THE SPONTANEOUS TRIGGERING OF SMALL-SCALE VAPOUR EXPLOSIONS

by

Terence Anthony Dullforce

A thesis submitted for the degree
of Doctor of Philosophy at the
University of Aston in Birmingham

October 1981

THE SPONTANEOUS TRIGGERING OF SMALL-SCALE VAPOUR EXPLOSIONS.

Terence Anthony Dullforce.

SUMMARY

This thesis presents the results of experimental work on the spontaneous triggering of vapour explosions, a phenomenon which can sometimes occur when two liquids at very different temperatures are brought into contact. The energy for the explosion is derived from the thermal energy in the hot liquid which is transferred very rapidly to the cold liquid by a fast fragmentation and intermixing process. The latter is vaporised so rapidly that a pressure pulse propagates from the explosion source.

The results of some 2000 small scale spontaneously triggered vapour explosion experiments are described, using four different liquid pairs. Spontaneous triggering is a term reserved here for those vapour explosions or interactions in the dropping mode of contact which occur without any external influence. In the case of molten metals it is generally associated with the collapse of an insulating vapour film at the liquid-liquid interface: hence a knowledge of the stability, heat transfer and breakdown characteristics of vapour films and bubbles is important to an understanding of spontaneous explosions. Small-scale experiments are described to investigate such characteristics by measuring the heat flux, (conventionally presented in the form of boiling curves), from metal spheres heated and rapidly quenched in water, and also the growth and collapse characteristics of spark generated vapour bubbles. A new technique is described for constructing minute surface thermocouples for surface temperature measurements on metal spheres.

The most important single result is the identification of regions in two-temperature space, called "temperature interaction zones" (TIZ) inside which it is possible for explosions to occur but outside of which they do not occur spontaneously. Some of the factors which affect the position of the zone boundaries have been identified and investigated and the variation of violence and dwell times across the zone have been related to the measurements of heat transfer and vapour stability in the quench and bubble experiments. A simple turbulent flow model for heat transfer from hot spheres has been developed. Particle size distribution in the finely fragmented portion of interacted metal debris, important to the modelling of heat transfer, has been shown to be predictable and essentially independent of the metal and water temperatures, mass and trigger mode over the ranges studied.

PhD Thesis, University of Aston in Birmingham, October 1981.

Key words: Vapour explosions.
Fuel-coolant interactions.
Liquid metal heat transfer

THE SPONTANEOUS TRIGGERING OF SMALL-SCALE VAPOUR EXPLOSIONS

LIST OF FIGURES

LIST OF TABLES

ACKNOWLEDGEMENTS

The work presented in this thesis was performed mainly at the Culham Laboratory as part of a UKAEA research programme supported by the Safety and Reliability Directorate (SRD), Culcheth. I would like to record my thanks to both SRD and the Culham Laboratory for allowing me to use the work as the basis of a PhD dissertation.

I would like also to thank my supervisors, Professor F.M.Page and Dr. R.S.Peckover, for their close involvement with the work, their advice and valuable time freely given. My division head and group leader, Dr`s K.V.Roberts and J.A.Reynolds, provided interest, support and encouragement throughout.

At Culham Laboratory many people over the years have contributed to the work in one way or another and I would like to record my gratitude to them and in particular to Dr´s J.A.Reynolds, R.S.Peckover, D.J.Buchanan and G.J.Vaughan for much discussion and collaboration. The experiments themselves have involved several people, but particular thanks go to G.J.Vaughan and A.N.Boucher for programming the data manipulation routines and to the latter for invaluable help in running the experiments. The excellent work of the various service departments at Culham (photographic, special techniques, electronic and manufacturing workshops) is also gratefully acknowledged.

The research has benefitted also from discussion by personal contact and letter with colleagues within the U.K. and throughout the world who have worked closely in the common pursuit of an understanding of the vapour explosion phenomenon. They are too numerous to mention individually, but close contact has been kept with researchers in Europe, the USA and in the UK (with colleagues at AEE Winfrith, AERE Harwell, AEE Windscale, CEGB Berkeley Nuclear Laboratories, Loughborough, Aston and Reading Universities, and the NII of the Health and Safety Executive).

Most PhD candidates would readily admit the impossibility of the task of producing a thesis without the support of their family. In this respect I am no exception and reserve special thanks for my wife, Joy, and children Rachel, Lucy, Daniel and Timothy, for their understanding and forebearence. My parents also have proved to be a constant source of moral support and practical help. I am grateful to my father and Mr R.Noyes who undertook the least satisfying task of all in proof reading the final version of this thesis in the attempt to find those last remaining errors. Mrs O.L.Morgan kindly stepped in to complete the typescript where the word processor proved inadequate and Mrs J.Williamson gave valuable assistance with the final preparation of the manuscript.

T.A.D.
Culham Laboratory,
October 1981.

EXTRACT FROM THE CANON`S YEOMAN`S TALE
THE CANTERBURY TALES
CHAUCER 1380 AD

Well, pass on to the story you require;
Before the pot is placed upon the fire
My master takes a certain quantity
Of metals which he tempers, none but he
-I can speak boldly now he`s gone away-
For he`s a cunning worker as they say,
At any rate he`s made himself a name;
He blundered very often just the same.
And how, d`you think? It happens, like as not,
There`s an explosion and goodbye the pot!
These metals are so violent when they split
Our very walls can scarce stand up to it.
Unless well-built and made of stone and lime,
Bang go the metals through them every time
And some are driven down into the ground
-That way we used to lose them by the pound-
And some were scattered all about the floor;
Some even jump into the roof, what`s more.
Although the devil didn`t show his face
I`m pretty sure he was about the place.
In Hell itself where he is lord and master
There couldn`t be more rancour in disaster
Than when our pots exploded as I told you;
All think they`ve been let down and start to scold you.
Some said the way the fire was made was wrong;
Others said, "No-the bellows. Blown too strong."
That frightened me, I blew them as a rule.
"Stuff!" said a third. "You`re nothing but a fool,
It wasn`t tempered as it ought to be."
"No" said a fourth. "Shut up and listen to me;
I say it should have been a beech-wood fire
And that`s the real cause, or I`m a liar."
I`ve no idea why the thing went wrong
Recriminations though were hot and strong.
"Well," said my lord, "there`s nothing more to do.
I`ll note these dangers for another brew;
I`m pretty certain that the pot was cracked,
Be that as may, don`t gape! We`ve got to act.
Don`t be alarmed, help to sweep up the floor
Just as we always do, and try once more.
Pluck up your hearts!" The muck was gathered up,
A canvas then was laid to form a cup
And all the muck was thrown into a sieve
And sifted for what it yet might give.

CHAPTER 1 INTRODUCTION

1.1 The vapour explosion phenomenon

Vapour explosions sometimes occur when two liquids are mixed together if one of them is very much hotter than the saturation temperature of the other. It is a phenomenon well known in metal foundries where mild explosions between some molten metals and water have been accepted as an occupational hazard, occurring almost daily without major consequence. Being one of the oldest scientific curiosities it was discussed in 1805 by the Society for the Promotion of Useful Knowledge and was most certainly known to the Alchemists in their attempts to turn other metals into gold. References to it date from the writing of Chaucer's Canterbury Tales, to the modern novelist. Solzhenitsyn sets one scene of his play "The Love-Girl and the Innocent" in a foundry, opening with the sputtering of molten metal from a wet casting mould.

1.2 Extent of the problem

The frequency of such minor events in modern foundries is believed to be high but incidents not involving injury or lost production are rarely reported. Occasionally, however, violent explosions occur causing personal injury and damage to property. For example, a furnace at Coalbrookdale was destroyed in 1801 when it was flooded with rain water. The aluminium industry is particularly prone to large scale explosions. It is estimated that between 1950 and 1960 hundreds of thousands of pounds worth of damage was caused in continuous casting

processes in the USA, Spain and the UK, with injuries and fatalities. There were 261 known explosions in Japan from 1935 to 1970, 80 people died and 800 were injured. The American Aluminium Association has collected data for the period 1944 to 1975, primarily concerning aluminium but involving also copper, magnesium, zinc, iron and steel. They record 75 explosions, 32 dead and 300 injured. In the UK 327 explosions were recorded in 1975 alone, many of them minor, but it is estimated that 10 to 15 incidents per year cause injury. The most recent example in the UK was at the Scunthorpe works of British Steel in 1975 where 11 people died when cooling water from a fractured pipe entered a torpedo containing 200 tons of molten steel, 180 tons of which were ejected in the process.

Vapour explosions are not restricted to foundries or indeed to molten metals and water but occur with a wide range of liquid pairs giving rise in several industries to apparently similar accidents and consequent concern for safety. It has been said that explosions are more frequent in paper making than in metal production with 59 recorded incidents between 1948 and 1973. They occur between fused sodium carbonate and water during quenching, and although there have been fewer injuries than with metal-water explosions, extensive damage has been caused to plant. In the nuclear industry, fuel cladding material has exploded with cooling water during deliberate melting experiments in research facilities. In the petroleum industry, liquid natural gas is known to be capable of violent explosion when spilled on water, although no industrial accident has yet occurred, and in the food industry the explosion of pork scratchings provides a more humorous example of a wide ranging and serious problem. Nor is the problem confined to industry but it has been suggested to account for, on the one hand, the mild spitting which occurs when wet chips enter cooking

oil, and on the other, for the violent explosion of sodium with water. In nature their occurrence has been postulated in astrophysical phenomena while the explosion of underwater volcanoes has been attributed to the same basic phenomenon. For instance in the destruction of Krakatoa in 1883 where the explosive yield was estimated to be the equivalent of 200 million tons of TNT. The statistics quoted above were taken mainly from references [1] [2] and [3] but several authors give excellent resumes of the more serious accidents, some of which are summarised in table 1.1.

1.3 Characteristics of vapour explosions

Considerable effort has been expended throughout the world, particularly since the early 1950s to identify the mechanism of these explosions. Over the past ten years the stimulus for such work has come from the nuclear industry, where there is interest in whether there are conditions under which reactor fuel can interact with the coolant in the highly unlikely event of melting in the core of a commercial reactor. The phenomenon has therefore been called a molten fuel-coolant interaction (MFCI) or fuel-coolant interaction (FCI), but other terms include: thermal explosion, thermal interaction, physical explosion, steam explosion (where water is the coolant) and vapour explosion. When used as a general term for the phenomenon, "fuel" refers to the hotter liquid, the energy source, while "coolant" refers to the colder liquid. In the present work vapour explosion has been used as a general description for all such events, while MFCI or FCI is reserved for particular reference to reactor fuel and coolant.

Table 1.1 Major industrial vapour explosion incidents

1954 Mallory-Sharon, Ohio	Water entered a crucible of a titanium arc melting furnace	$30,000 damage, 4 killed, 5 injured
1958 Reynolds aluminium, Illinois,	Explosion on loading wet aluminium scrap into a furnace	$1M damage. 25 mile area "rocked", 6 killed, 46 seriously injured
Quebec foundry	100 lbs molten steel fell into a trough containing 78 gals of water	$150,000 damage, 20 inch concrete floor cracked, 1 killed, some injured
1966 Western foundry	3000 lbs molten steel dropped into a water filled pit	Explosion heard 3 miles away, 3 injured
1967 Armco steel	30 tons molten steel fell on "damp" ground	6 killed 24 injured
East German slag incidents	Reports of several incidents when water entered cracks in slag crusts in open-hearth steel mills	Severe structural damage, deaths and injuries
1964 British slag incident	12-14 tons of slag exploded in a ladle that had been sprayed with lime water	Damage and injuries reported
1952 Canadian NRX reactor, Chalk River	Slow overpower transient led to 60 second nuclear excursion and fuel melting	Some damage and contamination of facility. No injuries
1954 Borax 1 reactor, Argonne, Idaho	Deliberate power excursion led to fuel melting	0.5 inch steel reactor tank ruptured. No injuries. 6-17 lb TNT equivalent. Conversion efficiency 7-20%
1962 Spert 1D reactor	Deliberate power excursion melted fuel	No injuries
1961 SL-1 reactor	Nuclear excursion damaged 12 fuel elements. 30,000 lb reactor vessel raised 9 feet into the air	3 KILLED ~~No injuries~~. Estimated 12 per cent conversion to mechanical work
1975 British Steel, Scunthorpe	400-700 gallons of water entered a torpedo containing 200 tons of molten steel. 180 tons ejected	11 killed, 8 injured, extensive damage
Tar-water	Hot tar exploded with condensed steam while loading a tanker	
1973 Tennent steel accident, Lanarkshire, Scotland	Molten steel exploded seconds after being poured into a 50 ton mould	2 killed, 5 injured
Oil-water	Small quantity of water settled beneath an immiscible light oil. Explosion occured when the oil was heated to more than 200 C	
Oil-water, New Zealand	Explosion with 60 litres of water covered by oil sludge in oil drying vessel of a greasemaking works	Factory destroyed by fire. Explosion generated 8 MPa, 5 killed
LNG-water, US bureau of mines	Unexpected explosions during tests on LNG spillage on to water	Apparatus destroyed. No injuries
1965 Transco cavern incident, Hackensack, New Jersy	Ten explosions occurred over 3 days when water leaked into a storage cavern freeze-sealed with LNG	No injuries
Soda recovery furnace incident	Large quantities of smelt (fused sodium carbonate) dropped into green liquor	Extensive damage to dissolving tank

It is generally accepted that chemical reactions cannot be the primary energy source for the vapour explosion because analysis of debris has not revealed the presence of significant quantities of chemically formed reaction products and because chemical reaction rates are often too slow for the materials of interest. Even so chemical reactions may play some part in for instance setting up the initial temperature conditions via exothermic reaction (eg sodium-water interactions). The phenomenon is, therefore, essentially physical in nature with the energy source being the excess heat in the hotter liquid, which is transferred on a millisecond timescale to the colder liquid. If the energy transfer is fast enough the increase in volume on vaporisation is inertially confined and the coolant is pressurised. A shock wave is produced which travels through both the coolant and the hot liquid and can do mechanical damage to the containing vessel and beyond.

If the hot phase can solidify in the coolant it can often be extracted as an extremely fine particulate with particle sizes ranging from a few micrometres to a few millimetres, the distribution being typically centred on a few hundred micrometres. It is tempting to consider the debris to be the result of the explosion, that is to say the results of the passage of the shock wave through the system, in much the same way that buildings are reduced to rubble by the shock wave from a chemical explosion. However, both Witte [4] and Roberts [5] have shown that the energy required to create the increased surface area of the debris would alone require heat transfer rates of several orders of magnitude greater than those observed normally in boiling processes, if this were to be achieved through the original sample surface. It seems, therefore, that the area increase necessary to obtain the required heat transfer and the fragmentation is not so much a result of the explosion but is actually a part of the mechanism required to produce the

explosive expansion. The energy in the increased surface area is, of course, only part of the total energy release, the remainder going to heat and vaporise the coolant and into the sound and shock waves. A fundamental problem of the vapour explosion is, therefore, that of understanding the fragmentation process, the conditions under which it can occur and the conditions required for the efficient transfer of thermal to mechanical energy.

1.4 Factors likely to affect vapour explosions

Experiments have shown that not all liquid pairs give rise to vapour explosions and for those that do the initial temperatures play an important role. The first requirement is of course that the hot liquid be above the saturation temperature of the colder vaporisable liquid. This may be, however, only one of several necessary but individually not sufficient criteria. Further, there is a wide range of parameters which may affect such criteria and have an effect on the likelihood and violence of an interaction. These include the physical properties of the liquids (specific heat, thermal conductivity, interfacial surface tension, melting point, viscosity, density etc.), the initial liquid temperatures, the quantity of liquids involved, the nature and availability of nucleation sites, the ambient pressure and the way in which the two liquids are brought together. The latter may be accomplished in a variety of ways, for example by the dropping, injecting or pouring of one liquid into the other and by the high velocity impact of one upon the other and either of the two liquids may form the bulk phase into which the other is introduced. Unfortunately, of the thousands of experiments that have been reported, not all have been done in a systematic way with the careful control of parameters

such as those listed above. Often several parameters have been varied at once.

1.5 Objectives of research

Despite considerable world wide attention there is still no complete understanding of the vapour explosion. The first steps in industrial safety are then to try and keep any possible reactants apart. If this fails, measures must be taken to minimise the effects. Clearly the latter approach is not satisfactory since at present such measures can only be based on empirical understanding.

The aim of the work presented in this thesis is, therefore, to enhance our fundamental knowledge of vapour explosions in one particular area, that of the spontaneous triggering of small drops, and to determine and if possible understand which liquids can be safely mixed and under what circumstances. With these broad objectives in mind it was therefore decided:

(i) to identify a few systems which were simple to experiment with, gave reproducible results and allowed the use of suitable diagnostics. (eg the coolant had to be transparent in order to film events),

(ii) to study predominantly a single contact/trigger mode; namely spontaneous triggering following vapour film collapse,

(iii) to identify and control as far as possible the parameters which may effect in any way interactions in this trigger mode,

(iv) to study specifically the effect of initial temperatures on the occurrence and nature of interactions and test the spontaneous nucleation theory (see chapter 2) in the chosen trigger mode,

(v) to study the effect of some other controlling parameters such as drop height, sample mass etc,

(vi) to perform such ancillary studies on vapour film growth and stability as appeared to be necessary to an understanding of the vapour explosion experimental results.

1.6 Organisation of thesis

A brief review of previous vapour explosion work is presented in chapter 2, which allows the work of this thesis to be placed in context. Chapters 3 and 4 describe the experimental procedures developed for studying vapour explosions, vapour stability and heat transfer. Chapters 5, 6 and 7 then present the raw data from the experiments, while the following chapter, 8, concentrates on data reduction and interpretation. Finally, the results, interpretation and extent to which the objectives set out above have been achieved are discussed in chapter 9.

The description of the experimental apparatus and procedures given in chapters 3 and 4 is more detailed than some would believe necessary. However, in view of the absence of strict reproducibility in experiments of this type, it may in retrospect be important to have recorded as precise a description of the experiments as possible in order to resolve some issues which have not yet been thought of or addressed.

CHAPTER 2 REVIEW OF PREVIOUS VAPOUR EXPLOSION WORK

2.1 Introduction

Very few topics in science can have been subjected to such rigorous investigation as the vapour explosion and there is an extensive literature on the subject which includes several excellent and lengthy reviews [1,3,4,6-18]. The review presented in this chapter draws much from those of Board and Caldarola [12], Williams [3] and Vaughan [1,14] and attempts only to extract the most significant points to emerge from a vast experimental and theoretical programme.

Experiments have been carried out with many different pairs of liquids over large ranges of temperature and mass (0.1 g - 30 kg) and in a variety of different geometries and contact modes. The cost of such experiments has similarly ranged from a few pounds to several hundred thousand pounds for a single in-pile experiment in reactor geometry. The reader is referred to the extensive tables summarising the experiments in the review articles.

There are three basic types of experiment that have been copied and performed internationally and conventionally classified according to the way in which the interacting liquids are brought together. These involve the dropping of one liquid into the other, the injection of one into the other and the high velocity impact of one on the other in a "shock tube". Other types of experiment include a range of in and out-of-pile simulation experiments specific to the nuclear industry. Experimental work is considered in sections 2.2 to 2.5 under these four

main categories, the last being given the general title "other geometries". Where appropriate the work presented later in this thesis is also included and referenced as [TT]. The current view of the stages involved in the triggering and propagation of explosions is then summarised in section 2.6.

Many different models have been proposed over the years to explain the experimental results. Some of these have been discarded as being of restricted application or inadequate as understanding of the phenomenon has progressed. One reference [1] lists 13 different models, but there are others. For convenience, the approach to understanding the vapour explosion is considered in sections 2.7 to 2.10 in four broad categories. Parametric models and temperature criteria, make no assumptions about the mechanism for fragmentation and mixing, but attempt on the one hand to predict the likely outcome of the explosion if it should occur, and on the other to find conditions of temperature or geometry where they have not been observed to occur. Some models for fragmentation are capable only of explaining incoherent events and are briefly listed in section 2.9, but the emphasis is placed on those theories that have received most attention within recent years as having the potential to explain coherent explosions in large masses of material.

2.2 Dropping experiments

By far the largest number of experiments have been performed by dropping or pouring one of the liquids into the other. In small quantities the dropped phase may enter the bulk phase as a single drop, and in larger quantities as a stream. Prior to the triggering of an explosion, except for very small drops, break-up occurs in the fall to

the bulk phase surface, or in falling through the bulk phase, or on impact with the container base. In larger quantities spreading across the base with break-up and folding gives a coarse mixture of the liquids. In all cases the dropped liquid enters the pool with its free fall velocity which distinguishes these experiments from some "injection" type experiments where a jet of one liquid has been directed on to the pool surface at high velocity [28,29].

Explosions have been observed to occur spontaneously without additional external influence only under specific conditions, but can be "forced" or "triggered" in a number of ways in many of the systems discussed below, under conditions where they would not normally have occurred. Such triggers have been provided by, for example, the dropping of a metal bar or pin [19], a hammer blow [20], a sudden step increase in ambient pressure [20], an oscillation to the system [19,21] an under-water spark [22], a chemical detonator [2,23] or an exploding wire [24,25,26]. The strength of the applied trigger pulse required to produce an interaction has so far not received much attention but there is evidence that the further temperature conditions are away from the conditions under which spontaneous triggering can occur [22,27], or the higher the ambient pressure, the stronger the trigger impulse must be [14,60].

The dropping of very large quantities and very small quantities (commonly referred to as large and small scale experiments) show different characteristics and the practice of distinguishing between them will be retained below. For convenience large scale is taken to mean those experiments in which the dropped phase mass exceeds a few hundred grammes, and ranges up to 30 kg. Small scale experiments involved smaller masses down to as little as 0.25 g.

The distance that the dropped phase travels while falling freely to the bulk phase surface is called the "drop height". The "pool depth" or "coolant depth" is the distance from the bulk phase free surface to the container base, and the time that elapses between initial contact of the liquids and the start of an explosion has been called the "delay time" or "dwell time".

Large scale dropping experiments. The most commonly used liquids have been molten metals and water. Experiments have been performed with molten aluminium [2,23,30-32], steels and cast iron [2,33], magnesium and magnox [2,30], copper [2,34], tin [2,23], lead [2], zinc [2], brass [2] and nickel [2]. In addition liquid freon [29,35], liquid natural gas (LNG) [36], molten sodium chloride [2,40], molten sodium carbonate [2] and molten sodium-potassium chloride mixtures [30] have also been dropped into water. Other combinations used were freon and mineral oil [29] and molten uranium dioxide and liquid sodium [37,38].

Without an external trigger, metal-water systems show the following general characteristics. Violent interactions can occur which in some cases has done extensive damage to strong metal containers, heating crucibles and reinforced enclosures [30,39,40]. Very fine scale spongy debris was produced in tin [23] and a fine powder in copper [39].

Not more than about 0.2 percent of aluminium was converted into oxide [43], observed by some workers as a white smoke [30]. This quantity is too small for the hydrogen produced to be the cause of the explosion as suggested in references [41,42], although some workers have observed a flash of light [31,41,42] others have not [30].

Visual observations [30] suggested interactions could occur before all the metal had entered the coolant and high speed cine film [23,39] has confirmed that molten metal, vapour blanketted [39], enters the water over a relatively long timescale (about 1 s). During this time it penetrates to the bottom of the container and spreads across the base while forming a coarse mixture of metal and water. Coarse mixing on a 10 mm length scale apparently expanded the metal volume by a factor of 10 for aluminium and 2 for copper [39].

The most violent interactions followed the coarse mixing and have been observed to start most often at a tank edge or corner [23,39]. These interactions were coherent and associated with a pressure shock wave which spread rapidly through the dispersion [23]. Propagation velocities from 30 to 400 m/s were shown to be proportional to the square root of the peak pressure (0.4 to 40 MPa) in accord with simple shock wave theory. Behind the well defined front, details of the mixture became obscured [23,32,39], either by rapid motion or vapour formation, but particle velocities here have been estimated as 25 m/s [23].

Incoherent spontaneous triggering of single drops of tin, or localised interactions on larger quantities, or a series of incoherent localised interactions at separate interaction centres have been observed to give mild explosions [23]. Peak pressures were low (1 MPa maximum) and rise times slow compared to the coherent explosions. No propagation front could be identified. Spontaneous triggering of aluminium and copper in free fall did not occur [39].

The geometry of experiments, physical dimensions of the water tank, water depth and drop height exert a strong controlling influence over

the occurrence of explosions. Mild explosions or none at all were observed in one series of experiments [32] in which large cylindrical containers were used, but very violent explosions have easily occurred with small rectangular tanks [30,32].

The use of a steel grid with 25.4 mm square openings, which broke-up a falling aluminium stream, also inhibited explosions as also did increasing the drop height to produce the same effect. With magnesium, however, the reverse effect was seen [44]. An increased drop height was required to ensure penetration of the lighter metal into the coolant before interactions could occur. Magnesium interactions were accompanied by persistent fires [30,44].

Some early work with aluminium [30], where metal was poured through a taphole in the crucible base, showed that a minimum taphole diameter was required to produce an interaction. No explosions were observed for diameters less than 63.5 mm.

Several authors have investigated the composition of the coolant tank base [30,42,44]. In one series of experiments [42] tanks with aluminium, glass and coated glass bottoms produced no explosions with molten aluminium. In another [30], coating the sides of metal coolant containers had no effect on aluminium explosions while coating the base could either promote or inhibit the explosions. Inhibition was achieved by painting with grease, oil or certain paints [30], while coatings with lime, gypsum, rust [30,42] or the hydroxides of iron or aluminium had the opposite effect.

Soluble oils [30], wetting agents [30] and acetone [39] added to the coolant also inhibited interactions.

Metal and water temperatures were important parameters. Most large scale experiments used cold (room temperature) water. Raising this above 333 K (60 C) inhibited interactions with aluminium [30]. There was also a lower metal temperature threshold which had to be exceeded to produce an interaction, and this was, for aluminium, a function of coolant depth, increasing with increased depth [30].

Similar temperature thresholds have been observed with other systems. For example saturated freon-22 dropped into water and water dropped into freon-22 [29] produce coherent explosions only for water temperatures above 350 K (77 C), and no interaction at all was observed below 327 K (50 C). Incoherent pops and bangs were produced for intervening temperatures. Freon-22 and freon-12 dropped into mineral oil also showed a lower oil temperature threshold for violent interactions to start. When hot mineral oil was poured into subcooled freon-22 [46] the lower threshold oil temperature was observed to increase with increasing subcooling.

Above the thresholds interaction pressures increased to peak at about 2 MPa or less. For freon dropped into water, peak pressures increased up to a water temperature of 353 K (80 C) only, beyond which temperature the interactions again ceased. The position of this upper, cut-off, temperature depended on contact mode and was absent for water dropped into freon, (ie interactions occurred for all water temperatures up to saturation).

Restricted ranges of temperature for interactions to occur were also found when pure hydrocarbons and hydrocarbon mixtures were poured onto water [36]. The pure hydrocarbons exploded when the difference in the initial bulk temperatures of the reactants was in the range 362 K -

395 K (89 C - 122 C) with a lower threshold water temperature of 315 K (42 C). Other mixtures such as methane poured on to pentane and liquid nitrogen poured on to propane also exploded. The experiments with hydrocarbon mixtures have demonstrated that liquid natural gas (LNG) can only interact after considerable "ageing", during which time the lighter constituent, methane, can "boil" off and the saturation temperature of the mixture increase.

Several kilogrammes of molten uranium dioxide have been melted in a resistance furnace [47] or produced by thermite reaction [38] and dropped into liquid sodium. Mixing was observed to take place, with sodium vapour being produced over a period of about 1 second. More vapour was produced with cold than with hot sodium [38]. The thermite produced oxide entered the sodium crucible as a stream of 10 mm diameter drops. No vapour explosions were observed, although the oxide finely fragmented on quenching to give angular shaped particles [38] similar to that produced in other experimental geometries with these materials. 200 - 700 ms after entry low energy incoherent pressure peaks of order 0.1 to 3 MPa (depending on the size of the vessel) were produced in the coolant and superimposed on the much slower coolant pressure rise.

Interactions between molten salt and water occur with apparently zero dwell time at high subcooling which prevented all the salt entering the water [40,45]. At low subcooling dwell times increased [40] and there was considerable penetration of the salt into the water before the explosion. These interactions could be inhibited by increasing the ambient pressure. At 0.1 MPa explosions occurred producing low peak interaction pressures, generally less than 1 MPa, but they were suppressed when the ambient pressure was increased to between 0.5 to

4 MPa in favour of a slow pressure rise over several seconds.

Small scale dropping experiments. A vast number of different liquid pairs have been used in small scale experiments and the reader is referred to reference [6] where many of them have been tabulated. High speed cine films have been taken by several authors [TT,20,48-51] and a description of a typical event is given later in section 5.5 of the present work. For most of the experiments the coolant has been water and the pool depth has been sufficient to ensure that interactions occurred spontaneously as drops fell through the water. When more than one drop was involved these interactions were generally incoherent but propagation through a dispersion of small drops has been observed [TT]. Not all liquid pairs have been induced to explode spontaneously, particularly those in which the melting point of the hot liquid was high (eg copper and aluminium [39,54]). Again, those pairs that have interacted spontaneously do so only under specific conditions.

All interacting pairs have shown a dwell time between contact and the explosion. For metal-water interactions dwell times rarely exceed a few hundred milliseconds [TT,52,53], while for experiments with refrigerants several seconds may elapse before interaction. As in large scale tests, the salt-water system showed extremely short dwell times in subcooled water [45]. With one exception [52] dwell times have increased with increasing temperature of both hot and cold liquids. Later it will be shown that the peak pressure was related to the extent of fragmentation in tin-water experiments which itself increased with both the hot and cold liquid temperatures [TT,49,58].

Film of tin-water drop experiments [TT,20,49] show that spontaneous triggering was followed by a cyclic expansion and contraction of the

interaction region, with successive cycles increasing in amplitude until fragmentation was complete. The number of cycles depended on the initial liquid temperatures and on the size of the sample. Very small drops generally exhibit only one cycle [53,54] of the interaction. The collapse of each cycle was accompanied by a pressure pulse in the coolant, which for tin-water rarely exceeded 0.1 MPa [TT] a few centimetres from the drop. There is evidence that the peak pressures (often observed on the second collapse) were a function of tin temperature and mass, and themselves peaked at about 973 K [48].

Many parameters have been shown to influence explosions, the initial liquid temperatures again playing a dominant role. Several workers have reported a minimum (threshold) temperature for the hot liquid which has to be exceeded [TT,60] for explosions to take place. The threshold temperature was independent of coolant temperature in metal water systems and increased with coolant subcooling in freon-water [TT] and freon-mineral oil experiments [69].

There was also a maximum coolant temperature beyond which interactions did not occur [TT,20,49,55,56,58,59]. This for metal-water experiments decreased as the metal temperature was increased, while in freon-water experiments it was generally fixed by the freon boiling point [TT]. In metal-water experiments the coolant cut-off temperature has been shown to be very sensitive to ambient pressure, decreasing with very small increases or decreases about normal atmospheric pressure [55]. The presence of non-condensible gas has also been shown to lower the cut-off [56].

It is shown later that the various threshold and cut-off temperatures form a closed boundary in temperature space outside of which

spontaneously triggered vapour explosions do not occur. Inside these closed regions spontaneously triggered interactions may occur. The regions have been called temperature interaction zones (TIZs) and are well established for several liquid pairs [TT,62].

A minimum mass of tin has been observed in tin-water experiments which had to be exceeded if interactions were to occur [TT,63]. The minimum mass was small and of no practical consequence, although its existence and its variation with the system temperatures must reflect the details of the triggering process involved. For small masses the position of the lower temperature threshold was moved towards higher tin temperatures.

The influence of contact with solid boundaries is complicated in small scale experiments. There is some evidence [TT,57] that contact with the container base before spontaneous triggering can occur inhibited these interactions. The mechanism for this is not understood and the phenomenon not confirmed by other workers [64]. If trapping of coolant between drop and container walls is allowed then, as in large scale experiments, base triggering can occur outside the normal TIZ [TT,57]. Externally applied triggers also violate the TIZ [20,60].

The presence of nucleating agents is also complicated and little investigated. The indications are that non-condensible gas [56] or lycopodium powder in the coolant [TT] diminish the size of the TIZ in tin-water and isceon-water interactions respectively. Oxide contamination of the metal surface similarly inhibited tin-water explosions [58] but was considered necessary in one series of experiments for the promotion of interactions between small copper drops and water [65].

2.3 Injection experiments

Experiments have been performed in which one liquid has been injected at high velocity into the other. The scale of the experiments varied from 1 g of water injected into 100 g of tin [70,71] to the 300 g of sodium injected into 3.2 kg of urania [72]. Very few liquid combinations have been investigated. Water and liquid sodium have been the most common coolants, and the former has been injected into molten sodium chloride [73] and the molten metals tin, lead and aluminium [70] and the latter into molten urania [74] and steel [75,76]. Injection velocities have ranged from 0.25 m/s for water into tin [70] to 30 m/s for sodium into steel [75] and the 80 m/s salt into water [73]. The injection of the hot liquid into the coolant has not given interactions between urania and sodium or sodium chloride and water.

In most of the experiments injection was accomplished by a hypodermic or similar fine tube which penetrated the melt surface before injection started. In some of the NaCl-water experiments [73], however, the water jet was squirted at the melt surface from above, but cine photography showed the water to penetrate the surface as a coherent jet.

The experiments were characterised by the rapid expulsion of various quantities of the melt from its container following dwell times that varied from a few milliseconds to several hundred milliseconds. The interaction could be accompanied by a flash of light [77], copious quantities of coolant vapour [77] and a pressure-time history consisting of one or more fast rising and narrow pressure spikes.

The most energetic explosions seem to have been those between urania and sodium (indeed this is the only experimental geometry to give energetic interactions between these materials) and between NaCl and water, while some systems gave very mild events (eg water into aluminium and lead [70]). It may be that the latter were due to violent boiling on timescales long compared to those associated with energetic vapour explosions. Even so, such interactions can liberate large amounts of energy as in the CORRECT I series of experiments where 100 kJ were liberated, with the system pressure rising from the static value of 0.5 MPa to 1 MPa over the "long" time of 0.5 s.

Water-molten salt experiments showed that the interaction violence was influenced by jet velocity. High injection speed (80 m/s) produced very mild events following short dwell times (a few tens of milliseconds). Only small quantities of the coolant had undergone injection when the interaction occurred. Lower injection velocities (as low as 1 m/s) produced longer dwell times (up to 250 ms), a greater volume of coolant penetration into the melt and more violent interactions.

The most systematic experiments seem to be those reported above for salt and water and those between molten tin and water. The latter have shown that dwell times are a function of metal temperature, increasing with T_h [71]. Furthermore, there was a low temperature threshold of 573 K below which interactions did not occur, and a higher temperature threshold at 723 K above which interactions were again inhibited. The low temperature threshold was the same as that for tin-water small dropping experiments but the upper cut-off temperature was much lower than that predicted by the small drop TIZ boundary. Above 773 K water was observed to rise to the tin surface and boil normally, as a water

drop would boil on the surface of a hot plate.

2.4 Shock tube experiments

The shock tube geometry, like injection experiments, has apparently little relevance to the industrial vapour explosion phenomena observed to date, although it was thought to be relevant to the confined geometry of coolant flow channels in nuclear reactor fuel assemblies. The first experiments were built in the USA but were followed by similar facilities in the UK (RDD Windscale and MOD Foulness), Germany and JRC Ispra, Italy.

A shock tube consists essentially of a long vertical column containing the cold liquid which is forcibly driven down by pneumatic pressure on to the surface of the hot liquid held in a small crucible at the bottom of the tube. Prior to initiating contact the coolant is held away from the hot liquid by a diaphragm which is subsequently ruptured. The hot liquid is usually heated by an RF heater and the diagnostics have included pressure transducers mounted in the tube walls and/or in the gas reservoir above the coolant column, thermocouples and high speed photography.

Film from some shock tube experiments [78,79] shows the following sequence of events. Following rupture of the diaphragm the liquid column moved down at high velocity (several metres per second) to strike the hot liquid surface where very rapid mixing and vapour generation resulted in some of the hot liquid being "scooped" out of the crucible to a depth of about one tube diameter. The expanding vapour drove the coolant column back up the tube taking with it the lifted hot phase. Condensation of the vapour then lead to the high

velocity return of the column, further mixing and so on. The coolant column was said to "bounce". At each bounce a sharp rising narrow pressure spike was observed.

The magnitude of pressures measured in different shock tubes are difficult to compare directly because they depend on the degree of constraint and on the position of the transducers within the apparatus. However, all experiments agree that the bounces correlated with the observed pressure spikes (typically 1 ms in width) and that the largest pressure was seen on the second bounce and not the first [80]. (Tin seems to be an exception here [79]. Pressure peaks were observed for temperatures above 573 K with the first peak ($\sim$10 MPa) always being the largest). It appears that the first bounce served to mix the reactants, with the dispersed hot liquid becoming quickly vapour blanketted. On the second bounce the insulating vapour film was collapsed and, on direct liquid-liquid contact, the enhanced surface area for heat transfer produced the very rapid heat transfer associated with a vapour explosion.

Increasing the degree of coolant subcooling and the impact momentum of the column [88] both increase the fragmentation, mixing and interaction pressures.

Water has been the most commonly used coolant and explosions have been observed between it and the metals aluminium [79,80,83,84], lead [78,79,81], silver [79,83], tin [79] and stainless steel [79,82,88]: the oxides of bismuth [79], boron [79] and uranium (as a powder [83] or granules [88]): magnox [79] and mixtures of lithium and potassium chlorides [78]. In all cases extensive fragmentation of the hot phase was observed, particularly with tin. The water temperature was in most

cases ambient or unspecified.

Most work has been done with aluminium and water where the peak pressures generated have been as high as 58 MPa (supercritical) but were typically 20 - 40 MPa [80,81]. There is some evidence that peak pressures increased linearly with aluminium temperature [83-86]. All other systems seemed to produce lower pressures. The presence of inert gas in the space above the crucible [81] and the generation of coolant vapour as the coolant column approached the melt surface [84-86], tended to cushion the impact, produce less efficient mixing and lower interaction pressures. With a lead melt less fragmentation was observed [81] and the interaction could be inhibited completely by inert gas [78].

The only other coolant to receive attention was liquid sodium which produced very low pressures with aluminium oxide [82,87,89,90] and urania, and extensive fragmentation. None of the sodium interactions, however, was considered to be an energetic vapour explosion.

2.5 Other geometries

A large number of in-pile and out-of-pile simulation experiments of reactor single and multiple pin geometries have been performed to determine whether vapour explosions can occur when these assemblies are deliberately subjected to overheating by loss of coolant flow or by a transient overpower of the fuel, or both. The reader is referred to reference [12] for further details and references. Suffice it to say that, although mild vapour explosions have occurred in some circumstances, no efficient conversion of thermal to mechanical energy has resulted, and there is no evidence of propagation between pins in

multiple pin assemblies.

The Q* type experiment [66,80], in which molten urania was produced by thermite reaction and released from its container within a pool of coolant, have shown, in the absence of an external trigger, a slow pressure rise over long timescales due to boiling. The type of energy release was classified with reference to the cover gas pressure and volume [66]. In some tests a mechanical impulse triggered vapour explosions between urania and water with small conversion efficiency.

Experiments in long tube geometry [67], in which a dispersion of molten tin was produced in a 1 m long tube filled with water at 358 - 368 K (85 - 95 C) and triggered either by detonator or spontaneously by allowing the tin to melt through a membrane into cold water beneath, has confirmed that 1-D self-sustaining shock waves can be produced, and that they can originate with, and escalate from, a spontaneous trigger.

2.6 Summary of main explosion features

There is general agreement that experimental studies have identified four stages in the development of coherent, large scale, vapour explosions which may be summarised as follows:

(1) A mixing stage during which the liquids intermingle on a length scale of order 10 mm. The production of coolant vapour seems important to this stage in insulating the liquids while mixing takes place. Heat flux to the coolant is relatively low and the vapour production helps mixing by stirring the components.

(2) A triggering stage where the trigger causes a pressure increase somewhere in the mixture sufficient to collapse the vapour blanket and start a fragmentation process. Triggering sometimes occurs spontaneously. Alternatively, vapour collapse can be initiated by the application of an external impulse.

(3) A propagation stage during which the fragmentation and rapid heat transfer travels at several hundred metres per second through the remaining volume of the mixture, liberating the energy of the hot liquid on a millisecond timescale. An essentially instantaneous energy release throughout the mixture is said to be coherent.

(4) An expansion stage in which expanding coolant or coolant vapour produces mechanical energy. Some of this energy is fed back to sustain the shock front.

Any model for the vapour explosion must explain the steps in the development of the explosion outlined above, and their outcome in terms of efficiency of energy transfer. In addition it should predict the circumstances under which the various stages may operate, ie, the position of temperature thresholds and cut-offs and the inhibition by gas and ambient pressure increases.

2.7 Hicks-Menzies and parametric models

Hicks and Menzies [91] calculated an upper limit to the energy available from the expansion of an initially perfect mixture of two liquids at different temperatures. Energy transfer between them was assumed to take place at constant volume. The mixture pressure rose until thermal equilibrium was established whereupon the mixture was

allowed to expand until its pressure had fallen to some predetermined value, usually atmospheric. Thermal equilibrium was maintained between the liquids throughout and no energy exchange with the surroundings was allowed. The saturation vapour pressure law was assumed in the two-phase mixture and the perfect gas law following complete vaporisation of the coolant.

The work output, or energy yield, from Hicks-Menzies calculations is often quoted as an efficiency, defined as the ratio of the mechanical energy released to the thermal energy available. The ratio of experimentally obtained efficiencies to the appropriate Hicks-Menzies efficiency has been called the fractional yield. In practice the available thermal energy is often difficult to define since the mass of the hot liquid involved in the interaction can be in considerable doubt. The energy yield is also difficult to quantify in some experimental geometries.

The Hicks-Menzies yield is a function of initial temperatures of the liquids and the ratio of quantities involved, peaking usually for approximately equal volumes of hot and cold liquid. The values predicted by Hicks-Menzies calculations are typically ten times larger than those observed in practice. The difference between this thermodynamic upper limit and observed energy yields can be too large for a realistic assessment of the damage potential of a vapour explosion. The theoretical models of section 2.10 seek to take into account the details of the less efficient fragmentation and mixing process obtained in practice as far as they can be understood at present.

An intermediate approach is that of the parametric model of which there are a number [92-102] and which have been compared in references [7,103,104]. These models require no details of, and make no prediction about, the fragmentation mechanism or the conditions under which fragmentation can occur, but simply assume that given contact of the hot and cold liquids, fragmentation and mixing will take place at a rate specified by characteristic time constants. Input parameters include the time constants, the liquid temperatures and the dispersed phase particle size, and the models can then be used to calculate the rate of energy transfer to the working fluid by conduction and/or convection and the pressure transients generated, and to determine the sensitivity of these to the input parameters.

By adjusting the values of the input parameters, the observed energy yields, pressures and timescales in experiments can be modelled and this gives an indication of the requirements of the physical mechanisms involved. Using these input parameters to then predict the outcome in other situations must be approached with caution. The physical mechanisms may not be the same, and in any case the scaling of the input parameters with, for example the masses of the liquids involved, is not understood.

Parametric models have been employed primarily in the study of nuclear reactor materials and the main conclusions have been summarised elsewhere [12]. They are only briefly stated here.

(i) The work done increases with decreasing time constants for fragmentation and mixing,

(ii) Vapour blanketting is important in cutting off heat transfer when fragmentation and mixing time constants are short,

see p28

(iii) Increased restraint increases mechanical work output,

(iv) Particle size distribution is important when the time constants are short, and

(v) there is no general agreement between models on the influence of non-condensible gas.

2.8 Empirical temperature criteria

A number of simple empirical criteria suggested by experiment have attempted to delineate conditions that have to be met for interactions to occur. The simplest and most obvious concern the bulk temperature of the reactants. For example the hot liquid has to be molten and above the saturation temperature for the coolant. Thus:

(i) $T_h > T_{sat}$ Vapourisation criterion

(ii) $T_h > T_m$ Baker melting point criterion

would form the very basic requirements, where T_h and T_m are the hot liquid temperature and melting point and T_{sat} is the coolant saturation temperature. The requirement for film boiling has, however, led some workers [TT,62,106] to further propose:

(iii) $T_h > T_{min}$ Minimum film boiling criterion.

where T_{min} is the minimum film boiling point for the coolant (see appendix 5). These criteria were soon found to be insufficient and more sophisticated variations of them based on the contact interface temperature, T_I, were added.

The interface temperature is the temperature common to both liquids established in the plane of contact of two materials when brought together. It has been calculated only for a plane interface between semi-infinite slabs of solid material and is determined by conduction only across the interface. T_I is given by:

$$T_I(1 + \alpha) = (T_h + \alpha T_c)$$

where T_c is the bulk coolant temperature and α^2 is the ratio of the product $k\rho c$ for the coolant to that of the hot liquid [107]. k, ρ and c are the thermal conductivity, density and specific heat capacity of the liquids respectively.

The interface temperature is established in times of the order of a picosecond, and for semi-infinite geometry is time invariant. In finite geometry and with a liquid-liquid interface it may fall with time or rise depending on the relative masses of the two liquids involved. Hence, in the application of the interface temperature criteria a fundamental difference exists between small quantities of hot liquid in coolant and vice-versa. Furthermore, with the high temperatures involved in some experiments, it is improbable that T_I is unaffected by radiated heat. The justification for its use, calculated as above, is based solely on the agreement obtained in some experiments

by so doing.

Interface temperature criteria are then:

(iv) $T_I > T_{sat}$ Modified vaporisation criterion

(v) $T_I > T_m$ Zivi melting point criterion

(vi) $T_I > T_{min}$ modified minimum film boiling criterion

(vii) $T_I > T_{spon}$ Fauske superheat criterion

There is little evidence for interface temperature criteria applying to anything but spontaneous triggering. Externally applied triggers can violate conditions (v) [22] and (vii) [60] and base triggering has violated (vii) [23].

The onset of interactions in spontaneously triggered systems, however, as the hot liquid temperature is increased can usually be identified with one or other of the conditions (i) to (vii), but there is no way of predicting which condition a given system should obey. The role of the film boiling criterion has been little studied but there is considerable evidence that some systems obey the spontaneous nucleation condition (vii) very closely. Others, however, obey condition (ii) or (v). It is not necessarily the higher temperature of these two that dominates. For example molten silver chloride dropped into water obeys the Baker melting point criterion (ii) which is lower than both the interface spontaneous nucleation criterion and the interface melting point criterion [60].

The role of the spontaneous nucleation criteria in safety assessments within the LNG and nuclear industries has aroused considerable controversy and will be considered in a little more detail.

Spontaneous nucleation (superheat) criterion. Following concern for the safe transport of LNG, the experiments outlined earlier led several authors [108-110,112-117,123] to an explanation of cryogen-water interactions based on the theory of homogeneous nucleation [111]. It was proposed that heat transfer across the liquid-liquid interface heated the cryogen beyond its normal boiling point into a metastable, superheated, state. Rapid, spontaneous nucleation and vaporisation then occurred when the limit of superheat, the homogeneous nucleation temperature, was reached, at which point the rate of vapour production was sufficiently fast to produce a shock wave in the coolant.

The most important (and controversial) of the superheat criteria is that due to Fauske [113]. Originally formulated to explain sodium into urania injection experiments, it has, over the years, been modified [118-121] to include all vapour explosion phenomena. The current basic requirements of the Fauske-Henry model are:

(i) direct contact must be made between the two liquids,

(ii) for $T_h > T_{spon} > T_I$ only small scale, incoherent, explosions are possible, and then only if T_I increases with time, ie the cold liquid is enclosed by the hot bulk liquid,

(iii) for $T_I > T_{spon}$ large scale, coherent, explosions are possible,

(iv) suitable system constraint is required with the third condition.

An attempt has been made to put the criterion on a firm theoretical base with the drop capture model [122] summarised in section 2.10. The model has been the subject of much critism and, as discussed above, while the position of the lower temperature thresholds in spontaneous triggered interactions in many experiments supports the hypothesis [TT,60], it does not apply when other trigger mechanisms are operative, or even, sometimes with spontaneous triggering [23,60]. In freon-water experiments there is controversy over the role of spontaneous nucleation, with one suggestion that the increase in violence observed when the condition is fulfilled is merely due to the provision of vapour blanketting which allows large quantities of reactants to mix before triggering occurs [148].

2.9 Incoherent fragmentation models

Many of the early models for fragmentation and mixing were essentially one-step processes with no obvious mechanism for the coupling or propagation of disturbances between adjacent drops or through coarse dispersions. For the most part they were suggested to explain small scale experiments where there was no requirement for coherence. For completeness the models are listed below with brief comments but will not be considered here in detail. References [1,4,14] discuss them more fully.

Gas release [123]. In general the solubility of gases in molten metals increases with temperature. This model suggests that rapid quenching of the metal causes it to become supersaturated with gas

which is released explosively and fragments the metal. This mechanism could "propagate" through a single drop with the gas release following the penetration of the thermal wave through the metal, and may conceivably be cyclic if vapour production interrupts the quenching process for short periods until it collapses or is otherwise dispersed. However, the energy available is small [1,12] and it is not likely to explain experiments performed in inert atmospheres where the gas solubility is very low [1].

Thermal stress fracture [124,125]. Freezing and contraction of the hot liquid surface is assumed to set-up stresses in a solid surface shell which are relieved by cracking. Hot liquid may then be squeezed through the cracks to contact the coolant and continue the process.

The energy available has been shown to be sufficient to account for the fragmentation of urania in liquid sodium [12] where angular shaped debris [126] indicates that some of the oxide was solid before fragmenting. The rate of fragmentation will, however, be limited by the solidification rate which is too slow to account for the pressures, timescales and energy releases observed in most experiments. The model assumes the solidifying phase is brittle and not plastic near the melting point [14], it ignores the possibility of supercooling, and it does not explain the interactions observed between water and molten bismuth, where the latter expands on freezing [1].

Shell (encapsulation, entrainment) model [59,127,128]. A number of mechanisms (eg Kelvin-Helmholtz instability and the folding of drops under hydrodynamic forces) have been proposed for the trapping of liquid coolant within the hot phase where its subsequent superheating and vaporisation cause internal pressures which disrupt and fragment

the system. An alternative scenario to the extrusion of hot liquid in the surface cracking model is that coolant could enter the cracks and become trapped. There is experimental evidence to show that entrainment can occur. Small water drops entering organic solvents have shown that the solvent can be entrained within the drop [128], water has been observed to blow molten aluminium and zinc into balloons which float [22] and small molten metal drops that have not exploded in water were often shown to be hollow [54]. The Kelvin-Helmholtz instability is considered not to be very effective in producing mixing at the interface [62] since the penetration depth would be small. There is evidence, however, for a surface instability from the surface ripples on small unexploded metal drops [54].

Capillary instability [105]. When the Weber number for a falling drop (the ratio of inertial to surface tension forces) exceeds a critical value it can fission to produce smaller, stable drops. The stable drop diameter depends on surface tension and the drop speed and is typically a few millimetres for molten tin drops falling with terminal velocity in water. The very fine fragmentation observed following an explosion in free fall cannot, therefore, be explained by this mechanism.

Coolant trapping (entrapment) [4,18,30]. Liquid coolant can be superheated under the inertial constraint of the bulk hot liquid when trapped between the hot liquid and a solid boundary. As with entrainment processes this entrapment can result in a spontaneous vaporisation and fragmentation. There is considerable evidence for this mechanism providing the trigger in large scale metal water experiments [18,23,30-32,39] and it has been observed in small scale experiments also [TT,19,21]. It cannot alone explain the fragmentation of all the metal in large scale experiments, or the spontaneous

triggering of falling drops.

Oscillating vapour blankets [129]. Vapour films on rapidly melted foils in water have been observed to oscillate at high frequency, producing an oscillating pressure at the surface which it is suggested is related to, and possibly responsible for, the fragmentation process.

Cavitation [130]. An alternative explanation to oscillating positive pressures themselves producing fragmentation is that these pressures at the surface create negative pressures and cavitation within the hot liquid drop which eventually fragment it. Again it is argued that this mechanism cannot supply the required energy [1,14].

Violent boiling [131-133]. In the transition boiling regime between nucleate and stable film boiling (see appendix 5) the heat flux increases as the hot surface cools. Transition boiling is, therefore, inherently unstable and is hydrodynamically violent compared with the other regimes. It is suggested that the forces associated with this boiling are sufficient to cause turbulence and mixing at the interface of the fluids. The violence of the collapse depends on the coolant subcooling. Heated spheres quenched in water [134] show that the collapse of a blanket can occur in less than a millisecond in highly subcooled water or much more slowly and less violently (taking up to 100 ms) in near saturated coolant. These processes were described as precipitous and progressive respectively.

Current opinion again is that entry into this region by cooling from the film boiling regime may provide a trigger to another fragmentation process, but that alone, violent boiling cannot explain the short timescales of large scale explosions. Neither can it explain the

explosion of liquid coolant dropped into a bulk hot phase where the surface temperature of the dropped phase increases with time. The transition from precipitous to progressive instability may give an explanation of the coolant cut-off temperature [1].

The demand in large scale explosions for a very fast fragmentation mechanism would appear to preclude those listed above. They can only be applied to the slower incoherent non-propagating events observed on the small scale. Even then, while these models might conceivably explain the fragmentation observed in individual small drop experiments, few of them are capable of extension to the explanation of all contact modes. Their role, however, in providing an initial trigger that could escalate by one of the self-sustaining mechanisms discussed below should not be dismissed. For example, molten metal and water experiments have demonstrated that explosions more easily occur in small vessels, where coolant can be trapped and heated under constraint until vaporisation produces the initial fragmentation. The escalation from small scale to large scale triggers has been observed [67] but the conditions for such have not been closely studied. Any of the above processes could provide a trigger in suitable circumstances.

2.10 Coherent, self-sustaining, models

To realise the damage potential of large masses of reactants, the explosion must take place coherently throughout the whole volume, which requires either a fast fragmentation mechanism which, triggered locally, can travel at high speed through the system, or the independent and simultaneous triggering of local events throughout the whole system. The latter seems unlikely, but as outlined above there is experimental evidence for the former. The models discussed in this

section are those currently in favour as having the potential to explain large scale energetic explosions.

BNL detonation model. Board et al [135] have shown that a detonating thermal explosion, analogous to a detonating chemical explosion, is possible in a coarse mixture of liquids given a fast enough fine fragmentation and mixing process.

Prior to an explosion in a large mass of molten metal, experiment has shown the metal and liquid coolant to be coarsely mixed. In its simplest form, the one-dimensional propagation model assumes such a mixture through which a plane shock wave is travelling at constant velocity. Ahead of the shock wave in the undisturbed mixture, the hot liquid is separated from the liquid coolant by coolant vapour. The arrival of the shock front collapses the vapour to give direct liquid-liquid contact and initiate fine fragmentation, mixing, and rapid heat transfer. Expansion of the coolant just behind the shock front drives the front forward.

To be self-sustaining, a detonation wave must move at the sonic velocity of the reacted mixture and at a velocity greater than sound in the undisturbed region, (the Chapman-Jouguet or C-J condition). This condition can be met if the energy transfer is completed within a very short distance behind the shock front, (ie between the front and the C-J plane where the velocity reaches the local speed of sound). The propagation velocity and pressure required to meet the C-J condition can be predicted without detailed knowledge of the fragmentation and energy transfer processes. Applied to metal-water systems the 1-D model implies the generation of very high pressures. For example [135], in a mixture of equal volumes of molten tin, water and steam

interaction pressures of 100 MPa are predicted with a propagation velocity of 300 m/s. These pressures were reduced to 5-10 MPa by extending the model to two-dimensional flow. The C-J condition can then be met with only partial energy transfer and efficiencies of about 10 percent, more typical of those observed in practice.

There are three aspects of the propagation model that require further comment. Firstly, the model assumes a pre-mixed (coarse) dispersion of the phases. While such dispersions have been observed in practice, the conditions for it are not predictable for all liquid-liquid systems, (eg sodium and urania). Secondly, a strong shock is assumed which can be provided in experiments by chemical detonator. But coherent explosions can be triggered naturally by the base trapping of coolant. It has been shown theoretically [146,147] and by experiment in long tube geometry [67] that steady state propagation can be attained by escalation from a small trigger. Finally, there is the question of a sufficiently fast fragmentation and mixing process. The original model suggested hydrodynamic mixing due to the relative motion between the hot and cold liquids behind the shock by virtue of their different densities. It has been criticised on the grounds that it was based on empirical relations for break-up times and drag coefficients for liquid drops subjected to shock waves in gases. Recent experimental data [136], however, shows that liquid-liquid systems behave in a similar manner to liquid-gas systems and that dense dispersed mixtures can be fragmented by weak shocks [137]. Besides hydrodynamic fragmentation, however, explosive boiling (spontaneous nucleation) and vapour collapse are being considered as alternative fragmentation mechanisms.

Bubble growth and collapse model. A cyclic model based on the collapse of coolant vapour bubbles which fragments the hot liquid and

enhances heat transfer locally to produce a second and subsequent bubbles has been suggested by several authors [20,61,138,139]. The collapse of vapour bubbles is associated with a pressure transient [TT] which may be capable of collapsing the vapour in adjacent regions and propagating the explosion. In common with other models a coarse mixture of the liquids would again appear to be the required initial state. As referenced in section 2.2 there is direct experimental evidence for cyclic bubble growth from high speed cine film and for propagation through drop dispersions [TT].

Buchanan [61] has divided the interaction for convenience into five stages. The first stage is a trigger which brings the coolant liquid, initially insulated by vapour, into contact with the hot liquid. In spontaneously triggered interactions the increase in dwell time with hot and cold liquid temperature and the shape of dwell time curves are compatible with the initiation of the explosion following natural vapour collapse through cooling of the hot liquid surface. Triggering is assumed to take place when the heat transfer flux exceeds some critical value in the transition boiling region. The observed coolant cut-off temperatures are explained on the basis of the displacement of the boiling curve with coolant subcooling (see appendix 5) which ensures that either the critical heat flux cannot be obtained at high coolant temperatures, or that it is attained at a surface temperature below the melting point of the hot liquid.

In the second stage, the heat transfer from the hot liquid to the cold liquid at the point of contact increases by at least an order of magnitude and very rapidly vaporises the coolant locally to form a vapour bubble. This bubble expands into cold coolant and at the same time again insulates the energy source. With the heat flux to the

bubble thus diminished and condensation taking place at the bubble wall in contact with cold coolant, the bubble begins to collapse. It does so asymetrically with the formation of a coolant jet travelling at high velocity towards the hot liquid surface.

The jet of liquid coolant penetrates the hot liquid surface in stage 3 of the model and disintegrates with a rapid increase in the liquid-liquid interfacial contact area.

In stage 4, during the penetration and break-up of the coolant jet, the heat transfer to the coolant (heat flux per unit area x area) rises rapidly and raises the temperature of the intermixed coolant.

In stage 5 at a certain temperature the jet vaporises and a high pressure vapour bubble is formed beneath the hot liquid surface. The rapid expansion of this bubble acts like a depth charge to shred and disperse the hot liquid between it and the surface into the surrounding coolant.

If sufficient energy can be transferred to the second bubble its size may exceed that of the initiating bubble in stage 2 and the process may escalate.

Quantitative results from the model have been derived by numerical simulation and we shall consider only briefly the mathematical formulations used.

The bubble dynamics for stage 2 were calculated from the classical results for the collapse of an empty spherical cavity in fluid by Rayleigh [140]. Bubble maximum radius, R_m, and the growth and collapse

time, t_g, were then given by:

$$R \frac{d^2R}{dt^2} + \frac{3}{2}\left(\frac{dR}{dt}\right)^2 = \frac{\Delta p}{\rho}$$

and

$$t_g = R_m \sqrt{\frac{\rho_c}{\Delta p}}$$

where R is the bubble radius, a function of time, t, ρ_c is the coolant density and Δp the pressure difference causing collapse. A bubble initial radius has to be assumed and it was further assumed that there was no heat transfer to the bubble during expansion and that at the maximum radius all the vapour suddenly condensed on the bubble walls.

Asymetric collapse with jetting has been observed experimentally [141] on high speed cine film and the process simulated numerically by Plesset and Chapman [142]. It is a phenomenon which occurs when the collapse takes place in a liquid adjacent to a boundary defining a change in the continuous phase density or viscosity. The jet forms when the bubble has collapsed to about 1/10 of its original size. Its final velocity, V_j, length, L_j, and diameter d_j, are given by:

$$V_j = \bar{V}_c (\Delta p / \rho_c)^{\frac{1}{2}} = 13.0 \left(\frac{\Delta p}{\rho_c}\right)^{\frac{1}{2}}$$

$$L_j = \bar{L}_c R_m = 0.493 R_m$$

$$d_j = \bar{d}_c R_m = 0.237 R_m$$

where $\bar{V}_c$, $\bar{L}_c$, and $\bar{d}_c$ are constants determined by the degree of asymmetry. The values given are for collapse against a solid wall.

The penetration of a liquid slug into another of equal density has been numerically simulated in two dimensions by Christiansen and Reynolds [143] who showed that the length of the jet increases exponentially with time from the start of penetration with a time constant proportional to d_j/V_j. Batchelor [144] has further shown that the contact area increases in a similar way with a time constant double that for the length increase. For liquids of different density Taylor [145] suggests the proportionality constant to scale with the square root of the ratio of the densities of the hot and cold liquids (ρ_h and ρ_c respectively). The time constant for area increase is then:

$$\tau = \frac{11}{4}\left(\frac{\rho_h}{\rho_c}\right)^{\frac{1}{2}}\left(\frac{d_j}{V_j}\right)$$

and the area of the jet, A, as a function of time, t, is given by:

$$A = A_o \exp(t/\tau)$$

A_o is the initial jet surface area. Solidification, vaporisation and surface tension could all limit the increase.

As the surface area increases conservation of mass dictates that the thickness of the interleaved liquid layers decreases. Heat transfer takes place across the thin layers into the coolant until the coolant vaporises at the saturation temperature or the spontaneous nucleation temperature. Spontaneous nucleation is so rapid that the latent heat cannot be supplied by the hot liquid and is taken from the coolant itself. Thus, a fraction (0.33 for homogeneous nucleation) of the coolant is vaporised to give a high pressure, high density gas bubble which expands and sends out a shock wave. Its subsequent motion is

described again from stage 2.

The efficiency of the energy feedback falls as the ambient pressure is increased providing a pressure beyond which interactions are cut-off. Further, it might be expected that the interaction is damped by the cushioning effect of non-condensible gas.

Drop capture model. The drop capture model [122] is based on the time-dependent behaviour of the thermal boundary layer established on initial contact of the two liquids and that of the number density of spontaneous nucleation sites (see appendix 6). Like other models it is convenient to consider as a number of separate stages.

Stage 1 requires that coarse mixing produces either a mixture of hot and cold liquid drops in a "sea" of vapour or collections of cold liquid drops in vapour bubbles within a continuous hot phase. In either event the hot and cold liquids must be separated by coolant vapour initially, not unlike the requirements of other models. No details are given of how such a mixture can be set-up.

In stage 2 the coolant spreads (wets) the hot liquid surface and conduction across the interface begins to superheat the coolant and develop a thermal boundary layer which increases in thickness with time.

Although the interface temperature is established in times of the order of a picosecond, nucleation cannot proceed until the thermal boundary layer thickness exceeds the diameter of the critically sized embryos. The latter is given by:

$$d_{crit} = 4\sigma/(P_v - P_\ell) \qquad \text{(see appendix 6)}$$

Since the vapour pressure, P_v, increases with temperature, the critical diameter falls as the interface temperature rises. Nucleation is also subject to certain time delays such as the acoustic relief time required for the pressure developed in the superheated coolant before it can expand, and the time to activate the first nucleation site, which is inversely proportional to the volumetric spontaneous nucleation rate, J, where:

$$J = \bar{A}N_L \exp(-W/\bar{k}T) \qquad \text{(see appendix 6)}$$

The Fauske criterion is introduced at this point. If the interface temperature on contact exceeds the spontaneous nucleation temperature (but not the thermodynamic critical temperature) the nucleation rate, J, is very high. Bubbles grow, interfere with each other and coalesce, to form a vapour blanket between the hot and cold liquids, essentially shutting off heat transfer. Drops enter film boiling and "capture" is not possible.

For a given interface temperature there is therefore a critical size for coolant drops, below which they become captured and explode and above which they become vapour blanketted and remain separated from the hot liquid by film boiling. Film boiling provides time for fragmentation down to the drop capture radius and a chain reaction can proceed to fragment all drops to capture size, at which point the capture and explosion of one drop initiates the explosion of all the others within a few milliseconds. A large scale, coherent, vapour explosion can then result.

Not clear.

Evidence for the drop capture model is provided by experiments in which small freon-12 drops were photographed at high speed entering a hot mineral oil surface. For interface temperatures less than the homogeneous nucleation temperature limit, drops of all sizes wetted the surface and vaporised from a thin film or by entrainment and incoherent nucleation. For interface temperatures greater than T_{hom} small drops were captured and vaporised within a few milliseconds, while large drops became vapour blanketted and floated until fragmentation or evaporation reduced them to drop capture size.

The model has been subjected to much criticism, particularly in reference [12] where the following remarks are made. Drops fragmented to the capture diameter should explode immediately and therefore the uniform mixture at the capture diameter could not be achieved. In any case the model requirement for fine fragmentation before the explosion takes place and the prediction of no explosions when the interface temperature exceeds the critical temperature are not in agreement with experiment. The assumption that bubbles cannot grow before acoustic relief and that their maximum size is restricted by the intersection of the mechanical stability line with the boundary layer thickness is also challenged.

2.11 Summary

The experimental characteristics of the main modes of contact used in laboratory experiments have been reviewed. The experimental evidence is wide ranging and sometimes appears contradictory, possibly because the controlling parameters and trigger mechanisms are not understood and cannot always be identified. The general consensus of opinion on the features of large scale coherent explosions has been summarised.

Hicks-Menzies and the temperature criteria are still the main tools for classifying events, while parametric models have provided some insight. A wide range of models exists for spontaneously triggered small scale explosions - this may indeed represent the richness of possible initiating mechanisms. For coherent propagating events the BNL model is the most attractive although the dominant fragmentation process has still to be identified.

CHAPTER 3 EXPERIMENTAL APPARATUS AND PROCEDURES I: VAPOUR EXPLOSION STUDIES

3.1 Introduction

In this chapter we describe the experimental apparatus and procedures for performing and monitoring some 2000 drop experiments. A number of liquid pairs were used, the four principal systems being molten tin, cerrobend* and cerrotru* dropped into water and refrigerant R12* dropped into water. Other systems briefly investigated were liquid nitrogen and water, molten tin and liquid nitrogen, molten tin and R12 and molten indium and water.

In the case of molten metals the coolant was always the bulk phase with small quantities of metals dropped into it. For the cryogenic liquids and water, however, the refrigerants were investigated as both the dropped phase (smaller volume) and the bulk phase. Also, in these systems, water was the hot phase and its role as both energy source and coolant could be compared.

The principal parameters varied were the initial liquid temperatures, but other parameters which were found to affect vapour explosions, such

---

* Cerrobend and cerrotru are trade names of the Cerro Corporation, USA, for two low melting point alloys. They are manufactured in the UK under licence by Mining and Chemical Products Ltd. Refrigerant R12 is one of a class of halocarbon refrigerants. It was purchased from the Imperial Smelting Corporation Ltd., Bristol who use the trade name isceon-12. It is more commonly known by another of its trade names, freon-12. The composition and properties of these materials are listed in appendix 1.

as drop height (the distance from the centre of the upturned crucible to the bulk liquid surface), sample mass, bulk phase depth and the presence of nucleating agents, were also investigated.

For those parameters which could affect the explosion but which were not investigated, (eg the quantity of dissolved air in the water and the degree of oxidation or other impurity in the metal), and which were difficult to assess quantitatively, an attempt was made by standardising the procedure for dropping to at least hold them as constant parameters. For example, water was always obtained from the same source with known impurity levels (see appendix 3) and was carefully prepared for each experiment in the manner described below.

Section 3.2 summarises the systems (liquid pairs) used and lists the parameter ranges studied. The experimental arrangements for dropping molten metals and cryogens are described in 3.3 and 3.4 respectively while section 3.5 describes the procedures developed to monitor such a large number of experiments systematically and the functions of computer routines for data storage and manipulation.

3.2 Systems and parameter ranges studied

Table 3.1 summarises the systems studied and parameter ranges investigated. In each system the first liquid of the pair was the dropped phase and the second liquid was the bulk phase (larger volume). The table lists for each system the initial temperatures of the hot and cold liquids, the quantities of the liquids involved specified by mass, volume or depth (the latter for the bulk phase) and the drop height.

Table 3.1 Systems and parameter ranges investigated

SYSTEM CODE	SYSTEM	VESSEL CODES	TEMPERATURE (K)		MASS/VOLUME/DEPTH		DROP HEIGHT (mm)	NUMBER OF EXPTS
			HOT PHASE	COLD PHASE	HOT PHASE	COLD PHASE		
1	Tin-water	0,1, 2,4,6	523 - 1273	273 - 373	0.5 - 44 g	20 - 600 mm	20 - 910	1179
2	Isceon-water	3	313 - 363	143 - 243	10 - 61 mm	10 cm3	30 - 340	560
3	Indium-water		1073					
4	Woods metal-water		no experiments performed with this system					
5	Isceon (+lyco. powder)-water	3	328 - 347	178 - 243	42 mm	10 cm3	90	40
6	LN2-water	3	273 - 371	77	40 mm, 500 cm3	44 cm3	100	16
7	Water-LN2	3	273 - 371	77	44 cm3	40 mm 500 cm3	100	11
8	Water-Isceon 12	3	304 - 368	243	1 - 40 cm3	40 mm	60	90
9	Cerrobend-water	1,4	473 - 1013	283 - 353	6.7 - 18 g	180 - 590 mm	30	40
10	Cerrotru-water	1,2	200 -1073	285 - 363	20 g	165 - 180 mm	30	85
11	Tin-LN2		about 1073	77	about 20 g	about 1 litre 200 mm	about 100	a few
12	Tin-Isceon 12		about 1073	77	about 20 g	about 1 litre 200 mm	about 100	a few

Besides the four principal systems already mentioned a number of experiments were performed with molten indium and water and with liquid nitrogen (LN_2) and water which will be reported in detail. Of the remaining liquid pairs, tin dropped into the cryogens at their saturation temperatures, spot tests only were performed.

The few experiments with indium were among the first performed. The metal, which was in the form of wire, was first cleaned with absorbent tissue to remove the oil in which it was coated and then heated in a stainless steel crucible under inert gas before tipping into several litres of distilled water. Oxidation was a considerable problem with the formation of a crust which had to be scraped away just before tipping.

3.3 Molten metal-water interactions

General description of the apparatus. The apparatus is illustrated by the block diagram of figure 3.3.1 and consisted essentially of a heated crucible containing the liquid metal pivoted above a container of water. Provision was made for tipping the crucible remotely, detecting the fall of the metal and triggering the recording electronics all from the start of the high-speed camera.

In laboratory experiments MaCracken [58] found that oxide coatings on the surface of metal melted in air led to unpredictable results. In the early experiments, therefore, a steel crucible, tipped by hand, was heated by Calor gas with the reducing region of the flame played on the metal surface to minimise oxidation. For the majority of the experiments, however, a small silica crucible (volume 3 cm^3) was

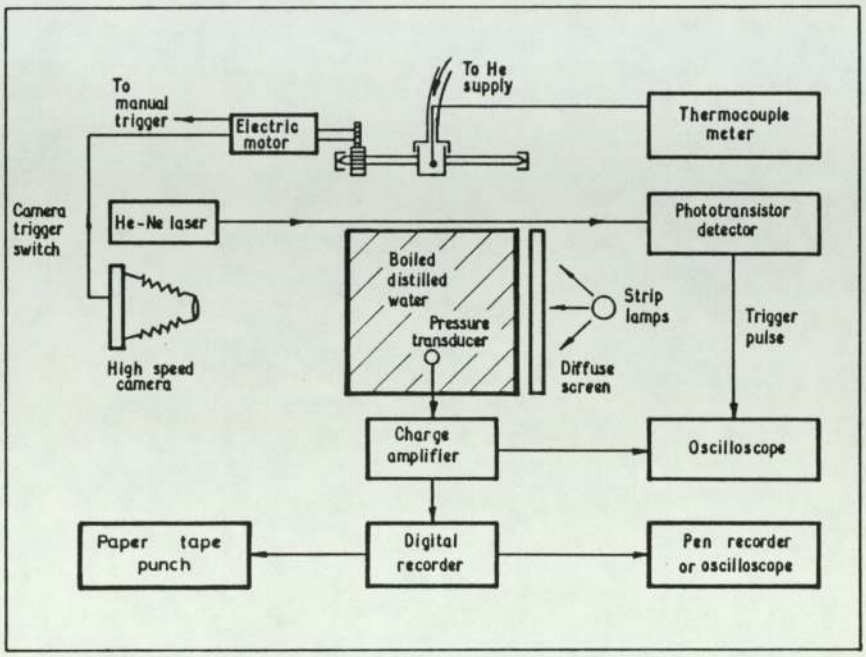

Fig 3.3.1 BLOCK DIAGRAM OF METAL-WATER EXPERIMENTAL APPARATUS

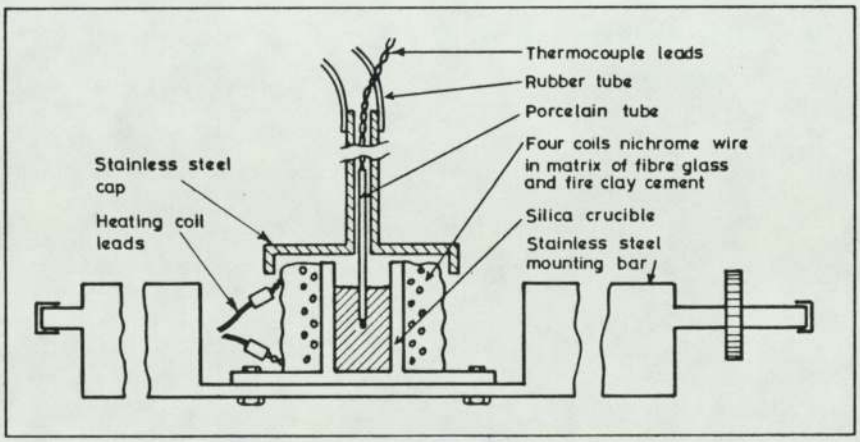

Fig 3.3.2 COVER GAS CAP AND CRUCIBLE ARM ASSEMBLY

resistively heated from the mains ac supply via a stepdown transformer. Details of the crucible assembly are shown in figure 3.3.2. Each crucible was made from a 25 mm length of 2.5 mm wall, 18 mm internal diameter silica tube fused to a rectangular silica plate, 55 mm by 26 mm by 3 mm thick, which formed the base and mounting flange. Three coils of nichrome wire (6.9 ohm per metre, 10 turns per coil) were wound on to each crucible, insulated from each other by fibre glass tape set in fireclay cement. Crucibles were then bolted on to a stainless steel arm as shown in figure 3.3.2 for mounting in the tipping assembly. They lasted for about 100 shots, depending on the temperatures reached, failing primarily through oxidation of the nichrome wires at the point where they left the fibre glass-cement matrix. A slow current of helium gas flushed the metal surface. The gas was introduced at the centre of a stainless steel cap, which loosely fitted over the crucible, and was then allowed to escape at the sides (see figure 3.3.2). Thermocouple leads also entered the crucible through the cover gas cap with the junction arranged to be roughly at the centre of the metal sample. Connecting wires were taken out through the side of the rubber tubing delivering gas to the cap.

A variety of coolant containers were used in the course of the experiments from simple glass beakers to specially manufactured tanks. Each vessel type was given a code number, and a list of these is given in table 3.2. By far the majority of the experiments were performed in the manufactured tanks (codes 1, 4 and 6). The base and walls were made from stainless steel while the other two walls were of clear perspex, (see figure 3.3.3), so that selected events could be recorded on high speed cine film. Illumination for filming, from the rear of the tank, was provided by three 1 kW tungsten-halogen strip lamps placed behind a diffusing screen and powered from the mains ac supply

Table 3.2 Vessel codes for vapour explosion studies

CODE	VESSEL TYPE, DIMENSIONS ETC.
0	Not recorded
1	Stainless steel sides and flat base, perspex front and back, 180 mm deep x 150 mm x 140 mm
2	As 1 but with a false, inverted, conical stainless steel base
3	Lower half of a 2 litre beaker, 40 mm deep x 125 mm diameter
4	As 1 but 600 mm deep
5	As 4 but with inverted conical base
6	Perspex sides, front and back with stainless steel, inverted conical base 100 mm deep x 157 mm x 142 mm

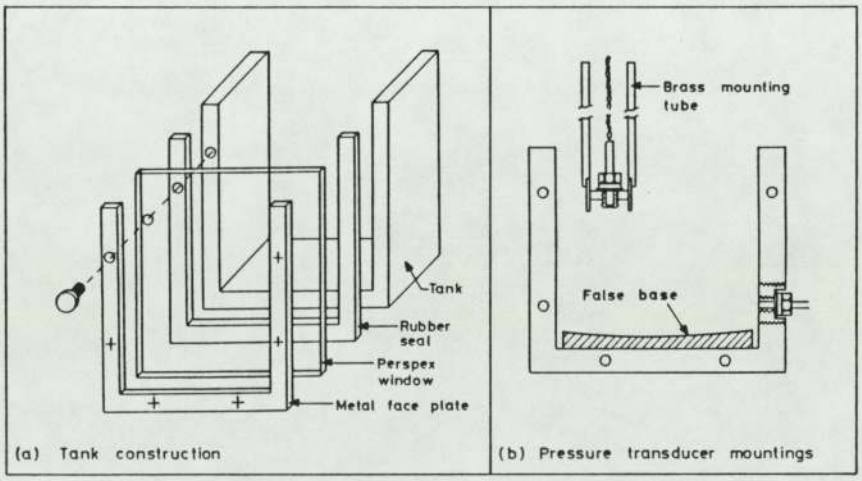

Fig 3.3.3 DETAILS OF COOLANT TANK CONSTRUCTION AND PRESSURE TRANSDUCER MOUNTING

via a transformer.

The time that the metal entered the water was initially monitored by the breaking of a light beam. 3 mm above the water surface the falling metal intersected a beam which was provided for convenience by a 0.5 mW He-Ne laser. This produced a voltage pulse from the phototransistor circuit illustrated in figure 3.3.4 which was used to trigger a Tektronix type 503 oscilloscope. This was a conventional circuit being basically a preamplifier for the phototransistor pulse followed by a bistable multivibrator with reset switch and an output amplifier which together delivered a 5 volt output trigger pulse.

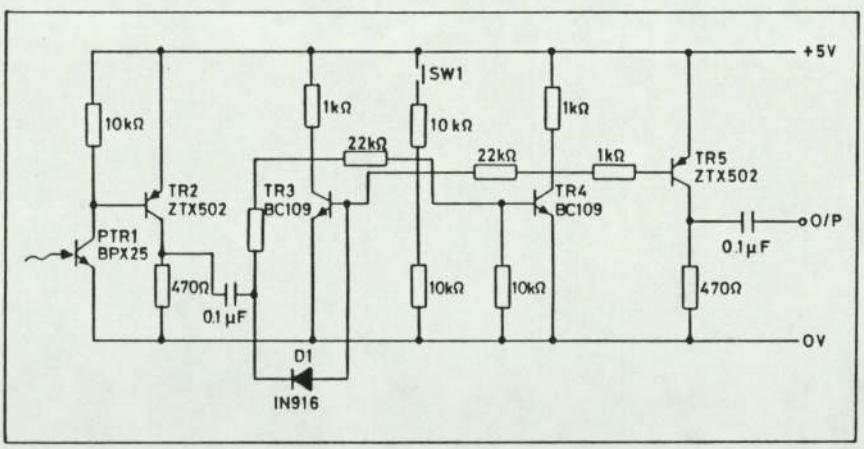

Fig 3.3.4 PHOTOTRANSISTOR TRIGGER CIRCUIT

With a tipping device there was difficulty in defining exactly where metal would fall. The light beam was not necessarily triggered by the leading edge of the tin drops. Occasionally the drops missed the beam completeley which could be subsequently broken by water ejected by the interaction. Dwell times, the time between the leading edge of the tin

drop reaching the water surface and the onset of the vapour explosion, were then apparently zero. It was also possible for the beam to be broken by a small drop of metal following the main drop, leading to an apparently short dwell time.

An alternative arrangement was therefore used in which the recording electronics were triggered from the closing of a microswitch attached to the rotating tipping arm and wired in series with a 4.5 volt dry cell. The tipping and fall time for the metal had then to be subtracted from the measured delays to obtain dwell times.

Experimental procedure. Each metal sample was heated to the required temperature which was then stabilised by adjusting the heating current. To minimise the possibility of oxidation of the metal the heating time was kept as short as possible, although sufficient time had to be allowed to ensure that the sample reached thermal equilibrium. Preliminary experiments with two thermocouples, one at the sample centre and the other near the crucible wall, showed that 3 - 5 minutes was generally adequate depending on the final temperature required. The crucible cap and thermocouple were removed vertically and the crucible was quickly and reproducibly tipped by a small electric motor actuated manually or by the event switch of the high speed camera which closed when the camera had reached the required speed. Tipping time was about 200 ms, fast enough to ensure that the crucible turned through 180 degrees before metal fell from it, which it then did as one or two drops (depending on the size of charge) rather than being poured in a stream over the crucible lip.

The metal fell through air through a known distance into a container of water. Care was taken to keep the distilled water as clean as

possible. Dissolved gases were removed prior to each experiment by boiling the water for three minutes using an immersion heater and then syphoning it into the reaction vessel where it was allowed to cool to within two degrees above the required final temperature before the metal was heated and dropped. At high coolant temperatures it was first necessary to re-heat the coolant with an immersion heater after syphoning.

After each experiment the tank was thoroughly cleaned and the water was replaced by freshly boiled and cooled water. Metal debris was collected and dried under an infra-red lamp for further examination. (In the case of the alloy cerrobend, with a melting point of only 343 K, the samples were dried over a low temperature hot plate to avoid melting the debris). Each sample was numbered and filed for storage in a small perspex box.

Diagnostics. In early experiments a crystal microphone was employed just outside the coolant tank wall to record the sound of the explosions which were displayed on an oscilloscope and photographed with a Polaroid oscilloscope camera. An example of such a trace is given in figure 3.3.5(a). It provided useful timing data but gave no indication of the size of the pressure pulses generated or the pulse shapes. A Kistler type 603B pressure transducer with a rise time of 1 microsecond and range 0-200 atmospheres was therefore substituted for the microphone and the output from its charge amplifier (Kistler type 5001) recorded either directly from the oscilloscope, triggered as described above, or more usually by a Datalab 901 transient digital analyser. Direct oscilloscope recording had the disadvantage that very fast rising pressure spikes were not seen by even the fastest film (Polaroid type 3000). Output from the transient analyser could,

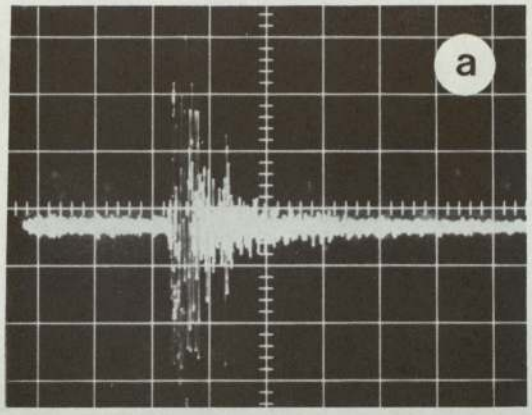

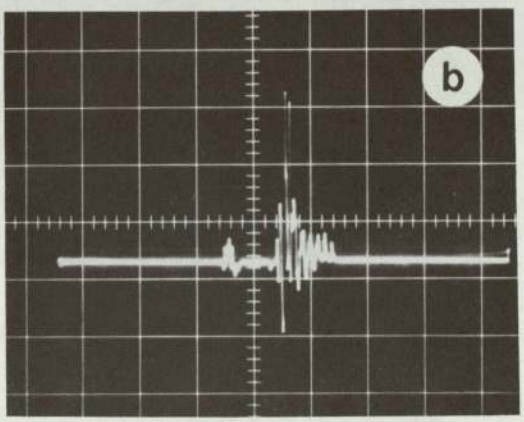

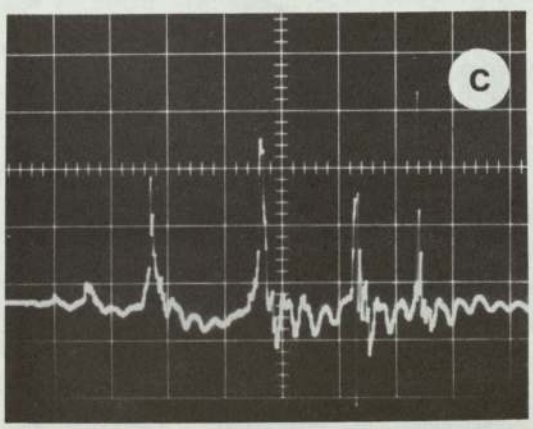

Fig 3.3.5 EXAMPLE PRESSURE RECORDS BY (a) CRYSTAL MICROPHONE,

(b) PIEZOELECTRIC TRANSDUCER IN THE TANK WALL AND

(c) PIEZOELECTRIC TRANSDUCER IN TUBE MOUNTING

Vertical sensitivity	(a) 5 mV/cm	(b) 0.04 MPa/cm	(c) 0.2 MPa/cm
Timebase	(a) 50 ms/cm	(b) 62.5 ms/cm	(c) 2.5 ms/cm

however, be displayed continuously on the oscilloscope where it could be examined in detail at leisure, expanding various portions of the trace if necessary, and hardcopy obtained by photographing the screen or from an Oxford instruments 3000 pen recorder. There was also the facility to output the digital information on paper tape for permanent record and computer analysis. The pressure transducer was mounted in the coolant in one of the two ways illustrated in figure 3.3.3. For most of the experiments it was mounted flush with the inside of the tank wall 30 mm above the base, but better pressure records could be obtained if the transducer was mounted at the bottom of a brass tube and immersed through the top of the tank. Figure 3.3.5(b) and (c) compares pressure records from both positions. With the transducer mounted in the tube and closer to the site of the explosion the effects of reflections were less important and the individual pressure peaks were much more clearly defined.

The pressure records from tin-water interactions varied little in character to that shown in figure 3.3.5(c). Two to five peaks were usually observed with the second generally being the largest. Peak pressures rarely exceeded 1 atmosphere.

Metal temperatures up to 1273 K were monitored by a chromel-alumonel thermocouple and Comark cold junction compensated digital thermometer.

16 mm high speed cine photography was performed using a Hycam rotating prism camera equipped with full height optical head and capable of up to 11,000 frames per second (fps). The framing rate was determined from neon timing markers at twice mains frequency along each edge of the film. Most of the filming was performed at 5000 fps using Ilford MK V motion picture film.

Debris examination. Each sample was visually examined and photographed on Polaroid type 52 sheet film using a Plaubel 5" x 4" plate camera with bellows extension, and a table lamp light source. Often it was possible to identify two fractions, a finely fragmented portion in which particle sizes could be as small as 6 micrometres, and lumps of metal that had clearly not been subjected to the dispersal mechanism and were too large to have been produced by Weber break-up. Although a subjective measurement, removing the latter and expressing the mass of the fine fragments as a percentage of the total sample mass, was used as a quick and simple method of assessing the extent of the interaction. This measurement has been called the percentage disintegration [58] or PD. A more precise measurement was obtained by expressing the mass of debris below a certain size, obtained by sieving the sample, as a percentage of the total mass. The choice of sieve size for this definition is explained in section 5.3. For tin dropped into water it was 2 mm. (To distinguish between them the latter will be called PD and the former the assessed PD or PDA).

For 67 metal samples, complete particle size distributions were determined. Samples were tipped into the largest mesh sieve at the top of an interlocking tower of 10 sieves with mesh sizes ranging from 0.1 mm to 3.35 mm, (Endicotes sieves: plain weave to BS 410). The sample was then gently brushed across the sieve mesh until only those particles too large to go through remained. The top sieve was then removed, inverted over clean paper and the particles tipped and brushed out. The sample obtained was then placed in a small weighed plastic box which was then re-weighed and the process repeated through the entire sieve range.

One tin sample for which the assessed PD was 100 per cent, was sent to AERE, Harwell, for surface area measurement by a radioactive absorption technique. This gave an area enhancement factor of 840.

3.4 Cryogen-water interactions

General description of apparatus. In general isceon-water interactions were much more violent than metal-water interactions and often led to the destruction of glass containers. Figure 3.4.1 illustrates such an interaction between just 10 cm^3 of refrigerant and 1 litre of water. For this reason the apparatus was enclosed by a much stronger outer container, but otherwise employed only minor changes to that described in the previous section. For those experiments in which isceon-12 was dropped into water, the electrically heated crucible was replaced by a small glass beaker (volume 30 cm^3) held in position on a steel rotating arm by two metal straps.

When the contact mode was reversed and smaller quantities of water were dropped into larger volumes of isceon, a plastic inner container was used in the tipping crucible to slow down the water cooling rate. This was particularly important with very small water volumes and enabled experiments to be performed down to 1 cm^3, below which a complete change of crucible design would have been necessary. Even so the maximum water temperature attained was about 348 K (75 C) and to obtain higher temperatures the tipping arm assembly was changed to that illustrated in figure 3.4.2. The essential feature of this design was the double skin wall through which boiling water from a heated reservoir was continuously run. The crucible was lagged with asbestos string and water temperatures up to 368 K (95 C) were easily achieved.

Fig 3.4.1 AN ILLUSTRATION OF THE DAMAGE POTENTIAL OF CRYOGEN-WATER INTERACTIONS

Experimental procedure. Most of the experiments involved isceon-12 dropped into water for which the procedure was as follows. Isceon was poured into the beaker and allowed to boil, cooling the beaker until boiling became quiet and about 10 cm^3 remained, at which point the steel arm was rotated and the cryogen tipped into a glass vessel (the bottom portion of a 2 litre beaker) containing boiled, cooled distilled water. For those experiments containing subcooled isceon the beaker temperature was first lowered by allowing a small quantity of liquid nitrogen to boil from it. Isceon, itself first cooled in liquid nitrogen, was then introduced and the temperature was allowed to rise until the required value was reached before tipping.

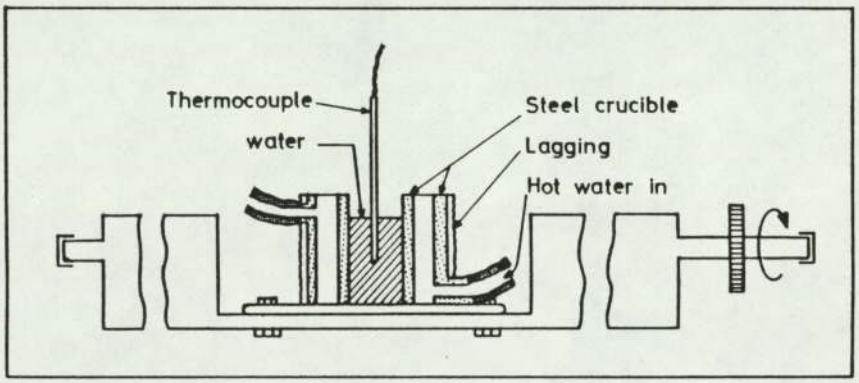

Fig 3.4.2 HEATED TIPPING ARM FOR ISCEON-WATER EXPERIMENTS

Diagnostics. Some pressure measurements were made using a force transducer arrangement in which the transducer was set in a massive stainless steel block, weighing 7 kg, and the downward impulse from the interaction communicated to the diaphragm through an anvil supporting the bulk phase vessel. The leading edge of the fast rising pressure pulse was used to trigger the transient recorder.

Figure 3.4.3 shows two typical records. About 50 per cent of the records were composed of one pulse occurring up to several seconds after contact between the isceon and water, and having pulse widths at half peak height of 1-10 ms. Figure 3.4.3(a) is such a record. The remaining 50 per cent had two or three pulses separated by a few hundred milliseconds. (Occasionally more than three pulses were recorded, up to a maximum of six). In general the second and subsequent pulses were lower than the first. Figure 3.4.3(b) shows this type of record. The pulses themselves were sometimes single peaks but more generally there was some fine structure as shown in figure 3.4.3(a). Three or four fine peaks per pulse was not unusual, but with the long sample times required to record the whole pressure history they were generally not well resolved.

Dwell times in these experiments were much longer than for metal-water interactions and were estimated in some of the experiments with the aid of a stop watch.

3.5 Data recording

It was realised at the outset that a large number of experiments would be performed, covering several parameter ranges, and which would result in the need for time-consuming searches during data reduction. Careful systematic recording of experimental details and results was therefore instituted at two levels. Firstly, all the details of each experiment were entered on four standard record sheets which acted also as check lists for procedure. These covered:

(i) Experimental conditions, system and vessel details, brief description of events from film, and summary of results.

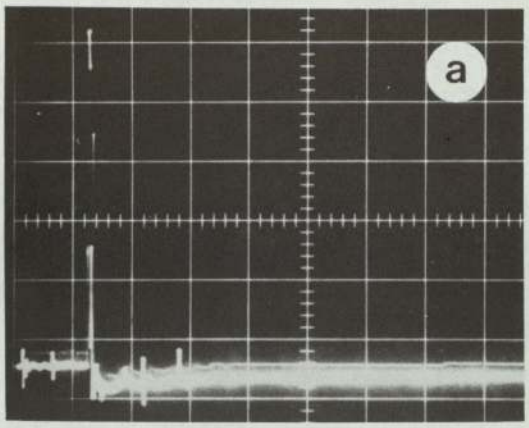

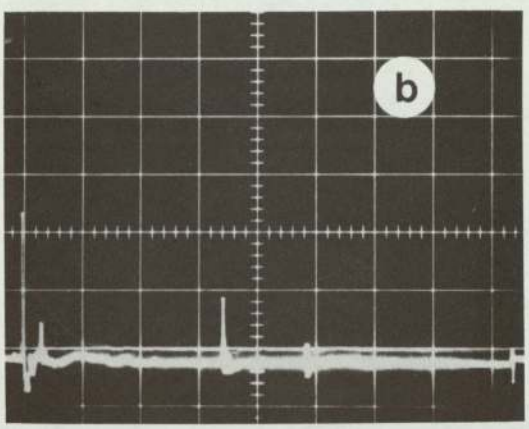

Fig 3.4.3 TWO TYPICAL PRESSURE RECORDS FROM ISCEON-WATER INTERACTIONS (T_h = 339 K, T_c = 243 K)

Vertical sensitivity	(a) 2 MPa/cm	(b) 0.8 MPa/cm
Timebase	(a) 100 ms/cm	(b) 100 ms/cm

(ii) Details of cine film, camera types, settings, lighting, lenses, and length scale factors,

(iii) Details of diagnostics, instrument types and settings,

(iv) Copies of oscilloscope recordings on polaroid film.

Secondly, the essential data and results were stored on computer. Table 3.3 lists the information and format recorded in this way. System codes are listed in table 3.1 and vessel codes in table 3.2. Input data was submitted on punched cards and a program (SORT) was written to search the experimental data over a maximum of six ranges and three integer parameters and to present the data in an easily interpreted format. The search program was initiated from a remote terminal. All the raw data plots of chapters 5 and 6 were produced from such searches. SORT enabled searches to be made on ranges, specified by maximum and minimum limits, of the following parameters:

(i) hot liquid temperature, T_h,

(ii) cold liquid temperature, T_c,

(iii) drop height, d_h,

(iv) pool depth, d_c,

(v) mass or volume of dropped phase, m

(vi) dwell time, t_D, and

(vii) percentage disintegration, or violence, PD.

A search could also be made on the three integer parameters to find all the experiments performed with a particular vessel, or a particular system, or all experiments that had been filmed.

Table 3.3 Punched card format for vapour explosion experimental data

COLUMN NUMBERS	PARAMETER	DESCRIPTION
2 - 6	experiment number	Each experiment was identified by an alpha-numeric string of the form AAXXX, where AA are identifying letters and XXX the experiment number
8 - 11	Temperature of the hot phase	To the nearest whole degree C
13 - 16	Temperature of the cold phase	To the nearest whole degree C
18 - 22	Drop height	The distance from the crucible centre in the tipped position to the bulk phase surface to the nearest cm
24 - 28	Pool depth	The depth of the bulk phase in cm
30 - 34	Mass or Volume of dropped phase	To the nearest 0.1 g or 1 cm^3 For system codes 1 & 3 - mass For system codes 2,5,6 & 7 - volume
36	Number of dwell times recorded	The dwell times themselves were recorded on a second card expected by program SORT when column was non-zero
40 - 42	PD or violence estimate	Assessed PD to the nearest 1 per cent. For systems which did not solidify the violence was estimated on the arbitrary scale 0, 25, 50, 75 & 100%
44	Vessel code	Integer in the range 0 - 9. See table 3.2
46 - 47	System code	Two digit integer. See table 3.1
49	Comment code	A zero or 1 indicating that the written record sheets contain observations or comments that should be borne in mind when interpreting the results
51 - 54	Film number	
	FORMAT OF DWELL TIME CARD	
2 - 6	Experiment number	
8 - 9	The letters DT	Signifying dwell time card to SORT
11 - 14	First dwell time	To the nearest millisecond, right adjusted
16 - 19 21 - 24 26 - 29	Any subsequent dwell times	Where those before did not lead to a complete interaction

CHAPTER 4 EXPERIMENTAL APPARATUS AND PROCEDURES II: HEAT TRANSFER AND VAPOUR STABILITY STUDIES

4.1 Introduction

It appears that in small drop experiments further sub-division (coarse mixing) of the hot and cold liquids is not required for a vapour explosion to start, although as discussed in chapter 2 fine fragmentation is required for the reaction to proceed to completion. Several authors have suggested that the self-triggering of vapour explosions is the result of the breakdown of stable film boiling which allows direct liquid-liquid contact to locally enhance heat transfer rates by several orders of magnitude and which starts the fragmentation process. Opinions differ as to whether violent boiling is alone sufficient to account for fragmentation or whether more sophisticated mechanisms, such as vapour bubble growth and collapse with coolant jetting, are required to explain this stage of the interaction. It is important, therefore, to understand the breakdown conditions for vapour layers at a rapidly cooling liquid-vapour interface and to know the effect of various parameters, which are known to effect vapour explosions, on the breakdown conditions. Such parameters include ambient pressure, nucleation site density and coolant subcooling. While some information exists in the open literature for saturated coolants, relatively little has been published with respect to the parameter changes listed above for any coolant other than water.

A simple method was therefore required to enable measurements to be made very quickly, primarily for the coolants and conditions of the

present studies. Section 4.2 describes such a technique, based on the rapid quenching of a heated stainless steel sphere, from which time-dependent heat transfer rates were derived. Although this technique is not new there is considerable disagreement in the reported results. For example, most authors agree that the minimum film boiling point for water decreases linearly with increasing water temperature, but there is considerable disagreement over the slope of the dependence. An excellent review of film boiling on metal spheres quenched in water is given by Benz [68]. Cine photography enabled the quenching process to be observed closely and the vapour layer thickness to be estimated using conventional illumination, while shadowgraphy, using a He-Ne collimated laser light source, gave valuable qualitative data concerning the distribution of heat in the coolant.

Metal-water interactions described later show the process to be cyclic, involving the shredding of hot liquid and the growth and collapse of near spherical vapour bubbles. The conditions under which coolant vapour bubbles can grow and collapse are then central to the spontaneous triggering mechanism. Section 4.3 describes experiments with spark generated bubbles beneath water, designed to investigate at least qualitatively such conditions. In particular, the growth and collapse times were measured as a function of coolant temperature for comparison with those observed in vapour explosions, and the nature of the collapse process with increasing coolant temperature, central to the condition for jetting to occur, was studied.

4.2 Sphere film boiling studies

General description of the apparatus. Film boiling on a 19.5 mm diameter heated stainless steel sphere was studied with the arrangement shown in figure 4.2.1. The sphere was attached to the bottom end of a 120 mm long ceramic tube, itself attached to a toothed metal rod that could be racked up and down by a 35 volt dc motor driven cog wheel, 95 mm in diameter. The extremes of vertical motion were set by microswitches attached to the motor support structure and operated by a contact on the rotating motor spindle. The distance between the switches was adjustable to control the depth of immersion of the sphere. Each microswitch was provided with a bypass switch to facilitate return of the arm.

In the raised position the sphere was at the centre of an electrically heated oven with the support arm passing through the oven top and the bottom closed with a manually operated sliding ceramic base. In the lowered position the sphere was immersed in a flat glass sided 120 mm square container of water, 120 mm deep, filled to within a few millimetres of the top lip. Travel from the bottom of the oven to the water surface was typically 30 mm.

All the mechanical parts were mounted on a perspex support structure inside a closed perspex container (300 mm x 380 mm x 500 mm tall) with a removable front which shielded the apparatus from draughts and maintained an inert argon gas atmosphere.

Why?

During the experiment the sphere surface temperature was monitored as a function of time and selected experiments could be filmed in either conventional white light or collimated laser light.

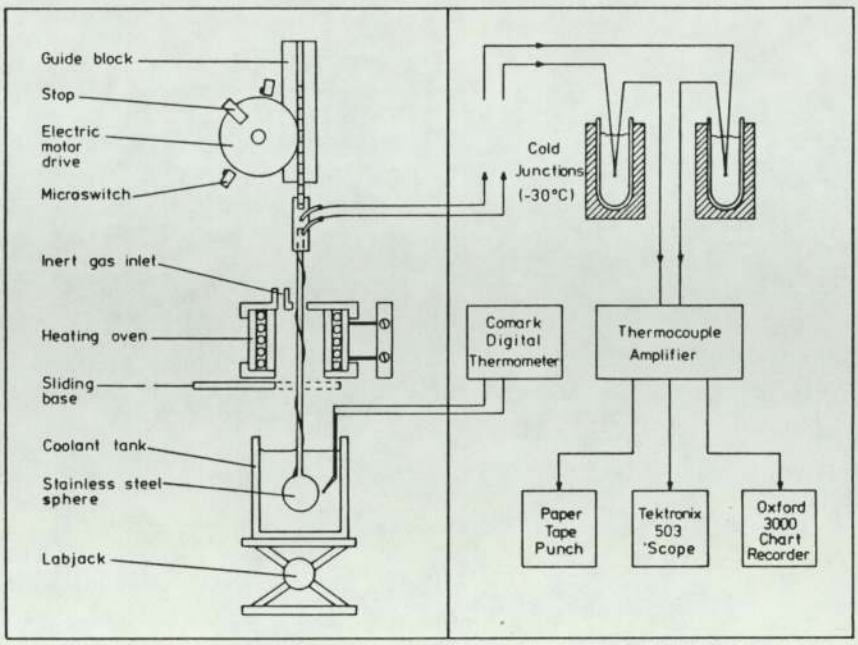

Fig 4.2.1 DIAGRAM OF SPHERE QUENCHING APPARATUS

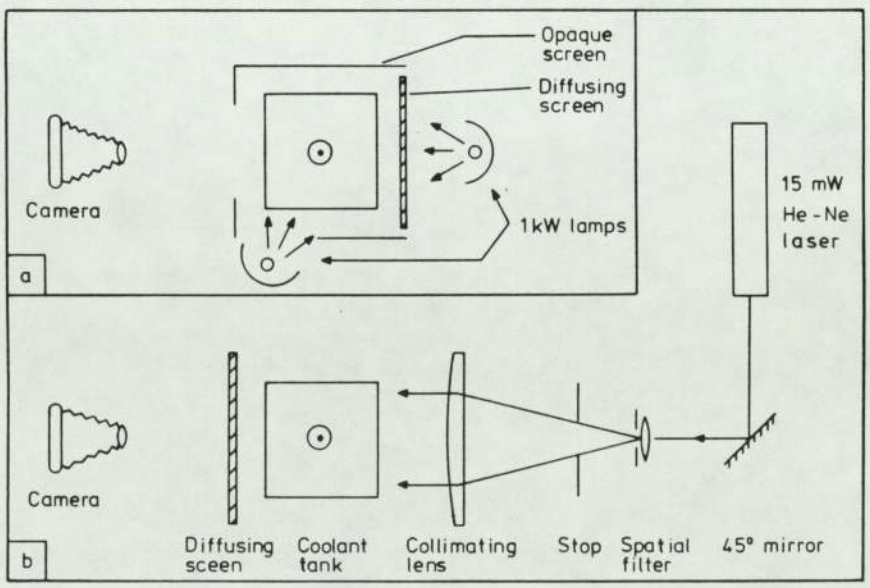

Fig 4.2.2 LIGHTING ARRANGEMENT FOR (a) WHITE DIFFUSE LIGHTING AND (b) LASER SHADOWGRAPHY

Diagnostics. Figure 4.2.1 contains a block diagram of the diagnostics, and lighting arrangements are shown in figure 4.2.2. For calibration purposes only, three chromel-alumonel thermocouples were included in the oven and these were monitored directly by a Comark 5000 ten channel cold junction compensated digital thermometer. The surface thermocouple leads were taken to cold junctions immersed in boiling isceon-12 at 243 K (-30 C) before amplification by factors of 100 or 200 by a purpose built ten input thermocouple amplifier. During quenching the output from this was recorded by a Datalab 901 transient recorder connected to a paper tape punch, oscilloscope and chart recorder. For calibration purposes the chart recorder only was used. Examples of temperature-time traces are shown later in chapter 7.

Some experiments were recorded on colour film using a 16 mm cine camera at 25 or 100 fps. Illumination from the rear was provided by a 1 kW lamp behind a diffusing screen with a second 1 kW lamp to give some oblique frontal illumination.

To record cine shadowgraphs, illumination was entirely from the rear from a 15 mW He-Ne laser. The laser beam was first expanded and spatially filtered by a X20 microscope objective and 25 micrometre pin-hole and then collimated by a 450 mm focal length 100 mm diameter plano-convex lens stopped down to give an 80 mm diamter beam. Shadowgraphs were projected on to one side of a frosted screen and filmed from the other.

Heating oven construction. The external dimensions of the heating oven were 45 mm diameter x 60 mm tall. It consisted essentially of two concentric ceramic tubes mounted between ceramic discs to form the top and base. A Kanthal heating element was wound on the inner ceramic

tube between the oven walls. Connecting wires to the heater entered the outer oven wall through two slots, one at the top of the oven and the other at the bottom. The oven assembly was supported by a 2.5 mm thick aluminium sheet.

The argon blanket gas was introduced directly into the oven through a ceramic tube in the top, and then allowed to escape into the main perspex container.

Oven temperatures of 1300 K were easily achieved with a 12 amp 40 volt current from the ac mains delivered via a variac transformer. This was taken as the practical limit of operation because Kanthal itself melts at about 1600 K.

Sphere construction and surface thermocouple calibration. Stages in the construction of the 30.3 g, 19.5 mm diameter stainless steel sphere assembly are shown in figure 4.2.3. The construction sequence on the right of the diagram only shows that part of the sphere near to the junction. A 1.5 mm diameter hole was drilled along a sphere diameter to within 0.5 mm of one surface (figure 4.2.3(a)). Penetration of the surface was completed by a 0.5 mm diameter drill along the same centre line. To support the sphere and insulate the thermocouple lead to the surface a 1.5 mm diameter ceramic tube with 0.8 mm bore was inserted into the larger hole leaving a 120 mm length protruding from one side. A 0.5 mm diameter chromel wire was then threaded through the ceramic tube to protrude about 1.5 mm above the steel surface, and electron beam welded into the surface leaving a small raised dimple of metal, figure 4.2.3(d), that was subsequently milled and polished. The final thermocouple junction was about 2 mm diameter and estimated at not more than 0.5 mm thick.

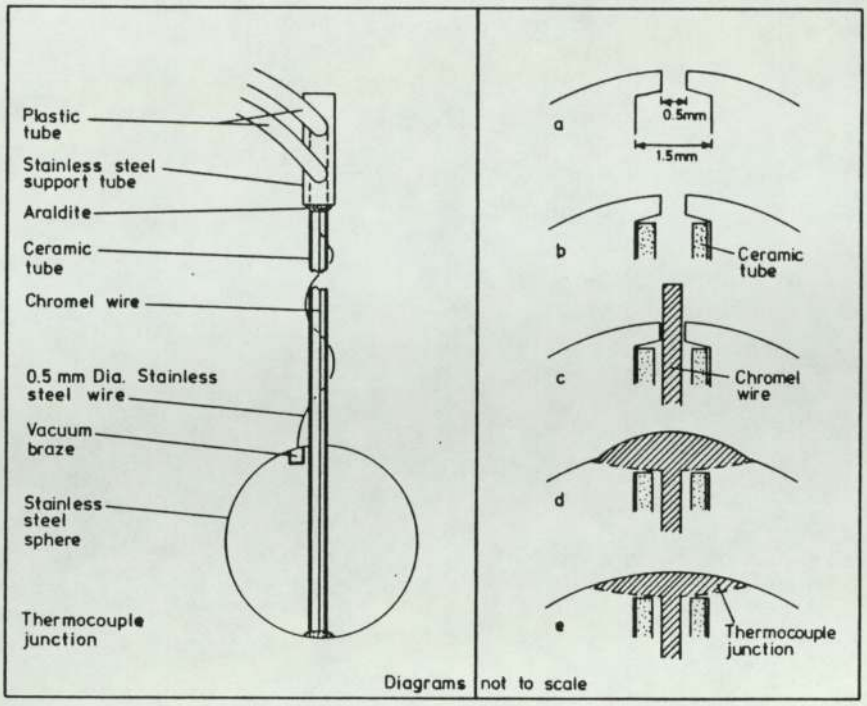

Fig 4.2.3 QUENCH SPHERE CONSTRUCTION

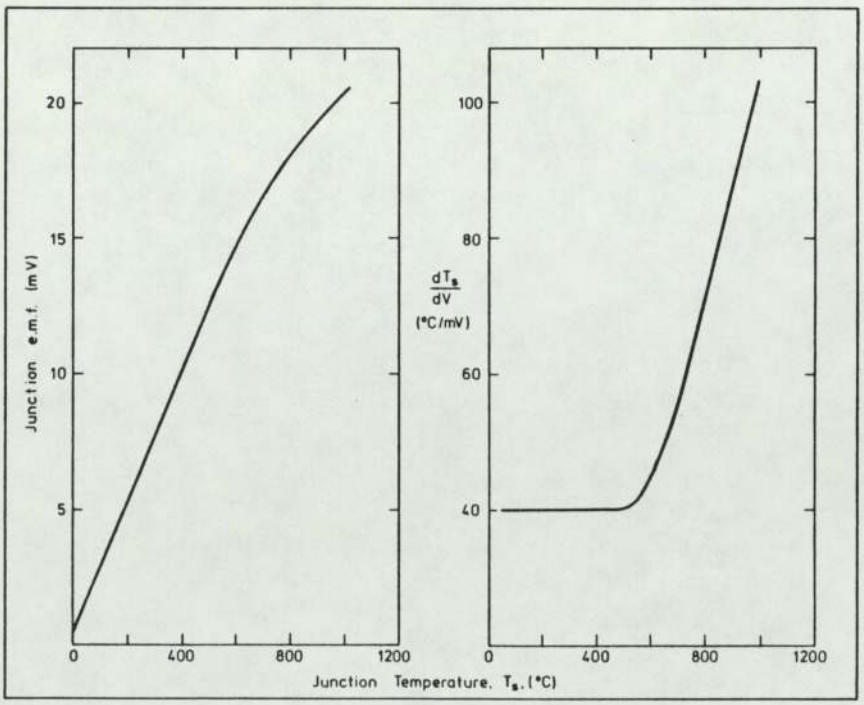

Fig 4.2.4 SURFACE THERMOCOUPLE CALIBRATION CURVES

Next a 0.5 mm diameter steel wire was vacuum brazed to the top surface of the sphere, in a well close to the ceramic support tube, and the wire coiled close to the support. The ceramic rod was then inserted into the stainless steel support tube and secured with Araldite epoxy resin, with the thermocouple leads leaving the side of the steel tube through plastic sleeving.

Uniform Temp.

Before any quenching experiments were performed the surface thermocouple was calibrated in the oven against the three small chromel-alumonel thermocouples placed against it. The test junction emf was amplified by a factor of about 200 and monitored by an Oxford 3000 pen recorder. The gain of the amplifier over the range 5 - 25 mV input was checked and the mean value found to be 198 $\pm$ 2.

The oven was purged for several minutes with about 2 litres per minute of argon gas before heating began. The current through the heater windings was fixed at some chosen value and the thermocouples monitored until the rate of change in temperature was less than 5 degrees in 15 minutes. The heater current was then altered and the procedure repeated several times to complete the calibration curve shown in figure 4.2.4. Calibration was checked several times during use. The rate of change of sphere surface temperature with time was determined by multiplying together the gradients of the recorded junction emf vs time curve and the reciprocal of the gradient of the calibration curve, ie:

$$\frac{dT_s}{dt} = \frac{dT_s}{d\bar{V}} \times \frac{d\bar{V}}{dt}$$

Contact between the chromel thermocouples and the metal sphere was ensured initially by measuring contact electrical resistance, but it was noted that after several hours, (the calibration procedure took over four hours), the contact resistance increased indicating surface contamination.

Experimental procedure. With the sphere in its lowered position its surface was carefully cleaned of any loose particles with soft tissue paper taking care not to touch the surface with bare fingers. The coolant container was then positioned below the sphere and raised to set the sphere above the tank centre and at the required depth. The sphere was then raised into the oven and the bottom closed. The tank was filled with distilled water, previously boiled for 5 minutes and allowed to cool to about 10 degrees above the final temperature required.

With the perspex container sealed, argon gas was fed to the oven at the rate of 2 litres per minute to purge, during which time the water continued to cool, until, within a few degrees of the required temperature the oven was heated to raise the sphere temperature to the required value. Heating time was typically 5 minutes.

The water temperature was then recorded, the heating current switched off, the oven door removed, the camera started and the sphere quenched.

Immediately following the experiment, the water final temperature was recorded together with the depth of the sphere top below the water surface and the position on the sphere surface at which the vapour film was observed to start its collapse. The recorded temperature-time trace was digitised, and plotted on the chart recorder, and the water

How? What use was made of this info.?

tank cleaned in preparation for the next experiment with freshly prepared water.

4.3 Bubble growth and collapse experiments

General description of experiment. The vapour bubbles were produced by a spark between two pointed under-water electrodes placed about 0.1 mm apart in a metal tank similar to that used for metal-water studies and as shown in figure 3.3.3. The tank was of aluminium 160 x 160 x 180 mm deep with perspex front and back and carried the replaceable spark electrodes which entered the metal walls through polythene insulating plugs. Electrodes were made by sharpening the ends of 2 mm diameter tungsten welding rods containing 1 per cent or 2 per cent of either zirconium or thorium. A 750 watt electrical heating element at the bottom of the tank was used to maintain water temperature.

The energy for the spark was provided by a 16 microfarad capacitor bank chargeable to 5 kV and switched on to the gap by a BK396 ignitron fired by a Harwell 7000 series trigger-delay unit. The latter was itself triggered remotely from the high speed camera switch in series with a 9 V dry cell. The closing of this switch, when the camera had reached operating speed, was also used to trigger simultaneously three transient digital recorders. The rise time of the trigger pulse was about 200 ns and the manufacturers specification dictates no more than 50 ns jitter on the transient recorders on reception of the trigger. Allowing for a full 9 V spread in the trigger voltage levels between the recorders, it was not possible for them to be more than about 200 ns out-of-step.

Experimental procedure. The electrodes were roughly positioned in the tank. Water from the laboratory still was then boiled in the tank for about 5 minutes to remove dissolved air and was allowed to cool to just above the required temperature before adjusting the electrode gap. The isolation cage was then closed on the tank, the capacitor bank charged and fired. Despite the provision of a gravity dump switch on the bank charging unit, the electrodes were grounded for safety with an earthing stick after each experiment. The electrode tips were re-ground after about five experiments.

Diagnostics. The block diagram of figure 4.3.1 illustrates the experimental arrangement and diagnostics. The rate of change of current through the spark was measured with a Rowgowski coil with a sensitivity of 180.5 kA/(ms)/V and the gap voltage was monitored by a Tektronix high voltage probe with an attenuation factor of 1000. The latter was determined by using the probe to measure a sine wave signal at the current frequency and of known voltage. Current and voltage signals were recorded by Datalab 905 transient analysers.

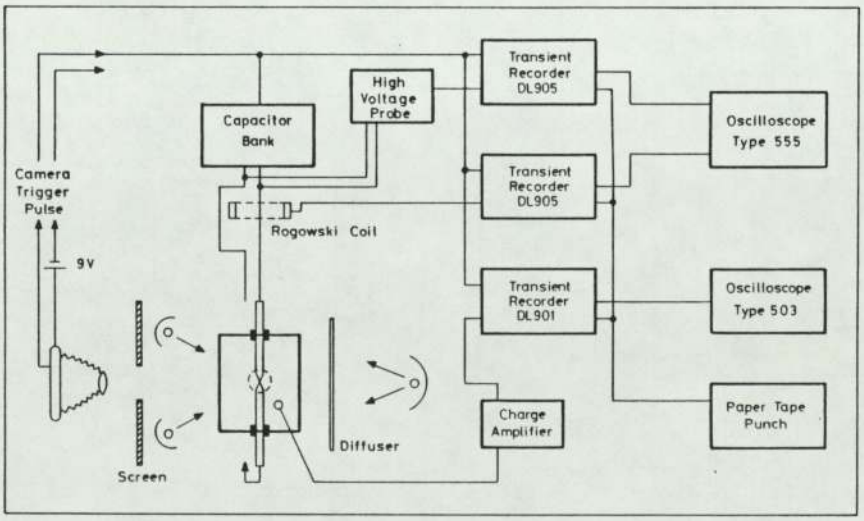

Fig 4.3.1 BLOCK DIAGRAM OF SPARK BUBBLE EXPERIMENTAL ARRANGEMENT

The pressure history in the water was recorded by a Kistler type 603B piezo-electric pressure transducer placed about 50 mm above the spark gap. The transducer signal was amplified by a Kistler 5001 charge amplifier and recorded by a Datalab 901 transient analyser. The transducer was housed in the cylindrical brass shielding tube shown in figure 3.3.3. A typical pressure record is shown later in chapter 7.

The analogue outputs from the transient recorders were displayed and photographed on oscilloscopes. The voltage and rate of change of current were monitored by a Tektronix type 555 dual beam oscilloscope and the pressure by a Tektronix type 503. Digital output was punched on 8-track paper tape using a Data Dynamics 1133 punch. Computer programs were written to process the tapes. Chapter 7 contains a typical set of computer generated curves.

The bubbles were photographed by the Hycam with high intensity diffuse rear lighting from the 3 x 1 kW tungsten-halogen strip lamps and some frontal illumination from two 750 watt lamps as illustrated in figure 4.3.1. The framing rate was generally about 7000 fps at f8. Timing marks were provided by the camera neon markers.

CHAPTER 5 EXPERIMENTAL RESULTS I:

VAPOUR EXPLOSION TEMPERATURE INTERACTION ZONES

5.1 Introduction

The most important single result from these experiments was the establishment of areas in "temperature space", called "temperature interaction zones", (TIZs), inside which interactions often occurred spontaneously as the metal fell through the water and before the container base was reached, but outside of which they were not observed to be triggered spontaneously. Inside the zones spontaneous interactions were not guaranteed, but outside them spontaneous interactions were not observed.

The TIZs are described in section 5.2 for the four main liquid pairs. The variation of violence with position in the TIZ is discussed in section 5.4. Dwell time measurements, which lend support to the vapour collapse triggering of these interactions in metal-water systems are given in section 5.6 while the other sections present the results of film analysis (5.5), to give some idea of interaction efficiency (5.7), debris analysis (5.3) and propogation experiments (5.8). Other systems are briefly discussed in section 5.9.

In any of the diagrams of the next three chapters a small number adjacent to an experimental point denotes the number of times the experiment was repeated with the same result.

5.2 Temperature interaction zones

The very broad classification of experiments into those which gave rise to a vapour explosion and those which did not has established the boundaries of the temperature interaction zones. Outside the zones no interaction occurred (NI). Inside the zones the samples were fragmented to an extent that depended on the initial hot phase and cold phase temperatures. For the alloys cerrobend and cerrotru, interacted debris was further subdivided into fragmentation interactions (FI) and explosive interactions (EI), based on the observed violence at the time of the experiment and on the form of the debris (see section 5.3). Isceon-water interactions were assessed subjectively on a five point classification as no interaction (NI), very mild (VM), mild (M), violent (V) and very violent (VV). The TIZs for each of the four primary systems studied are now considered separately.

Tin-water TIZ. Figure 5.2.1 shows the temperature interaction zone for 12 g tin drops falling through air into water. Experiments are included for drop heights up to 300 mm, coolant depths greater than 180 mm and tin masses from 10 g to 14 g. Within these ranges there is no evidence that varying these parameters effects the TIZ in any way. The zone is clearly defined in the figure where each experiment is marked by a cross or a circle to indicate repectively no interaction (zero PD) or an interaction (a few percent to 100 percent PD). Within the zone an interaction was not guaranteed but these have been left off the diagram for the sake of clarity. The important point is that spontaneously triggered interactions did not occur outside the zone.

The TIZ is characterised by essentially straight line boundaries which we can call for convenience the vertical, horizontal and sloping

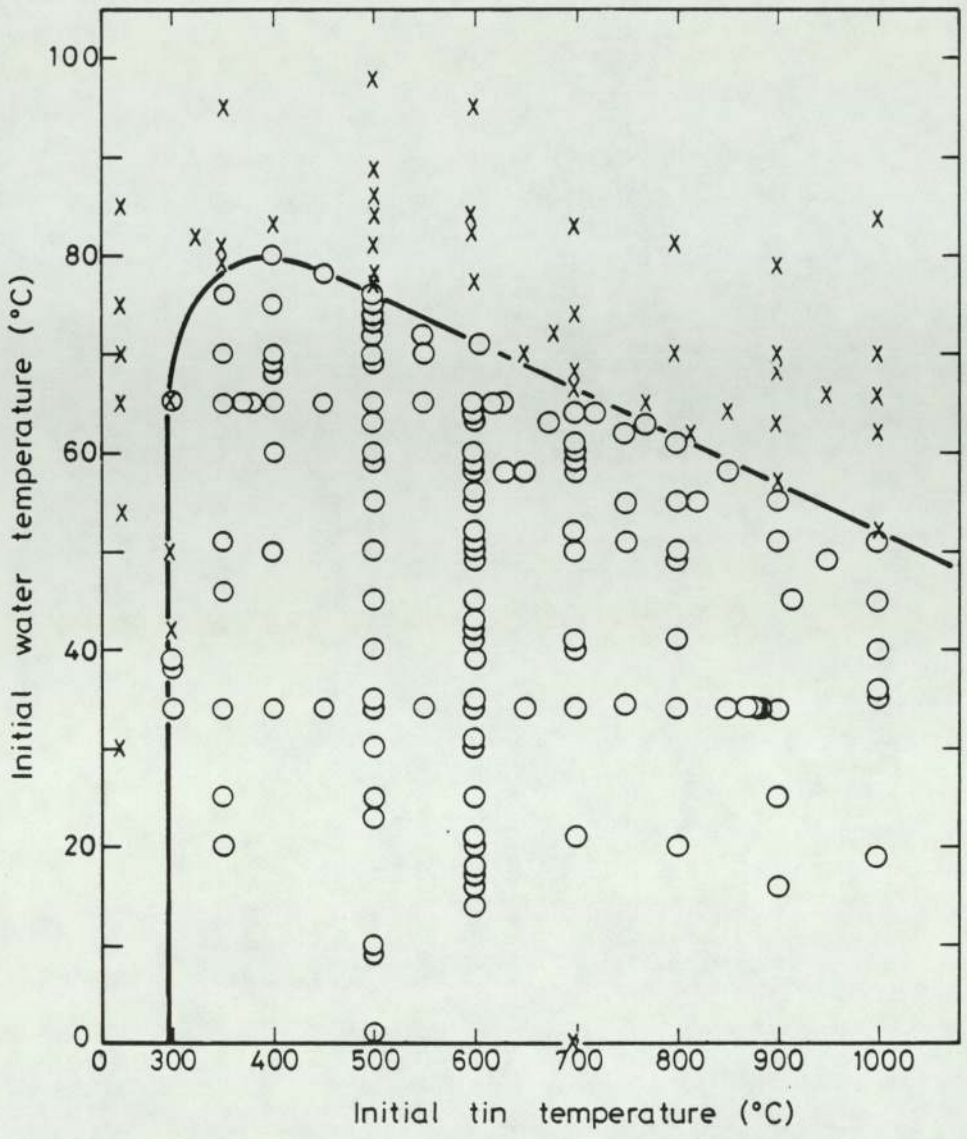

Fig 5.2.1 TIN-WATER TEMPERATURE INTERACTION ZONE

boundaries. One experiment with tin at 973 K (700 C) falling onto ice at 273 K failed to produce an interaction. The metal broke up on contact and solidified. An experiment at 773 K (500 C) however, with coolant at 275 K, produced an interaction. No other experiments were performed with T_c less than 283 K (10 C). The horizontal boundary has, therefore, been taken to be given by the coolant melting point. The vertical and sloping boundaries are not so easily explained. It is not

possible to say whether the sloping boundary can be extrapolated linearly to form a closed triangular region since tin temperatures could not be raised further with the existing apparatus. At any fixed value of tin temperature the sloping boundary gave a value for the coolant cut-off temperature which will be called the normal cut-off temperature, T_{nco}, and which was given by the empirical equation:

$$(T_h - T_{sat}) = \left(19T_{sat} - 20T_{nco}\right) \approx 20(T_{sat} - T_{nco})$$

Why this form of equn?

The suppression of base triggered interactions. Only those interactions which have taken place during the fall of the metal through the water are plotted in figure 5.2.1. Detailed discussion of the influence of the base in suppressing spontaneous triggering is postponed for consideration in section 6.4, but it was found that with a flat-bottomed coolant tank interactions occurred occasionally at coolant or fuel temperatures outside the sloping boundary and several seconds after initial contact of the liquids, a very much longer time than normally associated with spontaneous triggering. 12g tin drops falling into water at terminal velocity are marginally stable against Weber instability and split into several smaller drops on impact with the base. It was noticed that the long dwell time interactions occurred when these small droplets ran together at the sides or corners of the coolant tank and coalesced.

Initially it was thought that coalescence entrapped coolant within the metal leading to superheating and its subsequent rapid vaporisation. With a flat bottomed tank there was no guarantee that coalescence would always occur. It was encouraged by putting a false shallow conical shaped base into the tank (apex angle about 178 degrees) which ensured

that drops ran together at the base centre. About 20 experiments were then repeated outside the sloping boundary. Surprisingly, no interactions were observed, and the base was used in subsequent experiments with no further interactions beyond the sloping boundary.

It would appear from these results that base triggering is not caused by coalescence but is the result of trapping coolant between the molten tin and the container base and walls. Furthermore, the sharp geometry of the tank edges and corners was required in order to trigger in this way. In some large-scale experiments, (eg copper-water [39]), interaction is achieved by base triggering but, in the present experiments, it was a rare occurrence.

Cerrobend-water TIZ. Only a few results (about 40) with cerrobend and water were obtained. Because of the toxicity hazard associated with the cadmium content of this alloy the experiments were terminated in favour of the safer alloy cerrotru. Enough results were obtained, however, to indicate that a TIZ exists, with the left hand vertical boundary at a somewhat higher temperature than that for tin and water. The results are shown in figure 5.2.2 where the "standard" tin-water TIZ is superimposed for reference. Again, no interaction is marked by a cross, while fragmentation and violent interactions are marked by open circles and triangles respectively.

The position of the cerrobend sloping boundary has not been established but is apparently higher than that for tin, although we cannot be sure that those interactions with cerrobend above the sloping boundary of the tin system were not base triggered. The shaped base used in previous experiments to eliminate base triggering in the corners and edges of the coolant tank was not used in these experiments. The

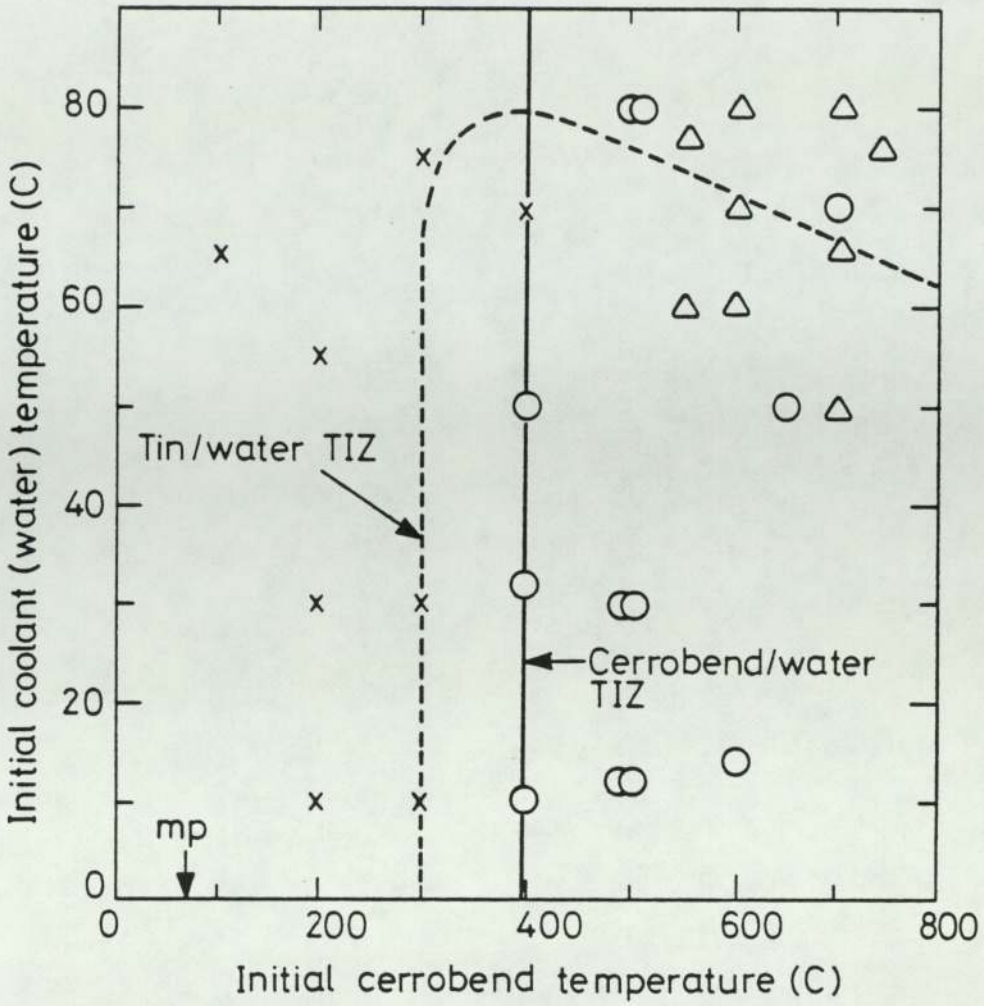

Fig 5.2.2 CERROBEND-WATER TEMPERATURE INTERACTION ZONE

cerrotru results below, however, suggest that they may be genuine spontaneous triggering.

Cerrotru-water TIZ. About 100 experiments have been performed in which 20 g samples of cerrotru were dropped through 30 mm of air into water 180 mm deep using the shaped base. Once again a well defined TIZ exists with straight line boundaries (see figure 5.2.3). As for cerrobend the sloping boundary is a little higher than that of the tin-water TIZ over the range of metal temperatures considered, though its slightly increased slope suggests on the basis of linear

extrapolation that it will fall beneath the tin boundary for temperatures above 1473 K (1200 C).

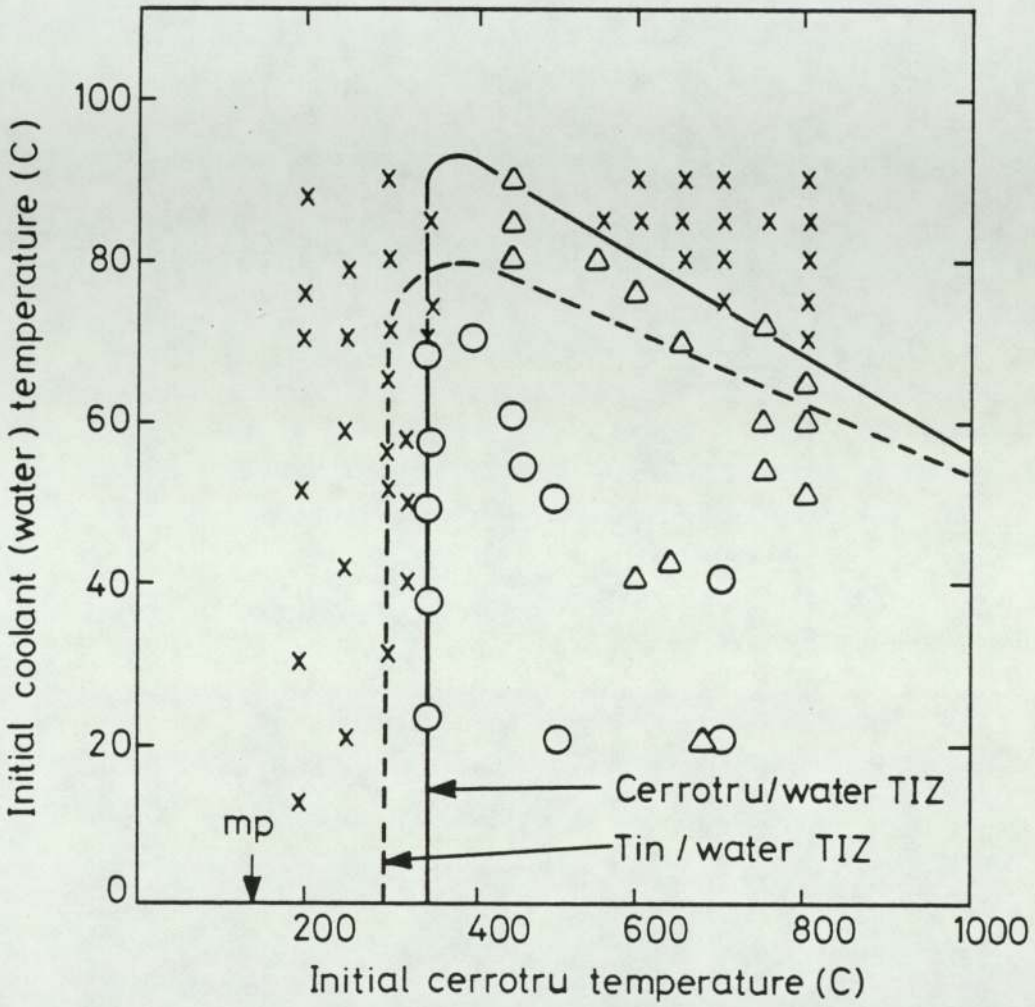

Fig 5.2.3 CERROTRU-WATER TEMPERATURE INTERACTION ZONE

Isceon-water TIZ. Figure 5.2.4 presents the results of about 500 experiments in which 10 cm^3 samples of isceon-12 were dropped into 500 cm^3 water, plotted in the usual way. Nearly all the experimental points were repeated once or more, those non-interacting combinations near the zone boundaries being repeated about five times. As with the

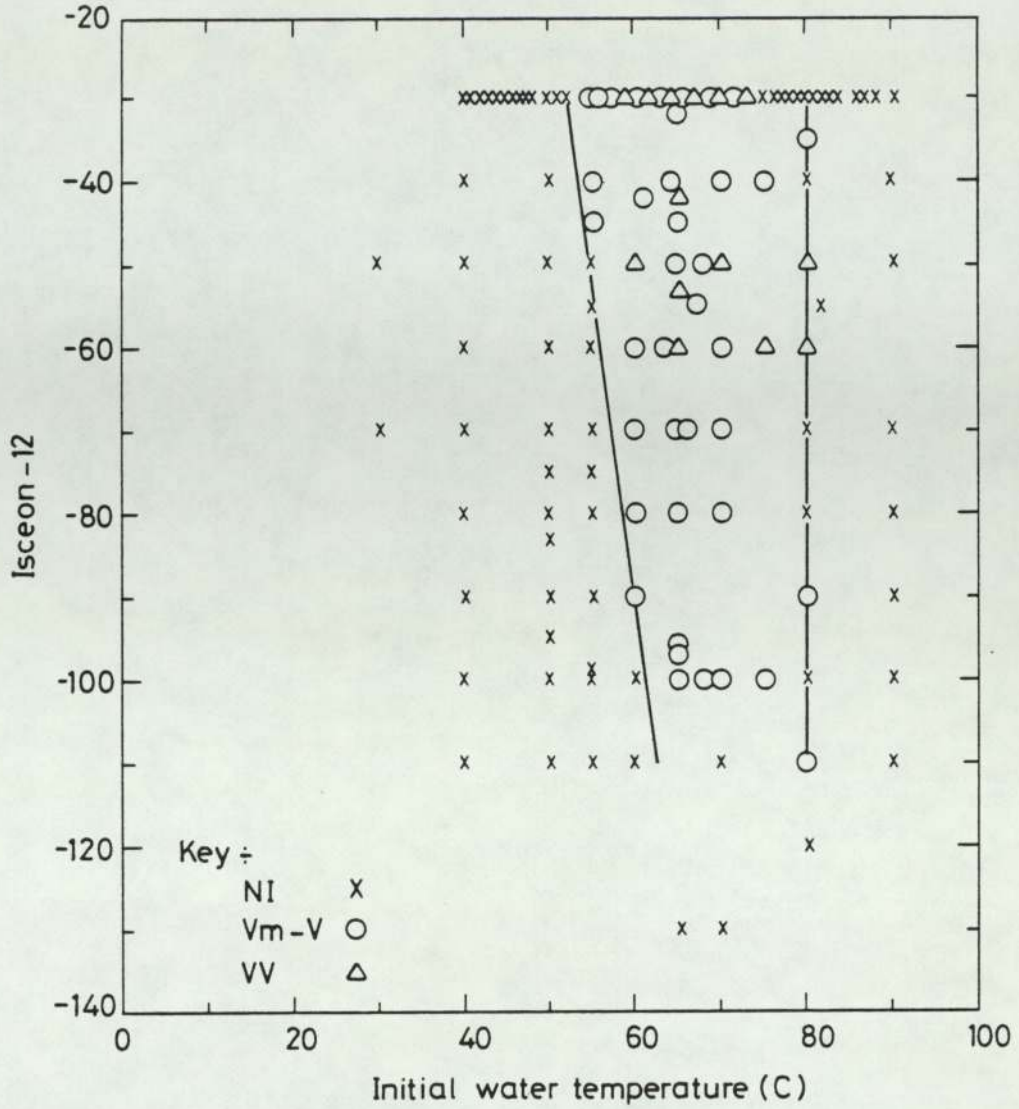

Fig 5.2.4 ISCEON-WATER TEMPERATURE INTERACTION ZONE

metal water system there is a well defined TIZ with straight line boundaries and a finite probability of no interaction within the zone. The latter have been omitted for clarity. Insufficient experiments were conducted with isceon temperatures below 163 K (-110 C) for the boundaries to be projected beyond this point. There was just one occasion when a very mild interaction occurred outside the zone, at T_h = 313 K (40 C), T_c = 243 K (-30 C). Many attempts to repeat it have failed and the result was therefore treated as, for some reason,

anomalous and not included in figure 5.2.4. It was the only anomaly in the 500 experiments.

5.3 Debris examination

The two broad categories of fragmented and non-fragmented debris outlined in section 3.3 were capable of further subdivision into several debris types. For clarity each of the systems studied is again described separately.

Tin-water system. The debris has been classified roughly in accordance with position within the TIZ. Non-fragmented debris occurred in two forms. At low tin temperatures, to the left of the TIZ vertical boundary, the metal solidified during fall through the water into a single solid lump of non-interacted tin. An example of this is shown in figure 5.3.1(a).

Partially interacted samples within the TIZ gave rise to the second form of non-interacted debris as shown in figure 5.3.1(c). The non-fragmented portion of these samples was in the form of thin twisted sheets of metal about 0.1 mm thick. This type of debris was found just inside the vertical TIZ boundary and was therefore always accompanied by a finely fragmented portion, albeit only a few percent when very close to this boundary.

For constant coolant temperature (ie on a given horizontal line in the TIZ) the fraction of the finely fragmented portion of the tin samples increased with increasing metal temperature. Finely fragmented debris was in the form of small sub-millimetre particles ranging in diameter from a few micrometres upwards. It ocurred basically in three forms.

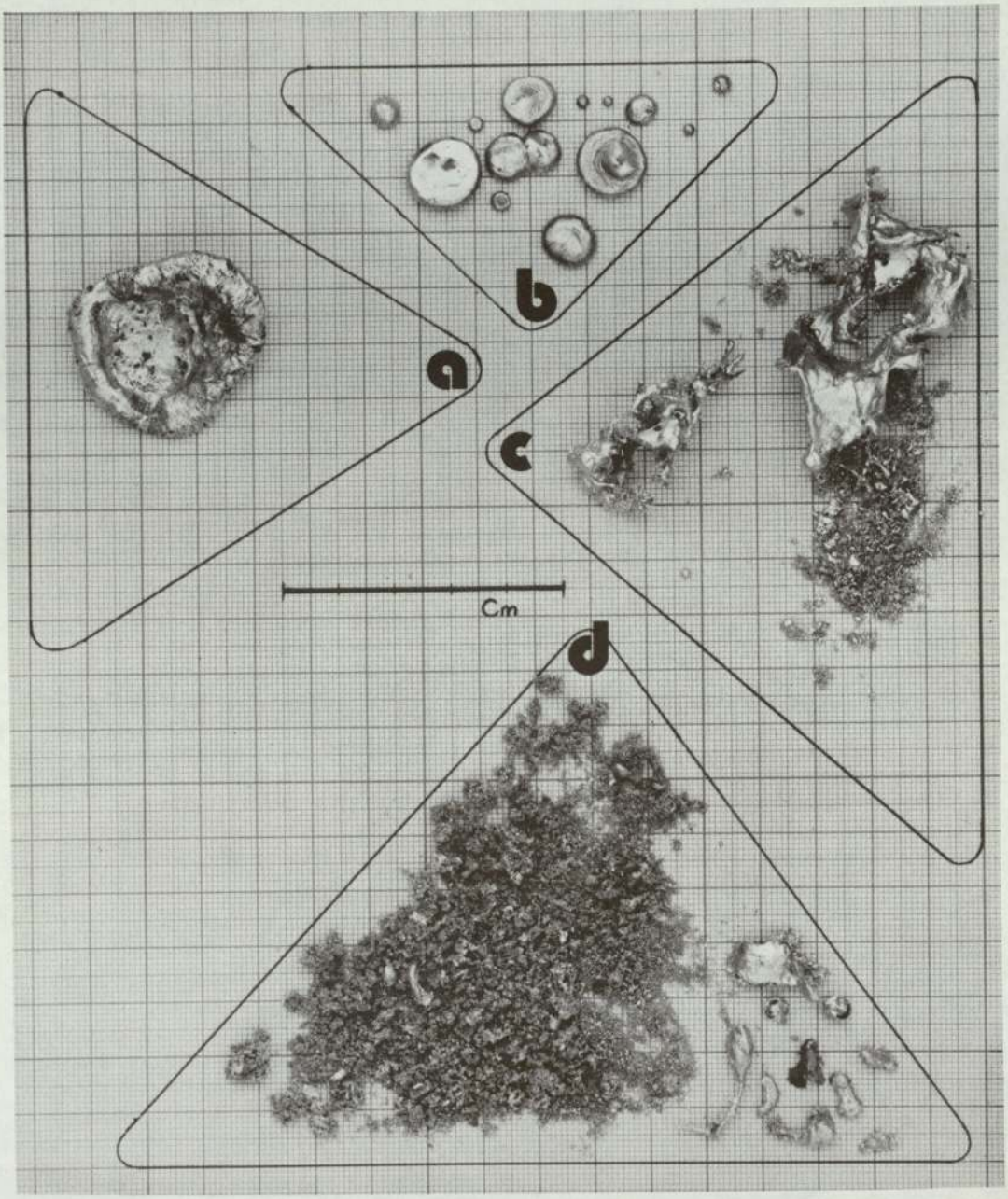

Fig 5.3.1 SELECTION OF TIN DEBRIS

Left of centre of the TIZ lumps of an inflexible "coke-like" debris was frozen and joined by interlocking filaments or stems of tin into a tangled mass with an overall "cauliflower" appearance. With increasing temperature this changed. Near the centre and right of centre, separation of the particles was still incomplete for most of the sample and solidification resulted in clumps of spongy, porous debris, which was flexible and easily broken down between the fingers. Such a sample is shown in figure 5.3.1(d).

The spongy debris was mixed with very fine completely separated (powdered) tin roughly spherical. The fraction of powdered debris increased towards the sloping boundary of the TIZ and the spongy material occurred in smaller clumps, with no completely solid lumps (ie coarsely fragmented debris) or stems of metal.

Finally, for any combination of tin and water temperature outside the sloping boundary, the metal broke into several smaller lumps either close to or on impact with the base to provide stable drop sizes compatible with the Weber number criterion. The example of figure 5.3.1(b) shows in addition some very small drops characteristic of the tiny Plateau spherules formed from the filament between two separating, larger, drops. Such coarsely fragmented debris was molten on contact with the base. The drops had one flat side which often contained pits and crevices indicating that water had been trapped between the drops and the base. Further evidence for trapping was given by some samples in which vapour had clearly forced its way from beneath the drop up through the surface and also from the ease with which drops outside the sloping boundary could skate over the base, presumably because of vapour generation beneath them.

The samples shown in figure 5.3.1 taken in the order (a), (c), (d), (b) are in order of increasing fragmentation such as would be observed in crossing the TIZ from some point outside the left hand boundary to a point outside the sloping boundary. The transition from no interaction to a few percent PD is clearly shown by samples (a) and (c), as is that from very high PD to zero PD at the sloping boundary (samples(d) and (b)). The latter corresponds to exceeding the sharp cut-off temperature reported by other workers (see section 2.2). It should be borne in mind that the foregoing description, and that which follows for the alloys, is a very broad characterisation of the main debris features and that there is no sharp change in debris type inside the TIZ such as was observed at the zone boundaries.

Cerrobend-water system. As for tin, non-interacted debris, (on the basis of which the position of the TIZ boundary was determined), could be unambiguously identified. There was no finely fragmented portion and the debris was either coarsely fragmented and consisted of large irregularly shaped lumps,or non-fragmented and in the form of flat plates. Only in a few samples, at very low cerrobend temperatures was the plate debris as thin or as twisted as the tin plate debris described earlier. Normally it was flatter, thicker (about 1 mm) and of irregular shape. The flatness was probably a consequence of the lower melting point of the cerrobend which ensured that the coarse or non-fragmented cerrobend was always molten on reaching the container base, so that however twisted the sample may have become in falling, it could flatten to a greater or lesser extent on reaching the base, depending on initial temperatures.

Fragmentation interactions were not violent. There was no loud bang, but some finely fragmented debris was produced. The remainder was

either in coarsely fragmented or non-fragmented form.

At the higher alloy and water temperatures explosive interactions were accompanied by a loud report, were clearly violent and produced very finely fragmented debris. Only a small quantity of these samples remained coarsely fragmented, if any. The finely fragmented portion was in the form of very small, nearly spherical drops with a size distribution ranging from micrometres (powder) up to 2 mm diameter, as in tin. Because of the lower melting point of cerrobend there was evidently sufficient time for complete separation of the particles before freezing which was, however, fast enough to prevent coalescence of the drops on reaching the tank base. "Coke" and "sponge" type debris was not produced.

The classification set out above was based on the experiments with water temperatures less than the melting point of cerrobend (343 K, 70 C). Above this, except for finely fragmented debris, debris could coalesce before solidifying on the container base.

It was noted that at all cerrobend temperatures the surface of coarsely fragmented debris was very shiny for water temperatures below 303 K (30 C), but above this temperature, where heat transfer rates were lower, the metal was dull with a crystalline surface (fibrous when viewed under a microscope) associated with crystallisation of the cadmium in the alloy.

Cerrotru-water system. Outside the cerrotru-water TIZ debris was very similar to that for tin and water, except that above the sloping boundary the coarsely fragmented drops were smaller than for tin. Just inside the left-hand boundary fragmentation interactions similar to

cerrobend occurred. At the higher alloy temperatures explosive interactions produced two types of finely fragmented debris. Water temperatures below 320 K (47 C) gave a spongy tin-like debris, while above 320 K, where cooling was slower, the debris was composed of fine spherical particles similar to that from cerrobend.

Measured particle size distributions. Traditionally particle size distributions have been obtained by taking the mass of debris below a particular size, expressing it as a percentage of the total mass of recovered debris and plotting this percentage against the particle diameter. 54 samples of tin debris were sieved and size distributions expressed in this way are shown for three of these samples in figure 5.3.2, together with one distribution curve for a cerrobend sample. The size distributions appear quite different and strongly dependent in some way on the initial tin and water temperatures.

In these experiments all of the initial tin sample was recovered and the total sample, therefore, could contain non-fragmented debris, coarsely fragmented debris (which could have been produced by drop break-up under inertial forces) and the very fine debris produced by vapour explosion. The size distributions in figure 5.3.2 are therefore not representative of those for debris produced by the vapour explosion alone, the difference being particularly significant for low PD events.

Before. How do we know this is due to VE?

It was decided, therefore, to determine the particle size distributions in the finely fragmented portion of each sample. Defining this portion in terms of the Weber stability criterion, however, did not produce a significantly better correlation. The stable drop diameter in the experiments was about 5 mm but break-up into particles of this size was accompanied by the production of as many smaller drops which formed

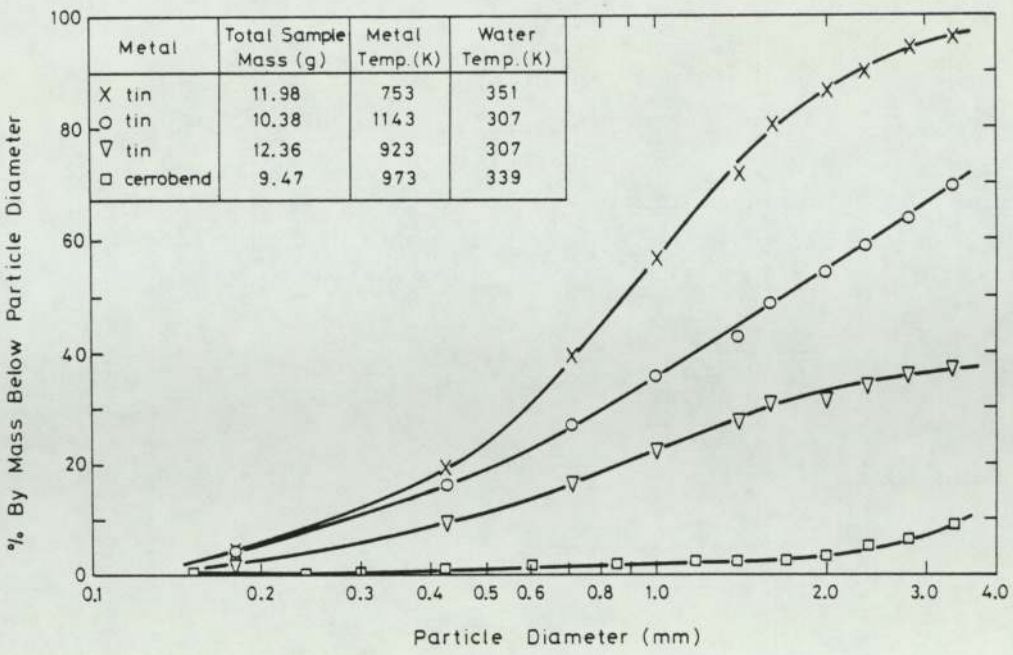

Fig 5.3.2 PARTICLE SIZE DISTRIBUTIONS IN SELECTED METAL SAMPLES

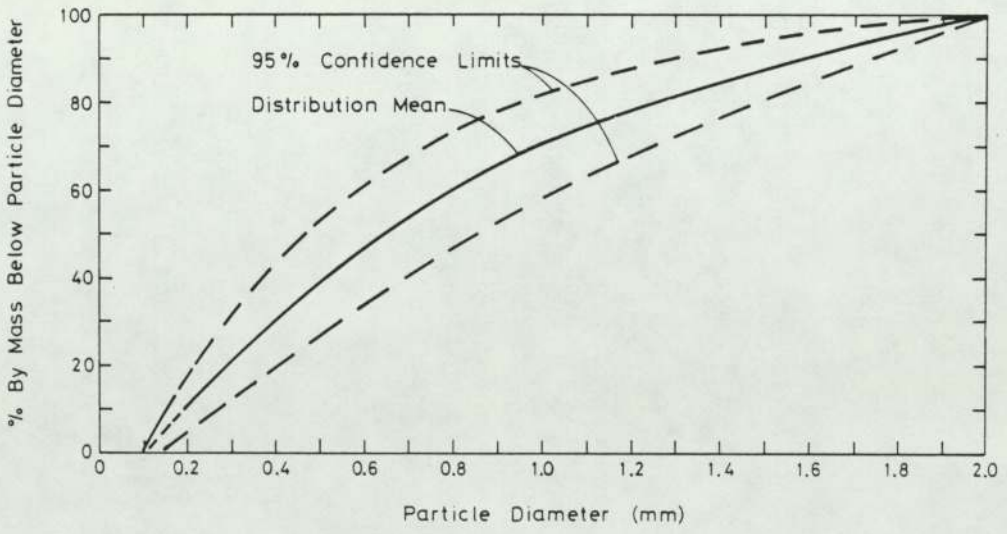

Fig 5.3.3 PARTICLE SIZE DISTRIBUTIONS IN THE FINELY FRAGMENTED PORTIONS OF 54 TIN SAMPLES

from the neck or filament between two separating larger drops. Examination of many non-interacted tin samples showed such small drops to be no less than 2 mm in diameter (see figure 5.3.1(b)). Only debris below 2 mm can, therefore, be confidently ascribed to result from a vapour explosion. The rather subjective measurement of percentage disintegration (PDA) used previously was, therefore, replaced by the more precise definition:

$$PD = \frac{\text{mass of debris below 2 mm}}{\text{total sample mass}}$$

which then gives a lower limit to the fraction of total sample mass that was involved in a particular interaction.

The particle size distributions of figure 5.3.2 were, therefore, re-plotted, together with those of 50 other tin samples, and are represented by the mean curve shown in figure 5.3.3 where the percentage by mass below a given particle diameter is now the percentage, not of the total sample mass, but of the mass of the finely fragmented portion of the sample (ie below 2 mm). The three tin samples of figure 5.3.2 fall exactly on the mean curve of figure 5.3.3. Statistical data for figure 5.3.3 are given in table 5.1 and the parameter ranges covered by the experiments in table 5.2. The dotted envelope represents the 95 percent confidence limits assuming a normal distribution about the mean. Clearly the spread in distributions is much reduced compared with those exemplified by figure 5.3.2 and, while showing statistical scatter, the distributions of figure 5.3.3 are essentially independent of the parameter ranges listed in the table.

Table 5.1 Data for particle size distributions in 54 tin samples

Mass of sample (g)	PD	Mass of fine debris (g)	Percentage mass below sieve size						
			0.18	0.425	0.71	1.0	1.4	1.7	2.0
11.95	36.9	4.41	4.8	23.1	45.4	64.6	76.6	89.3	100.0
10.29	51.6	5.31	18.8	32.4	52.4	67.0	80.8	89.8	100.0
11.59	82.1	9.51	7.9	33.4	56.0	73.5	86.9	91.8	100.0
11.98	86.6	10.37	4.9	22.3	45.7	65.5	82.9	92.5	100.0
11.80	76.9	9.08	7.5	31.3	53.3	70.9	86.3	94.2	100.0
11.52	81.0	9.33	9.9	36.5	58.7	76.1	89.0	94.4	100.0
11.54	81.7	9.43	8.4	35.4	57.9	73.8	86.9	93.5	100.0
11.51	84.4	9.71	9.6	40.5	64.8	80.5	91.5	96.5	100.0
11.1	38.8	4.31	3.5	16.0	34.6	55.0	75.9	88.6	100.0
11.11	43.7	4.86	2.5	14.0	35.4	54.9	76.5	90.1	100.0
10.41	74.4	7.74	7.1	32.2	55.8	74.5	88.8	95.5	100.0
11.31	90.8	10.27	7.0	31.9	58.8	77.6	90.9	94.6	100.0
11.68	61.9	7.23	9.1	32.4	50.8	66.3	81.5	91.0	100.0
11.6	79.2	9.19	11.0	41.1	62.7	77.8	89.3	96.6	100.0
11.46	83.7	9.59	6.9	36.2	59.2	74.1	87.6	94.5	100.0
11.96	82.7	9.89	11.8	46.5	70.6	83.4	92.6	96.6	100.0
11.36	37.1	4.22	11.4	34.6	53.6	68.2	81.5	92.9	100.0
11.35	43.6	4.95	12.9	37.6	55.8	70.7	82.0	93.9	100.0
10.34	56.7	5.86	11.4	40.6	60.9	75.6	87.5	94.0	100.0
12.23	78.3	9.57	11.3	39.9	61.3	75.8	87.8	95.1	100.0
11.84	95.9	11.36	10.4	41.1	66.9	83.7	93.7	98.1	100.0
11.95	88.4	10.56	7.9	31.3	53.9	71.1	86.2	95.0	100.0
11.78	40.8	4.8	8.5	30.4	49.6	67.3	83.8	92.9	100.0
11.82	43.6	5.15	13.1	38.3	56.9	69.5	84.3	93.2	100.0
11.84	56.7	6.71	10.9	40.2	62.4	79.0	89.7	94.3	100.0
11.53	92.6	10.68	11.0	44.6	68.4	83.9	94.0	97.8	100.0
11.88	89.1	10.59	10.0	39.2	61.7	77.8	88.2	94.5	100.0
10.34	54.5	5.64	16.1	42.2	60.1	73.4	86.0	92.7	100.0
11.63	29.3	3.41	11.1	32.6	51.0	67.7	83.0	91.9	100.0
11.5	39.4	4.53	12.1	36.6	55.0	69.5	83.2	92.7	100.0
11.58	55.4	6.42	10.1	34.7	53.4	67.9	80.5	90.7	100.0
11.76	43.5	5.12	13.5	37.3	56.4	70.3	84.4	93.4	100.0
11.12	34.0	3.78	10.6	33.3	52.1	67.7	81.7	91.5	100.0
10.88	58.3	6.34	8.0	31.9	52.8	69.4	85.8	94.3	100.0
9.17	71.4	6.55	9.8	38.9	61.5	75.9	87.8	95.6	100.0
10.38	54.1	5.62	8.2	29.9	49.8	65.5	79.0	89.9	100.0
10.78	47.7	5.14	7.4	30.9	50.0	65.4	82.9	90.9	100.0
10.9	40.8	4.45	6.5	31.7	52.4	67.6	82.5	91.2	100.0
9.68	40.6	3.93	6.1	28.5	48.6	65.4	81.4	91.6	100.0
11.51	35.8	4.12	5.6	28.6	50.2	66.0	79.6	90.3	100.0
11.02	68.0	7.49	8.1	41.1	54.1	70.8	83.6	91.9	100.0
12.11	64.0	7.75	7.1	29.4	50.3	67.0	83.7	92.1	100.0
10.38	39.2	4.07	9.3	36.6	54.1	67.8	80.8	89.4	100.0
9.72	52.6	5.14	10.7	33.5	50.4	65.8	80.0	90.5	100.0
10.78	33.9	3.65	5.8	28.2	47.9	63.0	79.5	88.2	100.0
11.05	58.3	6.44	6.5	32.3	55.1	70.7	85.1	93.8	100.0
12.36	32.4	4.01	6.3	28.8	49.3	67.1	82.9	94.0	100.0
12.09	62.9	7.6	9.5	35.7	57.2	72.7	87.6	93.4	100.0
10.58	74.0	7.83	7.3	32.2	55.3	74.1	88.5	95.9	100.0
10.52	71.3	7.5	4.9	26.4	47.9	65.2	82.3	91.5	100.0
10.97	55.8	6.12	3.3	21.4	42.8	60.1	78.3	90.8	100.0
9.81	73.2	7.18	10.0	38.6	59.7	74.9	86.6	95.2	100.0
10.85	64.2	6.97	8.5	35.7	57.2	72.6	87.9	95.5	100.0
mean			8.95	33.69	54.61	70.69	84.74	93.05	
standard deviation			3.06	6.50	7.02	6.20	4.33	2.34	
95 percent conf. limits			6.00	12.74	13.76	12.15	8.49	4.59	
99 percent conf. limits			7.89	16.27	18.11	16.00	11.17	6.04	

Also falling within the 95 percent limits shown, are the distributions for two 9.5 g cerrobend samples for which the PDs were 3 percent and 77 percent, one 44 g base triggered tin sample for which the PD was 70 percent, and ten cerrotru samples covering the parameter ranges also shown in table 5.2.

Table 5.2 Parameter ranges covered by sieved debris

	tin-water	cerrotru-water
metal temperature	632 - 1173 K (350 - 900 C)	633 - 1073 K (350 - 800 C)
water temperature	287 - 363 K (14 - 90 C)	293 - 363 K (20 - 90 C)
total sample mass (g)	9.72 - 12.36	9.5 - 20.7
percentage disintegration	29.3 - 95.9	1.3 - 91.1

5.4 Variation of interaction violence within TIZs

We now turn to the way in which interaction violence varied within the TIZ. The rate of energy release in vapour explosions will be proportional in some way to the factor by which the sample surface area is enhanced and to the size of the fragmented portion. It was shown above that the particle size distribution of the finely fragmented portion in metal water interactions was independent of the position within the TIZ although the fraction of the sample fragmented varied considerably. For a given sample mass it was reasonable, therefore, to take this size, as given by the PD, itself to be a measure of the rate of energy release and hence the interaction violence. Further justification for the use of PD as a measure of violence is given by

the correlation between PDA and the peak pressures observed at a fixed tin temperature of 873 K, shown in figure 5.4.1. A given PDA is an indication, not of the actual interaction pressure in a particular experiment, but of the maximum possible interaction pressure.

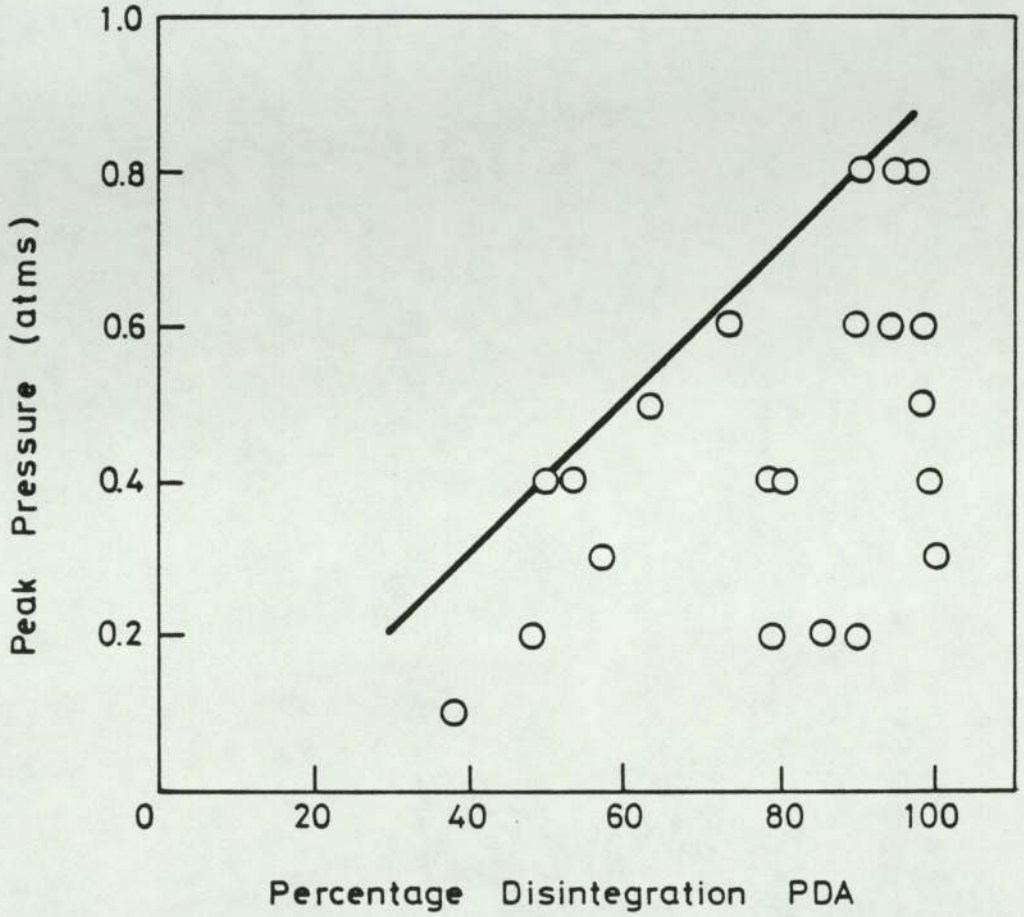

Fig 5.4.1 PEAK INTERACTION PRESSURES AS A FUNCTION OF PD

Temperature interaction zones may then be scanned vertically and horizontally to determine the variation of PD with water and metal temperatures respectively. Such scans are shown in figures 5.4.2 and 5.4.3 where PD was based on a 2 mm sieve.

In figure 5.4.2 PD is plotted against initial tin temperature for water at 338 K (65 C). The position of the left-hand vertical boundary and

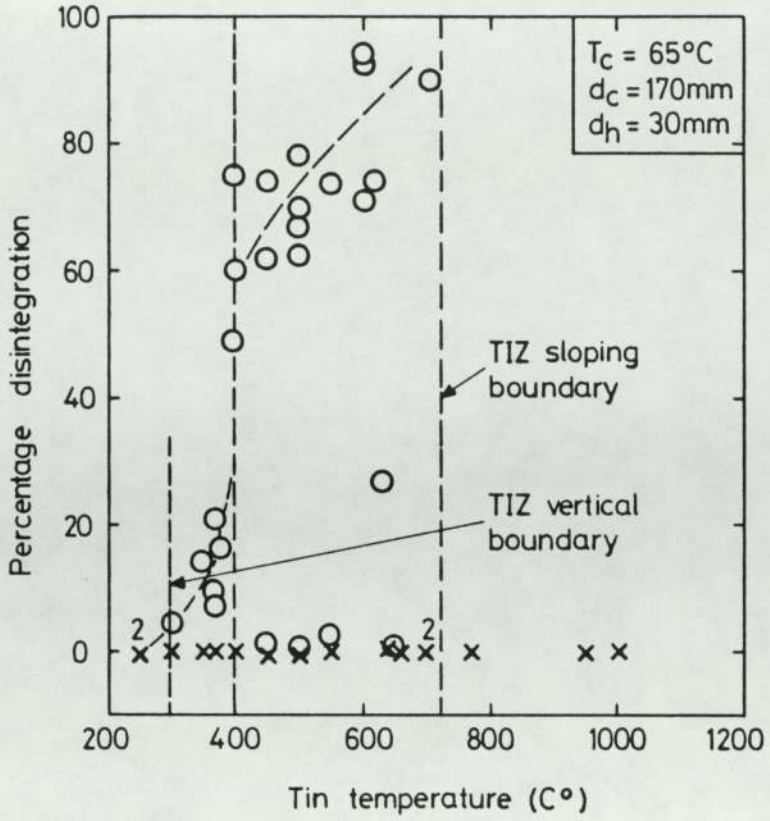

Fig 5.4.2 VARIATION OF TIN PD WITH TIN TEMPERATURE

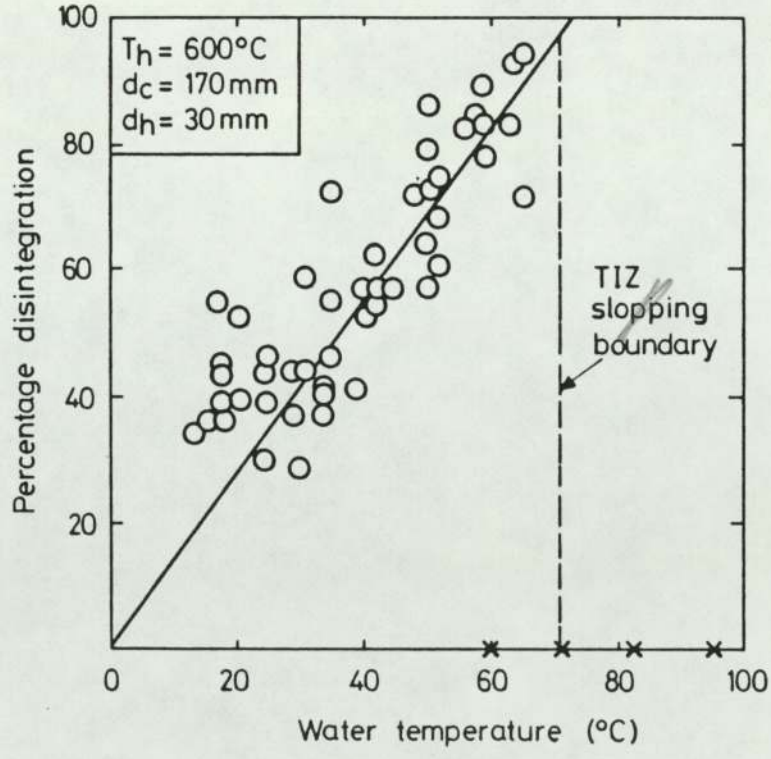

Fig 5.4.3 VARIATION OF TIN PD WITH WATER TEMPERATURE

of the sloping boundary of the 12 g TIZ are shown as dotted vertical lines. Within these boundaries the PDs increased from a very low value at low tin temperature to approach 100 percent near the sloping boundary. There was a sharp step increase at 673 K (400 C) where PDs increased suddenly from 20 percent to 50 percent, a feature shown by scans at other fixed water temperatures, although it occurred at higher tin temperatures as T_c was decreased.

A scan at a fixed tin temperature of 873 K (600 C) is shown in figure 5.4.3. PDs again increased as the sloping boundary was approached and were scattered fairly closely about a linear mean.

It was a general feature of PD plots that just below the cut-off temperatures (the point at which the scan cuts the sloping boundary) interactions occur with high PD or not at all.

Cerrobend and cerrotru interactions with water also exhibited an increase in violence as their TIZs were traversed towards the sloping boundaries. It is tempting and may be justifiable to equate the change from fragmentation to explosive interactions in these systems with that marking the step change in PD on the tin-water TIZ. Certainly tin interactions with PDs less than 20 percent could not by any stretch of the imagination be called explosive.

From the isceon-water interactions two points should be noticed in figure 5.2.4. First, interactions were observed for coolant temperatures up to the coolant saturation temperature, and were in fact at their most violent at T_{sat}. Second, the violence of interactions was again a function of position in the TIZ, this time not strongly dependent on the hot phase temperature (water), but more dependent on

coolant temperature. No very violent events were observed for T_c < 213 K (-60 C) and no violent events below 203 K (-70 C). These points are further illustrated by figures 5.4.4 and 5.4.5.

Figure 5.4.4 shows a scan across the TIZ at a fixed coolant temperature (T_{sat}) and illustrates quite clearly:

(i) the upper and lower water cut-off temperatures where the TIZ boundaries are crossed, and

(ii) the high probability, about 1 in 2, of no interaction occurring inside the zone.

A scan at constant water temperature (338 K, 65 C) is shown in figure 5.4.5 which shows the dependence of violence on coolant temperature. The most violent interactions occurred near $T_c = T_{sat}$ and fell off in violence as subcooling was increased. There is an indication that interactions cut-off at or below T_c = 173 K (-100 C) but further experiments would be required before the position of this boundary could be considered to be firmly established.

5.5 Film analysis

A typical film sequence, up to the point of triggering, for a 12 g tin sample dropped through 30 mm into water is illustrated by the line drawing of figure 5.5.1 which was traced from a projected film.

After entering the water the molten metal drop altered shape, particularly at the front which flattened under the the influence of

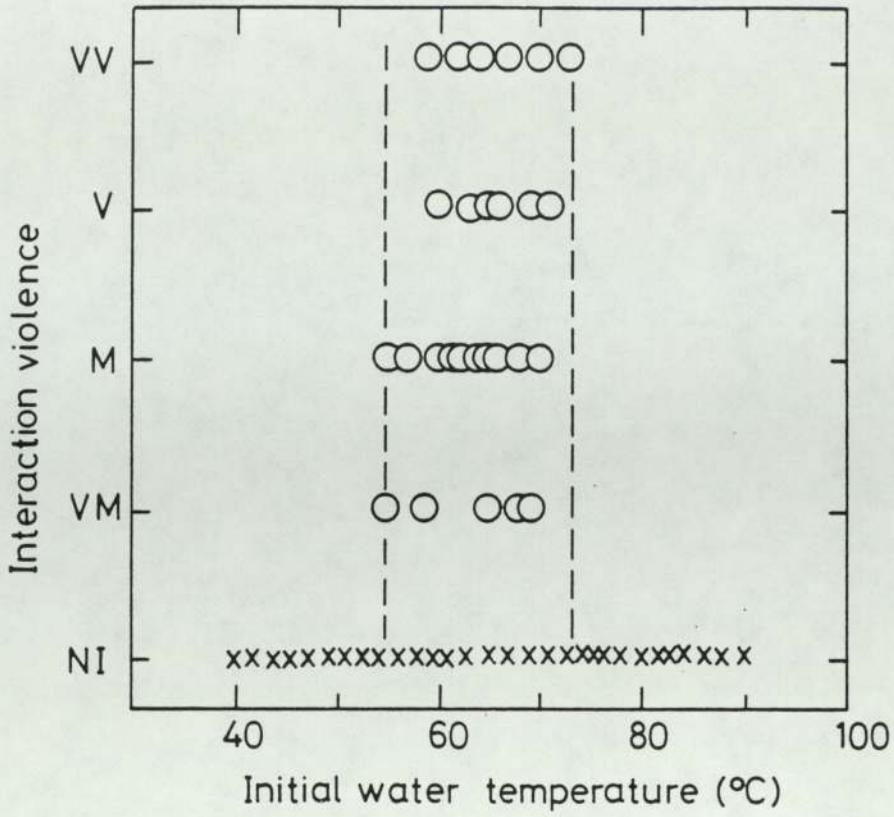

Fig 5.4.4 VIOLENCE OF ISCEON-WATER INTERACTIONS WITH WATER TEMPERATURE

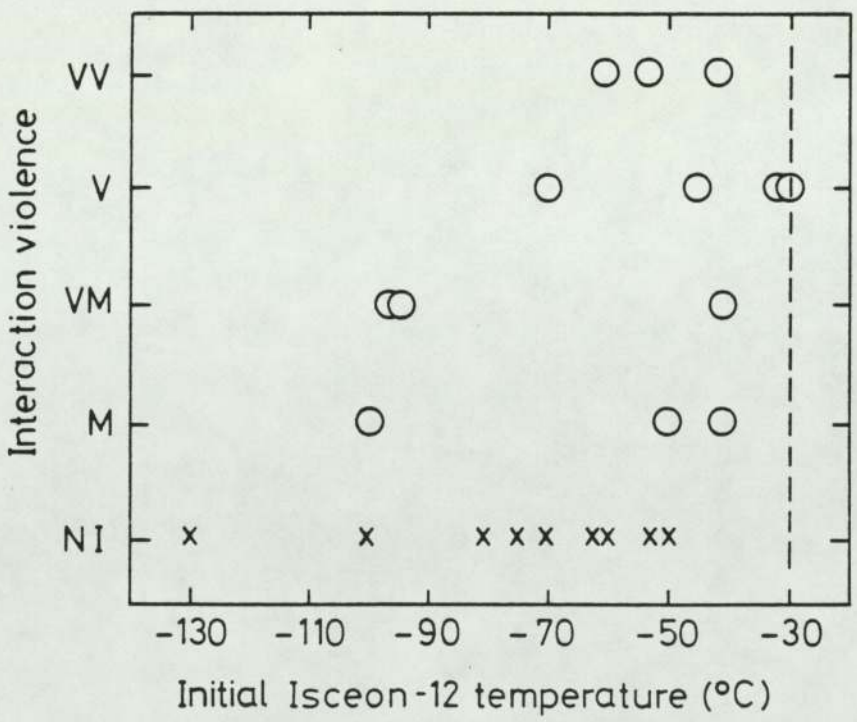

Fig 5.4.5 VIOLENCE OF ISCEON-WATER INTERACTIONS

WITH ISCEON TEMPERATURE

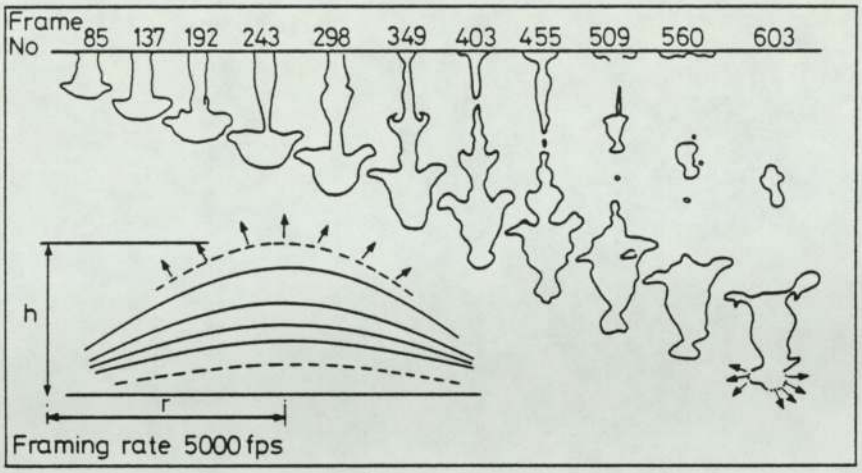

Fig 5.5.1 LINE DRAWING SEQUENCE OF A TIN DROP FALLING IN WATER UP TO THE POINT OF TRIGGERING

increased drag (see figure 5.5.1). Some air entrained on entry broke away and rose to the water surface while the irregularly shaped metal blob fell through the water at about 0.70 m/s. After a short time, 10 to 200 ms depending on the initial metal and water temperatures, the vapour explosion started. During the dwell time the metal had moved from 10 to 150 mm into the water but the start of the interaction occurred before the base of the coolant vessel was reached. The interaction started at some point on the metal surface where fine shredding of tiny quantities of the metal occurred, associated with a growing oscillation of coolant movement centred, as far as could be determined, on the site of the initial perturbation. During the outward movement of liquid, tin debris was dispersed into the coolant. After only three or four oscillations the tin sample had become engulfed by large quantities of fine debris and in the later stages of the interaction the dispersion of tin was clearly associated with the growth and subsequent collapse of large coolant vapour bubbles. The interaction was complete in about five oscillations with a period of

about 2 to 3 ms. The violence of the interaction clearly increased with each cycle until all the metal had been shredded. Sometimes, during the oscillation developing at the initial site, other sites became active but there was no apparent correlation between the oscillations at different sites. Often the initial perturbation or trigger was clearly seen but it failed to grow and there was no apparent preferred position on the metal surface where it occurred. In the last stages of bubble growth the bubble diameters were of the same order as the initial drop diameter, about 15 mm for a 12 g drop.

Similar films have been described by others, which show the same general phenomenon, (see section 2.2).

The penetration distance below the water surface as a function of time depends on the initial impact velocity, v_i, as shown in figure 5.5.2.

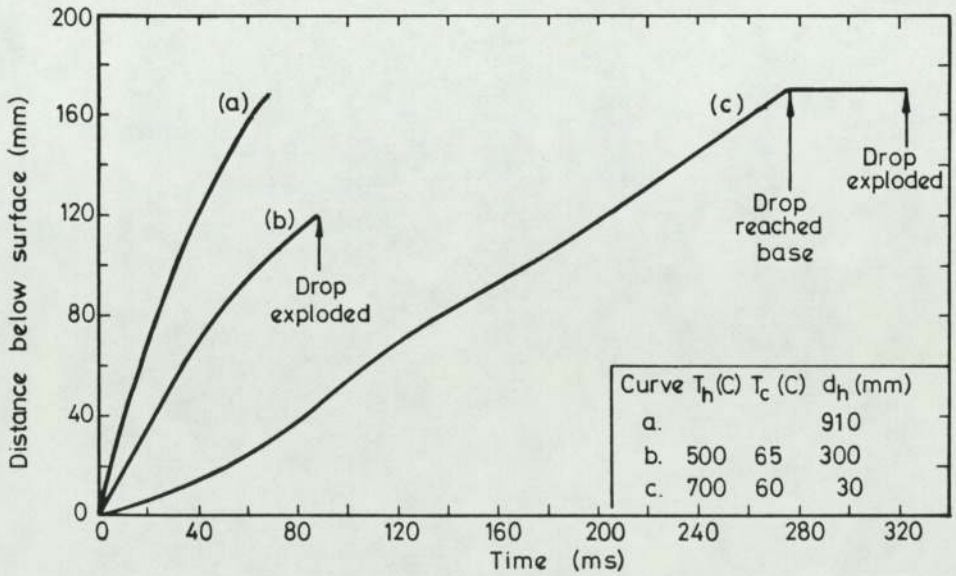

Fig 5.5.2 PENETRATION DISTANCE OF TIN DROPS BELOW WATER SURFACE AS A FUNCTION OF DROP HEIGHT AND TIME

Distance-time curves are shown for three drops with drop heights of (a) 910 mm, (b) 300 mm and (c) 30 mm. The calculated values of v_i are 4.23 m/s, 2.32 m/s (cf measured 2.27) and 0.77 m/s respectively. Terminal velocity was measured as 0.76 m/s for curves (b) and (c) which were 12 g drops, and was not much greater for curve (a), a 44 g drop for which a deep container was used. Only part of this curve is given in the figure.

5.6 Dwell time measurements

(a) Tin-water. The dwell time, t_D, was defined as the time between the leading edge of the tin drop entering the water surface and the initiation of the interaction. Dwell times were measured from film and from pressure records and increased with increasing fuel and coolant temperatures. Figure 5.6.1(b) shows the dwell time plotted against water temperature at a fixed fuel temperature of 873 K. The most striking feature of this curve was the sharp increase in t_D at about 328 K which appears to approach infinity as T_c approaches the normal cut-off temperature. Below 328 K t_D was low and only very slowly increasing.

A similar upward trend is shown also in figure 5.6.1 (a) where t_D is plotted against tin temperature at a fixed coolant temperature of 307 K (34 C). The fuel cut-off temperature, about 2273 K by extrapolation of the sloping boundary in figure 5.2.1, was however, not approached in this case.

(b) Water-Isceon. 90 experiments were performed in which 40 cm^3 water was dropped into saturated isceon-12. The dwell times ranged from very

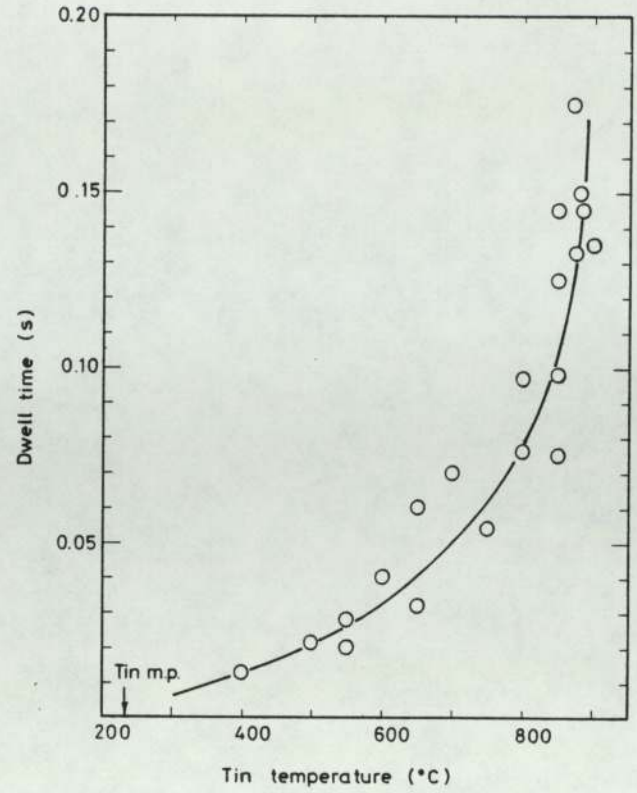

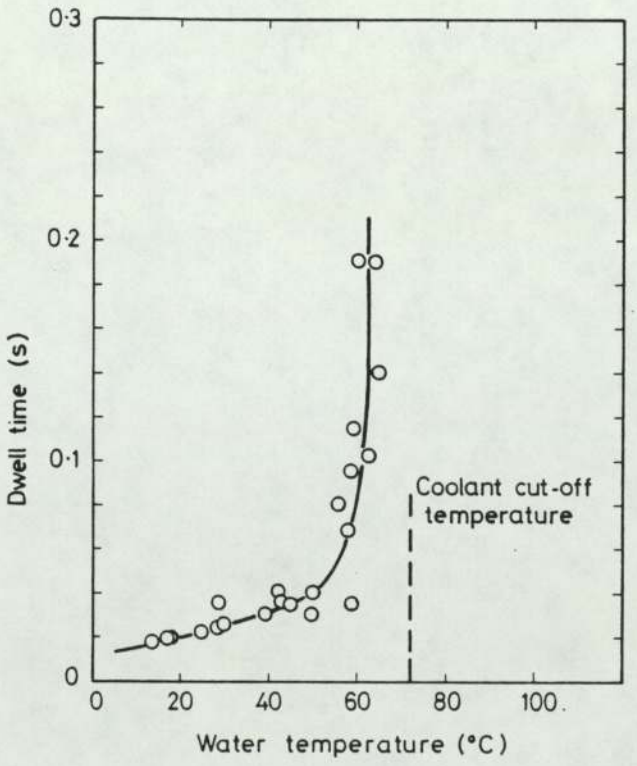

Fig 5.6.1 DWELL TIME MEASUREMENTS FOR TIN DROPPED INTO WATER FOR (a) CONSTANT TIN TEMPERATURE OF 873 K AND (b) CONSTANT WATER TEMPERATURE OF 307 K

short (very short being less than one second) up to seven seconds. At any value for T_h there was a wide range in measured t_D, but the general trend is, as before, for t_D to increase with increasing water temperature (figure 5.6.2(a)).

The most violent interactions were associated with the very short dwell times, as shown in figure 5.6.2(b). One series of experiments varied the volume of water dropped while keeping its temperature between 339 and 349 K (60 and 70 C). The results are shown in figure 5.6.3 where dwell times range up to 2 seconds, consistent with figure 5.6.2(a), and indicate that short dwell time violent interactions (5.5.1) occur with isceon volumes above 20 cm^3.

5.7 Interaction efficiency

Interaction efficiency was defined in section 2.7 as the ratio of the work done by the expanding vapour to the available thermal energy. The latter is given by

$$E = m_h c_h (T_h - T)$$

where T is the melting point of the hot phase where this is above the coolant saturation temperature, as for tin and water, or the saturation temperature if this is the larger, as for cerrobend and water.

In the case of metal-water interactions in which the dwell times are long and the explosion takes place deep in the coolant, cine film shows the coolant surface to rise in a well defined dome shape. The work done may be estimated from the energy density, $0.5\rho_c v^2$, in the moving

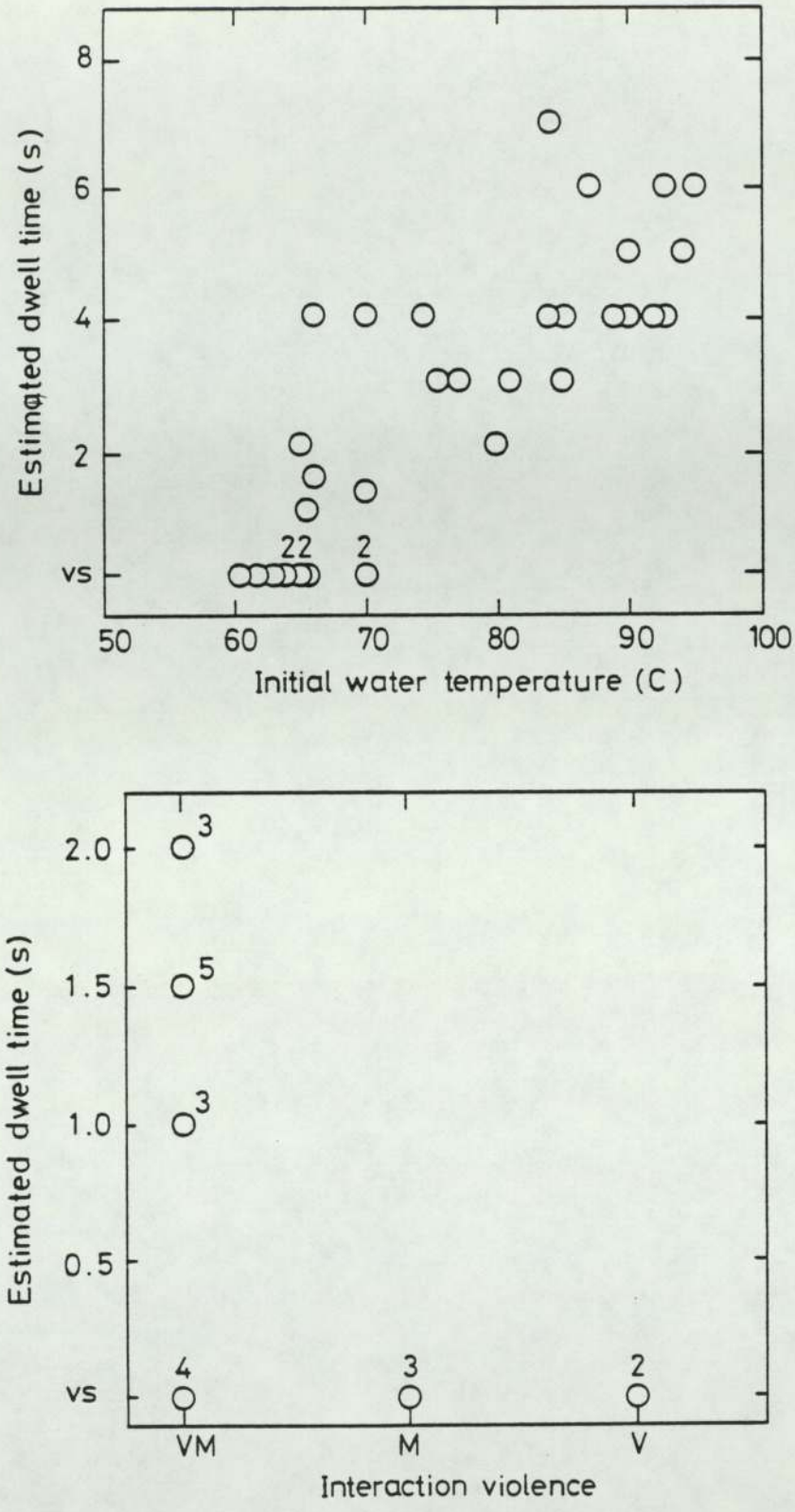

Fig 5.6.2 DWELL TIME MEASUREMENTS FOR WATER DROPPED INTO SATURATED ISCEON. (a) AS A FUNCTION OF WATER TEMPERATURE AND (b) CORRELATED WITH INTERACTION VIOLENCE

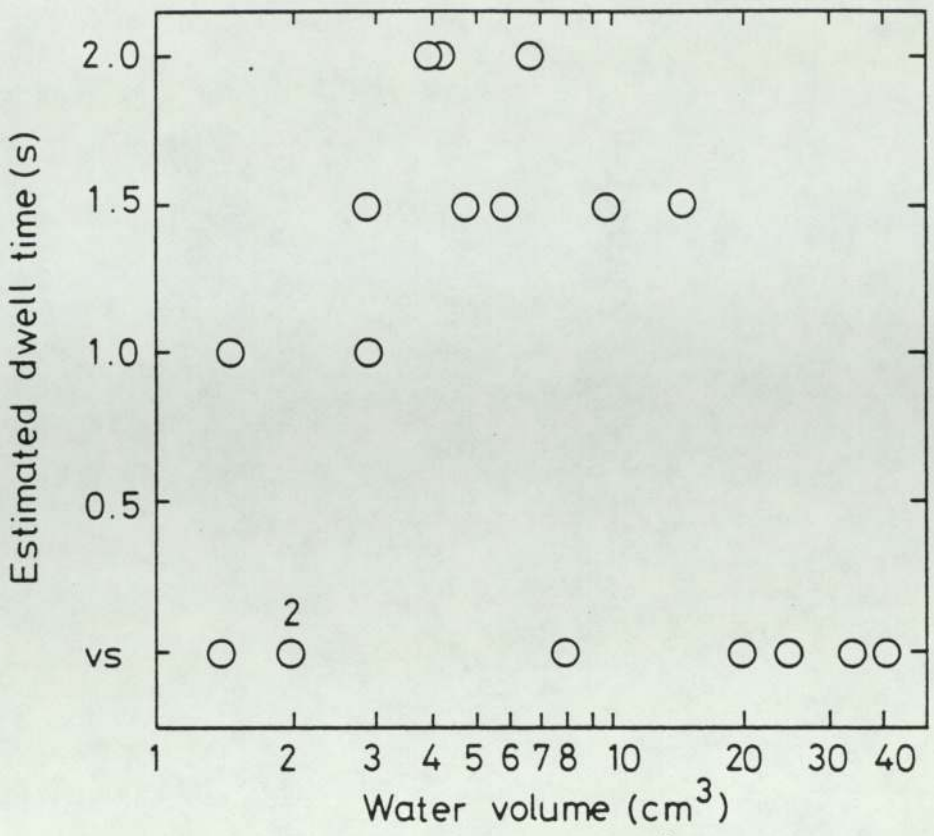

Fig 5.6.3 DWELL TIME MEASUREMENTS FOR WATER DROPPED INTO SATURATED ISCEON AS A FUNCTION OF WATER VOLUME

coolant multiplied by a volume, V . An upper bound to the work done, and hence the efficiency of an interaction, is given by assuming that all the coolant above the depth at which the explosion takes place moves upwards with the velocity v, and by taking for v the dome peak velocity, v_p. The work done is then given by

$$E = \tfrac{1}{2}\rho_c v_p^2 A d_e$$

Compressive energy?

where A is the coolant tank crossectional area and d_e the explosion depth. A line drawing sequence of the development of the dome profile following the interaction in figure 5.5.1 is shown in the bottom left

hand corner of that figure.

A lower bound to efficiency and work done is given by assuming that only that volume of coolant in the dome of raised liquid moves, where the dome dimensions are measured just prior to surface break-up (see figure 5.5.1). If the dome is considered part of a sphere this volume is given by:

$$V = \pi h(3r^2 + h^2)/6$$

and hence the work done is:

$$E = \pi h \rho_c v_p^2 (3r^2 + h^2)/12$$

The lower bound will still be slightly over estimated because not all the liquid moves with the dome peak velocity.

Measurements from a film of a 12 g tin drop at 873 K dropped into water, for which the PDA was 100 percent, gave an efficiency ranging from 0.37 to 3.77 percent of the available thermal energy above the tin melting point.

5.8 Propagation experiments

The detonation model of Board and Hall provides a mechanism for a coherent explosion to take place in a very large mass of hot material. Fragmentation and mixing must propagate very rapidly and large-scale experiments to detect this have been performed elsewhere. Propagation, albeit slow, has also been observed in the small-scale tin-water

experiments described in this thesis, in three quite different geometries. Velocities are low but could represent those at the start of an escalating process which is necessarily limited by the small quantities of tin available.

Propagation along a stream of tin. In one experiment the tipping crucible was slowed so that 20 g of tin at 1073 K (800 C) were poured over its lip in a steady unbroken stream. High speed cine film showed that in the water the leading edge broke away and pulled into a drop. After 70 ms the end of the stream started to fragment. Almost simultaneously the leading blob interacted and did so according to the usual expansion-contraction cycle. The leading edge of the stream followed in the same manner each contraction and expansion engulfing more tin so that fragmentation moved back along the still falling stream until it reached the water surface. The fragmentation propagation velocity along a stream length of about 50 mm was 2.4 m/s and was accomplished in 7 oscillations. A similar experiment has been reported by Witte [149] who injected hot mercury into water at the explosion propagation speed and thus sustained a continuous cycle of interactions.

Propagation through a dispersion of small drops. The second experiment involved a 44 g sample of tin at 823 K dropped through 300 mm into a deep container of water. The impact with the water surface (2.4 m/s) was sufficient to cause the drop to break-up on entry, into one large leading drop and very many smaller drops dispersed throughout the volume of the coolant (150 mm x 140 mm crossection and 470 mm deep). The leading drop triggered on reaching the container base, just out of view of the camera. It triggered simultaneously all the drops in the region 100 mm above the base which,

after a delay of 5.7 ms then triggered all the drops above them in the region 100 - 200 mm above the base. Propagation speed was estimated as 37 m/s.

Propagation across a flat "pancake" of tin. The last example of propagation comes from a 12 g drop at 973 K dropped through 30 mm of air into water at 333 K (60 C). The drop reached the tank base (170 mm deep) in 280 ms and the interaction occurred some 40 ms later. The drop was seen to spread on the base into a flat pancake, possibly trapping coolant and vapour beneath it which prevented direct contact. More will be said about this process in chapter 8. The vaporisation of this coolant could account for the slight swelling and lifting of the pancake just before triggering occurred at a point on the edge. The interaction travelled across the pancake at about 20 m/s.

5.9 Results from other systems

(a) Water poured into liquid nitrogen. In each experiment water sank to the bottom of the liquid nitrogen container and solidified. A few small pieces of ice bubbled around the bulk liquid but 95 per cent remained in one lump. Nothing remotely approaching a vapour explosion occurred.

(b) Liquid nitrogen poured into water. In all experiments the liquid nitrogen spread across the water surface with bubbling throughout the film, (ie vapour produced on the underside escaped by breaking through the film surface). For water temperatures below 298 K (25 C) the surface water froze and boiling took place from the ice surface. Breaking the ice only resulted in re-freezing. Small ice flakes could

be seen floating in the liquid nitrogen film, formed presumably from the freezing of airborne water vapour in contact with the upper film surface.

Above 298 K the liquid nitrogen film diminished first in thickness and then in diameter until it was able to float around the water surface. When it became small enough (about 30 mm dia.) all the vapour produced was able to escape from beneath the sides of the film and bubbling through the surface ceased. At about 10 mm dia. film boiling stopped and the liquid nitrogen fizzled away. The transition was quite definite but not accompanied by the Leidenfrost explosion reported for LNG-water interactions.

In all the experiments, (a) and (b), no vapour explosions were observed and observation was made difficult by the formation of dense clouds of condensed steam from the hot water in the cold liquid nitrogen vapour.

(c) Tin dropped into the cryogens at saturation temperature. Only a handful of spot check experiments were performed and in none of them did an interaction occur. In each case the tin simply film boiled on the container base and solidified.

(d) Indium dropped into water. The assessed PDs increased with water temperature in the familiar way as shown in figure 5.9.1. The coolant cut-off temperature was lower than that for the other metals and water at the same metal temperatures by some 15 degrees, and the maximum value of the assessed PDs did not exceed 80 per cent even close to the cut-off. They are, however, comparable with tin PDAs at the relevant position in the tin-water TIZ.

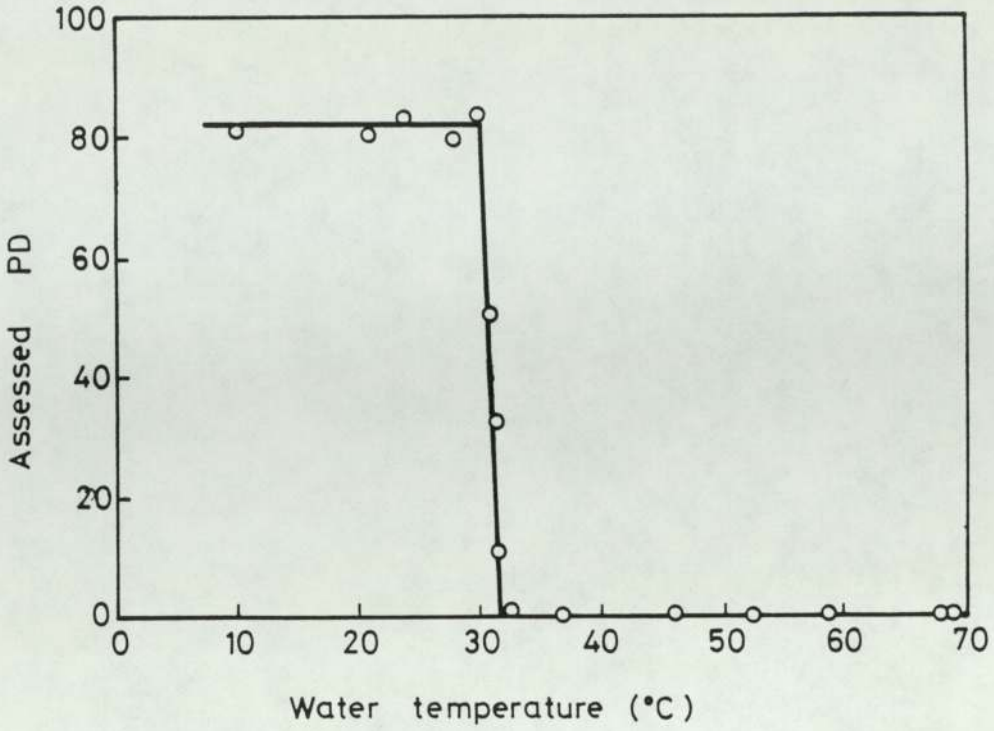

Fig 5.9.1 VARIATION OF INDIUM PD WITH WATER TEMPERATURE

CHAPTER 6 EXPERIMENTAL RESULTS II:

FACTORS AFFECTING THE POSITION OF THE TIZ BOUNDARIES

6.1 Introduction

When the initial drop experiments with tin and water were performed it was soon realised that there were many parameters which can influence vapour explosions, and a systematic approach to their evaluation was implemented. The initial choice of parameters such as coolant depth, drop height, fuel mass, etc., was then quite arbitrarily made, or at least made to comply with existing experimental facilities, and while providing a starting point for our studies some of these turned out to be not the most suitable choice that could have been made. For example 12 grams of tin was taken since it just suited crucible sizes made from stock silica tubes. Unfortunately 12 gram drops are just unstable and break-up in the water. From this point of view the choice of 170 mm for tank depth was unfortunate because break-up occurs at or near the base and without filming every drop it was not always possible to distinguish between break-up due to capillary instability and that due to impact with the base. Furthermore, the maximum dwell times measured near to the cut-off temperatures were about 200 ms and the time for metal to reach the container bottom was 250-300 ms, depending on drop shape etc.

This last point provided the motivation for the experiments of sections 6.3 and 6.4 because it was not clear whether or not the normal cut-off temperatures were determined by the approach of the metal to the tank base. Bulk phase depth and the fall distance to its surface, which

both effect the time for the dropped phase to reach the container base, were varied and their effect on the cut-off temperatures determined.

If vapour film collapse is the initiating event in these small-scale experiments then it is an essential requirement of the initial conditions that a vapour film be established on contact of the two phases. Any parameter which can influence these conditions will also determine the TIZ boundary positions. Such parameters are sample mass, which for small drops may determine the minimum film boiling temperature, the density and nature of nucleation sites and the contact mode which will determine if the interface contact temperature increases or decreases with time. These parameters were investigated and the results are presented in sections 6.2, 6.5 and 6.6.

In all the graphs that follow a small number next to any particular point on the graph is the number of times the experiment was repeated with the same result.

6.2 The effect of sample mass

Tin-water. A large number of experiments were conducted to find the effect of varying the mass of the tin on interaction violence at fixed values of tin and water temperatures, drop height and coolant depth.

It was found that there was a minimum mass required above which interactions occurred with PDs typical of the "normal" values, but below which they did not occur. Generally the value of the minimum mass was well defined. Figure 6.2.1 for instance shows three plots of PDA against tin mass for tin and water temperatures of 773 K (500 C) and 338 K (65 C) and varying drop height in the range 60-280 mm. In

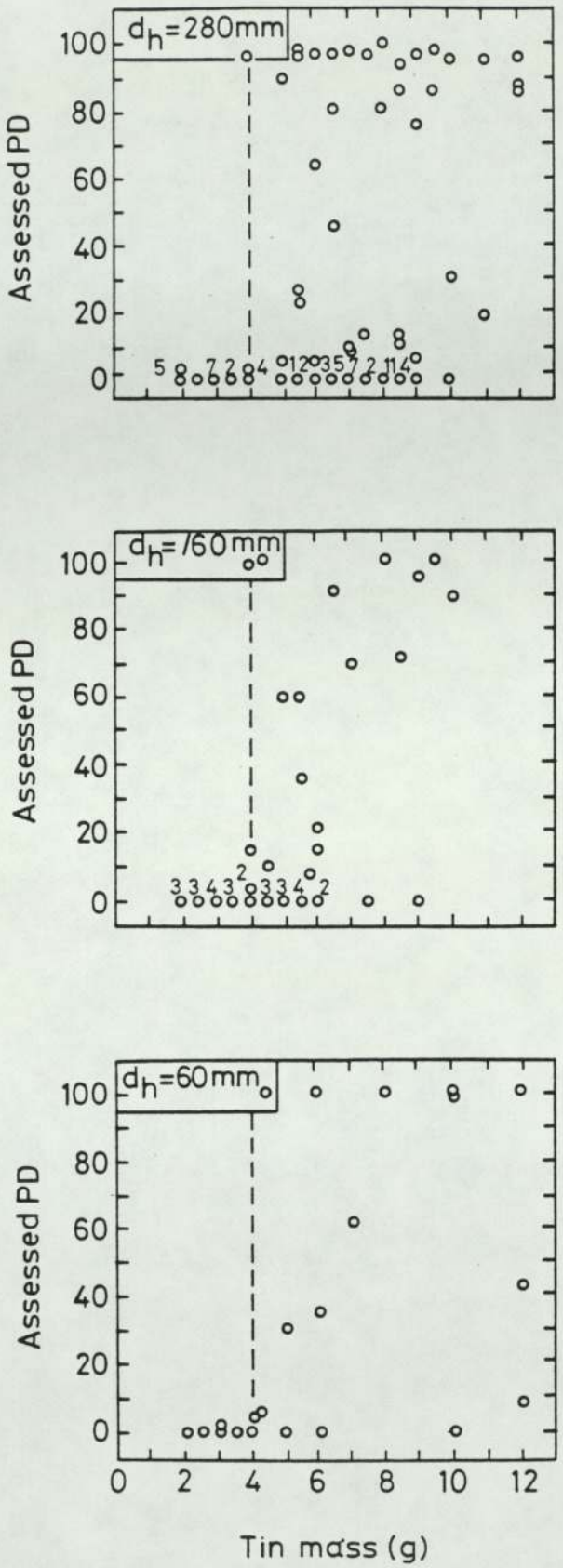

Fig 6.2.1 PLOTS OF PD vs TIN MASS AT VARIOUS DROP HEIGHTS

T_h = 773 K, T_c = 338 K

each case PD was zero for masses below 4 g, but increased very sharply above this value. The three graphs together represent 191 experiments, 52 of which were below the minimum mass. (On one occasion a 2 g sample did explode). This minimum mass was, therefore, very clearly established.

With the drop height fixed at 60 mm the effect of varying first tin and then water temperature was investigated and these results are summarised from plots such as those in figure 6.2.1 in figures 6.2.2 and 6.2.3. In figure 6.2.2 minimum mass is plotted against tin temperature for a coolant temperature of 338 K (65 C). Clearly, minimum mass decreases with increasing tin temperature.

Similarly, figure 6.2.3 shows how minimum mass increases with increasing coolant temperature for T_h = 773 K (500 C). The behaviour below 313 K (40 C) is still uncertain with the minimum mass going to zero somewhere between 294 K (21 C) and 313 K. At 294 K minimum mass was below 0.5 g, the smallest quantity of tin that could be used in the existing apparatus. Above 333 K (60 C) minimum mass seems to have become constant at 4 g.

Water-Isceon. 26 experiments were performed in which varying quantities of water between 1.5 and 40 cm^3 at 333 K (60 C) were dropped through 60 mm of air into 500 cm^3 of saturated isceon-12. Interaction violence and probability of occurrence both increased with increasing water volume (see figure 6.2.4). Above 4 cm^3 the interaction probability was 100 per cent. Below 4 cm^3 the probability decreased and at 1 cm^3 no interaction occurred in 4 experiments. It was not possible to experiment with smaller volumes. No single precise value for minimum mass (volume) was found although it seems likely that a

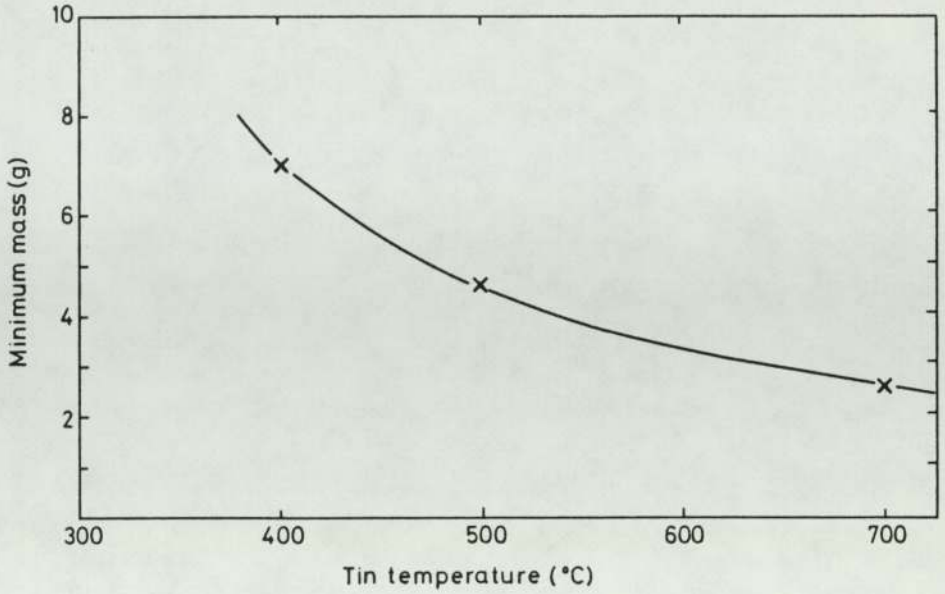

Fig 6.2.2 MINIMUM MASS AS A FUNCTION OF TIN TEMPERATURE AT A FIXED WATER TEMPERATURE OF 338 K

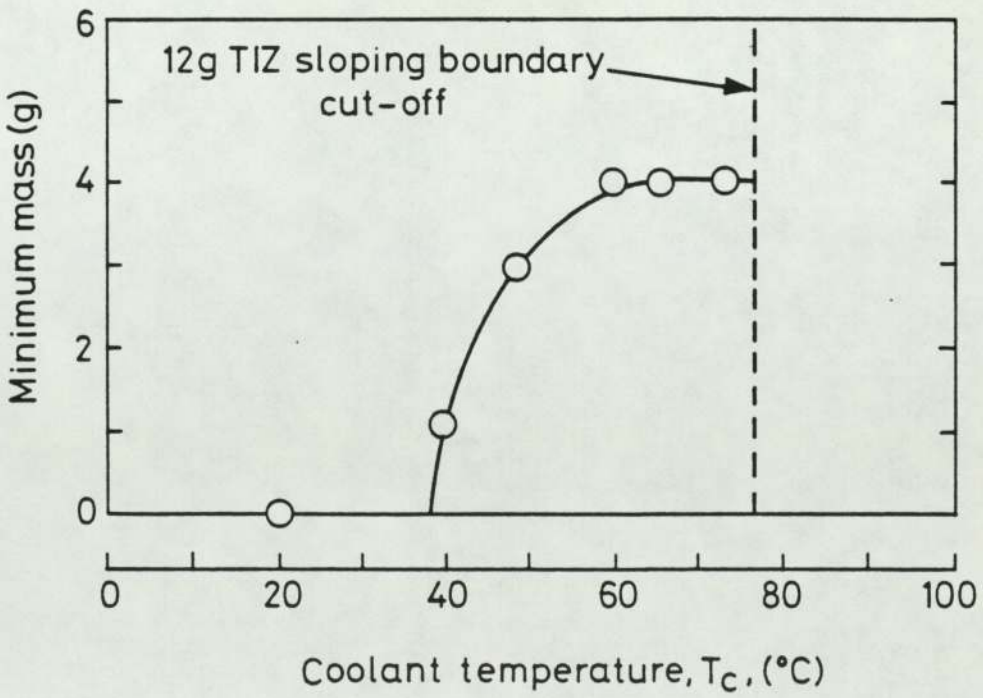

Fig 6.2.3 MINIMUM MASS AS A FUNCTION OF WATER TEMPERATURE AT A FIXED TIN TEMPERATURE OF 773 K

minimum may be defined for a given level of violence to be exceeded. For example, interactions rated greater than very mild in this system require water volumes in excess of 20 cm .

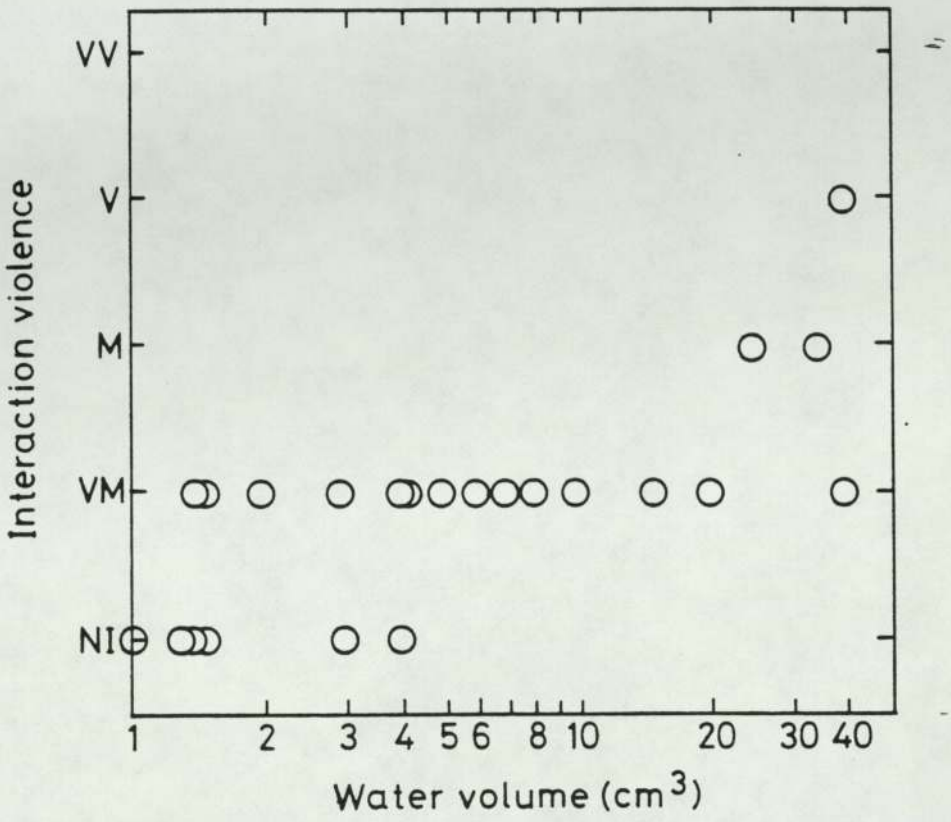

Fig 6.2.4 INTERACTION VIOLENCE AS A FUNCTION OF WATER VOLUME FOR WATER DROPPED INTO ISCEON

6.3 The effect of drop height

Tin-water. 97 experiments were performed in the 180 mm and 600 mm deep tanks with flat bases, to investigate the effect of drop height up to 910 mm on the sloping boundary of the "standard" TIZ. The results are shown in figure 6.3.1 and summarised in figure 6.3.2. Figures 6.3.1(a) and (b) show PD plotted against coolant temperature for tin temperatures of 823 K (550 C) and 1173 K (900 C) and a drop height of

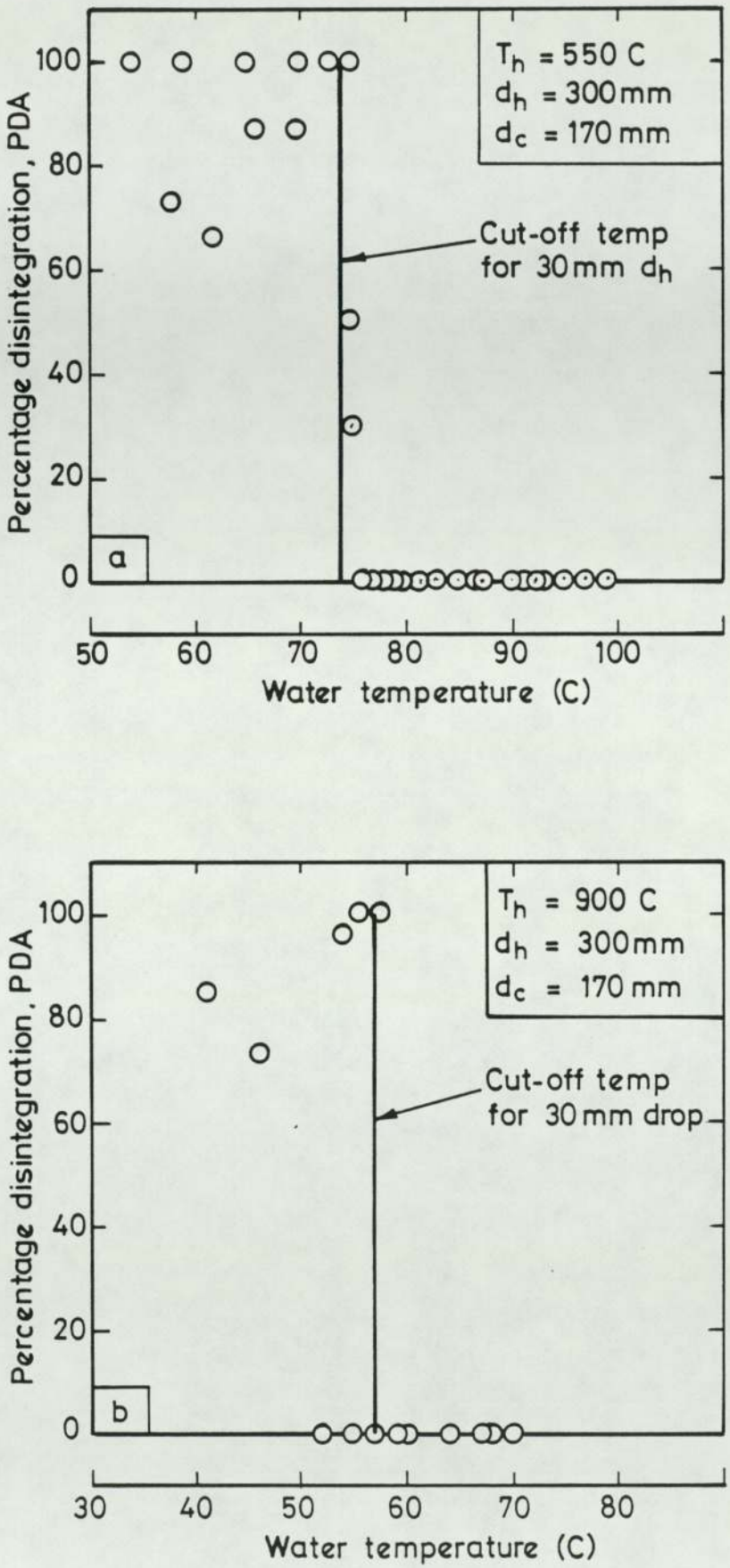

Fig 6.3.1 PD AS A FUNCTION OF WATER TEMPERATURE AND DROP HEIGHT

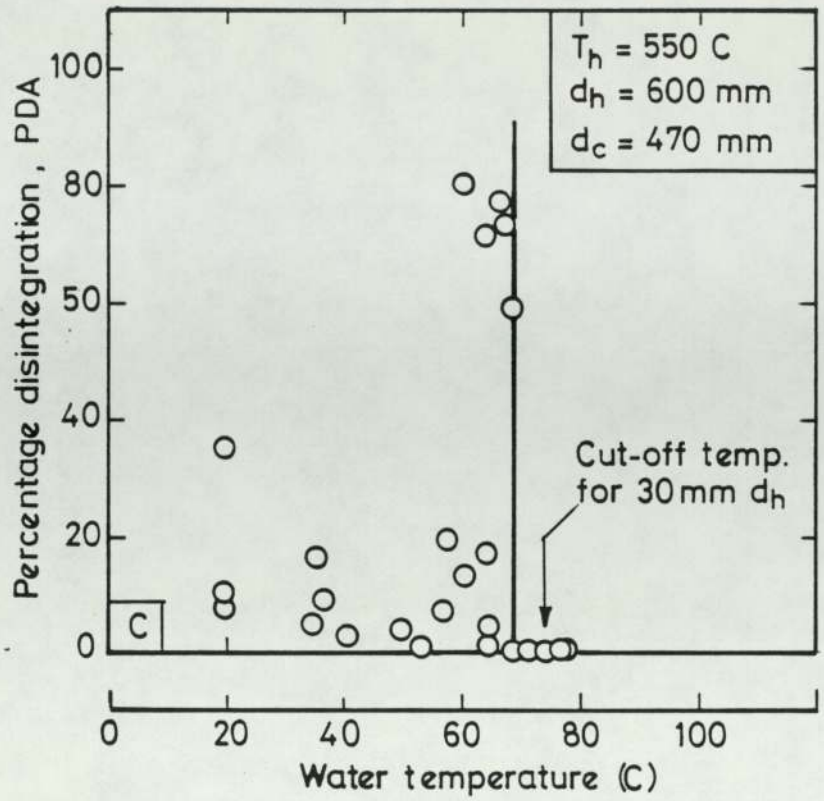

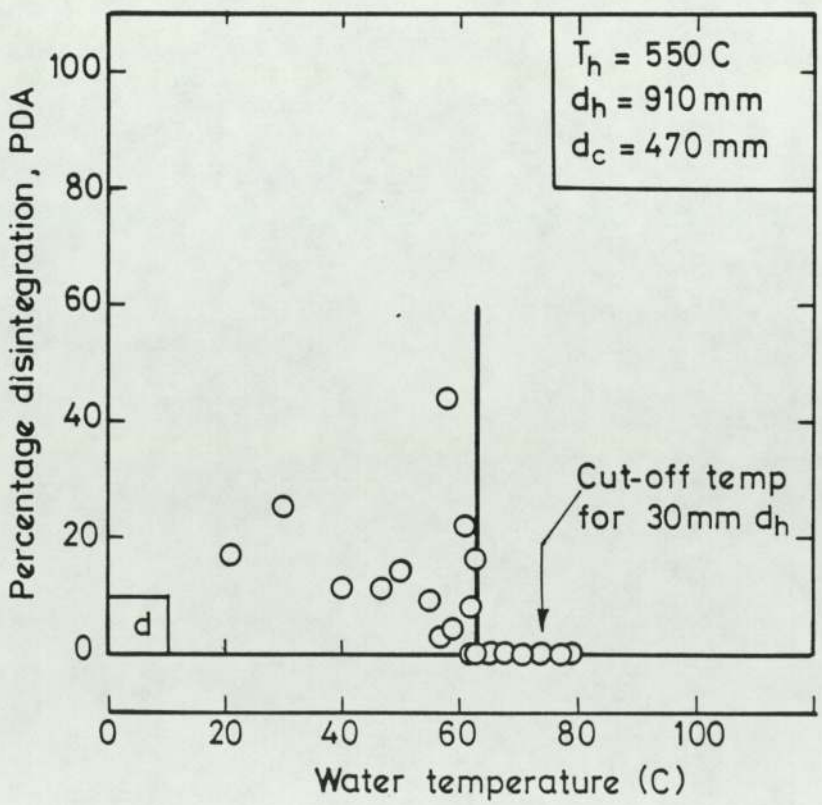

Fig 6.3.1 continued

300 mm. It can be seen that the coolant cut-off temperatures and hence the gradient of the sloping boundary were unchanged at the increased drop height. The normal values were taken from the "standard" TIZ of figure 5.2.1.

The effect of increasing drop height to 600 mm and 910 mm is shown in figure 6.3.1(c) and (d) at the constant tin temperature of 823 K. As with previous experiments, the highest PDs were obtained near to the cut-off temperature, but the value of this temperature decreased slightly as the drop height was increased. This is shown more clearly in figure 6.3.2 where the cut-off temperature is plotted against drop height.

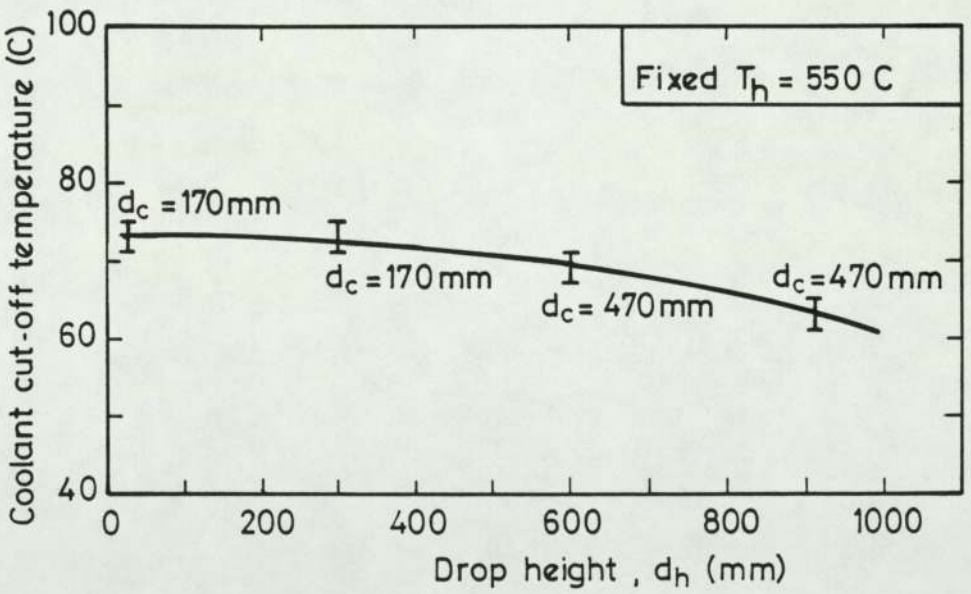

Fig 6.3.2 VARIATION OF COOLANT CUT-OFF TEMPERATURE WITH TIN DROP HEIGHT FOR T_h = 823 K

While the usual PD-T_c pattern was maintained at increased drop heights, (ie the maximum PDs were obtained close to the cut-off temperature), the value of PD in general fell below that for "normal" TIZ conditions.

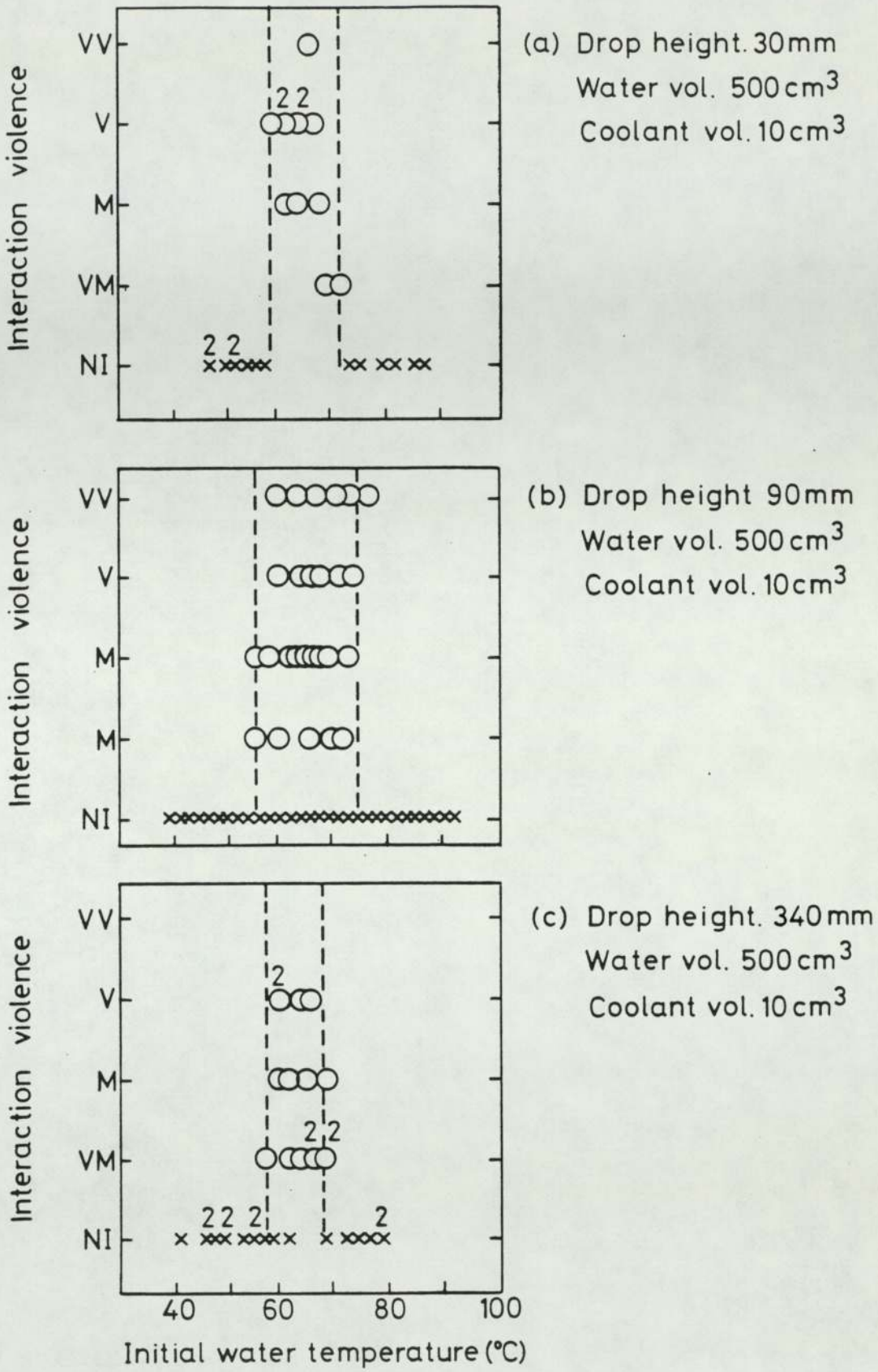

Fig 6.3.3 VARIATION OF VIOLENCE OF SATURATED ISCEON-WATER INTERACTIONS WITH WATER TEMPERATURE AND DROP HEIGHT

At d_h = 910 mm for example no value of PDA exceeded 45 per cent, while 100 per cent was common at the lower drop heights. At the higher drop height the coolant cut-off temperature has fallen by some 10 degrees.

Isceon-water. A small number of experiments were performed with drop heights of 30 mm and 340 mm into 500 cm^3 of water and these are compared in figure 6.3.3 with the results from the conditions for the "standard" TIZ (drop height 90 mm). A slight variation in the position of the zone boundaries is seen with the largest difference associated with the upper water temperature cut-off. The following statistics are interesting but need verification with more experiments.

(i) At the lowest drop height, 30 mm, the percentage of interactions within the marked zone was 100 per cent (cf 73 per cent at 90 mm)

(ii) At the largest drop height the probability of an interaction within the zone was 88 per cent, but no very violent interactions occurred.

6.4 The effect of bulk phase depth

Tin-water. 18 experiments were performed in a 600 mm deep tank with an initial tin temperature of 823 K (550 C) and drop height of 30 mm. The coolant cut-off temperature was found to be 349 K (76 C) which is not significantly higher than the 347 K taken from the "standard" TIZ for which coolant depth was 180 mm.

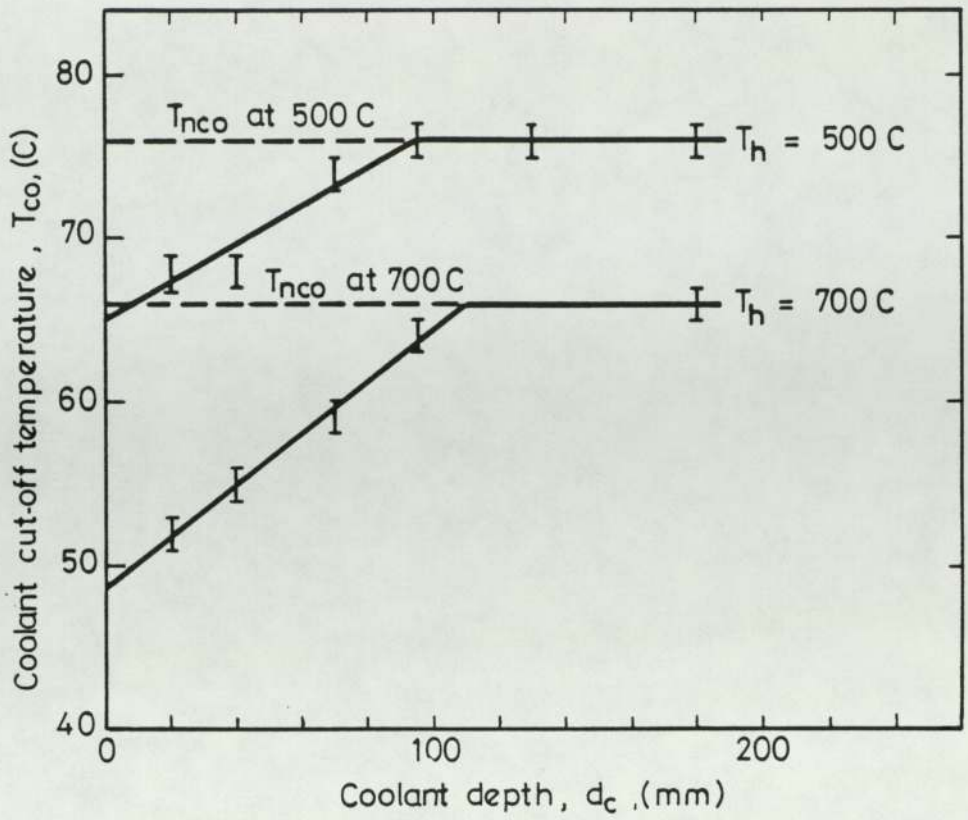

Fig 6.4.1 THE EFFECT OF WATER DEPTH ON COOLANT CUT-OFF TEMPERATURES FOR TIN DROPPED INTO WATER

Figure 6.4.1 shows the result of decreasing coolant depth on cut-off temperatures for tin initially at 773 K (500 C) and 973 K (700 C). The coolant was contained in the rectangular perspex tank 100 mm deep with the shaped base placed on supports of various heights to alter the effective depth of coolant between 20 and 95 mm. The drop height through air to the water surface was 20 - 30 mm. Each point on the graph was determined from a PD-temperature plot similar to figure 5.4.3. The effect was clearly restricted to shallow pools less than about 100 mm deep for which the cut-off temperature fell linearly with decreasing coolant depth. That depth above which the normal coolant cut-off temperature was obtained is labelled the normal cut-off depth, d_{nco}, and appears to be slightly dependent on tin temperature. d_{nco} is

95 mm and 110 mm at 773 K and 973 K respectively.

The data of figure 6.4.1 for depths up to d_{nco} is presented again in figure 6.4.2 in terms of the normalised parameters $(T_{sat} - T_{nco})/(T_{sat} - T_{co})$, the ratio of coolant subcooling at the normal cut-off temperature to that at the reduced cut-off temperature, and $(d_{nco} - d_c)/d_{nco}$, the ratio of the depression of the coolant depth below the normal cut-off depth to the normal cut-off depth. Both sets of data fall on a common straight line. As d_c approaches d_{nco} the normalised depth approaches zero and the normalised cut-off temperature approaches unity. As d_c is reduced to zero on the other hand the normalised depth approaches unity and the normalised cut-off temperature approaches the finite value of 0.65.

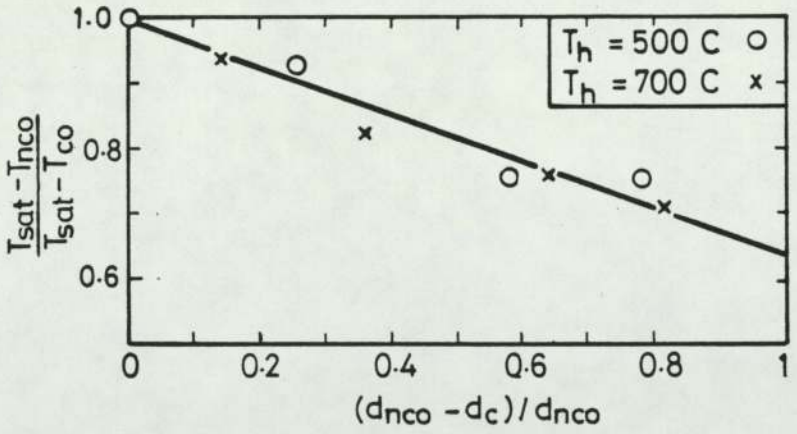

Fig 6.4.2 NON-DIMENSIONAL PLOT OF CUT-OFF TEMPERATURE AGAINST COOLANT DEPTH

The finite value of the intercept on the temperature axis of figure 6.4.2 reflects the non-zero values for T_{co} at zero depth suggested by the extrapolation of figure 6.4.1. Further, the single intercept value indicates that a limiting minimum value of cut-off temperature may be

found for any hot liquid temperature from the equation:

$$(T_{sat} - T_{nco}) = 0.65(T_{sat} - T_{co})$$

Isceon-water. Figure 6.4.3 shows the results of about 80 experiments in which 10 cm^3 of saturated isceon-12 has been dropped through 90 mm into 250 cm^3, 500 cm^3 and 750 cm^3 of hot water. These correspond to depths of 27 mm, 42 mm and 61 mm. respectively or to water-to-coolant volume ratios of 25:1, 50:1 and 75:1. In the figure the estimated interaction violence is plotted as a function of water temperature with x denoting no interaction and o denoting interactions in the usual way.

For each case interactions occurred over a narrow water temperature range with sharp upper and lower cut-off temperatures. The lower cut-off varied from 328 K (55 C) in figure 6.4.3(a) to 332 K (59 C) in figure 6.4.3(b) and the upper cut-off varied from 340 K (67 C) in figure 6.4.3(c) to 346 K (73 C) in figure 6.4.3(b). These variations are small and not significant in view of the smaller number of experiments performed at 750 cm^3 and 250 cm^3.

As with other TIZs, operation within the zone did not guarantee that interactions would occur, but outside the zone interactions definitely did not occur.

Bearing in mind the limited statistics, the following conclusions from figure 6.4.3 may be drawn but require verification by further experiments before they can be made general.

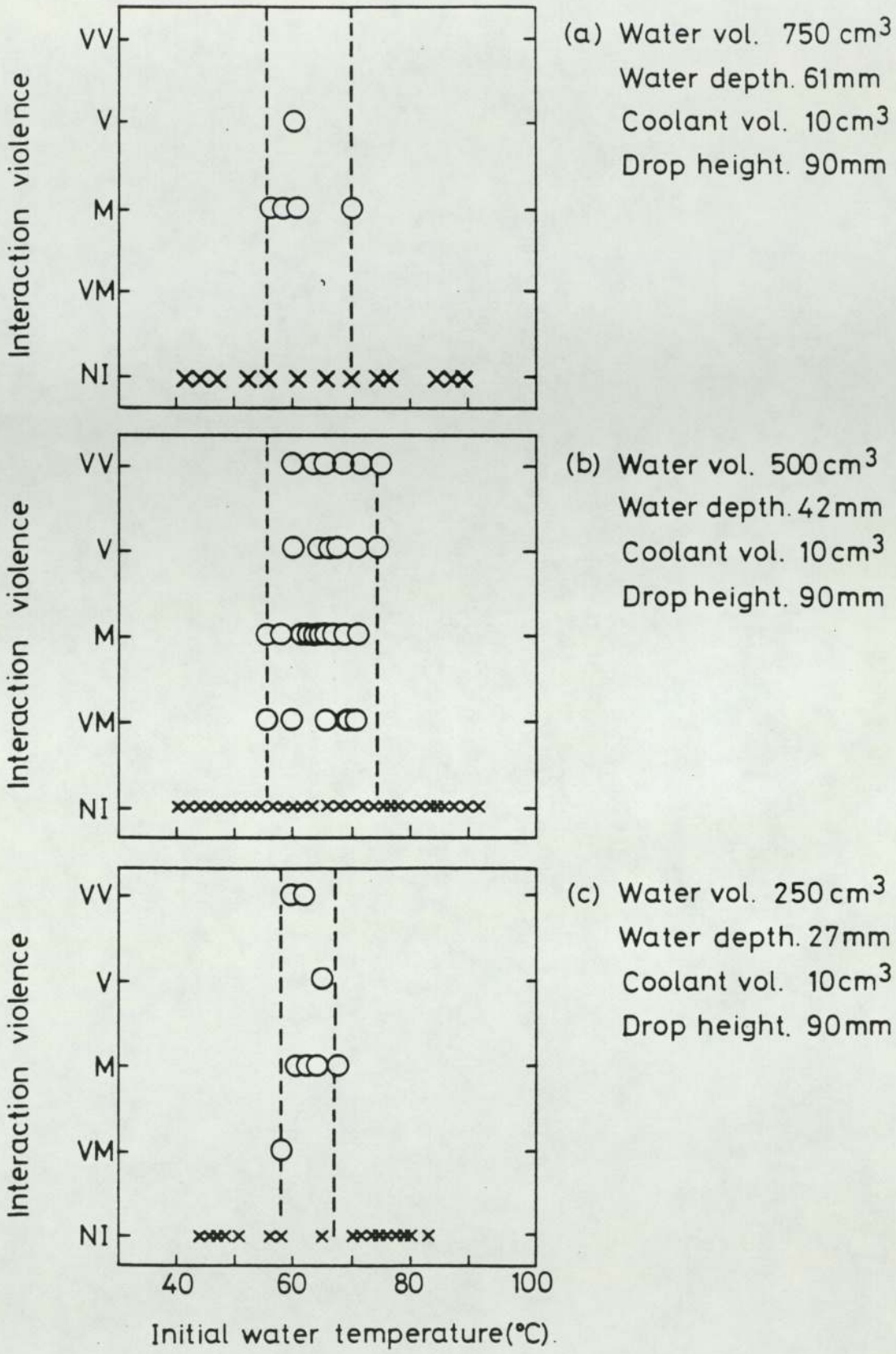

Fig 6.4.3 VARIATION OF VIOLENCE OF SATURATED ISCEON-WATER INTERACTIONS WITH WATER TEMPERATURE AND VOLUME

(i) In figure 6.4.3(a) no very violent interactions occurred and within the interaction zone marked, 56 per cent of experiments produced an interaction of some sort.

(ii) At 500 cm^3 interactions at all violence levels ocurred with 73 per cent probability of an interaction occurring within the marked zone.

(iii) At 250 cm^3 the probability of an interaction occurring within the narrow zone marked was 80 per cent.

There appears to be a roughly linear relationship between the probability of an interaction occurring and decreasing water depth or volume.

6.5 The effect of nucleating agents

Why?

25 experiments were performed in which about 0.2 g of lycopodium powder was added to the isceon coolant before dropping into water. There was no attempt to accurately control this weight. With a mean lycopodium particle size of about 30 micrometres and powder density of 0.25 g/cm^3 this represents about 10^{12} particles per cm^3 of isceon. The results are summarised in figures 6.5.1 and 6.5.2.

Figure 6.5.1 shows a scan across water temperature with pure saturated isceon-12 compared with a similar scan with lycopodium powder added. With the nucleation sites added experiments were only performed within the "normal" TIZ. The results again indicate a narrower zone than normal, but as with the influence of water volume and the drop height,

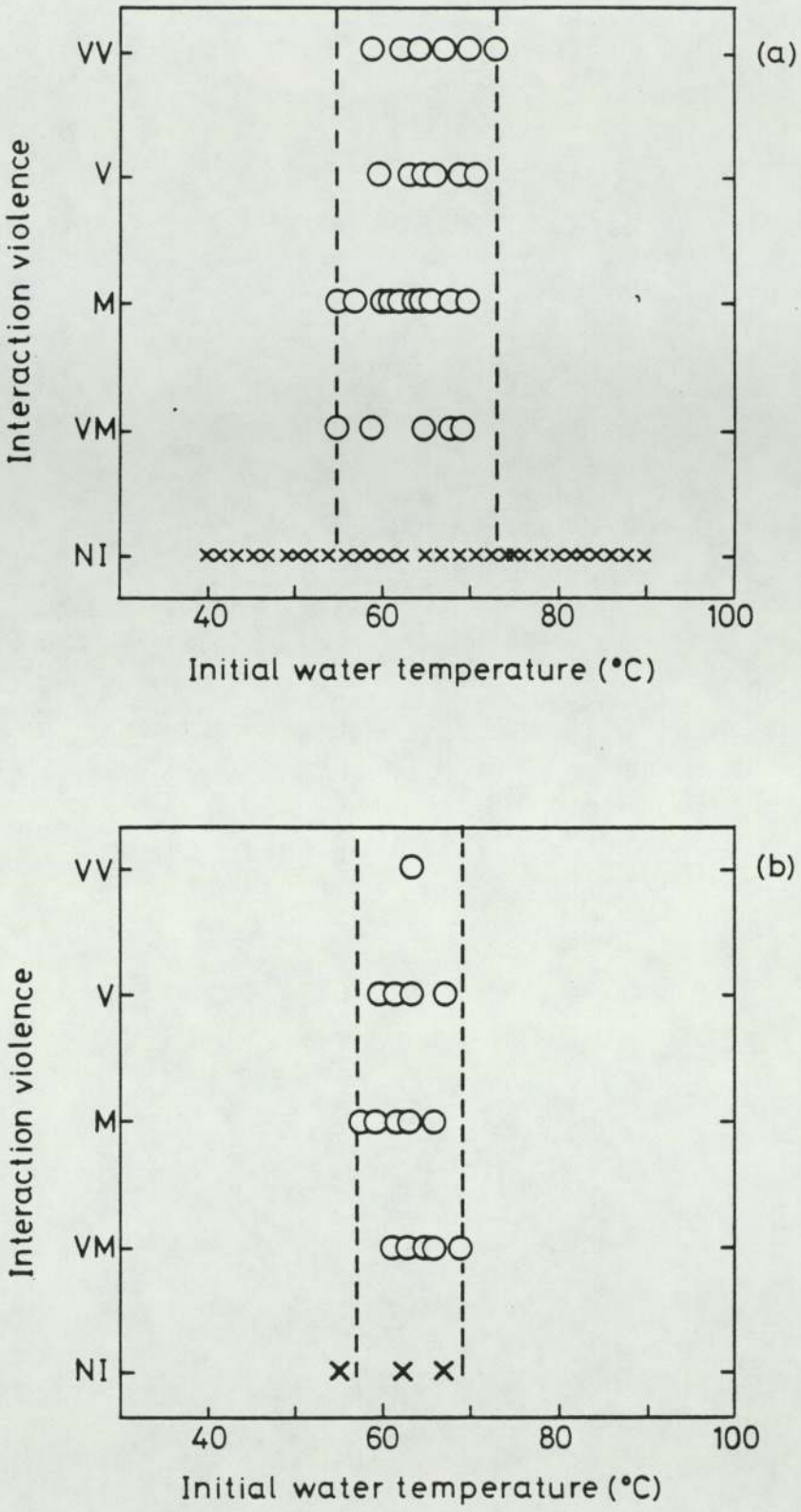

Fig 6.5.1 VARIATION OF VIOLENCE OF SATURATED ISCEON-WATER INTERACTIONS WITH (a) PURE ISCEON AND (b) ISCEON WITH LYCOPODIUM POWDER

further experiments are required to substantiate this. Within the zones marked on figure 6.5.1 there are fewer very violent interactions with the lycopodium powder added (1 in 17 or 6 per cent) in figure 6.5.1(a) compared to 6 in 37 (or 16 per cent) in figure 6.5.1(b), and a slightly higher overall percentage of interactions (88 compared to 73 per cent).

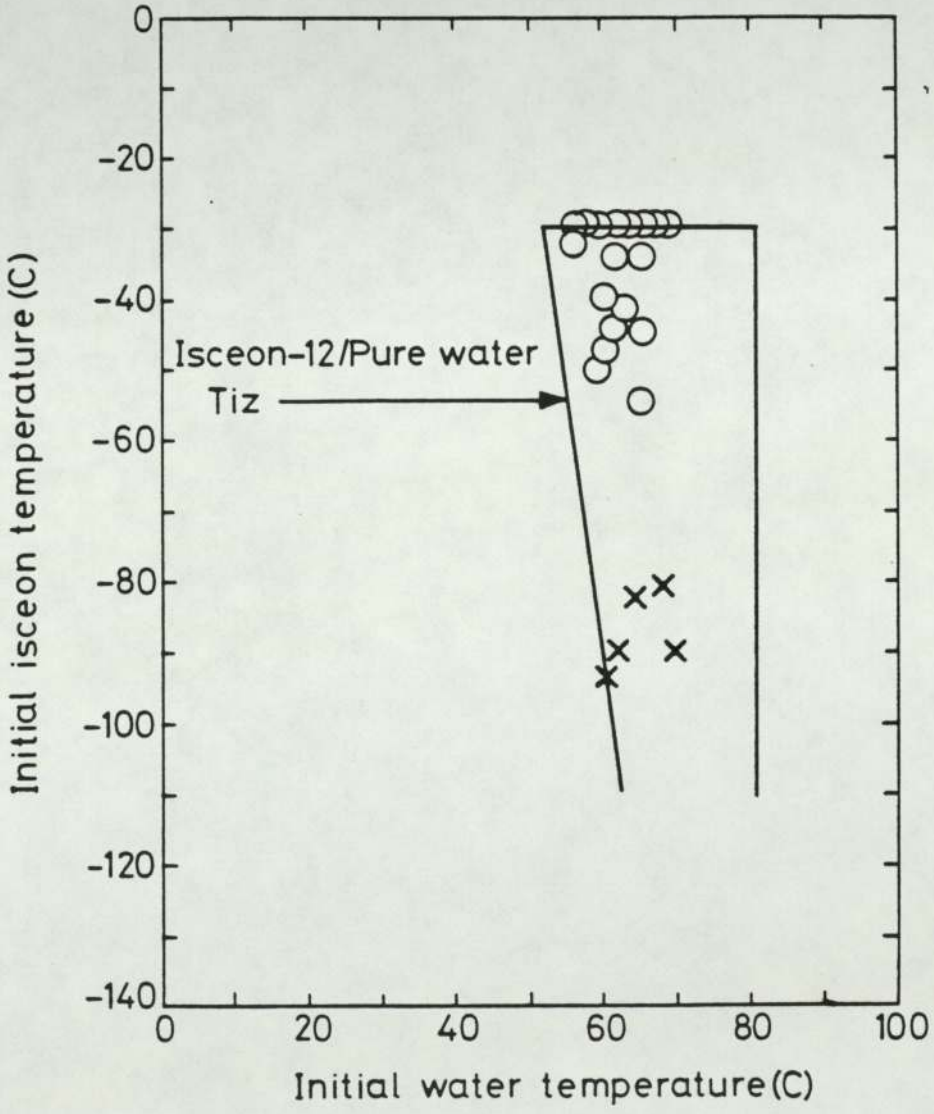

Fig 6.5.2 THE EFFECT OF SOLID NUCLEATION SITES IN THE COOLANT ON THE ISCEON-WATER TIZ

In figure 6.5.2 the results of figure 6.5.1 and those of a few experiments with subcooled isceon are superimposed on the "normal" TIZ of figure 5.2.4. Two interesting points emerge. First, with subcooled isceon-12 (up to 30 degrees subcooling) all 10 experiments produced an interaction when normally we would have expected about three failures. Second, at high degrees of subcooling all five experiments failed to produce an interaction when normally we would have expected 3 or 4 to have done so. Together the results suggest a smaller TIZ when solid nucleation sites are included in the coolant.

6.6 The effect of contact mode

Figure 6.6.1 shows the estimated violence plotted against water temperature for water dropped into isceon-12. Interactions again occurred in a fixed region of temperature space, the lower boundary coinciding, within experimental error, to that found previously for isceon dropped into water. There were, however, two important differences. First, the upper water cut-off temperature was not found in these experiments, interactions occurring for all water temperatures above the minimum up to 368 K (95 C). Second, no very violent interactions were observed at all and only three of the forty experiments inside the TIZ could be called violent, (less than 10 per cent).

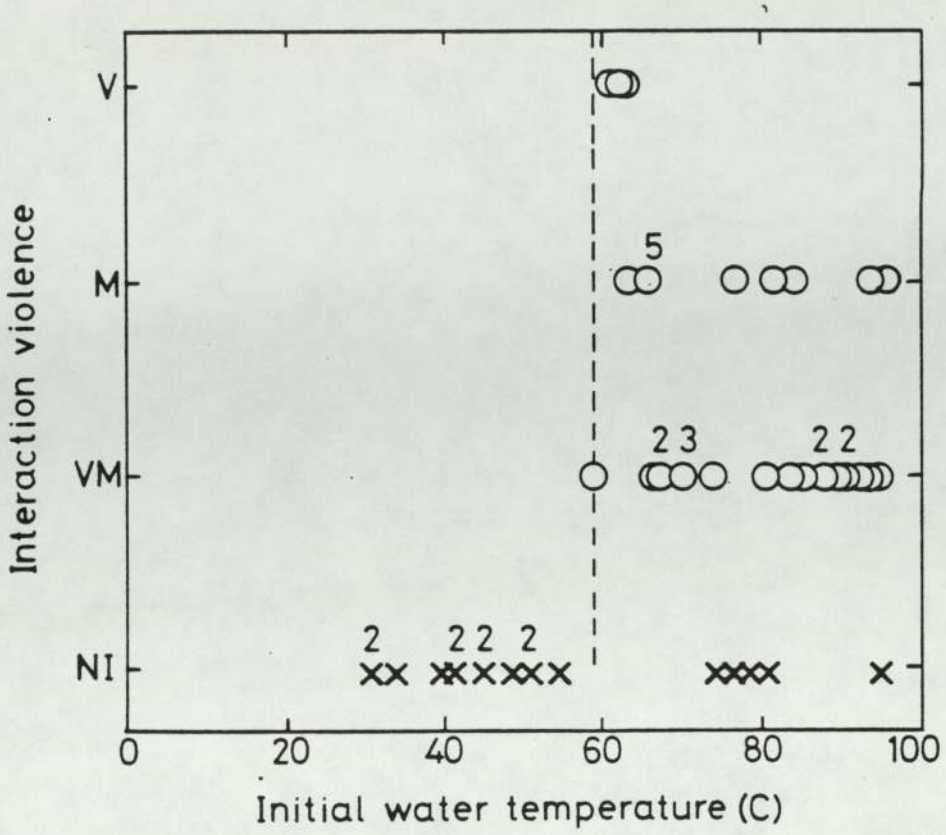

Fig 6.6.1 WATER-ISCEON INTERACTION VIOLENCE AS A FUNCTION OF INITIAL WATER TEMPERATURE

CHAPTER 7 EXPERIMENTAL RESULTS III:

HEAT TRANSFER AND VAPOUR STABILITY STUDIES

7.1 Introduction

Of the two ancillary experiments most work was done with film boiling on a stainless steel sphere. About 60 experiments were performed, the results of which are presented in section 7.2. It is shown in chapter 8 that a simple film boiling model for these experiments, when applied to the idealised case of spherical tin drops in water, might explain some features of the tin-water TIZ.

Only a few experiments were performed with spark bubbles, but the results do indicate that bubble collapse at high coolant temperatures, with jetting, is unlikely to occur. Such a model can therefore not explain the water-into-isceon drop experiments of section 5.2 where interactions were observed at the isceon saturation temperature.

7.2 Sphere film boiling experiments

General film description. Visual and photographic evidence have established three broad categories of behaviour of the sphere when quenched. In the first, at low sphere and water temperatures, nucleate boiling occurred immediately on quenching and there was no stable vapour layer formation anywhere on the sphere surface.

In the second category, at higher sphere and coolant temperatures, the sphere was immediately enveloped by a vapour film. For water temperatures above 333 K (60 C) the ceramic support tube was also surrounded by vapour. This collapsed within about two seconds, the collapse front moving down the tube towards the sphere like a burning fuse. Its collapse did not appear to affect the stability of vapour surrounding the sphere. The vapour generated over the sphere surface collected at the top of the sphere, near the base of the ceramic support tube, where bubbles pulsated and broke away. Below this perturbed area the vapour film, shimmering at first, stabilised within a few seconds and became very uniform and "rock steady". This stage in the process, shown in the photograph of figure 7.2.1(a), lasted for up to 30 seconds depending on the bulk coolant temperature, after which time the film broke down. Between entry into the water and vapour layer collapse the rate of vapour generation, judged by the rate of bubble departure, was high at first but became slower, almost ceasing in some cases, before increasing again as the breakdown was approached.

The break-down started usually at a well defined point on the surface, and usually near the top, where the vapour film was perturbed by the departing bubbles at the junction with the support tube. The vapour layer had, presumably, thinned sufficiently near this point for the perturbations to cause contact between the sphere surface and liquid coolant. The collapse front then proceeded to spread from the point of collapse in all directions, eventually to engulf the whole sphere surface. The speed of collapse depended on water temperature, being about 0.5 m/s at 319 K (46 C) and 1 m/s at 339 K (66 C). Throughout the collapse process the vapour layer ahead of the collapse front was essentially unperturbed by the front and remained a thin film close to the sphere surface (see figure 7.2.1(b)).

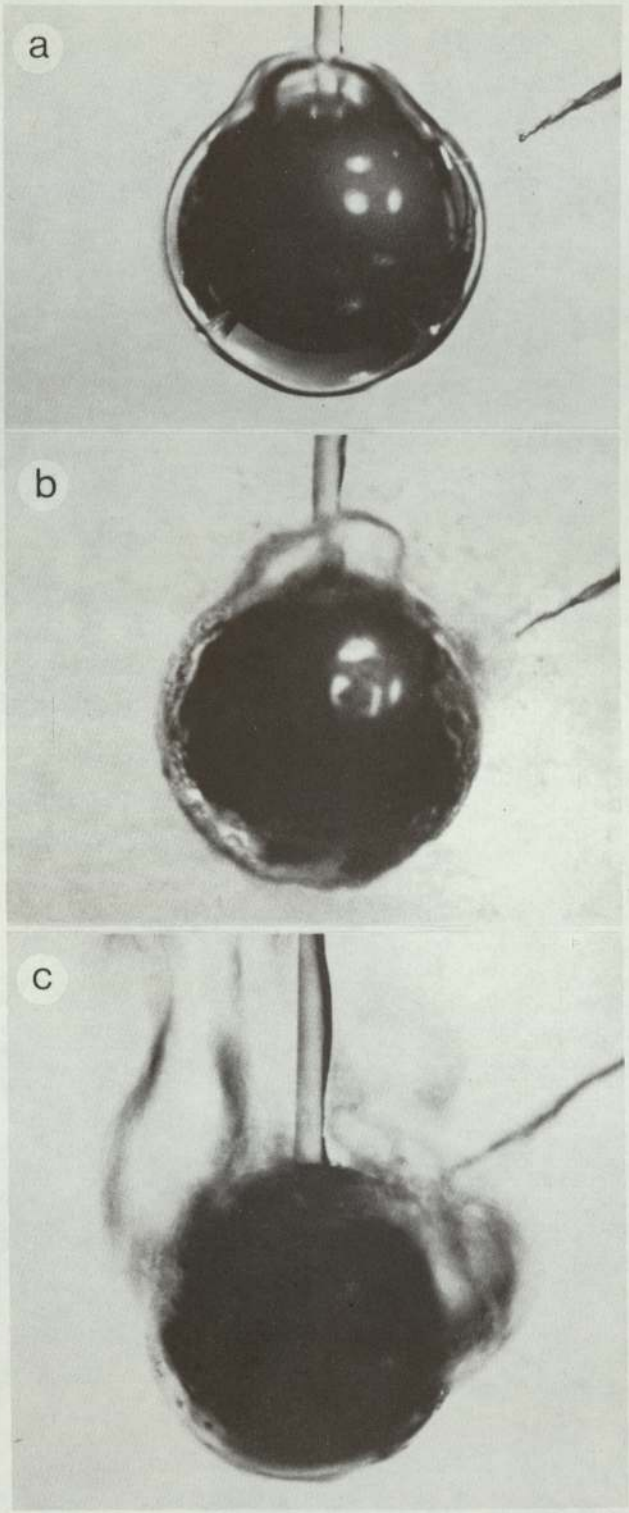

Fig 7.2.1 SELECTED PHOTOGRAPHS OF VAPOUR FILMS ON QUENCHED SPHERES

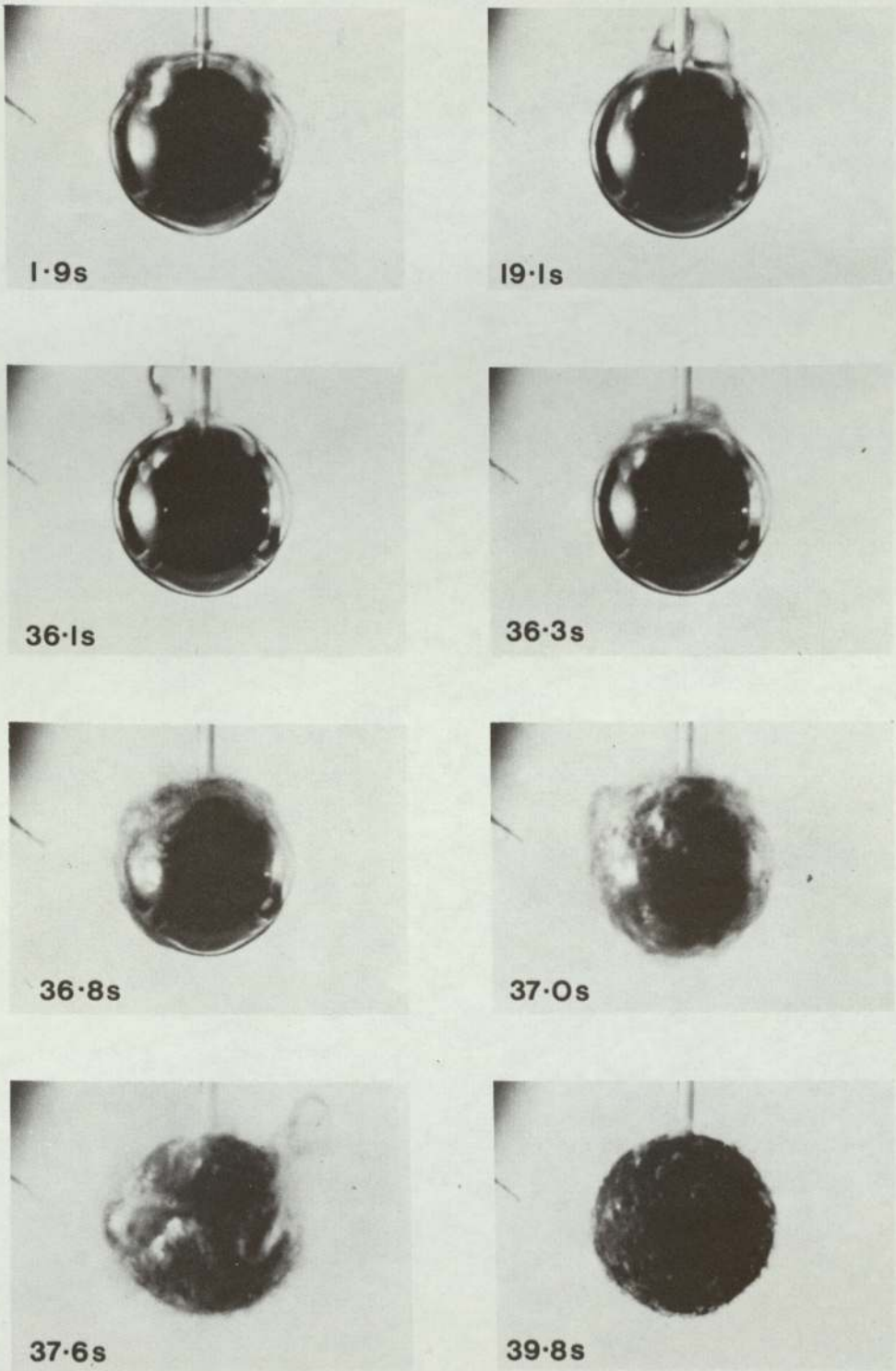

Fig 7.2.2 CINE FILM SEQUENCE OF A SPHERE AT 1223 K

QUENCHED IN WATER AT 341 K

The film in figure 7.2.1(a) appears to be much thicker than it really is because of the spherical lens action of the vapour cavity which appears to diminish the size of the sphere within it. A crude estimate from cine film suggests that the film thickness for a sphere initially at 1223 K quenched in water at 341 K is 0.35 mm or less.

Following collapse, nucleate boiling occurred with the surface generating bubbles of about 2 mm diameter which travelled quickly round the sphere surface to the top. The density and speed of escape of the bubbles decreased rapidly as the sphere temperature fell to the coolant boiling point.

Figure 7.2.2 shows a complete collapse sequence in which all the characteristics are visible. The initial sphere and water temperatures were 1223 K (950 C) and 341 K (68 C). Vapour layer collapse started near the support tube 36.3 seconds after immersion.

In the third category, for water temperatures greater than 343 K (70 C), a stable vapour film was formed as before but the breakdown was a gentle process with very little sound emitted and no propagating collapse front. On collapse the vapour layer appeared to unfold itself from around the sphere and disperse into the coolant above the sphere in the way shown in figure 7.2.1(c). The vapour was not held close to the sphere surface, or confined to leave the sphere near the support tube.

Laser shadowgraphy. Figure 7.2.3 shows two frames from a shadowgraph cine film which shows the turbulent mixing of cold water with that heated by the sphere. Shadowgraphy surprisingly showed no disturbance and mixing in the coolant close to the sphere surface (figure 7.2.3(a))

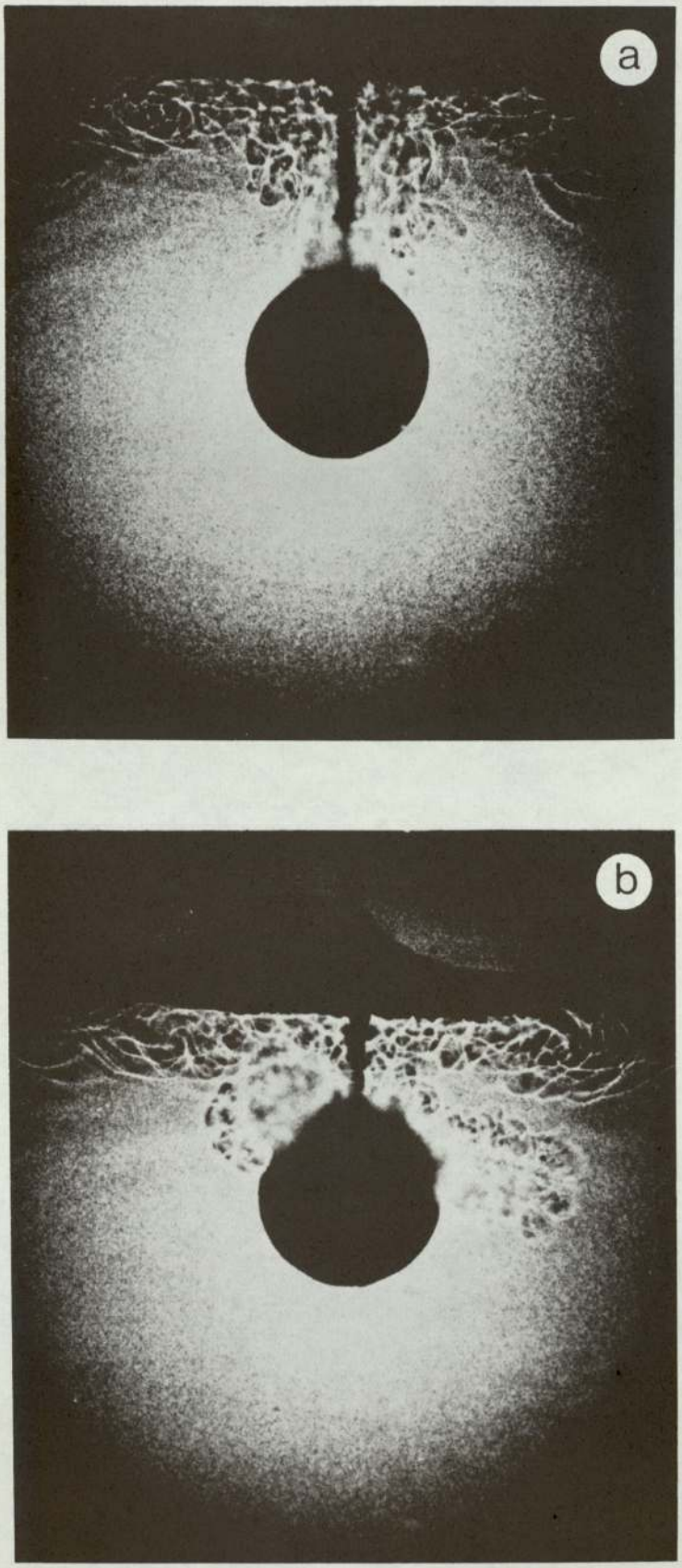

Fig 7.2.3 SELECTED SHADOWGRAPHS OF A QUENCHED SPHERE

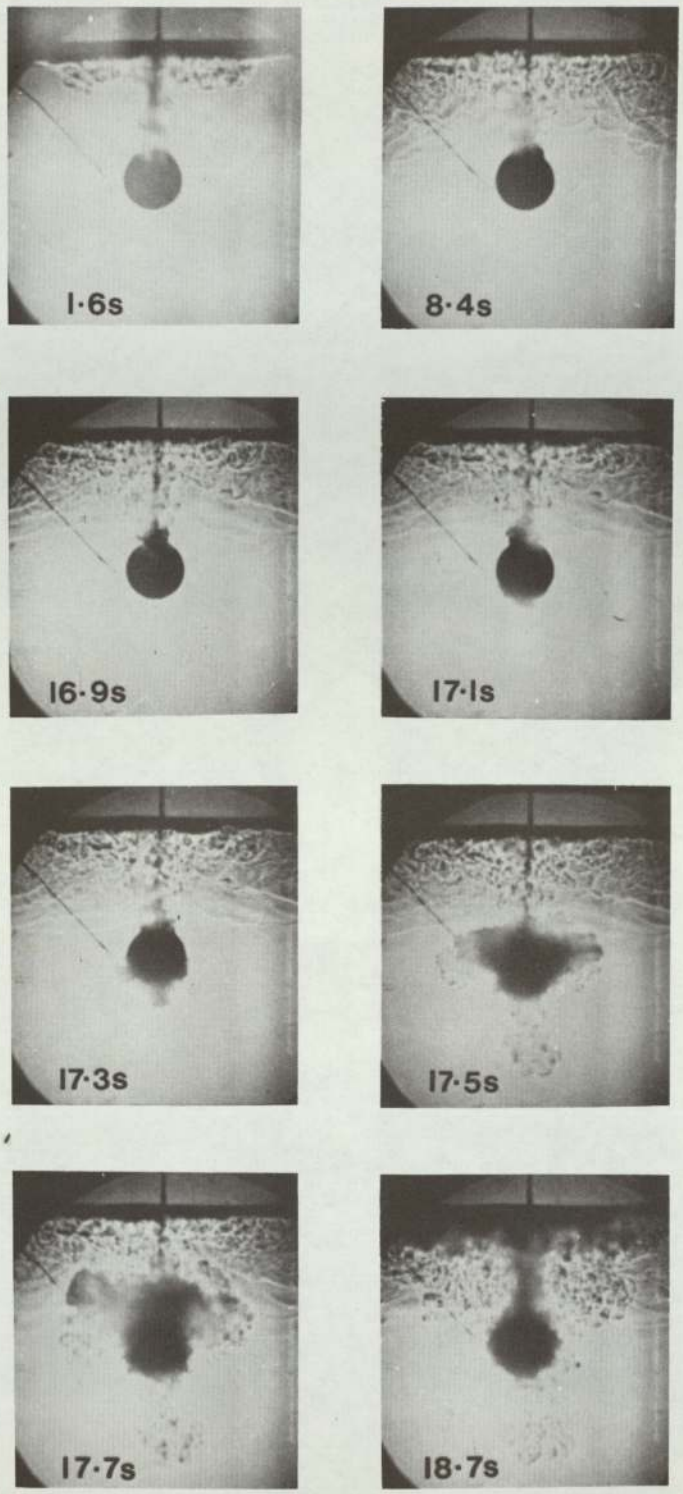

Fig 7.2.4 SHADOWGRAPH SEQUENCE OF A SPHERE AT 1265 K QUENCHED IN WATER AT 310 K

except near the junction with the support tube. Heated coolant rose from the top of the sphere, up the support tube, and spread out across the water surface. As time progressed the thickness of the surface mixing layer increased, penetrating down towards the sphere.

At the moment of vapour film collapse, (on the left and right hand sides of the sphere in figure 7.2.3(b), although occasionally it could be underneath the sphere), a jet of hot coolant and/or vapour was ejected from the point of collapse to penetrate deep into the coolant (up to 30 mm). Turbulent mixing then took place all round the sphere as the collapse front propagated. A complete shadowgraph sequence is shown in figure 7.2.4.

Temperature-time curves. In figure 7.2.5 two temperature-time curves are shown which characterise the quenching process. In the first, where no vapour blanket could be identified visually, the surface temperature fell quickly, within 4 seconds in the example of figure 7.2.5(a), to the bulk water temperature.

Where vapour blanketting was seen to occur the rate of cooling was initially slower. A typical temperature-time trace for this case is shown in figure 7.2.5(b) for a sphere initially at 1273 K quenched in water at 327 K (54 C). The surface temperature dropped by only 30 degrees during passage through argon to the water surface where the cooling rate increased on immersion. For about 30 seconds the sphere cooled under film boiling until breakdown occurred and the contact with water increased the heat transfer rate dramatically with a corresponding rapid, almost vertical, fall in surface temperature, down to the bulk water temperature. The length of the film boiling regime was a function of initial sphere and water temperature, as described

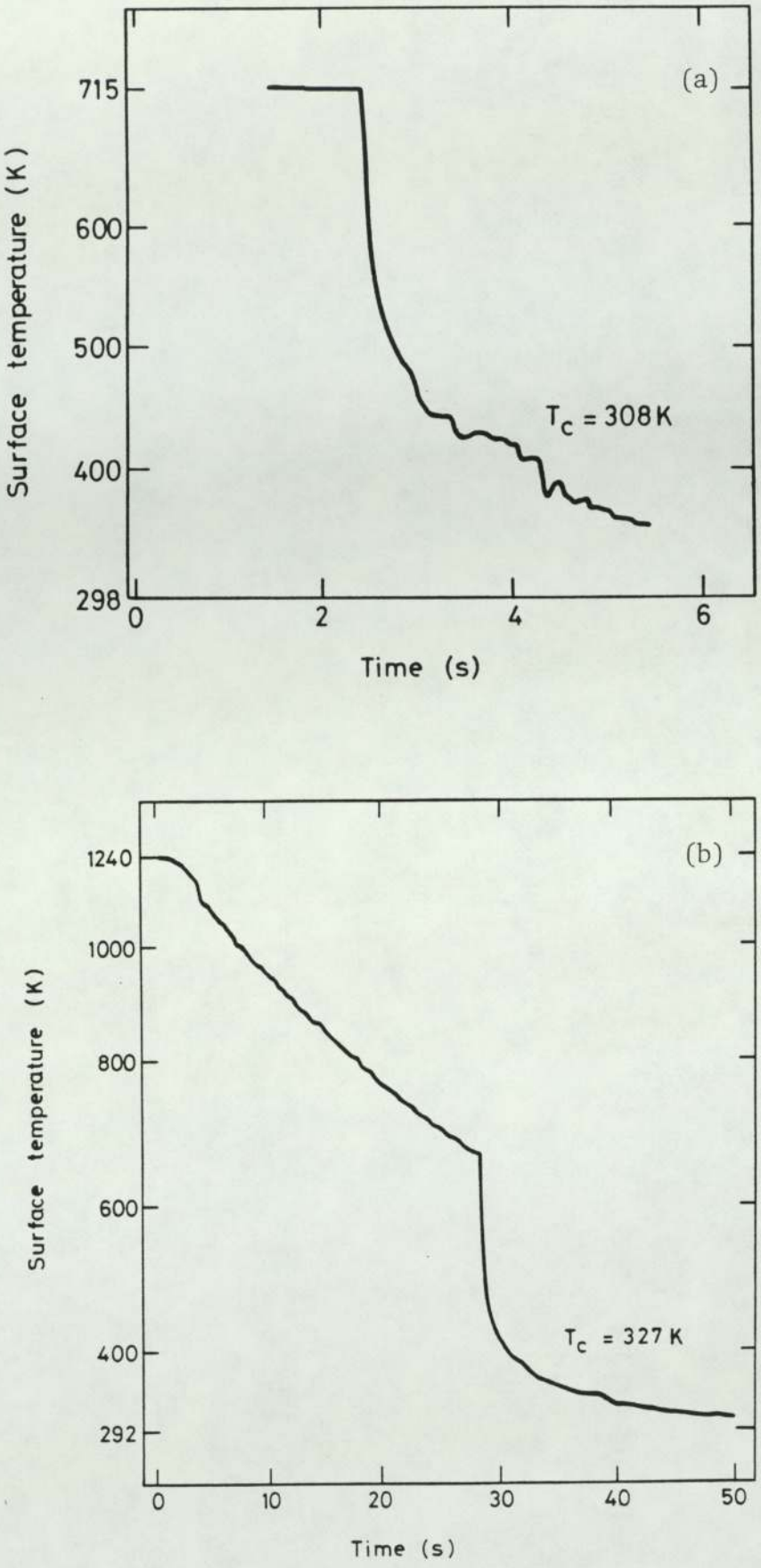

Fig 7.2.5 TEMPERATURE-TIME TRACES FOR QUENCHED SPHERES

below.

Cooling rate measurements. The rate at which the sphere cooled was found from the gradients of the temperature-time curves, and was shown to be a function of the water subcooling, T_{sub}, and the instantaneous value of the sphere surface temperature, T_s. Cooling rates, as a function of subcooling, are shown in figure 7.2.6. Curves (a) and (b) give measurements at surface temperatures of 1000 K and 750 K respectively (the initial sphere temperature ranging from 833 to 1288 K). Least square fits to the data of figure 7.2.6 give:

$$\left(\frac{dT_s}{dt}\right)_{1000} = 21.563 \exp(0.00724\ T_{sub})$$

$$\left(\frac{dT_s}{dt}\right)_{750} = 10.753 \exp(0.00965\ T_{sub})$$

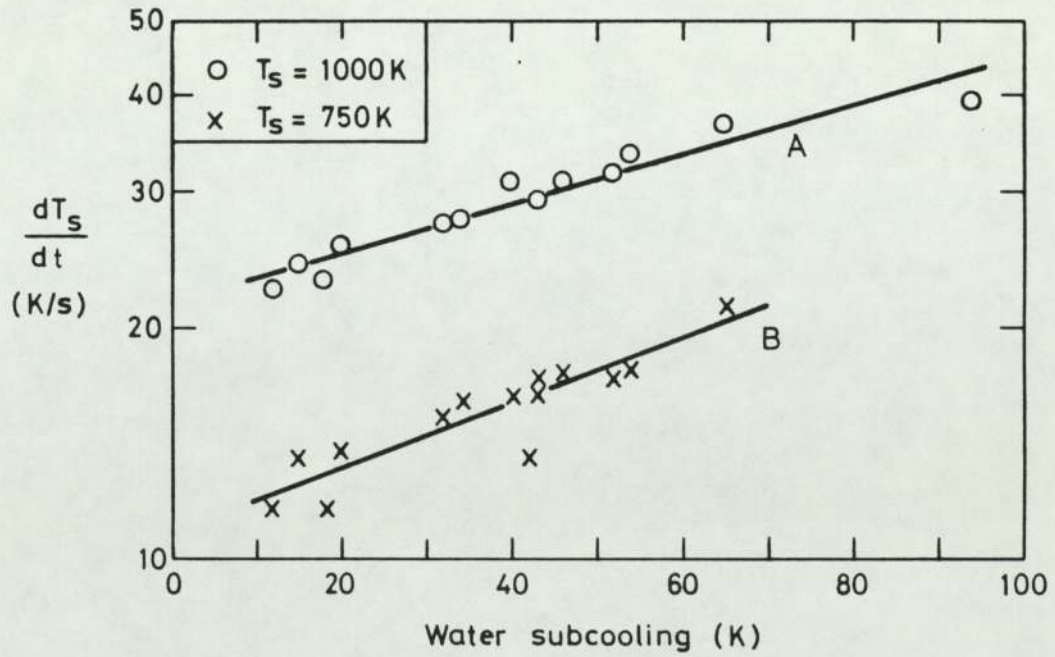

Fig 7.2.6 SPHERE COOLING RATE AS A FUNCTION OF SURFACE TEMPERATURE AND SUBCOOLING

Derived boiling curves. To derive boiling curves the simplest assumption that can be made is that the sphere cools isothermally with the temperature-time relationship given by the surface thermocouple measurements. For a sphere of mass m_s, radius r_s and specific heat capacity c_s the energy lost in cooling through dT degrees is given by

$$m_s c_s \, dT \qquad \text{joules}$$

If this is lost in time dt then the heat flux is

$$h = 0.33 r_s c_s \rho_s dT/dt \qquad \text{watts/m}^2$$

dT/dt is time dependent and given by the gradient, dT_s/dt, of the temperature time curves.

Not now.

Instantaneous heat fluxes plotted against the sphere surface temperature above the coolant saturation temperature ($T_s - T_{sat}$) gives boiling curves such as those in figure 7.2.7 for water at 327 K (54 C) and 358 K (85 C) respectively. The three regions of nucleate, film and transition boiling (-ve slope region) are reflected in the figure. At the lower coolant temperature the transition region was very sharp with the critical or burn-out heat flux and minimum film boiling point being very close. At higher coolant temperatures the critical heat flux was lowered in value and occurred at a lower surface temperature than T_{min}.

Establishment and breakdown of vapour films. Fig 7.2.8 shows the initial quench conditions plotted on a sphere temperature-water temperature graph (similar to a TIZ plot). Those experiments in which the sphere was seen to be completely vapour blanketted are indicated by open circles. The crosses are those for which the cooling curves

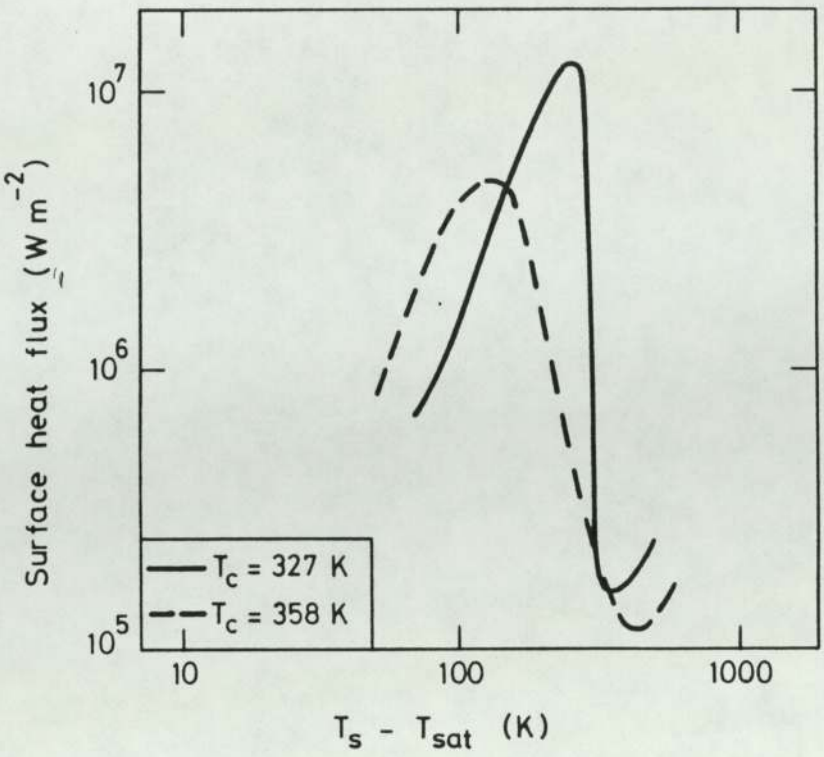

Fig 7.2.7 BOILING CURVES FOR QUENCHED SPHERES

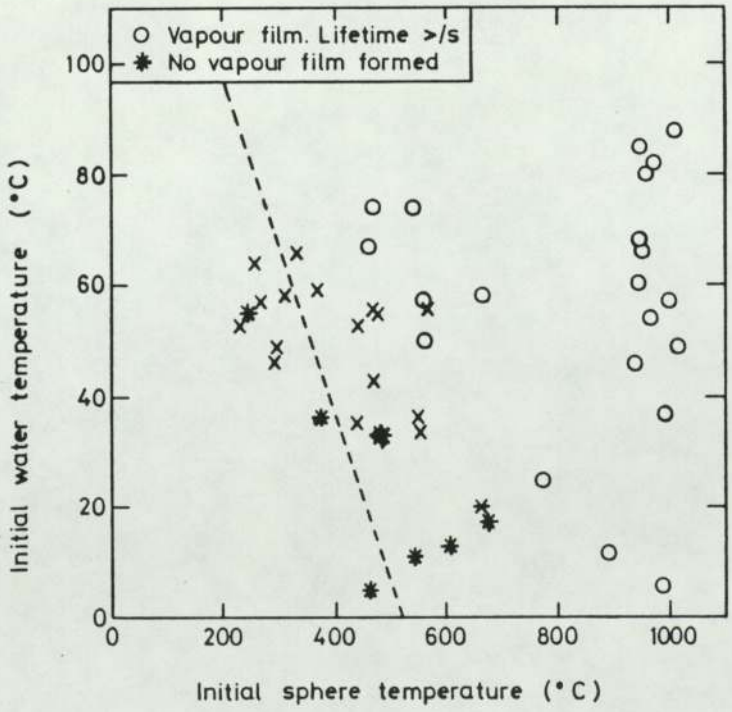

Fig 7.2.8 TEMPERATURE CONDITIONS FOR ESTABLISHING VAPOUR BLANKETTING

indicate a short-lived vapour film. Only for a few experiments did the cooling curves fail to indicate vapour coverage of the thermocouple, these being indicated by a *.

The temperature of the sphere surface at the time of collapse, which may be equated to the minimum film boiling temperature, is shown in figure 7.2.9 for the confirmed vapour blanketted experiments. The

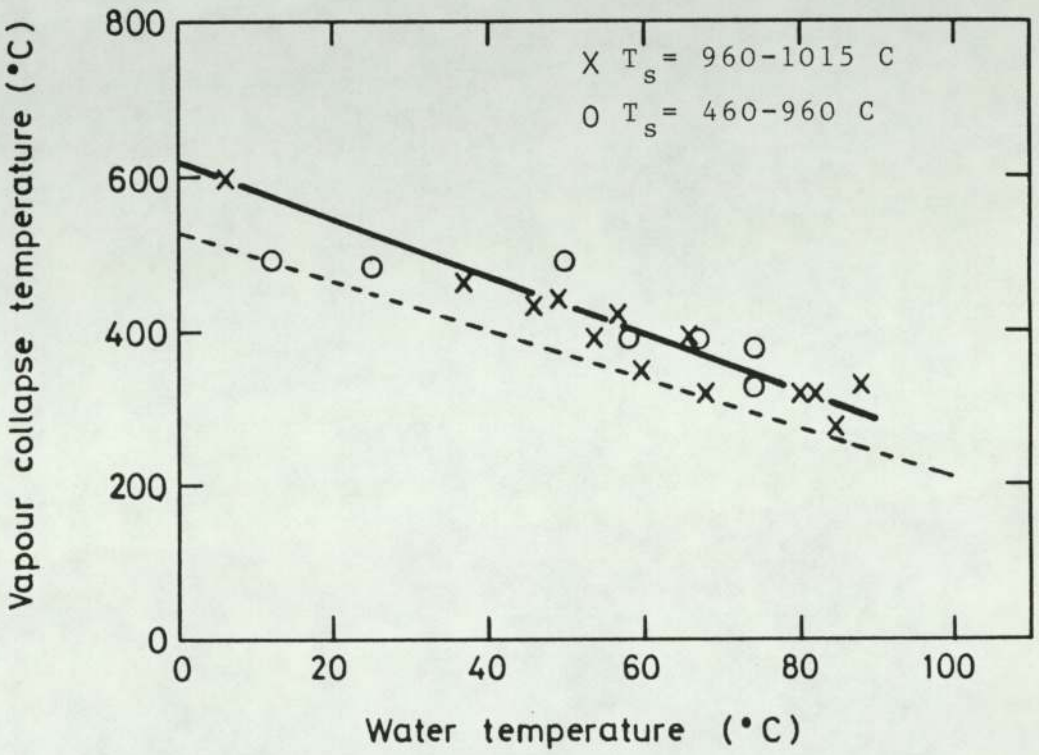

Fig 7.2.9 VAPOUR COLLAPSE TEMPERATURE AS A FUNCTION OF WATER SUBCOOLING

crosses indicate initial sphere temperatures of 960 C - 1015 C and the mean curve through these is given by the full line on the diagram. The other points indicate initial temperatures of 460 C - 960 C. Clearly, the minimum film boiling point is a linear function of subcooling and appears to be independent of the initial sphere temperature. The dotted line on figure 7.2.9 indicates the envelope of the lowest

observed values of breakdown temperature, and this line is also shown on figure 7.2.8. The position of this line might indicate that, at least at low water temperatures, the initial sphere temperature required to set up a vapour film is in excess of that at which the film, once established, would collapse.

The time to vapour collapse increased linearly with water temperature, as shown by figure 7.2.10 for initial sphere temperatures between 960 C and 1015 C. The vapour collapse temperature was independent of initial sphere temperature.

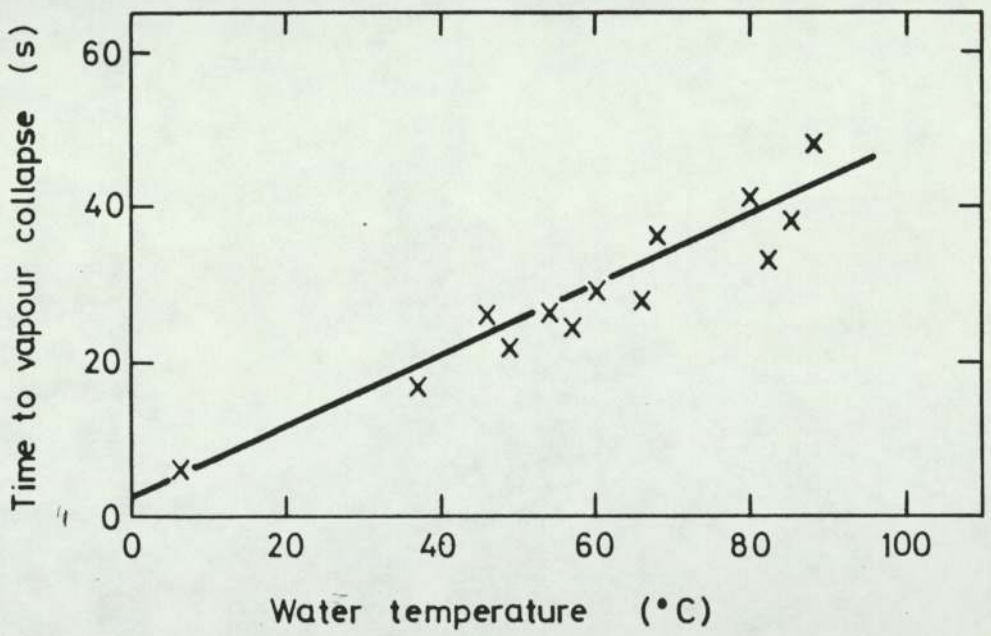

Fig 7.2.10 THE TIME TO VAPOUR COLLAPSE AS A FUNCTION OF SUBCOOLING

The effect of oxide coating. The effect of the oxide coating has not been systematically studied. Its presence was kept to a minimum. Spot tests, however, did indicate that when allowed to build up on the sphere, film breakdown temperatures were raised and the corresponding

lifetimes decreased.

7.3 Bubble growth and collapse experiments

Discharge characteristics. Figure 7.3.1 shows a sequence of computer generated curves, the first being the measured voltage across the spark gap, figure 7.3.1(a). The trigger pulse was applied at time zero and there was a 15 microsecond delay before the voltage was switched on to the gap. The gap voltage then remained constant for a time which varied up to 400 microseconds, the "hold-off" time, until breakdown occurred. A damped oscillatory discharge followed which extinguished in about 100 microseconds.

A similarly damped oscillatory curve (b) was obtained for dI/dT which jumped instantaneously to its peak value at breakdown. Taking the current as zero at the end of the discharge and integrating in reverse, generated the current-time waveform of figure 7.3.1(c).

The current flowing at the end of each time interval was multiplied by the corresponding gap voltage to derive the instantaneous values of power being fed into the discharge (see figure 7.3.1(d)). Integration of this by linear interpolation generated, with zero power at the beginning of the discharge, the energy fed to the spark as a function of time figure 7.3.1(e) and the total spark energy $E_s = \int_0^\infty I(t).V(t)\ dt$. In the example of figure 7.3.1 the spark energy was 50 J which was 61 per cent of the available bank energy ($E_b = 0.5CV_b^2$), and was deposited in the gap within 100 microseconds.

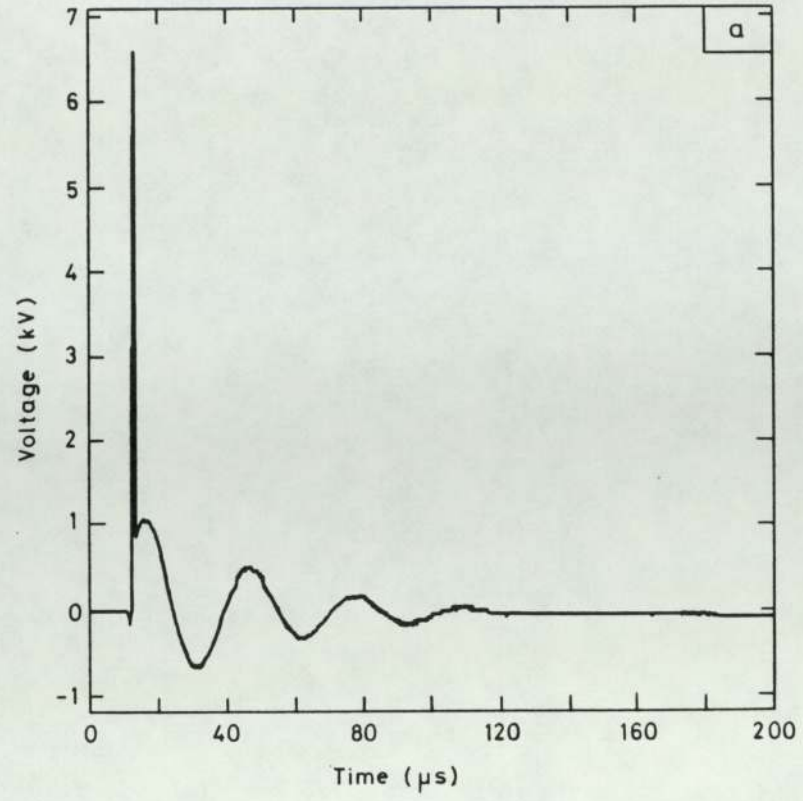

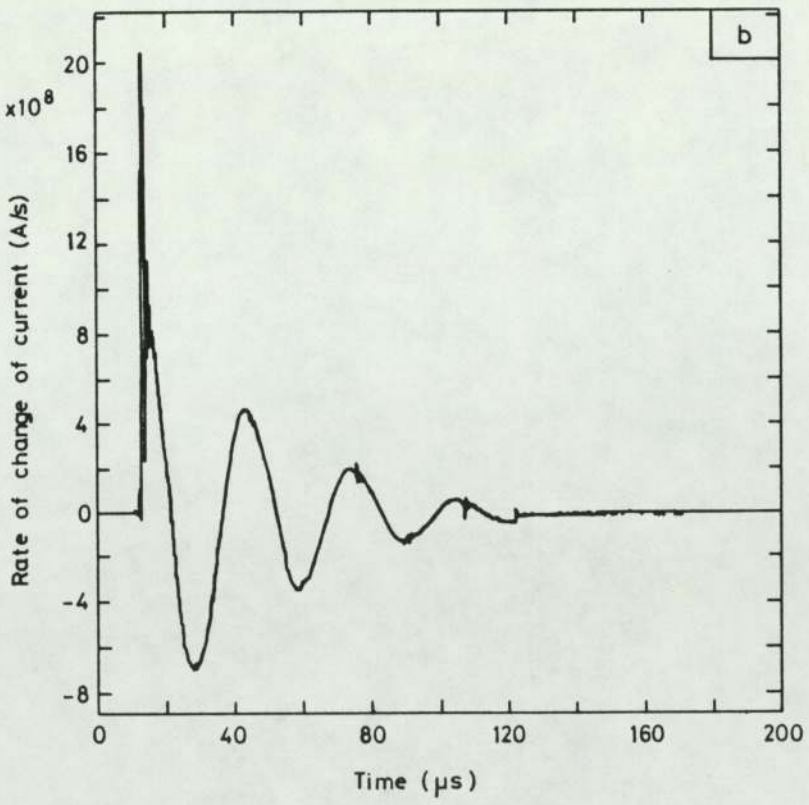

Fig 7.3.1 SET OF COMPUTER GENERATED CURVES

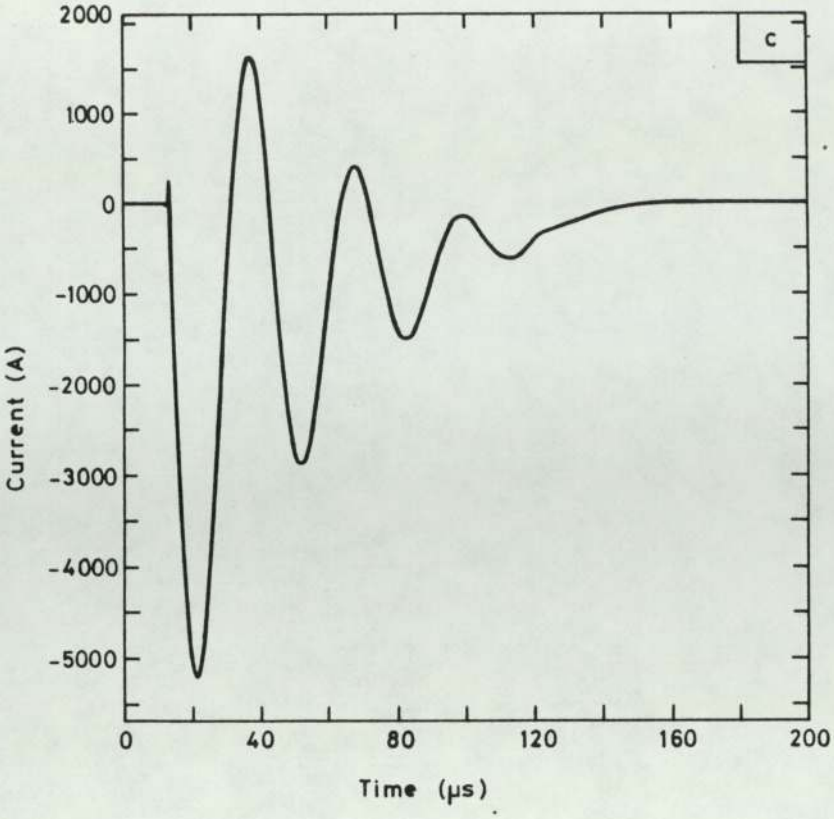

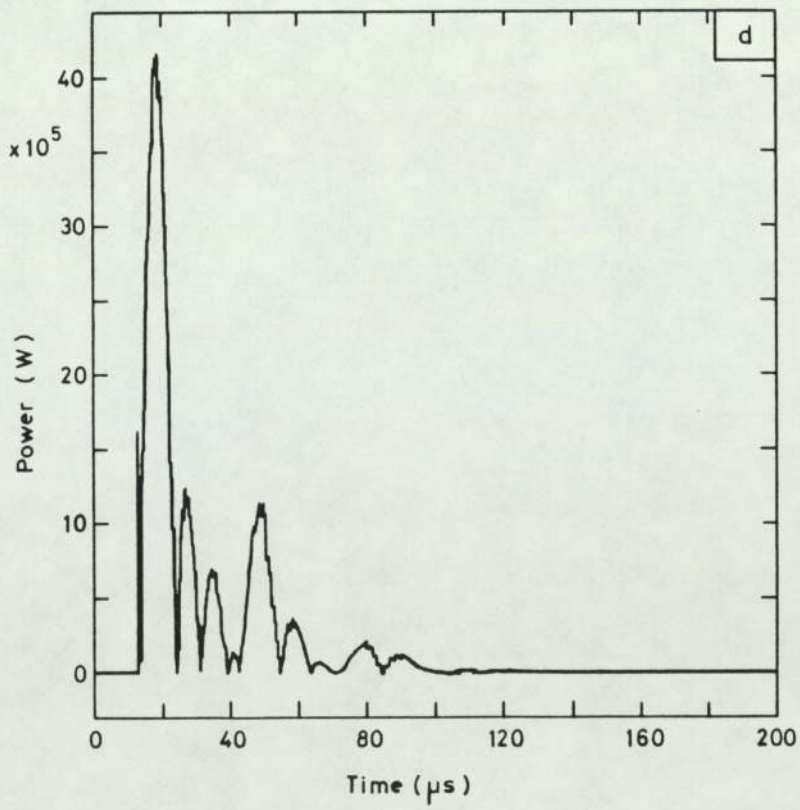

Fig 7.3.1 continued

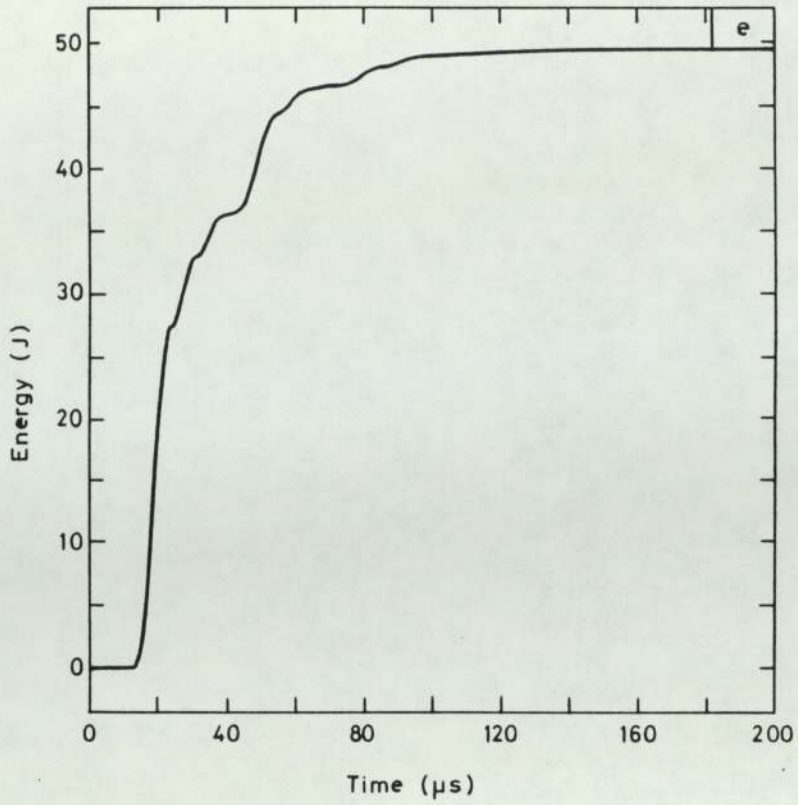

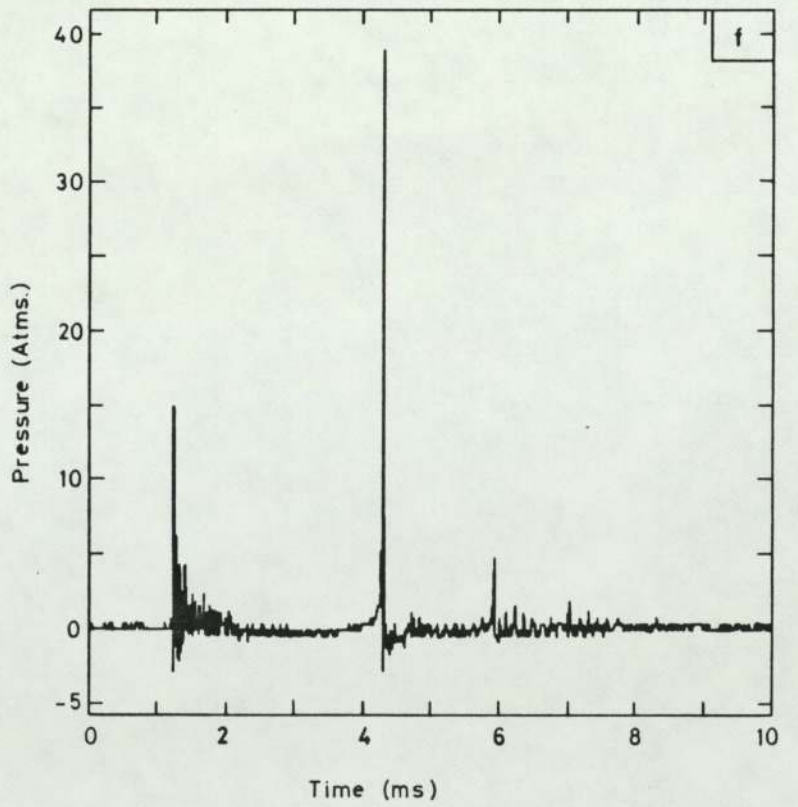

Fig 7.3.1 continued

A sensitivity study was carried out to find the effect of a 400 nanosecond displacement in V(t) with respect to dI/dT due to triggering jitter. This is twice the maximum possible error and was found to give less than 4 per cent error in E_s.

General film description. Electrical breakdown in the gap between the electrodes produced a flash of light lasting less than one frame interval but of such intensity as to momentarily overexpose the cine film if the emission did not occur between frames. This intense light, impossibility of synchronisation and the low framing rate combined to obscure the very early stages of the bubble, which could first be clearly distinguished only after reaching a diameter of about 3 mm. Bubble growth following the deposition of electrical energy was subsequently recorded.

The heated gas sphere initially expanded under the influence of its excess pressure over the surroundings, the inertia of radially outward flowing water maintaining the expansion even when the excess pressure had fallen to zero. Motion was finally arrested, when the bubble had reached its maximum diameter, by the pressure defect, and the bubble began to collapse. Loss of energy from the plasma sphere through mechanical work done on the coolant, the radiation of light and heat, thermal conduction across the bubble surface and condensation at the surface, rapidly collapsed the bubble. In the latter stages of collapse the remaining plasma and non-condensible gas was again compressed by the inertia this time of radially inward flowing coolant. It reached a minimum diameter from which it "bounced" to regrow and collapse several times, each bubble being smaller than the one preceding it.

At low coolant temperatures the bubbles could collapse, bounce, grow and collapse again several times before finally the remaining non-condensible gas was dissipated as tiny bubbles into the coolant. The first growth and collapse was centred on the electrode gap, but buoyancy ensured that subsequent bubbles drifted upwards. Similar films have been described by Kling [151].

At high coolant temperatures only one large bubble was produced, which, having reached maximum diameter, started to collapse. The collapse was suddenly halted, as if the bubble wall had come up against a solid core, and the bubble surface developed bumps or nodules rather like a raspberry and broke into a myriad of tiny bubbles dispersed into the coolant.

Bubble radius-time measurements. Bubble radii as a function of time were measured from projected cine film. Figure 7.3.2 shows two typical radius-time histories for low and high water temperatures. Only representative error bars are shown at selected points on the curves. Many more points, not shown, being used to define the curve. The dashed portions, at low radii, are extrapolations.

As the coolant temperature was raised the bubble maximum radius, growth and collapse times increased, while the number of bounces decreased. Between 335 K (62 C) and 348 K (75 C) only one bubble was observed to form. It grew and collapsed down to a few mm radius before disintegrating. At 360 K (87 C), however, bubbles grew but did not collapse completely, as described above and illustrated in figure 7.3.2.

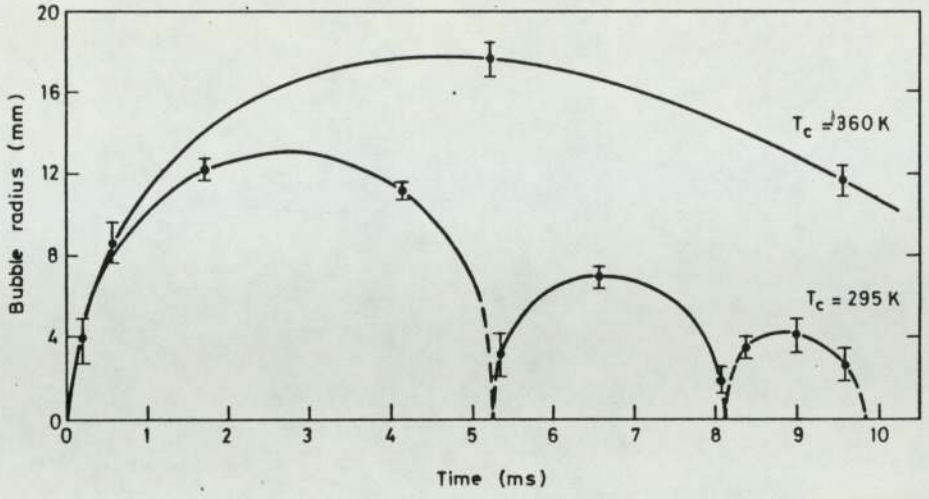

Fig 7.3.2 SPARK BUBBLE RADII AS A FUNCTION OF TIME AND WATER TEMPERATURE

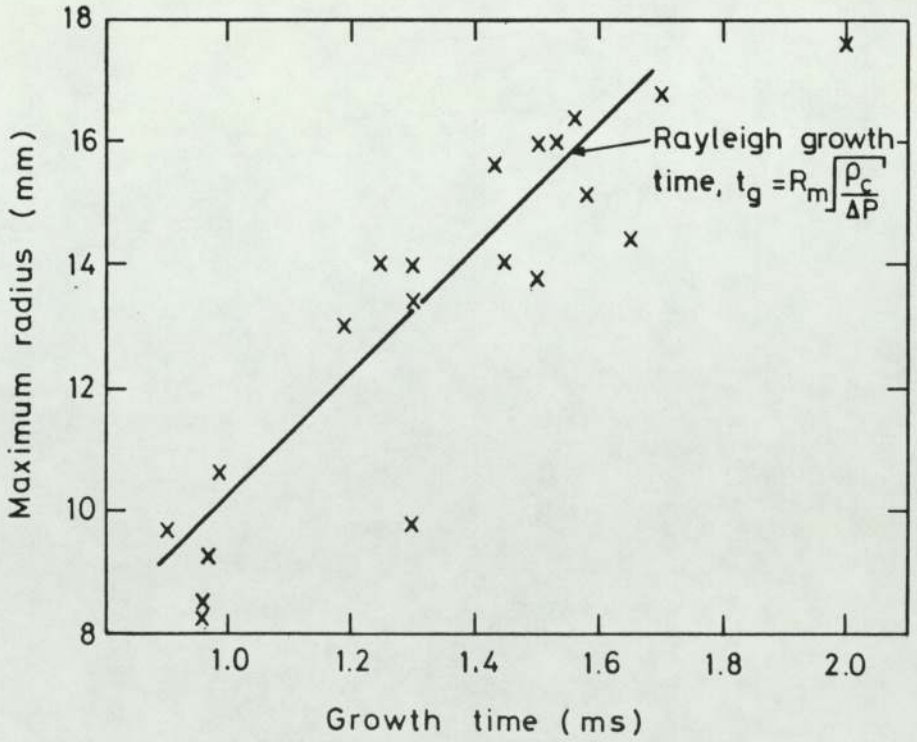

Fig 7.3.3 SPARK BUBBLE GROWTH TIMES AS A FUNCTION OF MAXIMUM RADIUS

What use was made of
these bubble-bounce data?

The bubble growth times are shown in figure 7.3.3 and increased with the maximum radius of the bubble, following closely the classical growth time given by the Rayleigh formula (see section 2.10)

Pressure measurements. The pressure-time history in the water showed a series of narrow pressure spikes separated by well-defined periods of time (see, for example, figure 7.3.1(f)). The first peak occurred when the spark gap was fired, time zero, and had the characteristics of a shock wave for which there was a sharp pressure rise, a discontinuity, on arrival of the shock wave at the transducer, followed by an exponential-like decay to hydrostatic pressure in about 1 ms. During this time the gas sphere, or bubble, was expanding and its pressure dropping. In the example of figure 7.3.1 the maximum bubble radius was reached in about 2.5 ms and the bubble commenced to contract, the inertia of in-rushing coolant compressing the permanent gas and uncondensed water vapour. The bubble bounced and the process repeated. At minimum volume very narrow acoustic pressure spikes were generated characterised by slower rise times, a much sharper decay and very much narrower pulse width. The first bounce produced a peak pressure over twice as big as that in the shock wave while the size of the pressures from the second and subsequent bounces was very much reduced.

CHAPTER 8 INTERPRETATION OF EXPERIMENTAL RESULTS

8.1 Introduction

It is the object of this chapter to interpret the main features of the vapour explosion experiments, particularly the position of the TIZ boundaries. An explanation is required for the onset of fragmentation interactions, the onset of violent interactions, and the upper temperature cut-off. It is shown that the latter two phenomena might be explained by some of the characteristics of film boiling, whilst the former corresponds closely to the interface superheat criterion in the systems studied.

Section 8.2 begins with a brief consideration of theoretical analyses of film boiling before developing a simple film boiling model for the quenched sphere experiments in section 8.3. This model is then used in sections 8.4 and 8.5 to interpret first the quenched sphere experiments and then the vapour explosion experiments. Section 8.6 then considers briefly the implications of interface temperature criteria for two other systems of interest to the nuclear industry, namely the probability of urania-sodium and urania-stainless steel interactions.

8.2 Film boiling theory

A review of film boiling is given by Jordan [150], where the success in predicting heat transfer coefficients is attributed to the orderliness of film boiling when compared to the transition and nucleate boiling

regions. Vapour is produced at the liquid-vapour interface, and therefore is influenced only by the hot surface temperature and not by the nature of the surface. Theoretical analyses generally assume that the vapour flows past the hot surface without turbulence. The heat transfer across the vapour film and the subsequent vapour production are then assumed to be the controlling mechanisms. Bromley [see Jordan] has shown that the data for boiling from horizontal cylinders to saturated coolant is well correlated by a laminar flow model. The assumptions of the Bromley model seem to form the basis of most others and can be summarised as follows:

(i) The vapour film is thin compared to the cylinder diameter.

(ii) There is no restraint on vapour removal.

(iii) Energy transport through the film is by conduction and radiation only.

(iv) Vapour flow is laminar, and controlled only by buoyancy and shear forces.

(v) The vapour-liquid interface is smooth (except where vapour is removed).

(vi) The vapour removal region covers a small area compared to the total surface area of the body.

(vii) Energy absorbed in evaporating coolant is very much greater than that used in raising the vapour temperature.

Reynolds has already explained the sloping boundary
Why was he wrong?
What is the distinction between thick + thin film boiling

(viii) Changes in the vapour momentum and kinetic energy on moving around the cylinder are negligible.

(ix) The vapour pressure is equal to the pressure in the liquid just across the interface (surface tension effects are negligible).

(x) The cylinder surface is isothermal.

(xi) The coolant is at its saturation temperature.

(xii) The physical properties of the vapour may be evaluated at the mean vapour temperature.

The Bromley theory was a good fit for $0.8 \leq \lambda_c/D \leq 8.0$ where λ_c is the Taylor critical wavelength, and D the cylinder diameter. For very small cylinders assumption (i) is not valid, whilst at large diameters the vapour removal mechanism becomes dominant. The theory has been modified by several authors (see Jordan's review) to provide a correlation over a larger range of λ_c/D and for data in sub-cooled coolant.

The success of the Bromley theory has prompted other authors to similar laminar flow analyses of film boiling on spheres [152,153] and Reynolds [153] has explained the sloping boundary of the tin-water TIZ on the basis of a simple laminar flow model in which the position of the boundary marks the transition from a thin to a thick film boiling region. In the latter, cooling times are very long and some suppression mechanism is assumed to act before vapour breakdown and triggering can occur. For example, the hot liquid surface may solidify

$$\mu \frac{d^2v}{dx^2} = \frac{dp}{dy} = \text{const} - C$$

$v = 0$ when $x = 0$, $x = \delta$

$$v = a + bx + \frac{c}{2\mu}x^2 \qquad a = 0 \qquad b\delta + \frac{c}{2\mu}\delta^2 = 0$$

$$b = -\frac{c\delta}{2\mu}$$

$$v = \frac{c}{2\mu}(x^2 - \delta x)$$

$$v_v \delta = \int_0^\delta v\,dx = \frac{c}{2\mu}\int_0^\delta (x^2 - \delta x)\,dx = \frac{c}{2\mu}\left(\frac{\delta^3}{3} - \frac{\delta^3}{2}\right)$$

$$v_v = \frac{c\delta^2}{12\mu}$$

$$c = \frac{dp}{dy} = (\rho_l - \rho_v)g \simeq \rho_l g \qquad \therefore v_v = \frac{\rho_l g \delta^2}{12\mu} = \frac{\rho_l g}{12\nu_l}\delta^2$$

Eqn 8.1 assumes no shear at vapour/liquid interface
True for vertical flow only

Wilke assumes the liquid flow to be inviscid, + the vapour to have the same pressure as the liquid
(ANL-7296, p 76) - gravity unimportant.
- moving sphere

or the container base may be reached.

In all these theories the vapour flow velocity, v_v, is proportional to δ or δ^2 where δ is the vapour layer thickness. Reynolds derived an expression for v_v by equating the viscous forces in the vapour to the drop weight to give :

$$v_v = \left(\frac{2\rho_h g}{3\nu_v \rho_v}\right)\delta^2 \qquad (8.1)$$

which was then used to eliminate v_v in a simple energy balance equation, in which the energy conducted across the vapour layer was equated to the sum of that required to produce the vapour and that removed by convection/conduction in the coolant.

In the quench experiment the temperature-time measurements enabled the vapour flow velocity to be determined from the experiment by equating the rate at which the sphere loses energy, to the sum of the energy flux required to increase the vapour temperature and that conducted across the vapour layer. v_v was found to decrease as δ increased, in contradiction to the common assumption. The correct trend of the $v_v - \delta$ relationship was derived by Witte [152] in his analysis by equating the pressure drop driving the flow, derived from the Bernoulli equation, to that generated by the viscous forces in the vapour layer. However, this would seem to violate the assumption in the derivation of Bernoulli's equation, that the fluid flow is inviscid. Bromley's laminar flow theory was similarly unsuccessful in predicting the heat flux from vertical tubes and plates where the experimentally observed heat transfer increases with the vapour flow Reynolds number. The theory suggests that it should decrease. This prompted Hsu and Westwater [see Jordan] to develop a turbulent flow model to explain

Why no bdy layer in vapour at liquid surface?

these results. The following is an adaptation of the Hsu and Westwater model for quenched sphere data.

8.3 A simple sphere film boiling model

It is assumed here that the rate at which the sphere cools, for a given subcooling, depends only on the instantaneous value of sphere surface temperature, and also that the sphere cools isothermally. The latter is a valid assumption for good metallic conductors. A simple quasi-steady state model may therefore be used in which the vapour film thickness is assumed to be determined by the instantaneous system temperatures, and not on past temperature history.

The flow pattern proposed by Hsu and Westwater, adapted to spherical geometry and simplified for the present purpose, is summarised in figure 8.3.1. The sphere temperature, T_s, decreases with time, but is independent of radius. In the vapour layer, the temperature falls from the sphere surface temperature to the coolant saturation temperature, T_{sat}, over the thickness δ_1 of a laminar flow sublayer, and remains at T_{sat} throughout the outer turbulent layer of thickness $(\delta_2 - \delta_1)$. Within the turbulent layer, the flow velocity profile is assumed to be flat, and the vapour velocity falls to zero as the sphere surface is approached through the laminar region. The mean vapour velocity is taken as v_v.

The heat removed by the coolant gives rise to a temperature fall from T_{sat} at the vapour-liquid interface, to the bulk coolant temperature, T_c, over the distance β, and the coolant is similarly assumed to flow

(1) These assemptions -
"uniform" δ, v_r, etc.

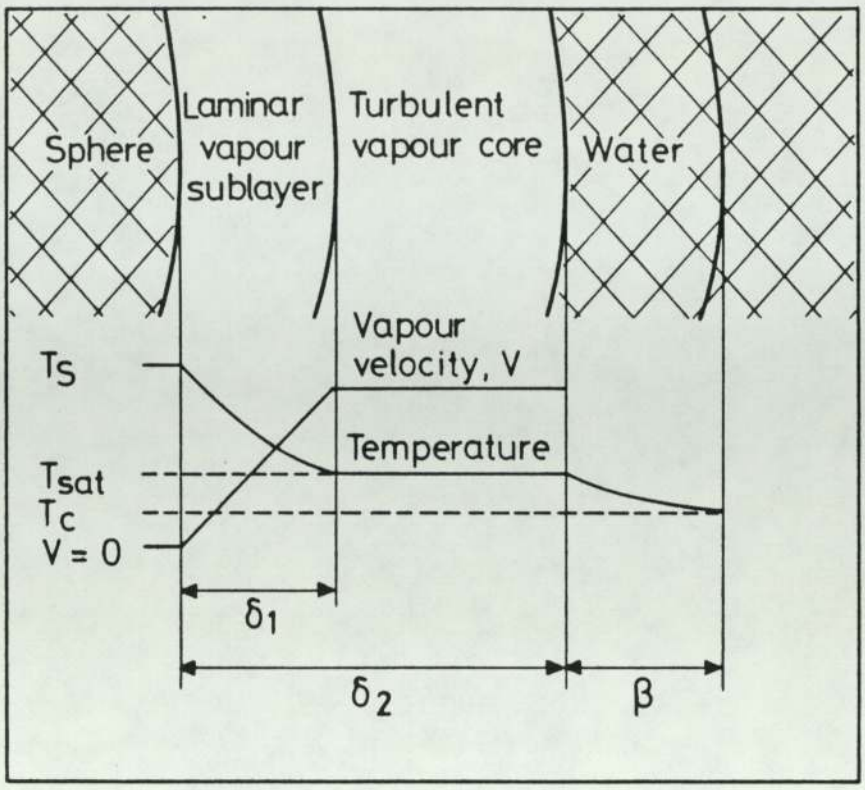

Fig 8.3.1 TURBULENT FLOW MODEL FOR FILM BOILING ON A SPHERE

within this depth with some mean velocity v_c.

It is also assumed for simplicity that the temperatures, flow velocities, and thermal diffusion depths are independent of position on the sphere surface, although the continuous generation of flowing vapour implies a loss mechanism which corresponds to the vapour bubble departure observed at the support stem. Bromley's assumption (vi) is assumed to hold. The perfect symmetry assumed is considered a valid approximation because the area of the sphere surface affected by bubble departure was seen to be small, and because of the absence of turbulent mixing in the liquid coolant over most of the sphere surface observed in the shadowgraph films. The aim of the model is to explain features of the sphere quenching experiments as a whole, so that this "lumped"

$\frac{dw_v}{dt}$ is total vap. gen. rate.

This gives S_i or N_v

approach is appropriate. It is intended that by so doing, the essential physics of the process will be accounted for.

The model equations. Heat transfer from the sphere surface is assumed to be by conduction only across the laminar sublayer, ie:

$$m_s c_s \left(\frac{dT_s}{dt}\right) = k_v A_s \frac{dT_v}{dx} \tag{8.2}$$

where A_s and dT_v/dx are the area of, and the temperature gradient in the vapour at the sphere surface. The conducted heat flux may be subdivided into that required to produce and heat the vapour, and that conducted/convected away by the liquid coolant, ie:

$$k_v A_s \left(\frac{dT_v}{dx}\right) = (c_v \Delta T_v + L)\left(\frac{dm_v}{dt}\right) + h' A_s \Delta T_c \tag{8.3}$$

c_v, ΔT_v and dm_v/dt are respectively the specific heat capacity, mean temperature rise and mass rate of flow of the vapour, and h' and ΔT_c are the surface heat transfer coefficient and the temperature fall in the coolant, across the thermal diffusion depth β. L is the specific latent heat of vaporisation for the coolant.

Hsu and Westwater used the the maximum vapour velocity, v_v, (that in the turbulent core and at its interface with the laminar layer), to define a critical vapour Reynolds number, Re*, which analysis shows must exceed a value of 100 for a turbulent core to develop (see Jordan [150] and Schlichting [159]). Thus:

$$R_e^* = \frac{\delta_l v_v}{\nu_v} = 100 \tag{8.4}$$

The Reynolds number for the overall flow is given by:

$$R_e = \frac{\delta_2 v_v}{\nu_v} \tag{8.5}$$

and hence:

$$\frac{\delta_2}{\delta_1} = \frac{R_e}{R_e^*} \tag{8.6}$$

ν_v is the vapour kinematic viscosity.

The following approximations are made to the terms in equations (8.2) and (8.3):

$$\frac{dm_v}{dt} = 2\pi r_s \rho_v \delta_2 v_v \tag{8.7}$$

$$\frac{dT_v}{dx} = \frac{T_s - T_{sat}}{\delta_1} \tag{8.8}$$

$$\Delta T_v = \tfrac{1}{2}(T_s - T_{sat}) \tag{8.9}$$

$$\Delta T_c = (T_{sat} - T_c) \tag{8.10}$$

k_c and T_c are the coolant thermal conductivity and bulk temperature, ρ_v is the vapour density, and r_s is the sphere radius.

The energy flux removed by the coolant may be obtained from the very substantial data available on natural convection from spheres. Clift et al [154], give the following correlation:

The boundary condition at the surface of a solid sphere is different from that for a vapour layer. (2)

8.11 – $Nu = N_a(Pr, (Pr.Gr))$

– but Pr, Gr for the liquid (7)

(3) – Apparent errors in eqns 8.16, 8.20

δ_1 – heat flux + conduction vap bdy layer.

8.4	δ_1, v_v	v_v – vap. bdy layer given by $Re^+ = 100$
8.6	δ_1, δ_2, Re	
8.15	$\delta_1, \delta_2, v_v,$	δ_2 – heat balance giving total vap. gen. rate

Define Nu

$$Nu = 1.7+0.3\{1+14.86\ [f(Pr)]Ra\}^{\frac{1}{4}} \tag{8.11}$$

where:

$$f(Pr) = \left[1 + \left(\frac{0.5}{Pr}\right)^{9/16}\right]^{-\frac{16}{9}} \tag{8.12}$$

Pr and Ra are the Prandtl and Rayleigh numbers (defined in the notation in appendix 7). The heat transfer coefficient, h´, then becomes:

$$h' = \frac{k_c Nu}{2r_s} \tag{8.13}$$

Equations (8.2) and (8.3) then reduce to:

$$\bar{a}\left(\frac{dT_s}{dt}\right) = \bar{b}\ \frac{(T_s - T_{sat})}{\delta_1} \tag{8.14}$$

$$\bar{b}\ \frac{(T_s-T_{sat})}{\delta_1} = \left[\bar{c}(T_s-T_{sat}) + \bar{d}\right]\delta_2 v_v + \bar{e}\ Nu(T_{sat}-T_c) \tag{8.15}$$

where:

$$\bar{a} = 4\pi r_s^3 \rho_s c_s \tag{8.16}$$

4/3

$$\bar{b} = 4\pi r_s^2 k_v \tag{8.17}$$

$$\bar{c} = \pi r_s \rho_v c_v \tag{8.18}$$

$$\bar{d} = 2\pi r_s \rho_v L \tag{8.19}$$

$$\bar{e} = 2\pi k_c r_s \tag{8.20}$$

4 2

8.4 Interpretation of the quenched sphere experiments

Vapour layer thickness. The conduction layer thickness, δ_1, was calculated from equation (8.14), as a function of subcooling, for surface temperatures of 1000 K and 750 K using the least squares fit to the data of figure 7.2.6. The vapour flow velocity, v_v, overall flow Reynolds number, Re, and δ_2 were then found in turn from equations (8.4), (8.15) and (8.6). The physical constants used for the vapour

phase were those at the saturation temperature and are given in appendix 1.

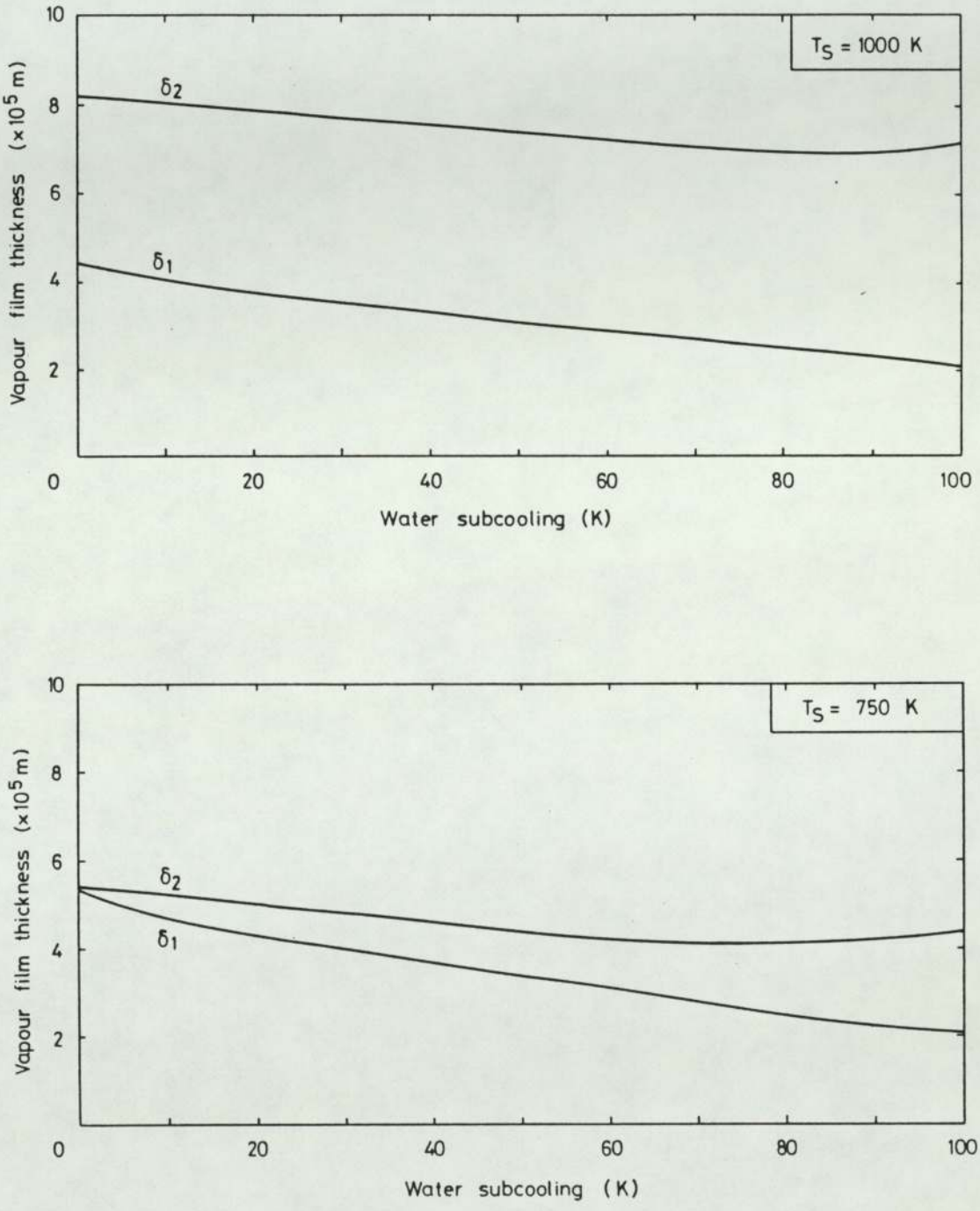

Fig 8.4.1 VAPOUR FILM THICKNESS AS A FUNCTION OF SUBCOOLING

"Values of $\delta_1 + \delta_2$ can only be order-of-magnitude.

The values of δ_1 and δ_2 are shown plotted against subcooling in figure 8.4.1. Both δ_1 and δ_2 are relatively weak functions of the subcooling. At high subcooling δ_1 is virtually independant of the surface temperature. As the surface temperature falls from 1000 K to 750 K the overall thickness decreases and, at low subcooling, that of the laminar sublayer increases. This is to be expected since at the lower surface temperature the heat flux from the sphere is diminished and the gradient required in the conduction layer to accomodate the flux will then also diminish. For T_s = 750 K and at low subcooling, $\frac{\delta_2}{\delta_1}$ is almost unity. This can be seen from figure 8.4.1 and also from figure 8.4.2 where the overall Reynolds number is shown as a function of subcooling and surface temperature. It might be expected that further cooling would result in δ_1 increasing only until it is equal to δ_2 at which point there would be no need for the turbulent core, and the flow

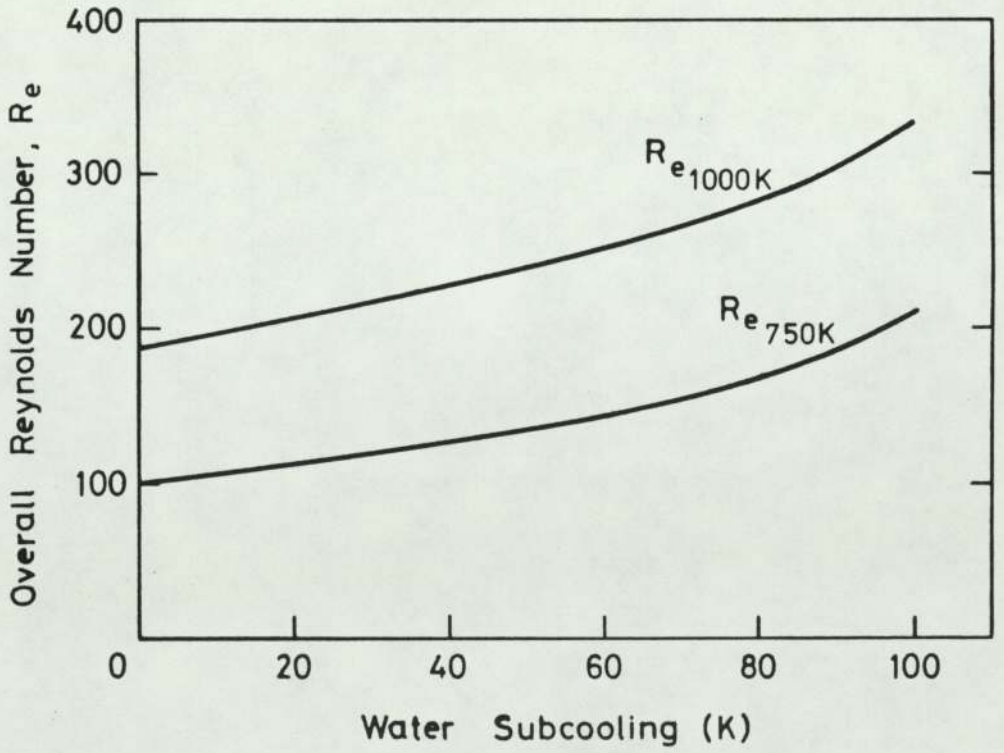

Fig 8.4.2 OVERALL VAPOUR FLOW REYNOLDS NUMBER AS A FUNCTION OF SUBCOOLING

would become purely laminar. The initial increase in δ_l to some maximum as T_s falls, followed by its subsequent decrease, would be in accord with pure conduction models.

Coolant flow velocity. The flux removed by the coolant is given in equation (8.15) by the Nusselt number for natural convection from a sphere. An alternative expression would be in terms of the coolant mass flow rate in the thermal boundary layer β. Equating the two gives:

$$\bar{e}\, Nu(T_{sat} - T_c) = c_c \Delta T_c \left(\frac{dm_c}{dt}\right) \tag{8.21}$$

where:

$$\Delta T_c = \tfrac{1}{2}(T_{sat} - T_c) \tag{8.22}$$

and:

$$\frac{dm_c}{dt} = 2\pi r_s \beta v_c \rho_c \tag{8.23}$$

The boundary layer thickness may be eliminated by equating the flux conducted into it, to $c_c \Delta T\, dm_c/dt$ from which:

$$\beta^2 = \frac{4k_c r_s}{v_c \rho_c C_c} \tag{8.24}$$

Equation 8.21 then may be rearranged to give the mean coolant flow velocity as:

$$v_c = \left(\frac{k_c}{\rho_c c_c}\right)\left(\frac{1}{r_s}\right)\left(Nu\right)^2 \tag{8.25}$$

v_c and β are functions only of subcooling, sphere radius and the coolant properties. For the steel sphere used in these experiments they are listed in table 8.1 where β is submillimetre (as suggested by the shadowgraphs) and v_c is extremely low.

TABLE 8.1 Coolant flow velocity and thermal diffusion depth

T_{sub}	Nu	v_c (mm/s)	β (mm)
20	23.17	9.8	0.78
40	30.95	14.8	0.63
60	35.21	19.2	0.55
80	37.16	21.4	0.52
100	30.53	14.5	0.64

8.5 Interpretation of TIZs

Superheat criterion and the onset of fragmentation. The results of the vapour explosion drop tests are summarised in figure 8.5.1 where the TIZs are reproduced as shaded regions in temperature space. The heavy shading represents that area within each TIZ where interactions could be violent and the light shading is the region where only fragmentation interactions were observed. Non-shaded (white) regions in figure 8.5.1(a) and (c) indicate areas where there were no experiments performed.

Also shown in the figure are the positions of the melting points for the hot liquid of each pair and instantaneous contact interface temperature lines corresponding to solidification of the hot liquid and homogeneous nucleation of the coolant, (labelled $T_I = T_m$ and $T_I = T_{hom}$

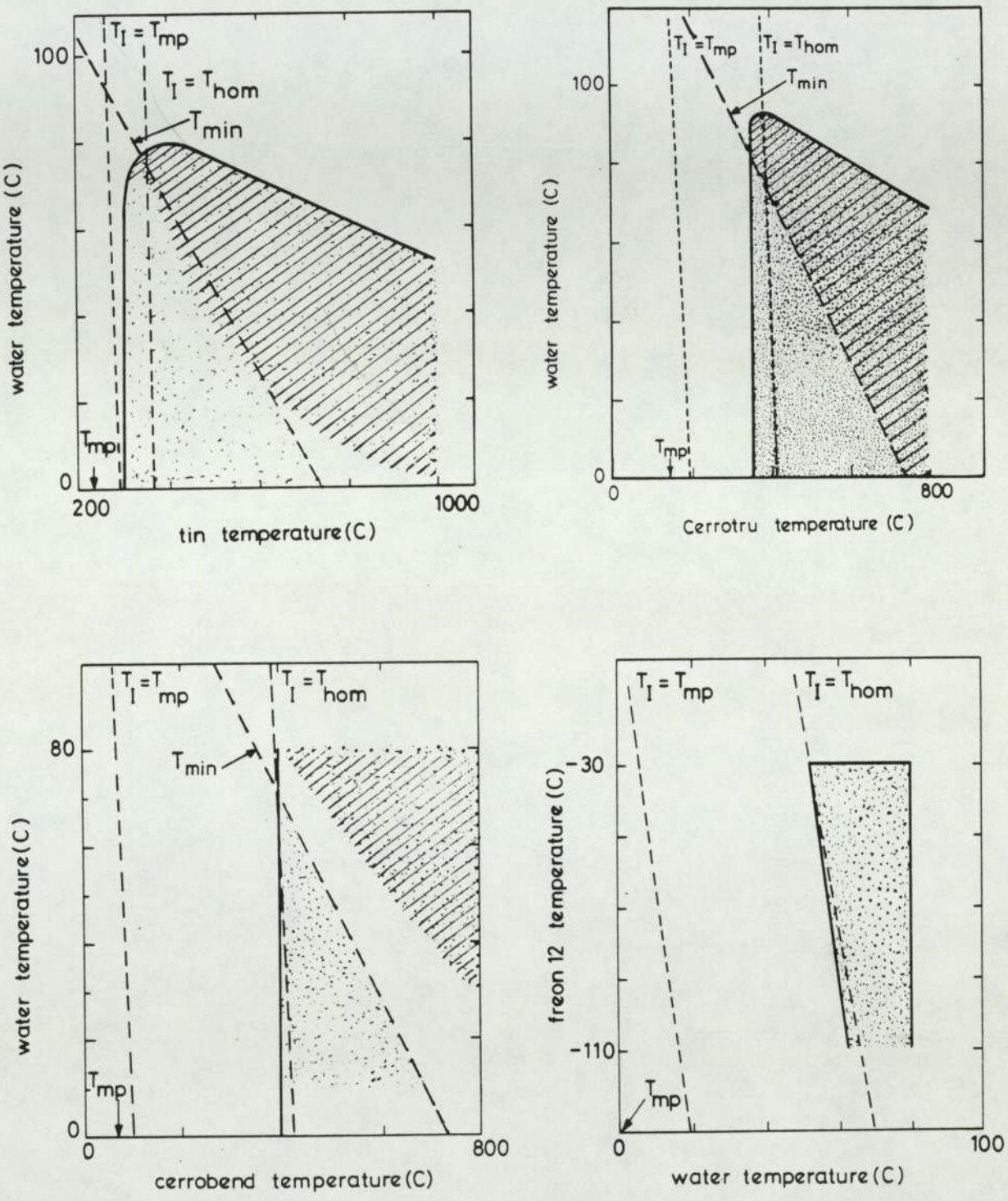

Fig 8.5.1 INTERFACE TEMPERATURE CRITERIA AND THE TIZ BOUNDARIES

(4) If this is original, it is important - but indep. of analyses

respectively).

The first experiments performed were with tin and water and showed that the left hand vertical boundary corresponded closely to either T_I equal to solidification or homogeneous nucleation. Later work with the other three systems confirmed that homogeneous nucleation rather than solidification determines the position of this boundary.

In the calculation of interface temperatures no account was taken of the temperature variation of the physical properties of the liquids involved or of convection or radiation at the interface. T_{hom} for water is generally taken to be about 573 K and this value was used here. For the refrigerant R12 the closest interface temperature line to the left hand boundary was drawn which corresponded to T_I = 312 K which is 0.81 x isceon critical temperature. 0.81 compares favourably with the Schins [155] approximation of 27/32 or 0.84.

Minimum film boiling and the onset of violent interactions. The homogeneous nucleation criterion clearly defines the position of the TIZ left hand boundaries, which mark the onset of mild fragmentation in these experiments. To produce violent interactions, however, some other criterion is required which could be provided by the minimum film boiling condition. Clearly, if triggering is to be the result of vapour film collapse, through whatever cause, then a film must be established in the first instance, although there is a strong case for arguing that in a liquid-liquid system film boiling should be assured by homogeneous nucleation. However, the application of the T_{min} criterion to the metal-water TIZs of figure 8.5.1, like the use of conduction-only interface temperature calculations, appears to produce some correlation, even though the existence of a minimum film boiling

Violent interactions only if bld depleaf
temp. is capable of causing film boiling.

But for any δ_1 there is a V_v - vapour is being produced, + the first term on the RHS of eq 8.15 is non-zero. (7)

I.e if $\delta = \delta_1$ there is still vapour to be produced.

(5) this criterion is just on the unsubstantiated, reverse of the Trinn law

temperature which is higher than the homogeneous nucleation temperature seems erroneous.

The minimum film boiling point lines plotted on figure 8.5.1 represent the lower envelope of the Bradfield data [156]. For cerrotru and tin this line adequately defines the division of the TIZs into regions of mild and violent interactions. For cerrobend the division is not violated, but how good a fit it is in this system cannot be judged because of the lack of data just above the dividing line.

A criterion for film boiling on tin drops in water. A simple condition for steady state film boiling is suggested by equation (8.15). For a fixed subcooling, the surface heat flux diminishes with surface temperature. Provided it exceeds that flux that can be removed by the coolant, vapour must be produced to accomodate the excess. When, however, the surface heat flux has diminished to a level that can be removed by the coolant alone, vapour production is not required. This condition is achieved when the heat conducted across the laminar sublayer is equal to the flux removed by the liquid coolant, ie:

$$\bar{b}\left(\frac{T_s - T_{sat}}{\delta_l}\right) = \bar{f}\sqrt{v_c}\,(T_{sat} - T_c) \qquad (8.26)$$

from which a stable vapour layer thickness, δ_s, may be defined as:

$$\delta_s = \frac{\bar{b}(T_s - T_{sat})}{\bar{f}\sqrt{v_c}\,(T_{sat} - T_c)} \qquad (8.27)$$

But $\bar{f}$ depends (I think) on the nat. conv. correlation for Nu - i.e. Nc as given by Table 8.1 - mm s^{-1}

If $\delta_1 = \delta_s$ implies film collapse, why is it not the same as T_{min}?

If δ_l is less than δ_s the film is stable. For δ_l greater than δ_s the film is unstable and would be expected to breakdown. In the forced flow conditions of the tin drop experiments v_c has been taken to be the observed terminal velocity of 0.8 m/s.

For a metal drop cooling isothermally the heat transfer coefficient is given by:

$$h' = \frac{mc}{A\Delta T}\left(\frac{dT_s}{dt}\right) \qquad (8.28)$$

where m, c and A are the drop mass, specific heat capacity and surface area respectively. ΔT is the driving temperature difference $(T_s - T_c)$ and (dT_s/dt) is the rate of fall of surface temperature. In film boiling h' is independent of the nature of the surface so that the rate of fall of surface temperature for a tin drop may be derived from the measurements on stainless steel with the same ΔT, by equating the expressions for their surface heat transfer coefficients, ie:

$$\left(\frac{dT_s}{dt}\right)_{sn} = \left(\frac{\rho_s c_s r_s}{\rho_{sn} c_{sn} r_{sn}}\right)\left(\frac{dT_s}{dt}\right)_s \qquad (8.29)$$

With a suitable adjustment also to the constants a and b values of δ_l and δ_s as a function of subcooling are plotted in figure 8.5.2 for surface temperatures of 1000 K and 750 K. The two curves cross for subcoolings of 55 K and 23 K respectively. Assuming a linear relationship, as observed with minimum film boiling temperatures, this line represents a division of the TIZ at somewhat higher temperatures than the Bradfield data suggests. It does, however, coincide with the temperatures at which the measured dwell times start to increase, and the Stevens-Witte transition line, as illustrated in figure 8.5.3. The

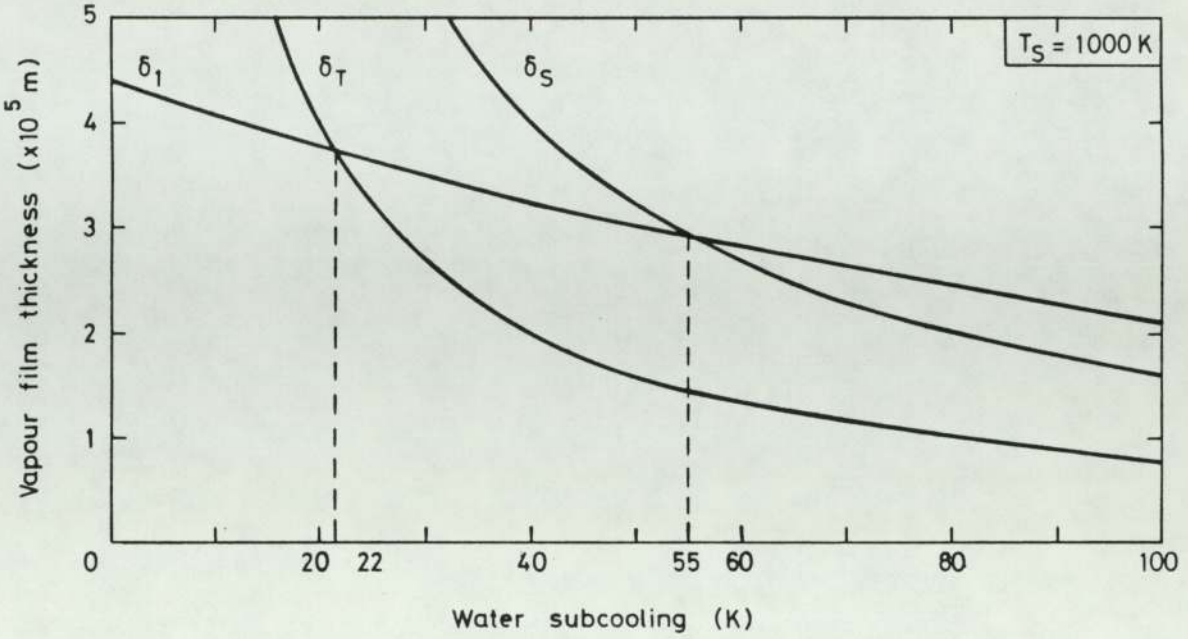

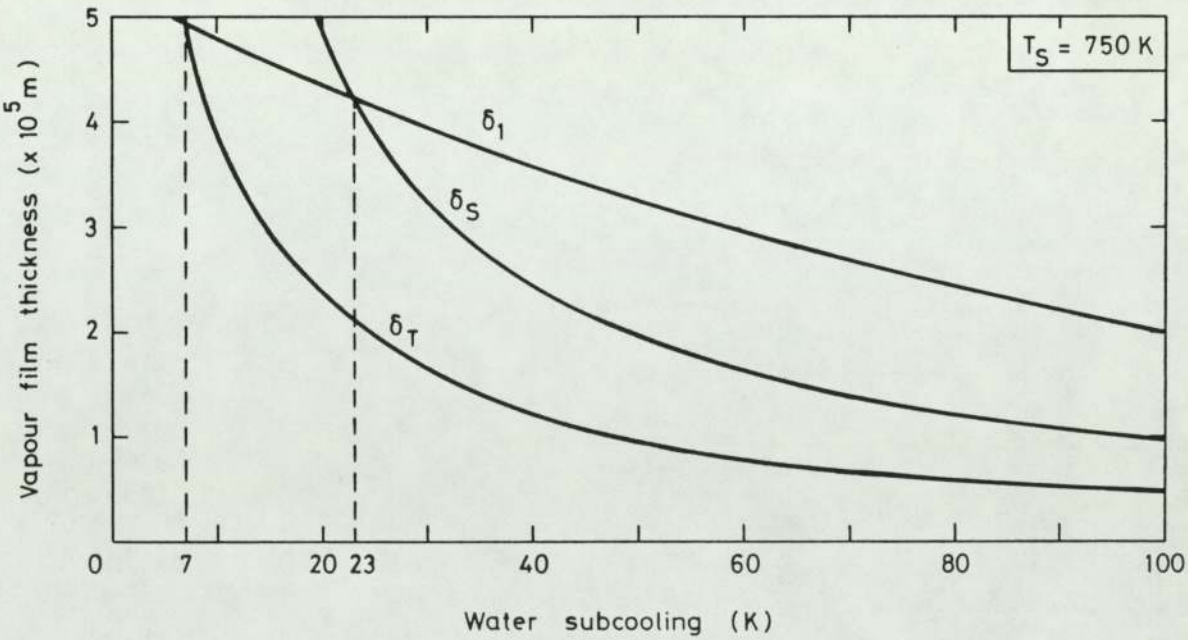

Fig 8.5.2 VAPOUR FILM THICKNESS, STABILITY AND TRANSITION LINES FOR SPHERICAL TIN DROPS

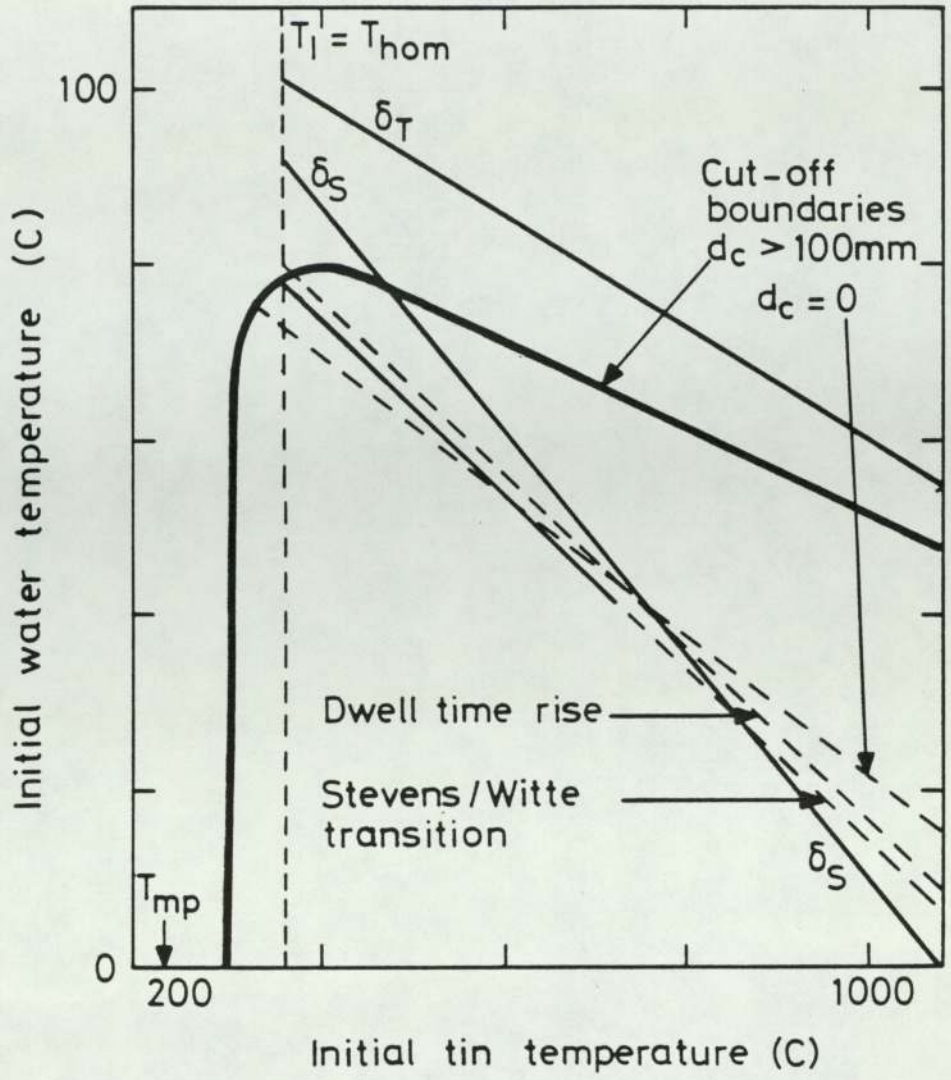

Fig 8.5.3 CHARACTERISTICS OF THE TIN-WATER TIZ

stability line departs most from the Stevens-Witte and dwell time lines at low subcooling and low surface temperature, where a laminar flow theory might be more applicable. The sharp increase in the gradient of the dwell time curves of figures 5.6.1 is better appreciated by plotting the dwell times against the reciprocal of the respective temperatures. Such plots are shown in figure 8.5.4.

The low and almost constant dwell times below the stability (minimum film boiling) line may indicate the timescales required for the development of the incipient instability of the collapse process.

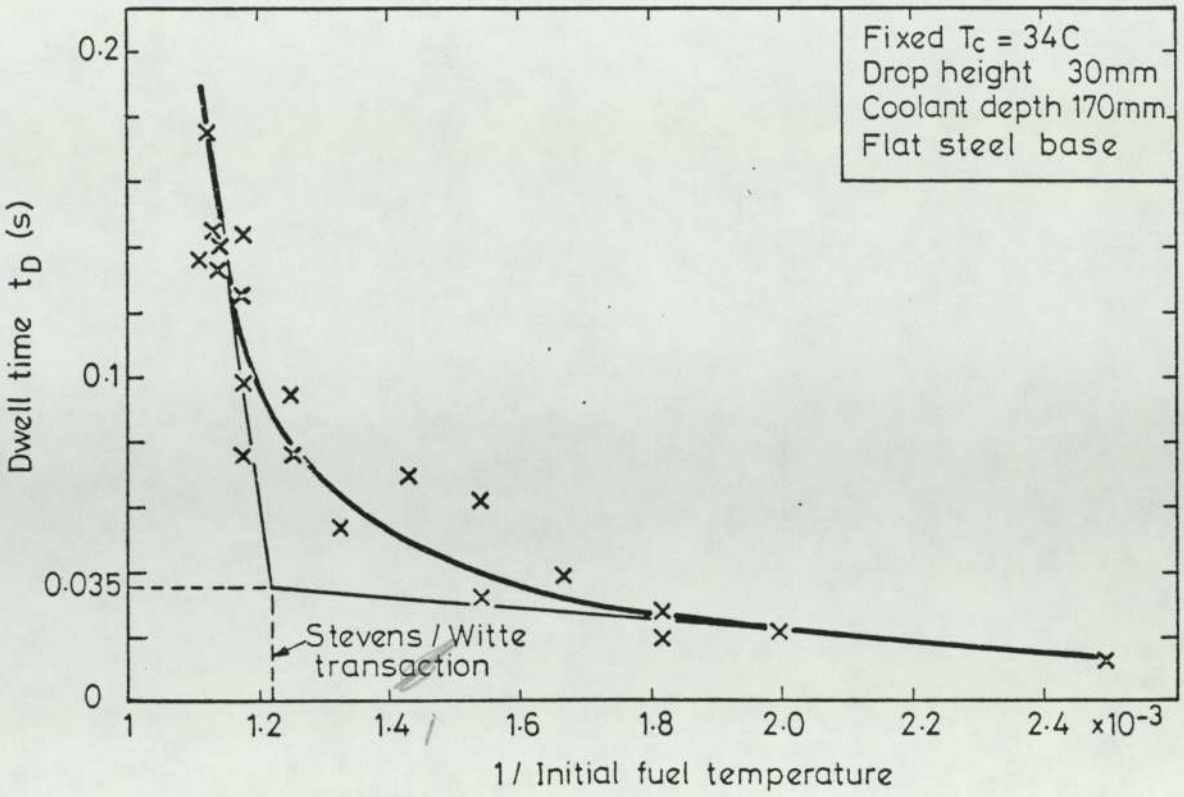

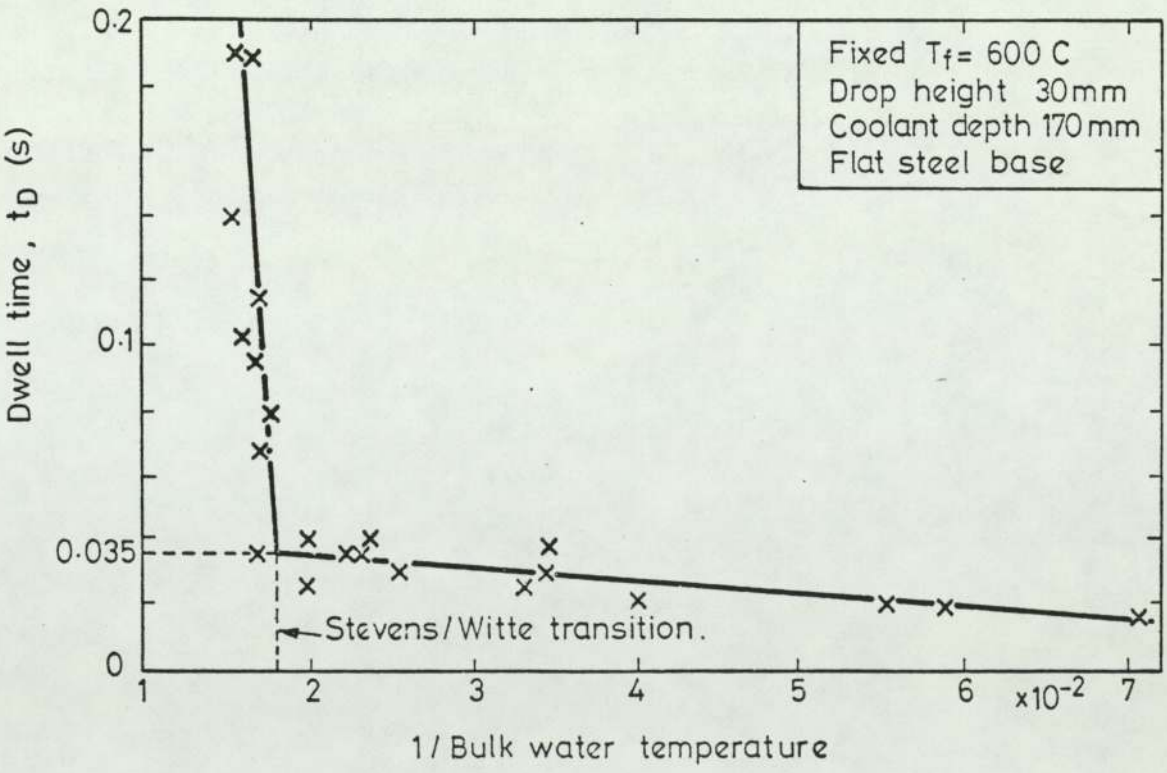

1/°C ? Why?

Fig 8.5.4 THE SHARP VARIATION OF DWELL TIMES WITH THE RECIPROCAL OF TIN AND WATER TEMPERATURE

(9) What about freon?

(10) Are tin drops spherical?

This is the only explanation of the sloping boundary. Is it all due to Reynolds?

Surely the Sloping Boundary must be $\delta_T = c\,\delta_S$ for $0.5 < c < 1$ (8)

The 0.5 is only arbitrary

Above the line film boiling is established and the dwell times then have also a cooling time component which increases more rapidly with the system temperatures.

Thick film boiling and the upper temperature cut-off. When the energy used to produce vapour exceeded that removed by the liquid coolant, was taken by Reynolds [153] as a criterion for a transition from thin- to-thick film boiling and an explanation of the sloping boundary of the tin-water TIZ. This condition corresponds to:

$$[\bar{c}\ (T_s - T_{sat}) + \bar{d}]\delta_2 v_v \geq f\ \sqrt{v_c}\ (T_{sat} - T_c) \qquad (8.30)$$

and is achieved when:

$$b\left(\frac{T_s - T_{sat}}{\delta_T}\right) \geq 2f\ \sqrt{v_c}\ (T_{sat} - T_c) \qquad (8.31)$$

where δ_T is the transition film thickness. Comparing equations (8.26) and (8.31) it may be seen that:

$$\delta_T = \tfrac{1}{2}\delta_s \qquad (8.32)$$

The transition lines for the tin drop experiments are also plotted on figure 8.5.2 and indicate that thick film boiling occurs for subcoolings less than 22 K and 7 K, for surface temperatures of 1000 K and 750 K respectively. Again, assuming a linear relationship, these figures suggest a line on the TIZ of figure 8.5.3 somewhat higher than the sloping boundary.

The inhibiting role of the container base. In shallow containers the coolant cut-off temperature was a function of coolant depth, increasing as the depth was increased. Since there was no evidence that the presence of the base could effect the spontaneous triggering of drops in the bulk coolant, contact with the base must determine the value of T_{co}, and it may be postulated that if the normal dwell time, a function of T_c, is greater than the fall time to the base, spontaneous interactions are inhibited by some base suppression mechanism.

Whatever the nature of this mechanism, the base will require time, which will be called the "waiting time", t_w, in which to take effect and it is then assumed that interactions may take place after reaching the base but before the waiting time has expired. If t_f is the drop fall time to the base, conditions for spontaneous triggering may be summarised as follows:

$t_f > t_D$	spontaneous triggering in bulk coolant
$(t_f + t_w) > t_D > t_f$	spontaneous triggering on base possible
$t_D > (t_f + t_w)$	spontaneous triggering prohibited

Estimates of the waiting time have been made from the experimental data and are shown in table 8.2 for a fixed hot liquid temperature of 873 K (the only value of T_h for which we have measurements of t_D as a function of T_c). At fixed values of coolant depth up to 100 mm the

Table 8.2 Estimates of waiting time from dwell and fall time data

d_c (mm)	$\frac{(d_{nco} - d_c)}{d_{nco}}$	$\frac{(T_{sat} - T_{nco})}{(T_{sat} - T_{co})}$	T_{co} (C)	t_D (ms)	t_f (ms)	$t_w = t_D - t_f$ (ms)
0	1.000	0.65	55	35	0	35
20	0.806	0.718	60	130	52	78
40	0.612	0.786	63	190	82	108
60	0.417	0.854	66	230	107	123
80	0.223	0.922	69	280	137	143
100	0.029	1.000	71	310	172	138

relationship of figure 6.4.2 has been used to predict the reduced cut-off temperature taking a value for d_{nco} of 103 mm (midway between those for 773 K and 993 K). Mean dwell times are tabulated from figure 8.5.4(b) and fall times from curve (c) of figure 5.5.2. Figure 8.5.5 shows how the waiting times decrease linearly with $1/T_{co}$.

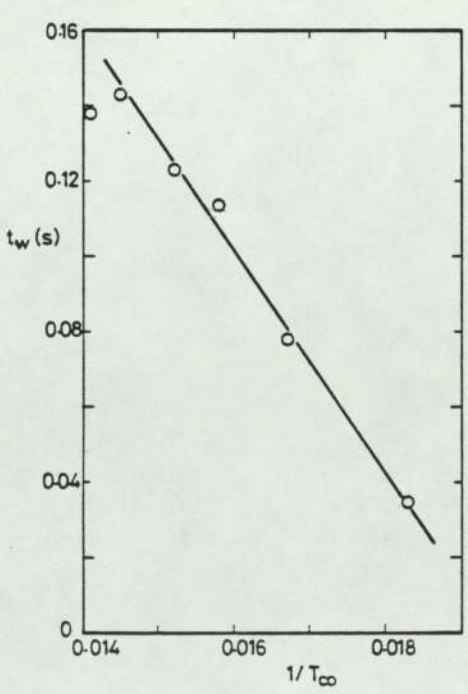

Fig 8.5.5 ESTIMATED WAITING TIME AS A FUNCTION OF COOLANT TEMPERATURE

Approaching the limit of zero coolant depth the fall time was zero and the waiting time was equal to the measured dwell time, in this case 35 ms. The corresponding coolant temperature was about 326 K (53 C). Below this, dwell times were generally less than t_w and interactions should occur. Above 326 K dwell times were greater than t_w and interactions should be inhibited. The lowest values of cut-off temperature, and hence the maximum depression of the sloping boundary, corresponds to the limit of zero coolant depth, in which position it lies very close to the film boiling condition, to the position at which dwell times rise sharply, and to the Stevens-Witte thin- to- thick film transition line (see figure 8.5.3).

Interactions with longer dwell times were observed, however, if the coolant depth was increased. Longer t_D corresponds to higher coolant temperature and higher values of t_w and, therefore, the position of the sloping boundary becomes dependent on coolant depth, moving up as d_c is increased. Above the film boiling condition derived above, however, t_D increases very rapidly and the dwell time curves become almost vertical. Very deep containers are then required for any change in cut-off temperature to be observed. The position of the sloping boundary in practice then becomes essentially independent of coolant depth as shown by the flattening of the curves of figure 6.4.1.

For a fixed coolant depth the cut-off temperature will be altered by any parameter which influences either the fall time or the waiting time. The fall time is shown in figure 5.5.2 to be strongly dependent on entry velocity, decreasing as v_i increases, and this leads to lower allowed values of t_D and the lowering of the cut-off temperature as shown in figure 6.3.2.

t_w depends on the details of the base suppression mechanism about which we may only speculate. Direct contact with the base may rapidly cool the tin so that when the normal dwell time has expired insufficient thermal energy is available to support the interaction. Alternatively the trigger mechanism itself may be inhibited by suppression of the instability at the coolant-vapour interface responsible for vapour collapse. For either mechanism we postulate that direct contact is necessary and a major contribution to t_w comes from the time after reaching the base required to achieve this. Large drops for instance spread on impact with a flat base and interactions can occur during this spreading as described in section 5.8. In the absence of a trigger, spreading proceeds until break-up into the very small drops of figure 5.3.1(b). Since there is no evidence from films of tin drop experiments that spontaneous triggering occurs after break-up it may be concluded that the sphericity of small drops facilitates the escape of trapped coolant and vapour and leads quickly to direct contact with the base.

Direct observation of the thermal insulation of molten tin above a thin metal sheet surrounded by water has been obtained by Sturgess [64]. Following contact and spreading across the sheet there was a waiting period after which time a vapour bubble formed and grew at a point on the underside of the sheet, presumably where the insulating film first collapsed and direct contact enhanced heat transfer locally. There is evidence from the debris from the experiments, and from that reported in this thesis, that trapping of coolant in cavities beneath drops does occur. The relatively slow vaporisation of this coolant across a thin vapour layer could then support the drop above the base until evaporation is complete.

8.6 Application of interface temperature criteria to other systems of interest

Experiments between molten steel and molten urania with liquid sodium have produced only mild interactions, the most energetic of them occurring in the injection mode. Dropping experiments, with which spontaneous triggering is associated, have resulted in extensive fragmentation but no energetic explosions. Experiments have not yet, therefore, established whether TIZs exist for the Urania - sodium or steel - sodium systems, but we can determine the maximum possible size for such zones. This is done in Figure 8.6.1. Interactions are only possible for temperatures between the melting points and boiling points of the hot and cold liquids. (The boiling point for iron was used as an estimate for that of stainless steel).

In Figure 8.6.1 interface temperature lines have been drawn corresponding to the saturation temperature and homogeneous nucleation temperature of the coolant and to the melting points of the fuels. In both systems the homogeneous nucleation temperature lines lie above the allowable areas in which the TIZs could be located, and the simple $T_I = T_{hom}$ criterion which applies to the four experimental systems using simulant materials would suggest that FCIs between the reactor materials are unlikely to occur in idealised conditions. It should be remembered, however, that the simulation experiments were performed under as clean a condition as possible with dissolved gas within the coolant being removed by boiling. It is therefore not surprising that the homogeneous nucleation limit determined the position of the left-hand boundaries of the TIZs.

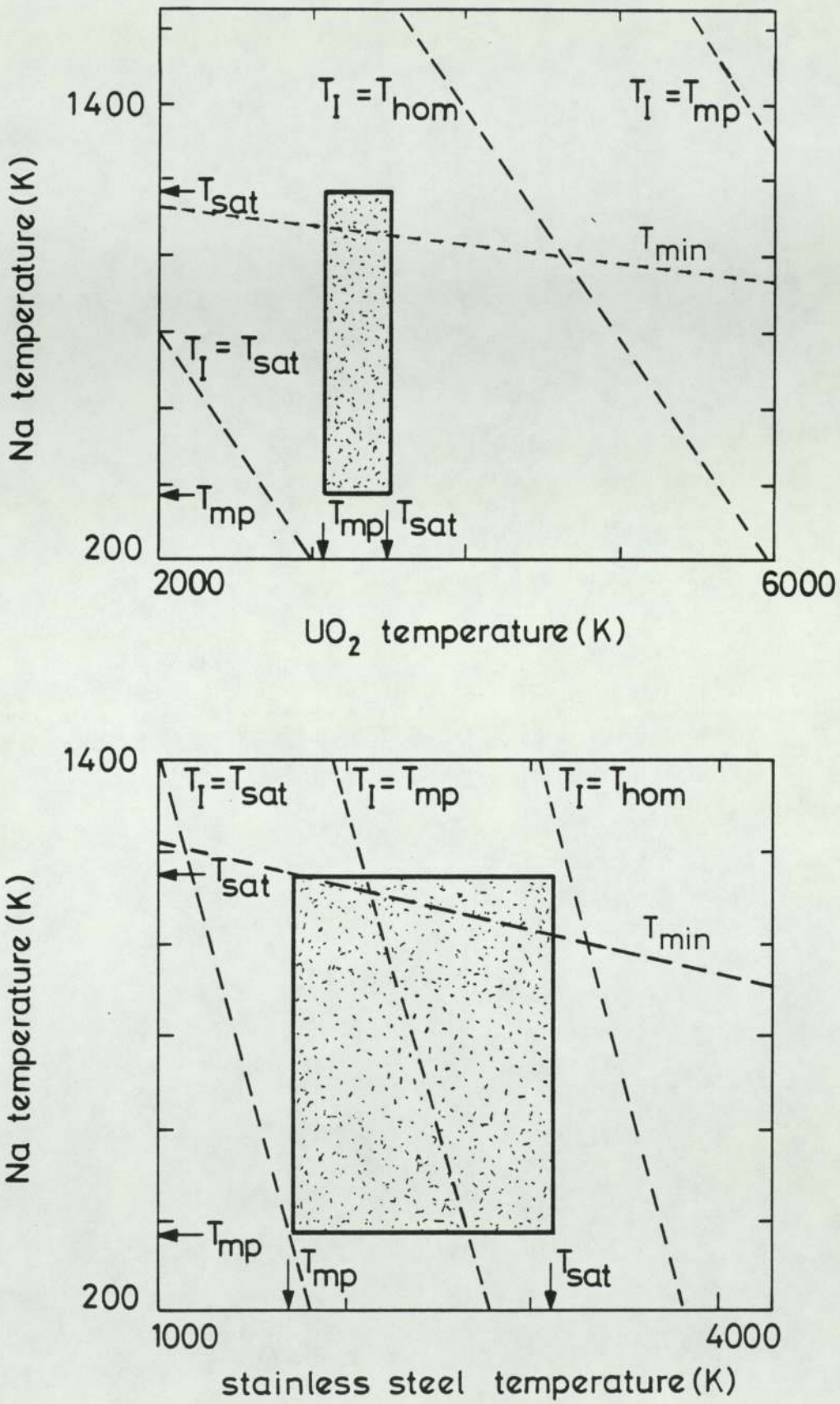

Fig 8.6.1 INTERFACE TEMPERATURE LINES AND THE CHARACTERISTICS OF POSSIBLE UO_2/Na AND STEEL/Na TIZs

However, the superheat criterion is that T_I must exceed T_{spon} and hence the critical interface temperature line could lie anywhere between those corresponding to T_{sat} and T_{hom}. In the stainless steel/sodium system the solidification line lies below the homogeneous nucleation line and cuts across the area in which the TIZ could lie. It is possible that the critical interface temperature line (corresponding to T_{spon}) could intersect the TIZ area between the lines $T_I = T_{hom}$ and $T_I = T_m$. FCIs might then be possible between stainless steel and sodium.

The critical line for the urania/sodium system could also cut the area in which a TIZ is allowable but in this system the solidification line is far above even the homogeneous nucleation line and solidification should occur for all possible values of T_{spon}.

T_{spon} could be lowered below T_{hom} by the presence of solid or gaseous nucleation sites or cavitation in the coolant provided the density of such sites is high enough within the thermal boundary layer at the fuel-coolant interface.

Also shown on the diagrams of Figure 8.6.1 are the minimum film boiling lines from the extrapolation of the data of Farahat [159]. Williams [3] has shown that the Henry correlation for T_{min} [158] produces a similar line. If the T_{min} criterion is valid in predicting the onset of violent explosions as opposed to mild fragmentation, then it further restricts the region in temperature space where there need be concern, to a very small area, and explains why only mild events have been reported in experiments, where relatively cold sodium has been used to date. Further experiments with these materials should aim at sodium temperatures approaching saturation.

Finally , there are a number of points that should be kept in mind before extending the results from the experiments described to a reactor situation.

(i) No account has been taken of radiative heat transfer. Below 1000 K the contribution of radiation is rather small [see Jordan] and does not effect the qualatative behaviour. For urania, or molten steel close to its boiling point, radiation can be important.

(ii) Solidification of the interface fuel will only limit FCIs if a continuous crust is formed thick enough to withstand the buffeting of pressure gradients accompanying vaporisation.

(iii) The superheat criterion is only applicable if liquid-liquid contact can be made between fuel and coolant. Reactor fuel can only melt if it is isolated from the sodium coolant by, for example, sodium vapour, and the question arises whether, in a practical situation, the vapour can leave the interface or otherwise allow liquid sodium to contact the fuel.

(iv) It should be remembered that these tentative conclusions are only applicable to falling drops in a large quantity of the bulk phase. The most violent FCIs are associated with the base contact mode, or with external triggering.

CHAPTER 9 SUMMARY

Following a review of the literature an area of study was identified, involving the spontaneous triggering of small drops, and experiments were designed to investigate some aspects of the basic physics of the vapour explosion. Several liquid pairs were considered of which four were chosen as satisfying the requirements set out in chapter 1. A substantial number of experiments were then performed and classified in terms of the violence of the interaction. Temperature interaction zones (TIZs) were found to exist in hot liquid - cold liquid temperature space, inside of which explosions were possible but outside of which they did not occur spontaneously.

The TIZs were characterised by straight line boundaries. The lower boundary was shown to be determined in these four systems by the Fauske superheat criterion, which seems to provide a condition for the onset of mild fragmentation. The extent of fragmentation increased as the TIZs were crossed in the direction of increasing hot or cold liquid temperature, and some other criterion is indicated as being necessary to determine when a significant portion of the hot liquid sample was fragmented and the interactions became violent. It has been shown, based on the measurements of Bradfield, that this might be provided by the minimum film boiling condition.

Interaction violence continued to increase with the system temperatures until an upper temperature cut-off was reached, (giving rise to a sloping boundary in the metal-water experiments), and beyond which

interactions were inhibited. Even the most violent of interactions involved very low conversion efficiencies of thermal to mechanical energy (0.37-3.7 percent).

Spontaneous triggering is widely believed to be due to the destabilisation of a vapour film surrounding the molten hot liquid as it cools through film and into transition boiling, and the cut-off temperature has been related to the establishment of a thick film boiling regime. Ancillary experiments were performed in which a heated metal sphere was quenched in water, to investigate the conditions necessary to establish vapour films. These led to the view that vapour flow is turbulent and not adequately described by the laminar flow models that have been traditionally assumed. A very simple model was therefore developed from an energy balance using the "average" properties of the sphere and vapour and assuming perfect symmetry. Conditions were derived from the model for film boiling, and for the thin-to-thick film transition used elsewhere to explain the sloping boundary of the tin-water TIZ. Applied to tin drops in water these conditions indicated that the minimum film boiling condition corresponded to the sharp increase in dwell time and to the position of the Stevens-Witte thin-to-thick film observations, but not to the minimum film boiling measurements of Bradfield. The transition line lies just above the TIZ sloping boundary.

It is not possible at present to put a satisfactory explanation to these latter observations. The model is relatively crude and there are uncertain numerical factors associated with many of the quantities, so that the precise position of the stability (film boiling) and transition lines should not be viewed as sacrosanct. Qualitatively the behaviour is encouraging, with the correct trends, and it is felt that

the model better describes the physics of the process, and could form the basis of a more sophisticated treatment. It should also be borne in mind that the Bradfield data is an arbitrary choice from much conflicting evidence in the literature; that the identification of the change to violent interactions is somewhat subjective; and that tin drops, as shown in figure 5.5.1 are far from being spherical.

A knowledge of the particle size distribution in fragmented debris is important in two areas. Firstly, in the modelling of heat transfer in the vapour explosion and secondly, in the post accident heat removal from a nuclear reactor in the very unlikely event of melting within the core. In the former, Bird [164] has shown that only the very small particles (less than about 280 micrometres) can contribute to significant heat transfer in the time available, while in the latter all sizes can contribute. Predictions of particle size distributions have been attempted [163], but the best that theoretical models can do is to provide some mean particle size and no knowledge of the range or shape of the distribution, and they usually involve arbitrary constants or assumptions somewhere along the way to force a fit to known experimental data, where size distributions have been based on the total sample mass. It has been shown in this thesis, however, that if the size distribution is based on that portion of the sample below a particle size of about 2 mm (above which fragments could have been produced by Weber instability alone) the distributions reduce to a mean curve with a well defined scatter. Unlike the size distribution in the total sample, the position of the mean curve is independent of the hot and cold liquid temperatures, sample mass and PD over the ranges investigated.

The independence of size distribution on PD (i.e. the fraction of the total sample fragmented by vapour explosion) is not incompatible with a bubble growth and collapse model for spontaneous triggering in which vapour bubble expansion shreds the molten metal and disperses it into the coolant. The collapsing bubble then produces further mixing with fresh metal which is shredded and dispersed on the next expansion phase into the same size distribution range and so on. The range of sizes is dictated by the break-up time for the shredding process, and the falling velocity of the expanding bubble wall. The sample PD then depends on the number of bubble growth and collapse cycles (a function of the hot and cold liquid temperatures) and the mass of hot liquid available. Such a shredding mechanism has been observed on high speed film of tin-water interactions.

If particle size distributions for large masses and for other contact - trigger modes can similarly be reduced, theoretical modelling may be simplified and reliable empirical predictions of size distributions could be possible.

Cine film of metal water interactions gives further support for the bubble growth and collapse model, with coolant bubbles being clearly visible in the later stages of the interaction. Growth and collapse times are on timescales comparable with those observed for spark generated vapour bubbles in pure coolant. Several authors report studies of spark induced bubbles. The limited results presented in this thesis extend those studies to higher coolant temperatures, and have shown that while the growth times continue to be given approximately by the classical Rayleigh formula, beyond some upper temperature, the bubbles are not able to collapse to the small volumes required by a model involving the formation of coolant jets.

This might provide an explanation for the observed coolant cut-off temperatures, although it is not clear with the limited results so far obtained, how the value of this cut-off can be made a function of the hot liquid temperature. Furthermore, it would be expected that vapour explosions with the coolant at saturation temperature would not occur and this is not in accord with the observed explosions, in this and other work, between refrigerants and water.

Since the work of Long (1957) in which 50 kg quantities of molten aluminium were dropped into water it has been recognised that the nature of the base plays an important role in the triggering of large scale vapour explosions. For industrial purposes it was possible to identify surface treatments which minimised the likelihood of explosions occurring, but despite continued efforts there is no real understanding of the processes involved. The role of the container base in small-scale experiments is complicated. It can have a similar effect. Interactions between molten tin and water have been observed to be triggered on the base with coolant above the cut-off temperature normally associated with spontaneous triggering. These interactions were rare and were not themselves considered spontaneous but (as with some large-scale experiments) due to a different triggering mechanism, possibly involving entrapment of the coolant between metal and base with subsequent superheating.

The results of the present study, however, showed that in small scale tin/water drop experiments the most important effect of the base was, not to trigger interactions by entrapment, but to inhibit interactions which would otherwise have occurred spontaneously. In shallow coolant, cut-off temperatures were shown to be a function of coolant depth, approaching the Stevens-Witte transition temperatures only in the limit

of zero depth. In deep coolant, cut-off temperatures approach a limiting maximum value given by the position of the sloping boundary of the tin /water TIZ. The results may be explained if a base suppression mechanism is postulated to inhibit those interactions with normal dwell times greater than the sum of the fall time to the base and a waiting time required for the base to take effect.

Some other parameters which affect the position of the TIZ boundaries for tin and water were also investigated. For example, at any point in the TIZ a minimum mass of tin was found to be required for interactions to occur. The minimum mass was small (a few grams) and decreased with (i) increasing tin temperature, and (ii) decreasing coolant temperature. No satisfactory explanation has been found for these observations.

Increasing the drop height to the bulk phase surface reduced the value of the coolant cut-off temperature, possibly by decreasing the fall time to the base, and hence the range of allowable dwell times, before base suppression of the interaction.

The addition of nucleating agents, in the form of lycopodium powder, added to the coolant in isceon-water interactions, appeared to diminish the size of the temperature interaction zone principally by inhibiting interactions at low coolant temperatures.

Contact mode was also found to affect the position of the upper temperature cut-off in isceon-water interactions. For isceon dropped into water this cut-off was at a water subcooling of 20 K and independent of the coolant temperature. When water was dropped into

isceon, however, the cut-off was removed and interactions occurred for water temperatures up to the saturation temperature.

The experiments reported in this thesis, together with others in the open literature, provide some support for, and some evidence conflicting with, the current theories for fragmentation criteria. None of the theories seems capable of explaining even the two simple variations of cold fluid dropped into hot and hot fluid dropped into cold, and it seems likely that several fragmentation mechanisms can operate under different circumstances to produce a vapour explosion. For a given system, one of them will dominate, although which one it is not possible to predict at present.

Finally, small scale experiments are for the most part incoherent and in themselves not likely to have serious damage potential in large systems. Some form of fast propagation in pre-dispersed mixtures is required for this, and the experiments reported do show the potential for an escalating propagation from a spontaneous trigger, provided a pre-dispersed state can first be established.

Appendix 1 Physical properties of materials of interest

PARAMETER	UNIT	Water	Tin	Cerrobend	Cerrotru
COMPOSITION		H_2O	Sn	Sn, Bi, Pb, Cd	Sn, Pb
MELTING TEMP.	K	273	505	343	412
BOILING TEMP.	K	373	2900	-	-
HOMOGENEOUS NUCLEATION TEMP.	K	573	-	-	-
CRITICAL TEMP.	K	647	-	-	-
SPECIFIC LATENT HEAT OF FUSION	J/Kg	3.33×10^5	6.07×10^4	-	-
SPECIFIC LATENT HEAT OF VAPORISATION	J/Kg	2.26×10^6	2.47×10^6	-	-
SOLID DENSITY	Kg/m^3	999 [1500]	7285	-	-
LIQUID DENSITY	Kg/m^3	960 [370]	6980	9300	8640
VAPOUR DENSITY	Kg/m^3	0.586 [373]	-	-	-
SOLID SPECIFIC HEAT CAPACITY	J/Kg/K	2000 [263]	224 [298]	-	-
LIQUID SPECIFIC HEAT CAPACITY	J/Kg/K	4179 [298]	257 [2000]	93.16	104.81
VAPOUR SPECIFIC HEAT CAPACITY	J/Kg/K	2060 [373]	-	-	-
SOLID THERMAL CONDUCTIVITY	W/m/K	2.3 [250]	63 [373]	-	-
LIQUID THERMAL CONDUCTIVITY	W/m/K	0.673 [353]	32.6 [773]	18.8	20.89
VAPOUR THERMAL CONDUCTIVITY	W/m/K	0.0246 [373]	-	-	-
SURFACE TENSION	J/m^2	0.0735 [15]	0.554 [878]	-	-
KINEMATIC VISCOSITY	m^2/s	0.31×10^{-6}	0.345 [593]	-	-
kpc		2.70×10^9	5.85×10^7	1.63×10^7	1.89×10^7
k/pc		1.68×10^{-4}	1.82×10^{-5}	2.17×10^{-5}	2.31×10^{-5}

PARAMETER	UNIT	Isceon-12	Stainless Steel(316)	Urania	Sodium
COMPOSITION		$CC\ell_2F_2$	Fe,Cr,Ni	UO_2	Na
MELTING TEMP.	K	115	1725	3069	371
BOILING TEMP.	K	243	3200 (Fe)	3500-4500	1155
HOMOGENEOUS NUCLEATION TEMP.	K	325	-	-	2365
CRITICAL TEMP.	K	385	-	-	2803
SPECIFIC LATENT HEAT OF FUSION	J/Kg	-	$2.75x10^5$	$2.75x10^5$	-
SPECIFIC LATENT HEAT OF VAPORISATION	J/Kg	-	-	$2.30x10^6$	-
SOLID DENSITY	Kg/m^3	-	7389 [1500]	9726 [3000]	-
LIQUID DENSITY	Kg/m^3	1500	6917 [2000]	8500 [3000]	777
VAPOUR DENSITY	Kg/m^3	-	-	-	-
SOLID SPECIFIC HEAT CAPACITY	J/Kg/K	-	682 [1500]	636 [3000]	-
LIQUID SPECIFIC HEAT CAPACITY	J/Kg/K	840	600	503.6	1259
VAPOUR SPECIFIC HEAT CAPACITY	J/Kg/K	-	-	-	-
SOLID THERMAL CONDUCTIVITY	W/m/K	-	23.2 [1000]	3.65 [3000]	-
LIQUID THERMAL CONDUCTIVITY	W/m/K	0.071	-	-	44.5
VAPOUR THERMAL CONDUCTIVITY	W/m/K	-	-	-	-
SURFACE TENSION	J/m^2	-	-	0.45	-
KINEMATIC VISCOSITY	m^2/s	-	-	$0.40x10^6$ [3190]	-
kpc		$8.95x10^4$	$9.63x10^7$	$1.56x10^7$	$4.35x10^7$
k/pc		$5.63x10^{-8}$	$5.59x10^{-6}$	$8.53x10^{-7}$	$4.55x10^{-5}$

Appendix 2 Properties of some systems of interest

system	α	a	b	B
tin-water	0.215	0.823	0.177	108.3
cerrotru-water	0.378	0.726	0.274	137.3
cerrobend-water	0.407	0.711	0.289	129.17
Isceon 12-water	0.182	0.846	0.154	2.98
stainless steel-sodium	0.672	0.598	0.402	0.123
uranium dioxide-sodium	1.669	0.375	0.625	0.0187

$$T_I = aT_h + bT_c$$

where $a = 1/(1 + \alpha)$,

$b = \alpha/(1 + \alpha)$ and

$$\alpha^2 = k_c\rho_c c_c / k_h\rho_h c_h$$

$$B = k_h\rho_c c_c / k_c\rho_c c_h$$

Appendix 3 Impurity levels in the water used in vapour explosion studies

element	concentration	element	concentration
Ag	0.03	Pb	0.1
Al	0.05	Pd	0.03 *
Ba	0.05	Pt	1.0 *
Bi	0.03 *	Sb	1.5 *
Ca	0.5	Si	50.0
Cd	0.5 *	Sn	0.15 *
Cr	0.03 *	Sr	0.03 *
Cu	0.05	Ti	0.05 *
Fe	0.5 *	Tl	0.3 *
Ga	0.05 *	V	0.05
In	0.05 *	W	0.3 *
Mg	0.03	Zn	1.5 *
Mn	0.03 *	Zr	0.1 *
Mo	0.03	Cs	0.5 *
Na	3.0	K	1.5
Ni	0.1 *	Rb	0.01 *

The distilled, deionised water used in the vapour explosion studies was supplied by A.E.R.E., Harwell, together with the analysis above.

(a) Concentrations are in microgrammes per litre.

(b) Only the elements listed were specifically sought.

(c) A starred figure (*) means the element was not detected and indicates the lowest concentration normally recorded by the method used.

(d) The silicon content was high because of the use of silica ware in production.

Appendix 4 List of cine films taken of tin-water interactions

Film No.	T_c (C)	T_h (C)	Mass (g)	d_h (cm)	PD2	Film No.	T_h (C)	T_c (C)	Mass (g)	d_h (cm)	PD2
54	600	43	12	3	57	90	500	65	20	3	80
55	600	59	12	3	83	91	500	65	20	3	70
56	600	45	12	3	57	92	500	64	6	3	63
57	600	29	12	3	44	93	500	65	6	3	7
58	600	14	12	3	75	94	500	66	20	3	1
59	800	49	9	3	68	95	500	65	15	3	18
60	650	63	10	3	0	96	500	65	15	3	63
61	500	65	4	28	0	97	550	82	44	30	66
62	500	65	9	28	53	98	550	68	44	30	-
67	500	65	7	28	3	99	550	65	44	91	34
68	500	65	7	28	1	100	550	80	44	91	18
69	500	65	12	28	-	101	550	70	44	91	10
70	500	65	12	28	59	102	550	73	44	91	6
71	500	65	6	28	8	103	550	72	44	91	7
72	500	65	6	28	0	104	550	77	44	91	5
73	500	65	6	28	0	105	550	67	44	91	15
74	500	65	2	28	2	106	550	67	44	91	11
75	500	64	3	28	1	107	550	67	44	91	6
76	500	65	4	28	93	108	550	67	44	91	14
77	500	65	5	28	82	109	550	56	44	91	17
78	400	50	12	3	6	110	550	60	44	91	15
79	400	60	12	3	12	113	250	58	12	3	0
80	400	70	12	3	82	114	250	44	12	3	2
81	500	60	12	3	-	115	799	64	12	3	80
82	500	50	12	3	46	116	600	86	12	2	0
83	700	60	12	3	-	118	500	65	20	28	60
84	700	50	12	3	81	119	500	65	18	28	43
85	800	50	12	3	86	120	500	65	16	28	30
86	800	41	12	3	69	121	500	65	10	28	38
89	500	65	6	3	0	122	500	65	8	28	16

Appendix 5 Characteristics of boiling processes

The characteristics of boiling heat transfer adjacent to a hot solid surface are described in many texts and research papers [e.g. 160 - 162]. There are three basic modes of energy transfer which can be distinguished from measurements of heat flux or heat transfer coefficient. The latter are normally displayed in the form of a boiling curve, a plot of flux or heat transfer coefficient against the surface temperature, or its excess above the coolant saturation temperature. A schematic of such a curve is shown in figure A.5.1 where the three boiling regimes, called nucleate, transition and film boiling, are distinguished.

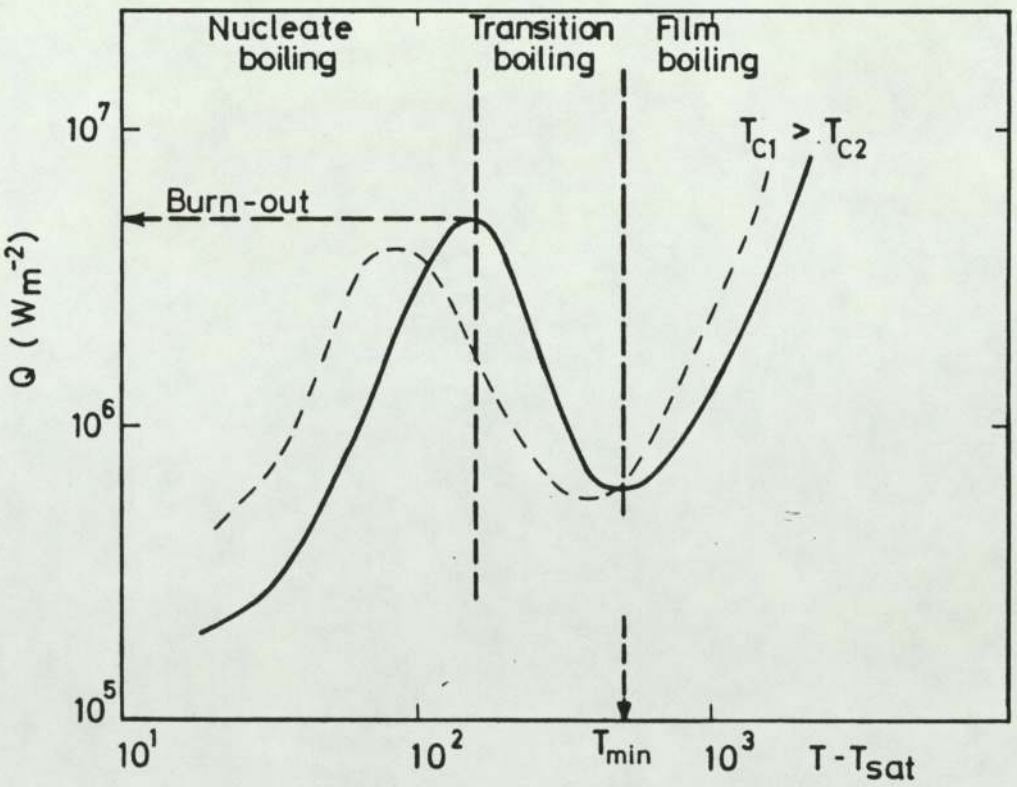

Fig A.5.1 TYPICAL BOILING CURVES AT TWO COOLANT TEMPERATURES

For surface temperatures below the coolant saturation temperature, heat transfer is by natural convection. Just above the boiling point,

however, vapour bubbles form at gas filled cracks and crevices in the surface, grow and detach themselves under buoyancy. The bubbles collapse as vapour condenses in colder liquid away from the interface and provide a mechanism for increasing the rate at which energy can be transferred to the bulk coolant. In this, the nucleate boiling regime, therefore, increasing the surface temperature increases the rate of bubble generation and hence the heat flux.

For this process to continue as the heater temperature is raised it is essential that there is access to the heater surface for fresh coolant, a condition that cannot be fulfilled as the bubble generation rate and surface density increase. Vapour anywhere on the surface insulates the surface and diminishes the heat flux locally. A maximum heat flux is thus obtained, called the critical or burn - out flux, beyond which the flux diminishes. Eventually adjacent bubbles begin to touch and coalesce before they depart from the surface and small areas of the surface become covered by a vapour film. The extent of the film increases with increased temperature until, at the minimum film boiling point, the surface is completely vapour blanketted and the flux has reached a minimum value.

Increasing the surface temperature further, again results in a rising heat flux with boiling taking place at the interface of the liquid coolant and its vapour. In this, the film boiling regime, the heat flux from the surface becomes independent of the nature of the surface and dominated by the coolant properties.

The negative slope, or transition region, between nucleate and film boiling is characterised by a rapid alternation between the other two boiling modes. Random pressure pulses are produced by vapour collapse

at the hot surface and it is thus the more violent of the three boiling regimes.

Of the several parameters which might affect the position of the boiling curve only the bulk coolant temperature and ambient pressure have been systematically evaluated. Increasing the coolant temperature for instance moves the boiling curve to the left and lowers the critical heat flux as illustrated in figure A.5.1. An increase in ambient pressure has a similar effect with the critical heat flux at first increasing as the curve moves left and then decreasing again. [162]

Appendix 6 Spontaneous nucleation

Superheating of the coolant at a liquid-liquid interface can occur because, unlike a solid-liquid system, the interface is smooth and free from gas filled crevices from which coolant vapour microbubbles can nucleate and grow. Spontaneous nucleation takes place in the absence of existing nucleation sites and as a result of statistical density fluctuations in the liquid. The volumetric nucleation rate is given by Skripov [165] as

$$J = \bar{A} N_L \exp(-Wf(\Theta)/\bar{k}T)$$

J is strongly dependent on the temperature, T, and increases from very low rates to very high rates over a small range in temperature. In sodium for example [166] $J = 1.68 \times 10^{-3}$ at 2120 K and 1.8×10^{5} at 2140 K. The temperature at which this sharp increase occurs (2140 K in this instance) is then defined as the spontaneous nucleation temperature of the liquid. W is the work of formation of the critical embryo from the liquid and is given by $(16\pi\sigma^3)/3(P_v - P_\ell)$ where σ is the liquid surface tension, P_v is the vapour pressure and P_ℓ the pressure in the liquid. $\bar{k}$ is Boltzmann's constant, and T the absolute temperature. N_L is the number of liquid molecules per unit volume and $\bar{A}$ is a constant $\sim 10^{10}\ s^{-1}$.

J is not sensitive to the product $\bar{A}N_L$ outside the exponential but is sensitive to (besides temperature) the function $f(\Theta)$, a relationship involving the contact angle between the liquids. For perfect wetting, $\Theta = 0$ and $f(\Theta) = 1$ and the spontaneous nucleation temperature assumes its maximum possible value called the homogeneous nucleation temperature, T_{hom}. Direct liquid-liquid contact with the cold liquid

heated beyond T_{spon} cannot be maintained and nucleation proceeds almost immediately.

Although the interface temperature of the cold liquid rises in 10^{-12} s nucleation cannot proceed until a sufficiently thick thermal boundary layer has developed to support vapour embryos of the critical size.

Appendix 7 Notation

$\bar{A}$ = a constant

A = coolant tank crossectional area

A_j = coolant jet surface area (a function of time)

A_o = initial jet surface area

A_s = quench sphere surface area

c = specific heat capacity

c_h = specific heat capacity of hot liquid

c_c = specific heat capacity of cold liquid

c_s = specific heat capacity of sphere

c_{sn} = specific heat capacity of tin

c_v = specific heat capacity of vapour

D = cylinder diameter

d_j = coolant jet diameter

d_h = drop height

$\bar{d}_c$ = a constant

d_c = bulk phase depth

d_{nco} = "normal" cut-off depth

d_e = explosion depth

E = energy

E_s = spark energy

E_b = capacitor bank energy

fps = frames per second

$f(\theta)$ = wetting function

Gr = Grashof number for quenched sphere = $(2r_s)^3\beta'(T_s - T_c)/g\nu^2$

g = acceleration due to gravity

h = Coolant dome height defined in figure 5.5.1

h' = surface heat transfer coefficient

$I(t)$ = spark gap current

J = volumetric spontaneous nucleation rate

k = thermal conductivity

k_v = thermal conductivity of coolant vapour

k_c = thermal conductivity of coolant

$\bar{k}$ = Boltzmanns constant

LN_2 = liquid nitrogen

$\bar{L}_c$ = a constant

L_j = coolant jet length

l = charecteristic length

M_m = minimum mass

m_c = mass of coolant

m_s = quenched sphere mass

m or m_h = dropped sample mass

m_v = mass of vapour

Nu = Nusselt number = $h'l/k$

N_L = number of liquid molecules per unit volume

$P(t)$ = coolant pressure

PD = percentage disintegration based on a 2mm sieve

PDA = assessed percentage disintegration

Pr = Prandtl number = $\eta c/k$

P_v = pressure in vapour

P_ℓ = pressure in liquid

Ra = Rayleigh number = $Gr.Pr$

Re = Reynolds number = $v_v \delta/\nu^2$

$Re^* = \frac{v_v \delta}{\nu^2} l = 100$

R_m = maximum bubble radius

R = bubble radius

r = see figure 5.5.1

R12 = refrigerant freon-12 or isceon-12

r_s = quenched sphere radius

r_{sn} = radius of tin drop

T = temperature

T_h = initial temperature of hot liquid

T_b = Sphere surface temperature at vapour collapse

T_c = initial temperature of cold liquid

T_s = sphere surface temperature

T_{co} = cut-off temperature

T_{nco} = "normal" cut-off temperature

T_I = interface temperature

TIZ = temperature interaction zone

T_{sat} = coolant saturation temperature

T_{spon} = coolant spontaneous nucleation temperature

T_{hom} = coolant homogeneous nucleation temperature

T_{crit} = coolant critical temperature

T_{sub} = coolant subcooling = $(T_S - T_c)$

T_m = melting temperature

T_v = temperature gradient in vapour at quenched sphere surface

T_{min} = minimum film boiling temperature

t = time

t_D = dwell time

t_f = fall time to base

t_g = bubble growth (or collapse) time

t_w = waiting time on base

V_c = volume of coolant

V_b = capacitor bank voltage

V = volume

$\bar{V}_c$ = constant

V_j = coolant jet velocity

V(t) = spark gap voltage

$\bar{v}$ = surface thermocouple emf

v, v_c = velocity of moving coolant

v_v = vapour flow velocity

v_i = impact velocity

v_p = coolant dome peak velocity

ρ = density

ρ_h = density of hot liquid

ρ_c = density of cold liquid

ρ_s = density of quenched sphere (stainless steel)

ρ_{sn} = density of tin

ρ_v = density of vapour

W = work of formation of critical vapour embryo

x = x-coordinate

ν_v = vapour viscosity

ν_c = coolant viscosity

$\alpha^2 = k_c \rho_c c_c / k_h \rho_h c_h$

β = thermal diffusion depth in coolant

β' = coefficient of expansion

ν = dynamic viscosity = η/ρ

ν_v = dynamic viscosity of vapour

σ = surface tension

λ_c = Taylor critical wavelength

δ_1, δ_2 = vapour layer thickness

δ_1 = laminar conduction layer thickness

δ_s = stable vapour layer thickness

δ_T = transition vapour layer thickness

$(\delta_2 - \delta_1)$ = turbulent core thickness

ΔP = pressure difference

ΔT = temperature difference

ΔT_v = mean temperature rise in vapour

ΔT_c = mean temperature rise in liquid coolant

$\bar{a}$ = constant defined by equation 8.16

$\bar{b}$ = constant defined by equation 8.17

$\bar{c}$ = constant defined by equation 8.18

$\bar{d}$ = constant defined by equation 8.19

$\bar{e}$ = constant defined by equation 8.20

$\bar{f}$ = constant defined by equation 8.30

Appendix 8 List of Publications

Buchanan, D.J. and Dullforce, T.A. "Fuel-coolant interactions: small-scale experiments and theory." 2nd specialist meeting on sodium-fuel interactions in fast reactors, Ispra, Italy, Nov. 1973.

Buchanan, D.J. and Dullforce, T.A. "Mechanism for vapour explosions." Nature, 245, pp 32-34, Sept. 1973.

Adlam, J.H. and Dullforce, T.A. "Spark-generated steam bubbles - experiment and theory." Culham Laboratory report CLM-R134, March 1974.

Dullforce, T.A. and Vaughan, G.J. "Thermal interactions between tin and water: preliminary results from Culham's minimum mass experiments." Culham Laboratory report CLM-M99, Jan. 1975.

Dullforce, T.A., Buchanan, D.J. and Peckover, R.S. "Self-triggering of small-scale fuel-coolant interactions: 1 Experiments." J.Phys.D: App.Phys., 9, ppl295-1303, 1976 [also UKAEA Culham Laboratory report no. CLM-P424]

Dullforce T.A., Jelphs, A.N. and Rimmer, W. "Thermal interactions between cerrotru and water." Culham Laboratory report CLM-RR/S2/17, 1977.

Dullforce, T.A. and Rimmer, W. "Thermal interactions between cerrobend and water." Culham Laboratory report CLM-RR/S2/18, 1977.

Reynolds, J.A., Dullforce, T.A., Peckover, R.S. and Vaughan, G.J. "Fuel-coolant interactions - some basic studies at the Culham Laboratory." 3rd specialist meeting on sodium-fuel interaction in fast reactors, Tokyo, Japan, March 1976.

Dullforce, T.A., Reynolds, J.A. and Peckover, R.S. "Interface temperature criteria and the spontaneous triggering of small-scale fuel-coolant interactions." Proceedings of the Deutsches Atomforum 1978 Reaktortagung, Hanover, West Germany, April 1978.

Dullforce, T.A. "The influence of solid boundaries in inhibiting spontaneously triggered, small-scale, fuel-coolant interactions." 4th specialist meeting on fuel-coolant interaction in nuclear reactor safety, Bournemouth, UK, April 1979.

Dullforce, T.A. and Sturgess, J.W. "Minimum fuel mass requirements in small-scale spontaneously triggered tin-water drop experiments." CSNI fuel-coolant interaction newsletter, SINDOC(78)135, July 1978.

Dullforce, T.A. "Fragmentation and explosive FCIs and the validity of the superheat criterion in spontaneously triggered small-scale drop experiments." CSNI fuel-coolant interaction newsletter, SINDOC(78)135, July 1978.

References

[1] Vaughan, G.J. "A consideration of some self-initiating mechanisms for FCIs." UKAEA Culham Laboratory report CLM/RR/S2/6U, August 1975.

[2] JSC on health, safety and welfare in foundries, sixth report of the subcommittee on continuous casting and high speed melting. "Molten metal and water explosions." HMSO London 1979.

[3] L.Williams. Private communication.

[4] Witte, L.C , Cox, J.E. and Bouvier, J.E. "The vapor explosion." J. Metals, 22, pp39-44, Feb. 1970.

[5] Roberts, K.V. "Theoretical calculations on fuel-coolant interactions." Paper no. 20, CREST meeting on sodium - fuel interaction in fast reactor safety, Grenoble, Jan. 1972.

[6] Buxton, L.D. and Nelson, L.S. "Core-meltdown experimental review". Chapter 6. "Steam explosions." Sandia report no. SAND74-0382, Aug. 1975.

[7] Teague, H.J. "Summary of the papers presented at the CREST meeting on fuel-sodium interaction at Grenoble in January 1972 and a report of conference papers 38a-k on fuel-sodium interactions." Proc. Int. Conf. on engineering of fast reactors for safe and reliable operation, Karlsruhe, pp812 - 838, Oct. 1972.

[8] Caldarola, L. "Current status of knowledge of molten fuel/sodium thermal interactions." GFK Karlsruhe report no. KFK1944, Feb. 1974. (also EUR-4973e).

[9] Fauske, H.K. "CSNI meeting on fuel-coolant interactions." Nuc. Safety, 16, no.4, July-Aug. 1975.

[10] Benz, R., Frohlich, G. and Unger, H. "Literaturstudie zur Dampfexplosion." GFK Karlsruhe report no. IKE, BMFT- QS-76, Feb. 1976.

[11] Board, S.J. and Hall, R.W. "Recent advances in understanding large scale vapour explosions." Paper SNI6/7 3rd specialist meeting on sodium-fuel interaction in fast reactors, Tokyo, Japan, March 1976. (also CEGB report no. RD/B/N3666).

[12] Board, S.J. and Caldarola, L. "Fuel-coolant interactions in fast reactors." Invited paper winter annual meeting ASME symposium on thermal and hydraulic aspects of nuclear reactor safety, Atlanta, USA, Nov. 1977.

[13] Bankoff, S.G. "Vapor explosions: a critical review." Keynote address 6th Int. Heat transfer conf., Toronto, Canada, Aug. 1978.

[14] Vaughan, G.J. "The metal/water explosion phenomenon - a review of present understanding." UKAEA SRD report no. SRD R177, May 1980.

[15] Cronenberg, A.W. and Benz, R. "Vapor explosion phenomena with respect to nuclear reactor safety assessment." Advances in nuclear

science and technology, 12, Plenum press, 1980.

[16] Bankoff, S.G. "Vapor explosions." Chapter 20, Nuclear reactor safety heat transfer, ed. by O.C.Jones Jr. pp695-728, Hemisphere press, 1981.

[17] Teague, H.J. "A summary of opening key issues in the science of fuel-coolant interactions and vapour explosions." Report of the chairman of the CSNI group of experts to the 4th CSNI specialist meeting on fuel-coolant interaction in nuclear reactor safety, Bournemouth, UK, April 1979.

[18] Zyzskowski, W. "Thermal explosion hazards in (fast) nuclear reactors." Atomic energy review, 16, no.1, pp3-87, 1978.

[19] Frohlich, G. and Mueller, G. "Experiences with vapor explosions caused by entrapment of water with melts." Trans. ANS, 26, p397, 1977.

[20] Board, S.J., Farmer, C.L. and Poole, D.H. "Fragmentation in thermal explosions." CEGB report no. RD/B/N2423, Oct. 1972.

[21] Frohlich, G, Mueller, G. and Unger, H. "Analysis of shapes of melts from entrapment experiments." Trans. ANS. 28, p449, 1978.

[22] Page, F.M. Private communication.

[23] Fry, C J. and Robinson, C.H. "Experimental observations of propagating thermal interactions in metal/water systems." Paper FCI4/P15 presented to the 4th. CSNI specialist meeting on fuel-coolant interaction in nuclear reactor safety, Bournemouth, UK, April 1979.

[24] Arakeri, V.H., Catton, I. and Kastenberg, W.E. "An experimental study of the molten glass/water thermal interaction under free and forced conditions." Nuc. Sci. and Eng. 66, pp153-166, 1978.

[25] Buxton, L.D., Nelson, L.S. and Benedick, W.B. "Steam explosion triggering and efficiency studies." Paper no. FCI4/P17 presented to the 4th. CSNI specialist meeting on fuel-coolant interaction in nuclear reactor safety, Bournemouth, UK, April 1979.

[26] Henry, R.E. and McUmber, L.M. "Vapor explosions of freon-22 with an external trigger." Paper presented at the 3rd. meeting of CSNI group of experts on the science of fuel-coolant interactions and of vapor explosions, Grenoble, Sept. 1978.

[27] Board, S.J. Private communication to G.J. Vaughan 1976 (cited in ref. 14).

[28] Anderson, R.P. and Bova, L. "Final report on the small-scale vapor-explosion experiments using a molten NaCl-H_2O system." Argonne report no. ANL-76-57, April 1976.

[29] Henry, R.E., Gabor, J.D., Winsch, I.O., Spleha, E.A., Quinn, D.J., Erickson, E.G., Heiberger, J.J. and Goldfuss, G.T. "Large scale vapor explosions." Proc. ANS fast reactor safety meeting, Beverly Hills, California, USA, April 1974.

[30] Long, G. "Explosions of molten aluminium in water. Cause and prevention." Metal progress, 71, no.5, pp107-112, May 1957.

[31] Hess, P.D. and Brondyke, K.J. "Causes of molten aluminium-water explosions and their prevention." Metal progress, 95, pp93-110, April 1969.

[32] Briggs, A.J. "Experimental studies of thermal interactions at AEE Winfrith." Paper SNI6/1 presented to the 3rd specialist meeting on sodium/fuel interaction in fast reactors, Tokyo, Japan, March 1976.

[33] Holtbecker, H. Private communication.

[34] JSC on health, safety and welfare in foundries, fifth report of the subcommittee on continuous casting and high speed melting. "Safety during semi-continuous and continuous casting of copper and copper alloys." HMSO, London, 1979.

[35] Armstrong, D.R. and Anderson, R.P. Argonne report no. ANL-RDP 49, 1976.

[36] Enger, T., Hartman, D.E. and Seymour, E.V. "Explosive boiling of liquified hydrocarbon/water systems." Paper presented to the cryogenic engineering conference, NBS, Boulder, Colorado, USA, Aug. 1972.

[37] Clerici, G., Holtbecker, H., Schins, H. and Schlittenbardt, P. "Interactions with small and large sodium to UO_2 mass ratios." Paper SNI6/13 presented to the 3rd specialist meeting on sodium/fuel interaction in fast reactors, Tokyo, Japan, March 1976.

[38] Johnson, T.R., Baker, L. and Pavlik, J.R. "Large scale molten fuel-sodium interaction experiments." Proc. ANS fast reactor safety meeting, Beverly Hills, California, USA, April 1974.

[39] Page, F.M. "Base triggered FCI in copper/water systems." Paper FCI4/P9 presented to the 4th. CSNI specialist meeting on fuel-coolant interaction in nuclear reactor safety, Bournemouth, UK, April 1979.

[40] Hohmann, H., Henry, H.E. and Kottowsky, H.M. "The effect of pressure on NaCl-H_2O explosions." Paper FCI4/P14 presented to the 4th. CSNI specialist meeting on fuel-coolant interaction in nuclear reactor safety, Bournemouth, UK, April 1979.

[41] Rengstorff, G.W.P., Lemmon, A.W.Jr. and Hoffman, A.O. "Explosion between molten aluminium and water - a review of knowledge." Battelle Memorial Institute report, April 1969.

[42] Laber, D. and Lemmon, A.W.Jr. "Explosions of molten aluminium and water." Battelle Memorial Institute report, Dec. 1970.

[43] Elgert, J.O. and Brown, A.W. "In-pile molten metal-water reactions." USAEC report 100, 16257, 1956.

[44] JSC on health, safety and welfare in foundries, fourth report of the subcommittee on continuous casting and high speed melting. "A study of the causes of molten metal and water explosions." HMSO, London, 1977.

[45] Davies, D. and Dullforce, T.A. Unpublished.

[46] Henry, R.E. and McUmber, L.M. "Vapour-explosion experiments with subcooled freon." Argonne report ANL-77-43, June 1977.

[47] Benz, R., Schwalbe, W., Hohmann, H. and Toselli, F. "Melt/water interactions in tank geometry: experimental and theoretical results." Paper FCI4/P16 presented to 4th CSNI specialist meeting on fuel-coolant interaction in nuclear reactor safety, Bournemouth, UK, April 1979.

[48] Bjorkquist, G.M. "Experimental investigation of the fragmentation of molten metals in water." MIT report TID 26826, June 1975.

[49] Dullforce, T.A., Buchanan, D.J. and Peckover, R.S. "Self-triggering of small-scale fuel-coolant interactions: 1. Experiments." J. Phys. D: App. Phys., 9, pp1295-1303, 1976 [also UKAEA Culham Laboratory report no. CLM-P424]

[50] Bjornard, T.A. "An experimental investigation of accoustic cavitation on a fragmentation mechanism." MIT report no. MITNE-163, 1974.

[51] Paoli, R.M. and Messler, R.B. "Explosion of molten lead in water." Proc. 8th Int. Congress on High Speed Photography. Stockholm, Sweden, June 1968.

[52] Witte, L.C., Vyas, T.J. and Gelabert, A.A. "Heat transfer and fragmentation during molten metal/water interactions." Trans. A.S.M.E. J. of Heat Transfer, pp521-527, 1973.

[53] Bjornard, T.A., Rosenow, W.M. and Todreas, N.F. Trans. ANS., 19, p247, 1974.

[54] Konuray, M.M. "The interactions of hot spheres and volatile liquids." PhD. Thesis, University of Aston in Birmingham, June 1975.

[55] Asher, R.C., Davies, D. and Jones, P.G. "Fuel-coolant interactions: Preliminary experiments on the effect of gases dissolved in the coolant." UKAEA Harwell report no. AERE-M2861, Dec. 1976.

[56] Asher, R.C , Davies, D., Kandiah, S.K. and Worthington, A.J. "The effect of ambient pressure on a vapour explosion (FCI)." UKAEA Harwell report no. AERE-M2862, Dec. 1976.

[57] Dullforce, T.A. "The influence of solid boundaries in inhibiting spontaneously triggered, small-scale, FCIs." Paper FCI4/P8 presented to the 4th CSNI specialist meeting on fuel-coolant interaction in nuclear reactor safety, Bournemouth, UK, April 1979.

[58] McCracken, G.M. "Investigation of explosions produced by dropping liquid metals into aqueous solutions." UKAEA Safety research bulletin, no.11, pp20-22, 1973.

[59] Brauer, F.E., Green, N.W. and Mesler, R.B. "Metal/water explosions." Nuc. Sci. and Eng., 31, pp551-554, 1968.

[60] Kondo, S. and Umehara, H. "Investigations of the development and propagation of fuel-coolant interactions using freezable simulant materials." Tokyo University, May 1978.

[61] Buchanan, D.J. and Dullforce, T.A. "Fuel-coolant interactions : small-scale experiments and theory." Paper presented to 2nd specialist meeting on sodium-fuel interactions in fast reactors, Ispra, Italy , Nov. 1973.

[62] Dullforce, T.A., Reynolds, J.A. and Peckover, R.S. "Interface temperature criteria and the spontaneous triggering of small-scale fuel-coolant interactions." Paper presented to the Deutsches Atomforum e.v. 1978 reactor meeting, Hanover, West Germany, April 1978.

[63] Dullforce, T.A. and Sturgess, J.W. "Minimum fuel mass requirements in small-scale spontaneously triggered tin-water drop experiments." CSNI fuel-coolant interaction newsletter, SINDOC (78) 135, July 1978.

[64] Sturgess, J.W. Private communication 1981.

[65] Zyskowski, W. "Thermal interaction of molten copper with water." Int. J. Heat Mass Transfer, 118, p271, 1975.

[66] Bird, M.J. and Millington, R.A. "Fuel-coolant interaction studies with water and thermite generated molten uranium dioxide." Paper FCI4/P19 Presented to 4th CSNI specialist meeting on fuel-coolant interaction in nuclear reactor safety, Bournemouth, UK, April 1979.

[67] Hall, R.W., Board, S,J, and Baines, M. "Observations of tin/water thermal explosions in a long tube geometry: their interpretation and consequences for the detonation model." Paper FCI4/P20 presented to the 4th CSNI specialist meeting on fuel-coolant interaction in nuclear reactor safety, Bournemouth, UK, April 1979.

[68] Benz, R., Burger, M. and Zach, O. "Comparison of experimental data on the minimum film boiling temperature for spheres." University of Stuttgart report IKE2-41, Nov. 1977.

[69] Henry, R.E., Fauske, H.K. and McCumber, L.M. "Vapor explosion experiments with simulant fluids." Proc. international meeting on fast reactor safety and related physics, Chicago, USA, Oct. 1976.

[70] Asher, R.C., Bullen, D. and Davies, D. "Vapour explosions (fuel-coolant interactions) resulting from the sub-surface injection of water into molten metals : preliminary results." UKAEA Harwell report AERE M2772, March 1976.

[71] Davies, D., Kelly, J.C. and Sanguine, S.J. "Injection of water into liquid tin - occurrence of explosions and measurements of dwell times." unpublished UKAEA Harwell report.

[72] Amblard, M., Costa, J. and Syrmalenios, P. "Recent JEF and CORRECT 1 sodium/fuel interaction results." Paper SNI 2/16 presented to 2nd CSNI specialist meeting on sodium/fuel interaction in fast reactors, Ispra, Italy, Nov. 1973.

[73] Anderson, R.P. and Bova, L. "Final report on the small scale vapour explosion experiments with NaCl-H_2O system." Argonne report ANL

76-57, 1976.

[74] Armstrong, D.R., Goldfuss, G.T. and Gebner, R.H. "Explosive interaction of molten UO_2 and liquid sodium." Argonne report ANL-76-24, March 1976.

[75] Asher, R.C., Bradshaw, L., Collet, R. and Davies, D. "Experimental work on the injection of sodium into liquid steel." Paper SNI 6/31 presented to 3rd CSNI specialist meeting on sodium/fuel interactions in fast reactors, Tokyo, Japan, March 1976, [also UKAEA Harwell report AERE-M2770].

[76] Abbey, M.J., Asher, R.C., Bradshaw, L., Davies, D. and Sanguine, S.J. "The injection of sodium into liquid stainless steel : a report of the second experiment Na-SS/1." Paper SNI 6/32 presented to 3rd CSNI specialist meeting on sodium/fuel interaction in fast reactors, Tokyo, Japan, March 1976, [also UKAEA Harwell report AERE-M2771].

[77] Asher, R.C., Bradshaw, L., Davies, D. Perry, J.E., Sanguine, S. and Vaughan, G.J. "The injection of liquid sodium into stainless steel : A report of further experiments Na SS/4 , Na SS/5 and Na SS/6." Paper FCI 4/P13 presented to the 4th CSNI specialist meeting on fuel-coolant interaction in nuclear reactor safety, Bournemouth, UK, April 1979.

[78] Hillary, J.J., Curry, P. and Taylor, L.R. "Preliminary experimental studies of the interaction of water with molten lead and molten salt mixtures." Paper presented to International conference on engineering of fast reactors for safe and reliable operation, Karlsruhe, West Germany, Oct. 1972.

[79] Higham, E.J. and Vaughan, G.J. "Molten fuel-coolant interaction studies: some results obtained with the Windscale small shock tube rig." UKAEA Windscale report no. ND-R-95(W), 1978.

[80] Darby, K.I., Guest, J.N., Pottinger, R.C., Rees, N.J.M., and Turner, R.G. "Progress at AWRE Foulness on the Al/water shock tube and UO_2/sodium thermal interaction rig." Paper SNI 2/1 presented to 2nd CSNI specialist meeting on sodium/fuel interaction in fast reactors, Ispra, Italy, Nov.1973.

[81] Derby, K, Pottinger, R.C., Rees, N.J.M. and Turner, R.G. "The thermal interaction between water and molten aluminium under impact conditions in a strong tube." Paper presented to the CREST meeting on sodium-fuel interaction in fast reactor safety, Grenoble, Jan. 1972.

[82] Goldhammer, H. and Kottowski, H.M. "Theoretical and experimental investigation of fuel-coolant interactions in a shock tube configuration." Proc. of the ANS/ENS international meeting on fast reactor safety and related physics, Chicago, USA, 4, Oct. 1976

[83] Zivi, S.M., Wright, R.W., Firstenberg, A.F. and Humberstone, G.H. "Shock tube experiments on pressure generation." USAEC STL-372-50, Dec. 1966.

[84] Wright, R.W. and Humberstone, G.H. Trans. Amer. Nuc. Soc., 9, (1), p305, 1966.

[85] Zivi, S.M. and Wright, R.W. "Kinetic studies of heterogeneous water reactors." USAEC Report STL-372-22, pp3-17, July 1965.

[86] Zivi, S.M. and Wright, R.W. "Dispersal and pressure generation by water-impact upon molten aluminium." USAEC report STL-372-30, pp62-74, Dec 1965.

[87] Lazarus, J., Navarre, J.P. and Kottowski, H.M. "Thermal interaction experiments in a channel geometry using Al_2O_3 and Na." Paper SNI 2/13 presented to the 2nd CSNI specialist meeting on sodium/fuel interaction in fast reactors, Ispra, Italy, Nov.1973.

[88] Kottowski, H.M. and Mol, M. "Importance of the coolant impact on the violence of vapour explosions." Paper FCI4/P12 presented to the 4th CSNI specialist meeting on fuel-coolant interactions in nuclear reactor safety, Bournemouth, UK, April 1979.

[89] Amblard, M. "Preliminary results on a contact between 4kg of molten UO_2 and liquid sodium." Paper SNI 6/14 presented to 3rd specialist meeting on sodium/fuel interaction in fast reactors, Tokyo, Japan, March 1976.

[90] Amblard, M. and Berthoud, B. "UO_2-Na interactions: The CORECT II experiment." Paper FCI4/P22 presented at 4th CSNI specialist meeting on fuel-coolant interactions in nuclear reactor safety, Bournemouth, UK, April 1979.

[91] Hicks, G.P. and Menzies, D.C. Argonne report ANL-7120, p654, 1965.

[92] Padilla, A. Trans. Amer. Nuc. Soc., 13, p375, 1970.

[93] Jacobs, H. Paper presented at the 3rd SMIRT conference, London, U.K., Sept. 1975.

[94] Caldarola, L. "A theoretical model with variable masses for the molten fuel-sodium thermal interaction in a nuclear fast reactor." Nuc. Eng. and Design, 34, pp181-201, (1975).

[95] Caldarola, L. "A theoretical model for the molten fuel-sodium interaction in a nuclear fast reactor." Nuc. Eng. and Design, 22(2), pp175-211, 1972.

[96] Cho, D.H., Ivins, R.O. and Wright, R.W. "A rate limited model of molten fuel/coolant interactions. Model development and preliminary calculations." Argonne report ANL-7919, 1972.

[97] Sawada, T., Hasegawa, Y. and Nishimura, A. "A parametric study on reactor containment response to fuel-sodium interaction." Paper SNI6/26 presented to the 3rd specialist meeting on sodium-fuel interactions in fast reactors, Tokyo, Japan, March 1976.

[98] Coddington, P., Fishlock, T.P. and Jakeman, D. "Calculations of the possible consequences of molten fuel-sodium interactions in subassembly and whole core geometries." Paper SNI6/25 presented to the 3rd specialist meeting on sodium-fuel interaction in fast reactors, Tokyo, Japan, March 1976.

[99] Breton, J.P. and Antonakas, D. "A model for SFI application to the JEF experiments." Paper SNI6/23 presented to the 3rd specialist meeting on sodium-fuel interaction in fast reactors, Tokyo, Japan, March 1976.

[100] Jacobs, H. and Thuray, K. "The calculation of the pressure history and the production of kinetic energy during a fuel-sodium interaction by solving the exact thermodynamic equations." Proc. Int. conf. on engineering of fast reactors for safe and reliable operation, Karlsruhe, October 1972.

[101] Fishlock, T.P. "EXPEL - A computing model for molten fuel-coolant interactions in fast reactor sub-assemblies." UKAEA Winfrith report no. AEEW RI029, Oct. 1975.

[102] Fishlock, T.P. Winfrith unpublished work 1977.

[103] Jakeman, D. "A review of the meetings of the working group on the comparison of calculational models." Paper SNI 6/21 presented to the 3rd specialist meeting on sodium-fuel interaction in fast reactors, Tokyo, Japan, March 1976.

[104] Potter, R. and Jakeman, D. "A review of the CREST comparison of the sodium-fuel interaction calculations covering seven methods." Paper SNI 2/20 presented to the 2nd specialist meeting on sodium-fuel interaction in fast reactors, Ispra, Italy, 1973.

[105] Hinz, J.O. "Forced deformations of viscous liquid globules." Appl. Sci. Res., A1, pp263-272, 1948.

[106] Dhir, W.K. "On the use of minimum film boiling temperature as a criterion for coherent molten metal-coolant interactions." Nuc. Sci. and Eng., 70, pp119-126,1979.

[107] Carslaw, H.S. and Jaeger, J.C. "Conduction of heat in solids." Oxford University Press, 1959.

[108] Katz, D.L. and Sliepcevich, C.M. "LNG/water explosions: cause and effect." Hydrocarbon Processing, pp240-244, Nov. 1971.

[109] Katz, D.L. Chem. Eng. Prog. 68, pp68-69, 1972.

[110] Yang, K. "Explosive interaction of liquified natural gas and organic liquids." Nature , 243, pp221-222, 1973.

[111] Doring, W. Z. physik. Chem., B36, pp371-386, 1973.

[112] Nelson, W. "A new theory to explain physical explosions." TAPPI, 56, no.3, March 1973.

[113] Nelson, W. "Recovery boiler explosions: new theory points to remedies." Pulp and Paper, Feb. 1973.

[114] Fauske, H.K. "On the mechanism of uranium dioxide-sodium explosive interactions." Nuc. Sci. and Eng., 51, pp95-101, 1973.

[115] Nakanishi, E. and Reid, R.C. "Liquid natural gas-water reactions." Chem. Eng. Prog., 67, no.12, Dec. 1971.

[116] Rausch, A.H. and Levine, A.D. "Rapid phase transformations caused by thermodynamic instability in cryogens." Cryogenics, April 1973.

[117] Blander, M. and Katz, J.L. "Bubble nucleation in liquids." AIChE. Journal, 21, no.5, pp833 -848, Sept. 1975.

[118] Fauske, H.K. "Nucleation of liquid sodium in fast reactors." Reactor Technology, 15, no.4, pp278-302, 1972.

[119] Fauske, H.K. "Mechanisms of liquid-liquid contact and heat transfer related to fuel-coolant interactions." Paper SNI2/18 presented to 2nd specialist meeting on sodium-fuel interaction in fast reactors, Ispra, Italy, Nov. 1973.

[120] Fauske, H.K. "Some aspects of liquid-liquid heat transfer and explosive boiling." Paper presented at the ANS fast reactor safety meeting, Beverly Hills, April 1974.

[121] Henry, R.E., Fauske, H.K. and McUmber, L.M. "Vapor explosion experiments with simulant fluids." Paper presented to the Int. Conf. on fast reactor safety and related physics, Chicago, Oct. 1976.

[122] Henry, R.E. and Fauske, H.K. "Nucleation characteristics in physical explosions." Paper SNI6/18 presented to 3rd specialist meeting on sodium/fuel interaction in fast reactors, Tokyo, Japan, April 1976.

[123] Epstein, M. "Thermal fragmentation - a gas release phenomenon." Nuc. Sci. and Eng., 55, pp462-467, 1974.

[124] Sallak, J.A. "An investigation of explosions in the soda smelt dissolving operation." Pulp and paper magazine (Canada), 56, no.9, pp114-118, 1955.

[125] Nelson, W. and Kennedy, E.H. "What causes Kraft dissolving tank explosions." Paper Trade Journal, 140, no.7, pp50-54, 1956.

[126] Armstrong, D.R., Testa, F.J. and Raridon, D. "Interaction of sodium with molten UO_2 and stainless steel using a dropping mode of contact." Argonne report no. ANL-7890, 1971.

[127] Flory, K., Paoli, R. and Mesler, R.B. "Molten metal-water explosions." Chem. Eng. Prog., 65, no.12, pp50-54, 1969.

[128] Groenveld, P. "Explosive vapour formation." Trans. ASME, J. Heat Trans., pp236-238, May 1972.

[129] Board, S.J., Clare, A.J., Duffey, R.B., Hall, R.S. and Poole, D.H. "An experimental study of heat transfer processes relevant to thermal explosions" Int. J. Heat Mass Transfer, 14, pp1631-1641, 1971.

[130] Kazimi, M., Watson, C., Lanning, D., Rohsenow, W. and Todreas, N.E. "Acoustic cavitation as a mechanism of fragmentation of hot molten droplets in cool liquids." MIT report COO-2781-6 TR, 1976.

[131] Vogel et al. Argonne report no. ANL-7553 , 118, 1969.

[132] Firstenberg, A.F. et al "Kinetic studies of heterogeneous water reactors." AEC Res. and Dev. Report. Annual summary report 1966 STL-372-20.

[133] Swift, D.L. and Baker, L. Argonne report no. ANL-7120, p839, 1965. MIT report no. COO-2781-6 TR, 1976.

[134] Stevens, J.W. and Witte, L.C. "Destabilization of vapour film boiling around spheres." Int. J. Heat Mass Transfer, 16, pp669-678, 1973.

[135] Board, S.J., Hall, R.W. and Hall, R.S. "Detonation of fuel-coolant explosions." Nature, 254, p319, 1975.

[136] Baines, M. "Hydrodynamic fragmentation in a dense dispersion." Paper FCI4/4, 4th CSNI specialist meeting on fuel-coolant interactions in nuclear reactor safety, Bournemouth, UK, April 1979.

[137] Theofanous, T.G., Saito, M. and Efthimiadas, T. "The role of hydrodynamic fragmentation in fuel-coolant interactions." Paper FCI4/P5 presented to 4th CSNI specialist meeting on fuel-coolant interactions in nuclear reactor safety, Bournemouth, UK, April 1979.

[138] Buchanan, D.J. and Dullforce, T.A. "Mechanism for vapour explosions." Nature, 245, no.5419, pp32-34, 1973.

[139] Vaughan, G.J., Caldarola, L. and Todreas, N. "A model for fuel fragmentation during molten fuel-coolant interactions." ANS/ENS international meeting on fast reactor safety and related physics, Chicago, USA, Oct. 1976.

[140] Rayleigh, Lord. "On the pressure developed in a liquid during the collapse of a spherical cavity." Phil. Mag., 34, pp94-98, 1917.

[141] Benjamin, T.B. and Ellis, A.T. "The collapse of cavitation bubbles and the pressures thereby produced against solid boundaries." Phil. Trans. Roy. Soc., 260, pp221-240, 1966.

[142] Plesset, M.S. and Chapman, R.B. "Collapse of an initially spherical vapour cavity in the neighbourhood of a solid boundary." J. Fluid Mech., 47, part 2, pp283-290, 1971.

[143] Christiansen, J.P. and Reynolds, J.A. UKAEA Culham Laboratory internal report.

[144] Batchelor, G.K. "The effect of homogeneous turbulence on material lines and surfaces." Proc. Roy. Soc., A213, pp349-366, 1952.

[145] Taylor, G.I. "The dispersion of jets of metals of low melting point in water." Paper 32, The Scientific papers of G.I. Taylor, 3, pp304-305, Cambridge University Press, 1963. (Edited by Batchelor, G.K.).

[146] Fishlock, T.P. "Calculations on propagating vapour explosions for the aluminium/water and UO_2/water systems." Paper FCI4/P2 presented to the 4th CSNI specialist meeting on fuel-coolant

interaction in nuclear reactor safety, Bournemouth, UK, April 1979.

[147] Jacobs, H. "Computational analysis of fuel-sodium interactions with an improved method." International meeting on fast reactor safety and related physics, Chicago, Oct. 1976.

[148] Board, S.J., Hall, R.W. and Brown, G.E. "The role of spontaneous nucleation in thermal explosions. Freon-water experiments." Proceedings of the fast reactor safety meeting, Beverly Hills, USA, April 1974.

[149] Bradley, R.H., Witte, L.C. and Cox, J.E. "The vapour explosion - heat transfer and fragmentation. Investigation of the vapour explosion phenomenon using a molten metal jet injected into distilled water." University of Houston technical report no. ORO-3936-7, October 1971.

[150] Jordan, D.P. "Film and transition boiling." Advances in heat transfer, 5, pp55-128, Academic Press, New York, 1968. (Edited by Irvine, T.F. and Hartnett, J.P.)

[151] Kling, C.L. "High speed photographic study of cavitation and bubble collapse." PhD thesis, University of Michigan, USA, 1970.

[152] Hsiao, K.H., Witte, L.C. and Cox, J.E. "Transient film boiling from a moving sphere." Int. J. Heat Mass Transfer, 18, pp1343-1350, 1975.

[153] Reynolds, J.A., Dullforce, T.A., Peckover, R.S. and Vaughan, G.J. "Fuel-coolant interactions - some basic studies at the UKAEA Culham Laboratory." Paper SNI6/2 presented to the 3rd specialist meeting on sodium-fuel interaction in fast reactors, Tokyo, Japan, March 1976. [Also Culham Laboratory report no. CLM/RR/S2/7].

[154] Clift, R., Grace, J.R. and Weber, M.E. "Bubbles , drops and particles." Academic Press, 1978.

[155] Schins, H.E.J. "Contribution to the boiling curve of sodium." Atomkernenergie (ATKE), 26, pp48-52, 1975.

[156] Bradfield, W.S. "On the effect of subcooling on wall superheat in pool boiling." J. Heat Transfer, 89, pp269-270, 1967.

[157] Farahat, M.M.K. "Transient-boiling heat transfer from spheres to sodium." PhD thesis, Northwestern University, USA. Also Argonne report no. ANL-7909, Jan. 1972.

[158] Henry, R.E. "A correlation for the minimum wall superheat in film boiling." Trans. ANS, 15, no.1, pp420-421, 1972.

[159] Schlichting, H. "Boundry layer theory." McGraw-Hill, New York, 1960.

[160] Collier, J.G. "Convective boiling and condensation." McGraw-Hill, London, 1972.

[161] Nukiyama, S. "Maximum and minimum values of heat transmitted from metal to boiling water under atmospheric pressure." J. Soc. Mech. Eng. Jpn, 37, pp53, 367-374, 1934.

[162] Farber, E.A. and Scorah, R.L. "Heat transfer to water under pressure." Trans. ASME, 70, pp369-384, 1948.

[163] Vaughan, G.J. "Theoretical considerations concerning molten fuel-coolant interaction debris size." Paper FCI4/P7 presented to 4th CSNI specialist meeting on fuel-coolant interaction in nuclear reactor safety, Bournemouth, UK, April 1979.

[164] Bird, M.J. Private communication.

[165] Skripov, V.P. "Metastable liquids." John Wiley and Sons, 1974.

[166] Henry, R.E. "A comparison of the sodium-UO_2 results with the spontaneous nucleation theory." Paper FCI4/P21 presented to the 4th CSNI specialist meeting on fuel-coolant interaction in nuclear reactor safety, Bournemouth, UK, April 1979.